NON-EQUILIBRIUM DYNAMICS IN QUANTUM SIMULATORS

im Fachbereich Physik der Freien Universität Berlin eingereichte Dissertation
zur Erlangung des Grades eines Doktors der Naturwissenschaften

MAREK L. GLUZA

eingereicht im Juni 2020

Dahlem Center for Complex Quantum Systems
Freie Universität Berlin

Reviewers
Prof. Dr. Jens Eisert
Prof. Dr. Piet Brouwer
Date of Disputation: 29th October 2020

Name: Gluza
Vorname: Marek Ludwik

Ich erkläre gegenüber der Freien Universität Berlin, dass ich die vorliegende Dissertation selbstständig und ohne Benutzung anderer als der angegebenen Quellen und Hilfsmittel angefertigt habe. Die vorliegende Arbeit ist frei von Plagiaten. Alle Ausführungen, die wörtlich oder inhaltlich aus anderen Schriften entnommen sind, habe ich als solche kenntlich gemacht. Diese Dissertation wurde in gleicher oder ähnlicher Form noch in keinem früheren Promotionsverfahren eingereicht. Mit einer Prüfung meiner Arbeit durch ein Plagiatsprüfungsprogramm erkläre ich mich einverstanden.

Datum: Unterschrift:

ABSTRACT

This thesis summarizes a course of investigation of various aspects of non-equilibrium dynamics in isolated quantum systems which can be controlled to the extent that one can speak of not just realizing but rather simulating a desired physical effect. The first subject considered concerns a general question of relaxation in a large class of physical models. It is rigorously proven that equilibration can occur for arbitrary local observables despite the entire system being perfectly isolated. Various mechanisms responsible for convergence to local equilibrium are highlighted. These involve in particular the memory loss of non-Gaussian correlations following an interaction quench, a notion of Gaussian ergodicity and a proof of the emergence of translation invariance of correlations due to the presence of this symmetry in the Hamiltonian governing the evolution. These results provide the long time and large system size asymptotics facilitating a thermodynamic limit, but at the same time are relevant for state-of-the-art quantum simulation experiments with large numbers of ultra-cold atoms: A related effect has been observed in a one-dimensional phononic quantum field simulator and additionally a method is provided to study relaxation dynamics of this type in optical lattice quantum simulators. Within the second theme explored in this thesis a novel quantum read-out method is proposed and applied in continuous field quantum simulators which allowed for the first time to measure experimentally various thermodynamical properties of one-dimensional quasi-condensates. In particular, tomographic results concerning thermal properties, non-commuting observables, momentum and time-resolved occupation numbers of phonons are presented. Finally, ideas for practical benchmarking of the dynamics of certain closed quantum systems are put forward, based on the concept of a fidelity witness. It is demonstrated that fidelity, despite being a sensitive measure for large systems, can be efficiently estimated for non-equilibrium dynamics in coherent quantum simulators implementing paradigmatic models of condensed matter physics. The method developed has already found an independent application in studies of variational quantum circuits aiming at achieving so-called quantum chemistry accuracy using the Sycamore quantum processor. The fact that all three themes of research laid out in this thesis have found an experimental realization hints at a prognosis for future developments in physics that it will become standard that quantum simulators will realize experimentally novel theoretical ideas on demand and the time between theoretical insights and experimental observations will be dramatically shortened.

ZUSAMMENFASSUNG

Diese Dissertation fasst eine Reihe von Untersuchungen zu unterschiedlichen Aspekten von Nichtgleichgewichtsdynamik in isolierten Quantensystemen zusammen, die in einem Maße präzise kontrolliert werden können, dass man nicht nur von der Realisierung eines physikalischen Effektes, sondern von seiner Simulation sprechen kann. Das erste Thema befasst sich mit einer allgemeiner Frage der Relaxationdynamik in einer grosser Klasse von physikalischen Modellen. Es wird in diesem Rahmen rigoros bewiesen, dass eine Equilibrierung von beliebigen lokalen Observablen auch dann generisch vorliegen kann, wenn das System perfekt isoliert bleibt. Unterschiedliche Mechanismen werden herausgestellt, die für die Konvergenz zu lokalem Gleichgewicht verantwortlich sind. Dies betrifft insbesondere der Gedächtnisverlust von nicht-Gaußchen Korrelationen nach schnellen Änderungen von Wechselwirkungen, eine Begrifflichkeit von Gaußscher Ergodizität und der Beweis einer Emergenz von Translationsinvarianz in Situationen, in denen der Hamiltonoperator eine solche Symmetrie aufweist. Diese Resultate ergeben die Asymptotik eines Übergangs zu langen Zeiten und großen Systemen, die einen thermodynamischen Limes abbilden. Sie sind aber gleichermaßen relevant für moderne Quantensimulationsexperimente, wie sie derzeit mit großskaligen Systemen ultrakalter Atome durchgeführt werden: Ein artverwandter Effekt wurde in einem eindimensionalen Quantenfeldsimulator beobachtet. Aufbauend auf diesen Ergebnissen werden Methoden bereitgestellt zur Untersuchung der Nichtgleichgewichtsdynamik von Systemen ultrakalter Atome in optischen Gittern. Im zweiten Teil der Arbeit wird eine neuartige Auslesemethode vorgeschlagen und auf Quantensimulatoren kontinuierlicher Quantenfelder angewendet, die tatsächlich experimentell erprobt wurde, was erstmals erlaubte, verschiedene thermodynamische Eigenschaften von eindimensionalen Quasikondensaten experimentell zu vermessen. Insbesondere werden tomographische Resultate über thermische Eigenschaften präsentiert, über Erwartungswerte von nichtkommutierenden Observablen und auch Besetzungen von Phononenmoden, in Impuls und Zeit aufgelöst. Schließlich werden Ideen vorgestellt über die Zertifikation der Quantendynamik abgeschlossener Quantensysteme, basierende auf der Idee eines sogenannten Fidelitätszeugen. Es wird gezeigt, dass die Fidelität - eine inhärent fragile Größe für große Quantensysteme - effizient geschätzt werden kann für die Nichtgleichgewichtsdynamik kohärenter Quantensimulatoren, die paradigmatische Systeme aus der Physik der kondensierten Materie implementieren. Die so entwickelte Methode hat bereits eine unabhängige Anwendung gefunden in Studien variationeller Quantenschaltkreise, die darauf abzielen, das Genauigkeitsniveau der Quantenchemie zu erreichen, den Sycamore Quantenprozessor verwendend. Die Tatsache, dass alle drei in dieser Dissertation präsentierten theoretischen Forschungsrichtungen bereits experimentell realisiert werden konnten, deutet darauf hin, dass hier eine Prognose aufgegriffen werden kann, nach der es Standard wird, dass Quantensimulatoren theoretische Ideen gezielt aufgreifen können und die Zeit zwischen theoretischer Einsicht und experimenteller Bestätigung dramatisch verkürzt wird.

CONTENTS

1 INTRODUCTION 1
1.1 Non-equilibrium dynamics in quantum simulators 3

2 EQUILIBRATION VIA GAUSSIFICATION IN FERMIONIC LATTICE SYSTEMS 6
2.1 Formulation of the problem 7
2.2 Our results 7
2.3 The implications of the result 8
2.4 Open problems 9

3 EQUILIBRATION TOWARDS GENERALIZED GIBBS ENSEMBLES IN NON-INTERACTING THEORIES 31
3.1 Formulation of the problem 32
3.2 Our results 32
3.3 The implications of the result 33
3.4 Open problems 34

4 QUANTUM READ-OUT FOR COLD ATOMIC QUANTUM SIMULATORS 84
4.1 Formulation of the problem 85
4.2 Our result 85
4.3 The implications of the result 86
4.4 Open problems 87

5 FIDELITY WITNESSES FOR FERMIONIC QUANTUM SIMULATIONS 109
5.1 Formulation of the problem 109
5.2 Our results 110
5.2.1 Fidelity witnesses 110
5.2.2 Experimentally relevant fidelity witnesses 110
5.3 The implications of the results 111
5.4 Open problems 112

6 SUMMARY 127

Climate footprint estimates 137

Acknowledgments 138

PUBLICATIONS OF THE AUTHOR

The four first-author publications featuring in this thesis are:

[1] *Equilibration via Gaussification in fermionic lattice systems*, M. Gluza, C. Krumnow, M. Friesdorf, C. Gogolin, J. Eisert, *Physical Review Letters*, **117**, 190602, (2016), doi.org/10.1103/PhysRevLett.117.190602

My main contribution in this project was to provide the blueprint of the calculations involved in the derivation of the result with both significant individual initiative but also following the input of the co-authors.

[2] *Equilibration towards generalized Gibbs ensembles in non-interacting theories*, M. Gluza, J. Eisert, T. Farrelly, *SciPost Physics*, **7**, 38, (2019), doi.org/10.21468/SciPostPhys.7.3.038

My main contributions to the project were the formulation of the problem and its proof strategy, the derivation in collaboration with the co-authors of the central results of the paper and the numerical calculations.

[3] *Quantum read-out for cold atomic quantum simulators*, M. Gluza, T. Schweigler, B. Rauer, C. Krumnow, J. Schmiedmayer, J. Eisert, *Communications Physics*, **3**, 12 (2020), doi.org/10.1038/s42005-019-0273-y

My main contribution to this project was to formulate the tomographic reconstruction method following a suggestion of prof. Schmiedmayer and to implement it numerically applying it to the experimental data.

[4] *Fidelity witnesses for fermionic quantum simulations* M. Gluza, M. Kliesch, J. Eisert, L. Aolita, *Physical Review Letters*, **120**, 190501, (2018), doi.org/10.1103/PhysRevLett.120.190501

My main contribution to this project was to provide the blueprint of the calculations involved in the derivation of the result with both significant individual initiative but also following the input of the co-authors.

Other publications:

[5] *Construction of exact constants of motion and effective models for many-body localized systems*, M. Goihl, M. Gluza, C. Krumnow, J. Eisert, *Physical Review B*, **97**, 134202, (2018), doi.org/10.1103/PhysRevB.97.134202

[6] *Holography and criticality in matchgate tensor networks*, A. Jahn, M. Gluza, F. Pastawski, J. Eisert, *Science Advances*, **8**, eaaw0092, (2019), doi.org/10.1126/sciadv.aaw0092

[7] *Neutrino mixing, interval matrices and singular values*, K. Bielas, W. Flieger, J. Gluza, M. Gluza, *Physical Review D*, **98**, 053001, (2018) doi.org/10.1103/PhysRevD.98.053001

[8] *Majorana dimers and holographic quantum error-correcting codes*, A. Jahn, M. Gluza, F. Pastawski, J. Eisert, *Physics Review Research*, **1**, 033079, (2019), doi.org/10.1103/PhysRevResearch.1.033079

[9] *Edge mode locality in perturbed symmetry protected topological order*, M. Goihl, C. Krumnow, M. Gluza, J. Eisert, N. Tarantino, *SciPost Physics*, **6**, 72, (2020), doi.org/10.21468/SciPostPhys.6.6.072

[10] *Contracting projected entangled pair states is average-case hard*, J. Haferkamp, D. Hangleiter, J. Eisert, M. Gluza, *Physics Review Research*, **2**, 0131010, (2020), doi.org/10.1103/PhysRevResearch.2.013010

[11] *Dynamical structure factors of dynamical quantum simulators*, M. L. Baez, M. Goihl, J. Haferkamp, J. Bermejo-Vega, M. Gluza, J. Eisert, *PNAS*, **117**, 42, (2020), doi.org/10.1073/pnas.2006103117

[12] *Decay and recurrence of non-Gaussian correlations in a quantum many-body system*, T. Schweigler, M. Gluza, M. Tajik, S. Sotiriadis, F. Cataldini, S-C. Ji, F. S. Møller, J. Sabino, B. Rauer, J. Eisert, J. Schmiedmayer, *arXiv preprint*, arXiv:2003.01808, (2020), arxiv.org/abs/2003.01808

[13] *Recovering quantum correlations in optical lattices from interaction quenches*, M. Gluza, J. Eisert, *arXiv preprint*, arXiv:2005.09000, (2020), arxiv.org/abs/2005.09000

[14] *Quantum field thermal machines*, M. Gluza, J. Sabino, N. H. Y. Ng, G. Vitagliano, M. Pezzutto, Y. Omar, I. Mazets, M. Huber, J. Schmiedmayer, J. Eisert, *arXiv preprint*, arXiv:2006.01177, (2020), arxiv.org/abs/2006.01177

1

INTRODUCTION

The vision of developing a quantum computer with unparalleled computational capabilities [15--17] has lead to enormous experimental advances allowing for an unprecedented degree of control over quantum dynamics of various systems [18--21]. In fact, so much progress has been made that achieving fault-tolerant quantum computing, i.e., implementing quantum algorithms which would not be corrupted by imperfections of quantum gates, seems to be a matter of continuing the existing efforts [22, 23]. Successfully completing this programme would be a significant milestone in the development of our civilisation as it would constitute a 'quantum' leap in our capabilities of doing computations. However, this major technological advance necessitates further sophisticated engineering feats developed in a collective effort. The roadmap to do this seems clear and if the progress is not interrupted by external issues such as the, ironically, man-made climate warming [24] then the bold idea of quantum computing should become reality within our lifetime.

This thesis will exemplify some of the possible ways for studying paradigmatic questions in physics by making use of the exciting innovative tools brought about by recent advances in quantum technologies. In this chapter an overview of the existing possibilities will be provided. It has the aim to set the scene by introducing the main quantum simulation platforms in their own right but it is hard to do justice to the wealth of exciting observations that have been made in the past years of research. Thus, primarily the focus will be on works that will be necessary for the later chapters, where some of the platforms will make an appearance, so that it will be possible to assess the publications presented in this cumulative thesis in context of state-of-the-art contributions at the front lines of contemporary research. It must be stressed that the newly emerging field of quantum simulation is transforming at a very rapid pace. Therefore only time will tell whether the studies that will be referenced in this chapter as being representative at the time of writing for the experimental possibilities will prove to become landmark scientific achievements in a broader perspective but it seems that some of the developments have excellent chances. After discussing the current state and goals of research on quantum computation and simulation a section follows which focuses on non-equilibrium dynamics in isolated quantum systems with the goal of presenting the subject using only a minimal number of formulas. This general description will be further refined in the other chapters which describe the core publications presented in this cumulative thesis and, of course, the publications themselves will provide the detailed formulations and evidence for the essential claims.

Currently there are two platforms which are major contenders in the effort towards building a quantum computer. In setups using trapped ions [18] it has been demonstrated that it is possible to perform quantum gates, i.e., elementary building blocks of quantum algorithms, which fail once out of thousands of applications [25]. While this astonishing feat has not been achieved yet for the specific systems implementing quantum algorithms, e.g., for the Innsbruck platform which is one of the pillars of the European flagship of quantum technologies [26], still trapped ions allow to run sophisticated quantum algorithms [27]. Superconducting qubits offer a completely different approach and allow for easy scalability of the system. However, the main challenge in the past decades was to improve their coherence [19]. This in fact has been successful, and did not go unnoticed even in popular media [28], as one of the leading groups has demonstrated that a quantum device of around 50 qubits can be used to draw random samples from a probability distribution which is effectively out of reach of any classical device [29]. Somewhat surprisingly, studies of this type despite being funded through private corporate investments do not demonstrate something of immediate monetary value, but rather a particular insight concerning nature, in the sense of a fundamental law concerning the physics of computation [15, 30, 31]. Namely, we find that predictions of quantum mechanics are seen to hold in the regime of extreme computational complexity [32], demonstrating that some of the limitations of classical computation can be surpassed. This milestone however, is not the end of the story. Due to the lack of quantum error-correction the currently existing quantum computation platforms have been termed noisy intermediate-scale quantum (NISQ) devices and there are more exciting physical observations to come once fault-tolerant systems become available [33].

The search for good applications of quantum computers is a research field in itself [34], and certainly quantum computers should not be limited to factoring large numbers efficiently. Here, we will be interested in a specific branch of this avenue of research, namely, we would like to know which aspects of dynamics can we understand for quantum many-body systems. The term many-body means that we are interested in systems where many particles

come together and interact in a sophisticated manner. In many instances this gives rise to a collective behavior and emergent phenomena which are not possible without interactions of a large number of constituents [35]. We understand a great deal about these thanks to insightful ideas of many physicists [36]. Various emergent phenomena in quantum many-body systems have been studied in condensed matter systems experimentally and have lead to many interesting developments. However, there are certain limitations that obstruct progress in understanding quantum many-body systems better. In generic applications, a theoretical physicist can only make progress by means of approximations and it is exceedingly difficult to substantiate these rigorously beyond merely physical intuition. The reason for this is not lack of trying hard: It turns out that often being able to answer specific questions about quantum many-body systems would automatically allow to solve seemingly unrelated and abstract computational tasks [37--39] which are unlikely to be solved by a classical algorithm [40]. Various complexity classes, similar to those characterizing tasks tackled by ordinary classical computers have been developed and studied, broadly falling under the scope of the field of Hamiltonian complexity [41--43]. The link between quantum physics and computational complexity theory can be thought of as talking about the elephant in the room: Quantum many-body systems are computationally hard to simulate and we might not be able to compute quantities of interest even with aid of largest supercomputers. This motivates quantum simulation which is the idea to use quantum systems to simulate the dynamics of other quantum systems making use of the fact that oftentimes markedly different physical systems are described by identical effective models.

The line of research aiming at realizing quantum simulators is somewhat independent from the efforts to build a fault tolerant quantum computer. Quantum simulators are devices that do not necessarily allow for full programmability, in particular operating a quantum simulator does not usually involve thinking about quantum gates or quantum computing circuits. It is also not the focus to develop systematic ways of correcting errors which is central to the effort of building a quantum computer that operates regardless of its classical environment. The main aim when devising quantum simulators is to achieve a profound degree of quantum coherence, i.e., bring the system to conditions where quantum effects are overwhelmingly important, e.g., using strongly coupled atoms that are well isolated. That is, one wants to make use of constituents that already show strong quantum effects and interfere with their idle behaviour only to the extent that is necessary to bring about an interesting physical feature or effect.

Thus a quantum simulator is typically operated by having an understanding of the types of interactions present in the system and aiming at changing their strength appropriately. This can involve changing the distributions of couplings in space, e.g., making two continuous one-dimensional systems interact, or suddenly doubling up the lattice of a discrete system. While these two ideas are clearly not the only ones possible, they will both feature in this thesis. The former scenario allowed us to study the details of the emergence of Gaussian correlations [12] and recurrences in isolated systems [3,44], but more generally also allows for devising thermal machines where the working fluid consists of ultra-cold atoms that necessitate quantum mechanics to model it [14]. The latter scenario has proven to be an excellent test-bed for studying relaxation dynamics in isolated systems [45] but going beyond that we have also shown that it allows to read out quantum correlations in the system [13] which is crucial for observing via quantum simulation the theoretical ideas presented in this thesis [1,2,4]. This particular aspect, namely that the various superbly controlled quantum systems may be capable of realizing exciting quantum phenomena but these may turn out to be invisible as the natively available read-out is restricted, is thematic for the frontier of the currently ongoing research in the field of quantum simulation and the research that is summarized in this thesis provides possible solutions towards alleviating the read-out bottleneck.

There are various experimental demonstrations of steering a gas of ultra-cold atoms so that the effective dynamics will resemble the physics of various interesting condensed matter systems. Specifically using ultra-cold atoms trapped in optical lattices one can aim to understand question about strongly correlated fermions in solid state materials. This includes equilibrium and non-equilibrium phenomena including among others studies of phase transitions, many-body localization, or topological effects [20,46--54]. Instead of creating a lattice resembling those appearing in crystals one can restrict the dimensionality of the system and focus on observing fundamental field-theoretic aspects of the quantum system [44,55--59]. It is also possible to study transverse Ising models that appear naturally in arrays of trapped ions or Rydberg atoms which stand out by having a long range of interactions [60--64].

Currently, one of the main topics in cold atomic quantum simulators is to achieve colder temperatures which could allow us to study the physics of high-temperature superconductors or frustrated quantum magnets [65] or realize quantum field thermal machines [14]. With these efforts underway, it is particularly appealing that one can study the physics of the system in the quantum simulator throughout the continuous effort to reduce the single physical parameter that enhances quantum effects. This should be contrasted with quantum error-correcting codes

which become advantageous only once a certain threshold of coherence has been reached and only when this is done it will yield a tremendous gain for realizing exciting physical phenomena via quantum computation [66].

1.1 NON-EQUILIBRIUM DYNAMICS IN QUANTUM SIMULATORS

Condensed matter systems are often modelled by assuming thermal equilibrium [67--69]. In some quantum simulators, one can start from a zero-temperature state which is essentially pure [45]. At the same time, the system is almost perfectly isolated from the laboratory environment which is essential to study experimentally quantum effects, especially in a many-body system. How then can we be able to perform a quantum simulation at finite temperatures if the system is closed?

This question is one of the motivating cornerstones for the study of equilibration and thermalization in finite closed quantum systems and is a central topic of this thesis. The cleanest setting for studying it is motivated by the availability of experiments with cold gases where one changes the Hamiltonian abruptly, faster than the relevant time-scales of dynamics in the system. This is called a quantum quench which is theoretically defined by an instantaneous change of the initial Hamiltonian $\hat{H}$ to a new Hamiltonian $\hat{H}'$. This implies, in particular, that the energy defined by the quantum expectation value $\langle\cdot\rangle$ of the Hamilton operator changes instantaneously

$$E = \langle\hat{H}\rangle \quad \rightarrow \quad E' = \langle\hat{H}'\rangle \, .$$

Of course one should remark that this is only an abstraction which models a very sudden change of parameters in the system. Nevertheless, in many cases a quench neglecting the finite duration of the change Hamiltonian is a valid approximation.

After a quench the expectation value of a generic local observable $\mathcal{O}$ will typically become time-dependent

$$\mathcal{O}(t) = \langle\hat{\mathcal{O}}(t)\rangle$$

where $\hat{\mathcal{O}}(t) = e^{it\hat{H}'}\hat{\mathcal{O}}(t)e^{-it\hat{H}'}$ denotes the Heisenberg evolution of the observable generated by the post-quench Hamiltonian. Whenever the time variations of $\mathcal{O}(t)$ become significantly larger than the experimental error bars, we say that one is observing non-equilibrium quantum many-body dynamics.

It goes beyond the scope of this thesis to provide a detailed account of existing studies of quench dynamics in isolated systems which can be obtained from a number of reviews [70--75]. One of the crucial aspects to discuss is that a system undergoing non-equilibrium dynamics at long times should at some point thermalize, meaning that the expectation value of an observable should not vary in time, but rather agree with a value that one would obtain by assuming the state to be a thermal state given some temperature. This in particular is expected to take place for systems that feature non-trivial interactions and lack local symmetries and conservation laws [70--75].

However, there are several cases where thermalization may take unusually long to occur, or even may not happen at all. The presence of a large amount of symmetries can render a system to be integrable, but in this case we do not expect thermalization but rather convergence to generalized Gibbs ensembles [1, 2, 76--82] which are parametrized by a number of generalized temperatures. Many-body localized systems [83, 84], in which disorder leads to the appearance of an extensive number of local constants of motion [5, 84] are one particular example of systems that are not expected to thermalize. Moreover, even in translation-invariant systems some memory of the initial state [83, 85, 86] may remain or even non-equilibrium fluctuations may persist over very long times, apparently to no end [87--90].

We hence are faced with a difficult problem: Most systems are expected to thermalize, but it is very difficult to know just by inspecting the form of the Hamiltonian whether it will occur for a particular isolated system. It is clear that dephasing is an important part of the process [91, 92], but analytical arguments are difficult to make due to the generality of the question and the possibility of counter-examples. Whenever available, analytical arguments tend to be quite instructive because they reveal the mechanisms responsible for a system relaxing. This is in contrast to studying relaxation using numerical calculations for a fixed model [78, 93--100] which allows us to map out the possible phenomena but it is difficult to gain insight at to why these occur. One way forward is to attempt proving rigorously just equilibration without considering the question of thermalization. This distinction consists in showing observables relaxing to an equilibrium value without making a statement about the equilibrium value [73, 101--103]. Thus we see that a result showing equilibration is a weaker statement than proving thermalization, however, the latter may simply not be occurring following a quench. Thus focusing on equilibration should be seen as a step which allows to aim for general arguments that do not have to take into account counter-examples constituted by systems

which equilibrate to non-thermal steady states. Currently, the generality of the arguments makes it difficult to derive accurate predictions on how fast this process will occur [76, 104--110] unless one takes a drastic step of considering a randomized Hamiltonian in order to avoid considering examples of systems with slow dephasing [111--116].

In this context, many different experiments have been performed where various choices of the observable have lead to striking observations by means of its non-equilibrium dynamics. A pioneering achievement was the observation of the Mott-superfluid phase transition in optical lattice quantum simulators [49] by tuning the interaction which leads to the competition of two orders, one where local occupation numbers of atoms in the lattice are good quantum numbers, and one where momentum is. This has been followed up by studies of dynamics of phase transitions [117], transport [118], breakdown of ergodicity due to disorder [50] and more [52--54, 119]. In analog quantum simulation platforms using trapped ions additionally various effects were observed such as effective causality breakdown due to long-range interactions, dynamical phase transitions and others [62--64]. Finally, in a one-dimensional continuous field quantum simulator in which rubidium atoms are controlled on an Atom Chip prethermalization and observation of non-thermal steady states has been observed [44, 55--59].

It is, therefore, possible to explore experimentally a fundamental question: If initially one observes non-equilibrium dynamics of certain observables, will the system relax? If so then we will find that for large enough times the variations of $\mathcal{O}(t)$ are contained within the experimental error bars. Then the second question to study is whether the effectively constant long-time value $\overline{\mathcal{O}}$ agrees with the expectation value of that observable in a thermal ensemble?

In Ref. [56] a striking observation has been made motivated by theoretical studies of various effective models which the quantum simulator effectively implements. Namely, it has been demonstrated that depending on the initial state preparation the 'same' gas relaxes towards two different steady states. This means that at least one of them must be non-thermal. A quantum simulation has therefore demonstrated that a closed system evolving under unitary dynamics governed by a specific Hamiltonian did not thermalize.

Steady states of this type are referred to as generalized Gibbs ensembles and it will be the goal of the first two chapters of this thesis to provide a mathematically rigorous theoretical prediction for their necessity in certain quench scenarios. Specifically, in the following chapter Ref. [1] will be presented which shows that any state of fermions with a finite correlation length Gaussifies under free hopping dynamics on a lattice. By Gaussification we mean that an initially non-Gaussian state after a quench of many-body interactions becomes Gaussian over time in the sense that all correlation functions satisfy Wick's theorem. Gaussification can be viewed as a refined statement compared to directly aiming to show equilibration. This is because a system that was initially non-Gaussian can become Gaussian over time but stay out-of-equilibrium. If in addition to Gaussification one shows equilibration of the covariance matrix of the system then one can conclude that local equilibration has taken place. Making this distinction turned out to be fruitful as this allowed us to show equilibration for many practically relevant scenarios and in these cases equilibration occurs according to a power-law in time. This includes in particular scenarios that can be studied in optical lattice quantum simulation experiments via a quench of a many-body interaction parameter. At the same time, the result is relevant for understanding the foundations of statistical mechanics because the system throughout the dynamics of the Gaussification process is perfectly isolated. We derive a precise understanding of a mechanism for memory loss in large systems without the need for coupling to the environment or 'random shaking' of some sort from the outside - we show that the onset of scrambling of the memory of initial conditions occurs via internal dynamics of the isolated system. On the technical side, this is facilitated by detailed understanding of how to treat the question at hand despite possible obstacles such as Poincaré recurrences or reversibility of the unitary dynamics which only seemingly stands in contradiction to memory loss effects. All this is shown to be possible and additionally it is demonstrated that the rate at which the Gaussification process scrambles the memory of the initial non-Gaussian condition is functionally tight, matching numerical experiments using tensor network techniques.

In the chapter following the work on Gaussification a subsequent study is presented which largely brings to completion the program on equilibration following interaction quenches [2]. Here we demonstrate a detailed understanding of the phenomena at hand deriving a general result showing power-law equilibration time scales for initial states that are not necessarily translation invariant. This result is primarily rooted on a technical advance that we establish which allows us to compute dephasing rates without resorting to otherwise common approximations in field theory. This allows us to treat a wealth of models, that are restricted essentially only by the range of interactions, for evolution times where other methods would be ineffective. To arrive at our result it was necessary to understand what are the relevant constants of motion which additionally gives an intuition concerning which kind of generalized Gibbs ensembles are realized following equilibration after an interaction quench.

The third chapter will be concerned with the experimental platform of Ref. [56] where generalized Gibbs ensembles have been observed experimentally. This is a shift of the physical setting from fermionic systems hopping on a

lattice to bosons constrained to a single dimension which are described by a continuous field theory. Additionally, in contrast to the works on Gaussification where dispersion of wavepackets is crucial this effect does not feature in the bosonic quasi-condensates considered. This is due to the fact the relevant effective degrees of freedom in this system are phonons which are the collective excitations of the system and they have an approximately linear spectrum. The chapter presents the results obtained using a novel tomographic method that we have developed which allows to time- and momentum- resolve occupation numbers of the phonons in the system [3]. The successful functioning of the method constitutes a quantitative test of the effective theoretical models of the system developed in a long tradition of theoretical studies and is a crucial result of this thesis. This constitutes a significant extension of the read-out capabilities of the continuous field quantum simulation platform at hand and the key feature is non-equilibrium dynamics which we craft into a tomographic resource enabling state reconstructions.

The last chapter will present a method allowing to make progress on the conceptual question of how to benchmark and verify non-equilibrium dynamics in powerful quantum simulators given simple experimental observables and limited repetitions of the experiment [4]. Once more non-equilibrium dynamics is in focus but the task considered in this chapter stands in contrast to previous chapters as the physical question which is tackled could be viewed as being more abstract. The presented results fall into an area of research that is very much timely and important for emerging quantum technologies with the aim to develop methods allowing to make sure that a quantum simulation or computation was successful, i.e., certify the computation [120]. This is important as ultimately the task tackled by quantum computing should go beyond what we can compute classically. Certification, however, is challenging as the systems tackled have to be assumed to be large and not every single observable can be measured in practice. We show how to approach the problem by means of fidelity witnesses which are experimentally friendly observables that allow to certify that the operation of a quantum protocol was successful. While the task of certification of quantum dynamics may seem unusual compared to common questions in physics it is very much relevant for various systems in nature that we can practically engineer. In fact, the method of fidelity witnesses has been successfully employed to certify the preparation of Hartree-Fock states on the Sycamore quantum processor [121].

The thesis is summarized by giving a more detailed overview of the subjects presented in the thesis with one of the conceptual conclusions being that we seem to be witnessing a transformative time in physics due to the newly emerging quantum technologies. This is exemplified by the fact that it was possible for all three of the main theoretical ideas presented in this thesis to find an experimental application which is rather unusual for questions concerning quantum systems that may otherwise need a long time to be devised experimentally. However, this can well become a standard for the future when programmable quantum devices become more widely available.

2

EQUILIBRATION VIA GAUSSIFICATION IN FERMIONIC LATTICE SYSTEMS

In this chapter a rigorous result will be discussed concerning the question of memory loss of the initial conditions for a system undergoing unitary dynamics. That is to say we would like to understand how in a closed system the details of the initial configurations or correlations between constituents can become obscured by some mechanism which we would physically interpret as a scrambling process.

On a higher, conceptual, level it is highly desirable to derive results of this type for closed quantum systems. Indeed philosophers, and arguably this is the preference of many a physicist, find it quite unsatisfactory to say that a closed box with a gas thermalizes because the system is coupled to the surrounding environment - as then the question arises what thermalizes the environment? One could follow such arguments ad infinitum as any part of the observable universe comes to equilibrium by exchanging entropy with its own observable universe. Such reasoning does not deliver a deep understanding of why nature seems to realize ubiquitously thermal ensembles. And there is a need for that inquiry.

Specifically in the context of this thesis, we ask: Can a quantum simulator made of cold atoms thermalize because of a minute coupling to the auxiliary parts of the laboratory system? Or a solid state material in which the relevant couplings lead to much faster dynamics than would be caused by the coupling to the environment? It is not plausible that a weak coupling to the environment would be able to thermalize a system sufficiently fast.

Non-relativistic lattice systems interacting only between local sites exhibit effective causality, known as the Lieb-Robinson bound [122]. Should the environment be thermalizing the system by a flux of entropy through the boundary then the bulk of the system will remain non-thermal until it can causally exchange entropy with the environment. That is not what generically happens. And interestingly enough, we can rigorously prove instances of systems that come to equilibrium without the need of an environment. What we shall see is that a system can act as its own bath. Hence, scrambling ensues anywhere in the system in the same way without the need for an environment to trigger thermalization.

The questions highlighted here have a long standing history of inquiry [123]. The subject has received a flurry of interest in the recent decade and several in-depth reviews on the subject are available [70--75]. Indeed through several interesting contributions it has become clear that the effect sketched in plain language above can be substantiated in various ways for many-body systems.

The crucial contribution that is the starting point of this part of the thesis is the work by Cramer et al. [76]. In this work, it has been for the first time shown that a very simple yet paradigmatic system can act as its own bath. Specifically, it was proven for bosonic lattice systems that on-site particle measurements that initially exhibited non-Gaussian statistics over time become Gaussian. An instance of this behaviour would be to consider the observable corresponding to the local particle number $\hat{N}_x$ at site x and to show that even if initially we have that the moments do not factorize then this is the case for large times t to an increasingly improving approximation

$$\langle \hat{N}_x^2 \rangle \neq \langle \hat{N}_x \rangle^2 \quad \overset{t}{\mapsto} \quad \langle \hat{N}_x^2(t) \rangle \approx \langle \hat{N}_x(t) \rangle^2 \, .$$

This happens despite the system being perfectly homogeneous and even finite.

Below we will give the specific details but let us already now reveal the answer to the most pending riddle: If the system is homogeneous and translation invariant, how do we identify which part of it will play the role of its own bath? For this to happen necessarily some aspect of the protocol 'measure moments of the local particle number' must break the symmetry of the problem. But if the system is everywhere the same this may not be entirely obvious. The resolution of this lies in the fact that we are interested in local observables. To describe all moments of the observable it suffices to merely know the reduced density matrix where the observable acts. Similarly to the study of entanglement of pure states, we find then that considering the quantum equivalent of a marginal distribution can allow for local entropy increase and hence memory loss has a chance to appear. This is because we discard the information about the distribution of the rest of the system and its relation to the small subsystem where the observable acts. In Ref. [76] these elementary ingredients were shown to suffice for a rigorous derivation of a memory loss effect in a bosonic system. This result for essentially a single mode reduced density matrix was then improved for arbitrary local subsystems in Ref. [124]. This latter work established a quantum

central limit theorem for distributions where the variables are weakly correlated but not necessarily independently and identically distributed hence improving the results of Refs. [125--127] and giving the convergence rate not discussed in detail in Ref. [128]. Here, we will show how to derive a quantum central limit theorem for fermionic systems and how to draw conclusions about an equilibration mechanism based on it.

2.1 FORMULATION OF THE PROBLEM

We say that a quantum system described by a density matrix $\hat{\rho}$ locally equilibrates under a Hamiltonian $\hat{H}$ in the time interval between some relaxation time t_0 and some recurrence time t_{Rec} if the state at any time $t \in [t_0, t_{Rec}]$ is practically indistinguishable from the time-averaged state $\hat{\rho}^{(eq)}$ on the level of local observables [71]. Quantitatively, we fix some small $\epsilon > 0$ such that for every local observable $\hat{A}$ we have

$$|\langle \hat{A} \rangle_{\hat{\rho}(t)} - \langle \hat{A} \rangle_{\hat{\rho}^{(eq)}}| \leqslant \epsilon \tag{2.1.1}$$

for all $t \in [t_0, t_{Rec}]$, where $\langle \hat{A} \rangle_{\hat{\rho}} = \mathrm{tr}[\hat{\rho}\hat{A}]$ denotes the quantum expectation value of a local observable $\hat{A}$ which is local and has unit operator norm and $\hat{\rho}(t)$ is the initial state evolved unitarily according to the Hamiltonian $\hat{H}$.

In general, we would like to characterize precisely when systems equilibrate in this sense. However, this is notoriously difficult both on the practical side of attempting to prove such results but also from the perspective of computational complexity theory as Hamiltonian evolution is BQP-hard and so we would be making an interesting statement about quantum algorithms and their long-time behavior. For this reason it is interesting to concentrate first on the case of so-called Gaussian dynamics. These are evolutions whose Hamiltonians are special as they are a quadratic form in creation and annihilation operators. The ground and thermal states of such Hamilton operators are called Gaussian.

There are two specific questions we have investigated. The first problem is: Show that there exist Gaussian dynamics under which non-Gaussian states equilibrate on the level of local observables in finite time intervals. To find a solution and understanding of this statement one has to navigate around subtle issues. One of them being that non-Gaussian states in principle necessitate a large amount of parameters to be specified that can be hard to compute numerically for large systems if, e.g., the state represents a ground state affected by many-body interactions. Thus one has to tackle the problem without referring to particular properties of the state. Secondly, we aim to show that for a fixed Hamiltonian a number of states which are possibly non-Gaussian equilibrate. This is necessary to be able to claim having obtained a deeper understanding of foundations of statistical mechanics in isolated systems as empirically we expect this framework to become applicable after relaxation largely regardless of initial conditions. The statement of the second problem we considered is: When is the equilibrium state thermal and what are its properties otherwise? Quenches to free evolution have an extensive number of constants of motion and it has been discussed in literature that this can lead to the necessity of considering the equilibrium ensemble to be more general than thermal ensembles. Thus even if initially non-trivial interactions have been imprinted onto the state by means of non-Gaussian correlations their memory may be lost over time after the quench to free evolution. However, it is expected that the conservation laws should in various instances lead to the memory of non-equilibrium initial conditions and the equilibrium state will not be captured by a single temperature but to accommodate the various conserved charges one needs to describe it by means of a generalized Gibbs ensemble.

2.2 OUR RESULTS

The paper discussed in this chapter should be viewed in conjunction with the subsequent work presented in the following chapter together amounting to a remarkably general result. Ref. [1] presented in this chapter shows how Gaussian dynamics ''Gaussifies'' a non-Gaussian system, that is, turns a non-Gaussian quantum state into a Gaussian quantum state. This is true to an arbitrarily good approximation if the evolution time and system size are large enough. More precisely, we arrived at the following statement.

Theorem 1 (Fermionic generic Gaussification)**.** *Consider the initial fermionic state* $\hat{\rho}(0)$ *with exponential decay of correlations and a non-interacting translation-invariant post-quench Hamiltonian with dispersion relation* $E(p)$ *such that there are no points with* $E''(p) = E'''(p) = 0$ *for any* p*. Then there exist a constant relaxation time* t_0 *and a recurrence time* $t_{Rec} = \Theta(L)$ *such that, for all* $t \in [t_0, t_{Rec}]$*,*

$$|\langle \hat{A} \rangle_{\hat{\rho}(t)} - \langle \hat{A} \rangle_{\hat{\rho}_G(t)}| \leqslant Ct^{-1/6} \tag{2.2.1}$$

where $C > 0$ *and the state* $\hat{\rho}_G(t)$ *is Gaussian with the same covariance matrix as* $\hat{\rho}(t)$.

The formulation of this theorem already takes into account additional insights which follow from the publication [2] presented in the subsequent chapter. In the paper presented here we have proven this result under an assumption concerning the dynamics and showed that this property is valid, e.g., for the nearest-neighbor hopping of fermions on a ring. The updated formulation already includes the strengthening that essentially any local translation invariant hopping Hamiltonian on a ring gives rise to Gaussification.

2.3 THE IMPLICATIONS OF THE RESULT

The most important physical condition about the initial state is that of a correlation length. This property has been proven for ground states of gapped Hamiltonians and for high temperature states [129--132]. Hence, the result essentially implies that any 'equilibrium' state, which tend to have a finite correlation length, will Gaussify following an interaction quench. Other than that we demonstrate that it is not necessary to know more about the initial state.

This is the first hallmark of the general success of the program that is being brought to fruition by the works presented here and in the next chapter: We do not need to know precisely the quench model or the initial state to make a general and rigorous statement concerning equilibration. For a non-Gaussian state with a finite correlation length we prove that translation invariant Gaussian dynamics will render the initial state Gaussian. This implies equilibration according to a power-law in time for initial non-Gaussian states that are translation invariant. The work presented in the subsequent chapter further studies non-translation invariant initial conditions and proves equilibration in many natural instances with a comprehensive understanding of counter-examples.

It should be stressed that we do not need to know the precise values of the couplings of the model only its physical properties such as translation invariance or the range of hopping. We also do not need to know the precise initial values of the correlations, only that they satisfy a certain natural clustering property. And still with an analytical result we can prove equilibration according to a power-law in time. This should be contrasted with numerical studies where it is only ever possible to check individual cases for fixed values of couplings and initial conditions and hence it is difficult to give conclusive evidence for the occurrence of equilibration for a class of initial states and quench models. On a higher level, we hence have shown that an analytical approach, despite being less straightforward in general can lead to success in this type of general questions.

The most important instance of equilibration that our theorem implies is when the initial state is taken to be translation invariant in the same way as the non-interacting quench Hamiltonian. In this case the second moments do not change in time after the quench, as can be seen by considering the problem in momentum space where both the initial second moments and the couplings of the quench Hamiltonian are simultaneously diagonal. In this case to obtain an equilibrium state one needs to show that the higher moments over time become Gaussian, and this is precisely what the statement of our theorem implies. Specifically in this case we have that $\hat{\rho}_G(t) \equiv \hat{\rho}_G(0)$ because the second moments do not change in time and hence our bound (2.2.1) becomes

$$|\langle \hat{A} \rangle_{\hat{\rho}(t)} - \langle \hat{A} \rangle_{\hat{\rho}_G(0)}| \leqslant Ct^{-1/6}$$

showing that for an arbitrary local observable $\hat{A}$ its expectation value will become time independent and the deviation from the average is suppressed by a power-law envelope in time. Here we also notice the possibility of memory effects and the necessity of generalized Gibbs ensemble. Indeed, thermal states with respect to the quench Hamiltonian are a one parameter family giving for each choice of temperature a unique covariance matrix with a fixed average value of the energy. However, for a local quench Hamiltonian the energy is determined only by some particular correlation functions while many other correlation functions are not constrained by fixing the total energy and after starting out-of-equilibrium they may differ from the values expected in a thermal ensemble even after the relaxation has been completed.

That is to say, we find that thermalization does not always occur despite all local observables equilibrating. This comes from the fact that non-interacting Hamiltonians have an extensive number of conserved quantities which are the eigenmode occupation numbers. Given the Hamiltonian spectrum, these have unique values for any given temperature (the Fermi-Dirac distribution for fermions and for bosons the Bose-Einstein distribution). Whenever the initial state happens to have a distribution of eigenmodes that is not thermal this feature will be perfectly preserved in the dynamics. In this case, one is lead to generalize the notion of thermal states to systems with local conservation laws and consider generalized Gibbs ensembles. Our work shows an equilibration towards such generalized Gibbs ensembles.

We have subsequently developed a method that will allow studying this type of dynamics and equilibrium states in optical lattice quantum simulators [13]. This should allow to observe using optical lattice quantum simulators the Gaussification effect described in the paper presented in this chapter. Additionally, we have studied a related effect concerning the dynamical emergence of Gaussian correlations in one-dimensional quantum field simulators [12]. Interestingly, this experimental observation hints towards a more general mechanism of Gaussification. The result presented in this chapter relies on spatial mixing of correlations: After a quench Gaussification occurs because due to the finite correlation length the initial correlation agree with a Gaussian state for correlations between distanced points. Hence the correlations between points much further than the correlation length play the role of a Gaussian 'bath' with which the local correlations become mixed over time. In the experiment presented in Ref. [12] we are dealing with a system of phonons where correlations can range over substantial portions of the system and hence it is not an instance directly covered by the theory presented in this chapter. However, even in this case we observe Gaussification and can link it to a different type of a Gaussian bath with the mixing not relying on spatial spreading of wave-packets but rotation of canonically conjugated quantum fields.

2.4 OPEN PROBLEMS

Our work makes progress on certain interesting questions. At the same time it opens up new challenges or highlights the difficulty of long-standing problems such as stability of Gaussian dynamics with respect to interactions. Below, as will be done in the subsequent chapters too, some examples of interesting problems are listed that seem to remain unresolved.

Problem 1. Let $\hat{H}_0$ be a Hamiltonian leading to Gaussification. What remains of this effect in the thermodynamic limit after adding a many-body interaction of some small but finite strength which induces scattering of particles? Specifically, for an initially non-Gaussian state does one find at first a power-law decay of non-Gaussianity which then reaches a transient behavior and levels off towards a constant non-zero value? Is this constant proportional to the interaction strength?

Problem 2. (Partially solved [2], see next chapter.) How generic is the effect of Gaussification described above? Does it appear for a large variety of models?

Problem 3. (Partially solved [2], see next chapter.) Assume that Gaussification occurs. When do second moments equilibrate and hence the entire state becomes relaxed?

Problem 4. Rigorously prove a tighter dynamical exponent, e.g., that for nearest-neighbour hopping non-interacting particles on a ring the 4-point correlation functions tend towards the Wick expression according to the envelope $\propto t^{-1+\epsilon}$ where $\epsilon > 0$ can be chosen arbitrarily small. The observations about the size of the wave-front from Ref. [133] may be useful.

Problem 5. Rigorously prove Gaussification for non-translation invariant models. The observation that eigenmode wave-functions remain in general oscillatory facilitating the use of stationary phase approximation as suggested in Ref. [133] may be useful.

Equilibration via Gaussification in Fermionic Lattice Systems

M. Gluza,[1] C. Krumnow,[1] M. Friesdorf,[1] C. Gogolin,[2,3] and J. Eisert[1]
[1]Dahlem Center for Complex Quantum Systems, Freie Universität Berlin, 14195 Berlin, Germany
[2]ICFO-Institut de Ciencies Fotoniques, Mediterranean Technology Park, 08860 Castelldefels (Barcelona), Spain
[3]Max-Planck-Institut für Quantenoptik, Hans-Kopfermann-Straße 1, 85748 Garching, Germany
(Received 19 February 2016; published 4 November 2016)

In this Letter, we present a result on the nonequilibrium dynamics causing equilibration and Gaussification of quadratic noninteracting fermionic Hamiltonians. Specifically, based on two basic assumptions—clustering of correlations in the initial state and the Hamiltonian exhibiting delocalizing transport—we prove that non-Gaussian initial states become locally indistinguishable from fermionic Gaussian states after a short and well controlled time. This relaxation dynamics is governed by a power-law independent of the system size. Our argument is general enough to allow for pure and mixed initial states, including thermal and ground states of interacting Hamiltonians on large classes of lattices as well as certain spin systems. The argument gives rise to rigorously proven instances of a convergence to a generalized Gibbs ensemble. Our results allow us to develop an intuition of equilibration that is expected to be more generally valid and relates to current experiments of cold atoms in optical lattices.

DOI: 10.1103/PhysRevLett.117.190602

Despite the great complexity of quantum many-body systems out of equilibrium, local expectation values in such systems show the remarkable tendency to equilibrate to stationary values that do not depend on the microscopic details of the initial state, but rather can be described with few parameters using thermal states or generalized Gibbs ensembles [1–3]. Such behavior has been successfully studied in many settings theoretically and experimentally, most notably in instances of quantum simulations in optical lattices [2,4,5].

By now, it is clear that, despite the unitary nature of quantum mechanical evolution, local expectation values equilibrate due to a dephasing between the eigenstates [3,6–12]. So far it is, however, unclear why this dephasing tends to happen so rapidly. In fact, experiments often observe equilibration after very short times, which are independent of the system size [5,13], while even the best theoretical bounds for general initial states of concrete systems diverge exponentially [2,12]. This discrepancy poses the challenge of precisely identifying the equilibration time, which constitutes one of the main open questions in the field [1–3].

What is more, only little is known about how exactly the equilibrium expectation values emerge. Because of the exponentially many constants of motion present in quantum many-body systems, corresponding to the overlaps with the eigenvectors of the system, there seems to be no obvious reason why equilibrium values often only depend on a few macroscopic properties such as temperature or particle number. In short: it is unclear how precisely the memory of the initial conditions is lost during time evolution.

To make progress towards a solution of these two problems, it is instructive to study the behavior of non-interacting particles captured by so-called quadratic or free models. In these models, the time evolution of so-called Gaussian states, which are fully described by their correlation matrix, is particularly simple to describe. While studying the time evolution of such states provides valuable insight into the spreading of particles and equilibration, it is unclear if and under which conditions general non-Gaussian initial states out of equilibrium end up appearing Gaussian.

In this Letter, we address this question: we show under which conditions very general non-Gaussian initial states become locally indistinguishable from Gaussian states with the same second moments. This mechanism is much reminiscent of actual thermalization, in that an initially complex setting appears to converge to a high-entropy state that is defined by astoundingly few parameters only. In this way, we present a significant step forward in the theory of equilibration of quantum many-body systems that have been pushed out of equilibrium. Furthermore, our work suggests that for quadratic models, Gaussification can be seen as a genuine mechanism of nonequilibrium dynamics, complementing and playing a significant role in equilibration.

Our results hold for a remarkably large class of initial states, gapped interacting models evolving, after a so-called *quench*, in time under a quadratic fermionic Hamiltonian with finite ranged interactions. This family of Hamiltonians notably includes the case of noninteracting ultracold fermions realizable in optical lattices. By virtue of the Jordan-Wigner transformation, our results also apply to certain spin models. We formulate our results in the form of a rigorously proven theorem, which at the same time provides an intuitive explanation of the physics behind our result. We find Gaussification to be a consequence of two natural assumptions, namely exponential clustering of correlations in the initial state and what we call delocalizing transport.

Setting.—We begin by precisely stating the physical setting that we consider. For notational convenience, let $\mathcal{L}$ be a $d_{\mathcal{L}}$-dimensional cubic lattice with V lattice sites. Each site $r \in \mathcal{L}$ is associated with a fermionic orbital with fermionic creation and annihilation operators $f_r^\dagger$ and f_r. We collect them in a vector $c = (f_1, f_1^\dagger, \ldots, f_V, f_V^\dagger)$. All results can be generalized to fermions with internal degrees of freedom on Kagomé, honeycomb, or other geometries. The Hamiltonian of a quadratic fermionic system is then of the form

$$H = \sum_{j,k=1}^{2V} c_j^\dagger h_{j,k} c_k, \tag{1}$$

with Hermitian coupling matrix h. The time evolution of annihilation operators in the Heisenberg picture under such a Hamiltonian is given by

$$c_j(t) := e^{iHt} c_j e^{-iHt} = \sum_{k=1}^{2V} W_{j,k}(t) c_k \tag{2}$$

with the propagator $W(t) := e^{-2ith}$.

Next, we introduce the concept of Gaussian states and Gaussification. Define the correlation matrix γ of a state ρ as the matrix of its second moments, i.e., $\gamma_{j,k} := \mathrm{tr}(\rho c_j^\dagger c_k)$. A convenient characterization of Gaussian states is the following: they are the states that maximize the von Neumann entropy given the expectation values collected in the correlation matrix. For every state ρ, we hence define its Gaussified version ρ_G as the Gaussian state with the correlation matrix of ρ, i.e., $\mathrm{tr}(\rho_G c_j^\dagger c_k) = \mathrm{tr}(\rho c_j^\dagger c_k)$.

Assumptions.—Our main theorem holds for initial states (including non-Gaussian ones) with a form of decay of correlations that evolve under quadratic Hamiltonians that exhibit a form of transport that we define below. We now make these two conditions precise, starting with the correlation decay:

Definition 1.—(Exponential clustering of correlations) We say that a state ρ exhibits exponential clustering of correlations with length scale $\xi > 0$ and constant $C_{\mathrm{Clust}} > 0$ if, for any two operators A, B with $\|A\| = \|B\| = 1$, we have

$$|\mathrm{tr}(\rho AB) - \mathrm{tr}(A\rho)\mathrm{tr}(B\rho)| \leq C_{\mathrm{Clust}} |\mathrm{supp}(A)||\mathrm{supp}(B)| e^{-d(A,B)/\xi}. \tag{3}$$

Here $d(A, B)$ is taken to be the natural distance on the lattice between the supports $\mathrm{supp}(A)$, $\mathrm{supp}(B)$ of A and B and $\|\cdot\|$ denotes the operator norm.

Ground states of interacting gapped local Hamiltonians [14,15] as well as thermal states of arbitrary nonquadratic fermionic systems [16] at sufficiently high temperature have exponential clustering of correlations as defined in Definition 1. Thus, the initial state could be prepared within a quench scenario where the Hamiltonian is changed from a gapped interacting model to a quadratic Hamiltonian which governs the nonequilibrium dynamics. To reemphasize, by no means is the initial state assumed to be in any specific relation to properties of the latter quadratic Hamiltonian.

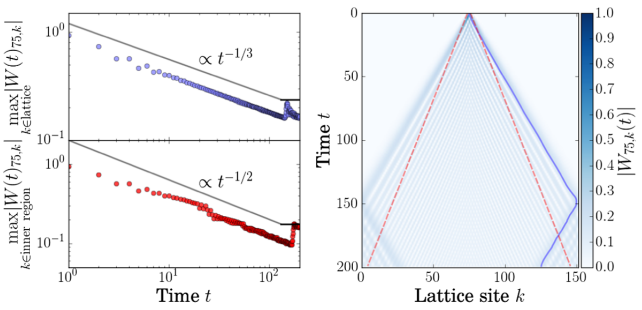

FIG. 1. The right panel shows a numerical study of the spreading of the support of a fermionic annihilation operator described in Eq. (2) under the evolution of the quadratic hopping Hamiltonian $H = -\sum_j (f_j^\dagger f_{j+1} + f_{j+1}^\dagger f_j)$ on a one-dimensional chain of 150 sites with periodic boundary conditions. The support expands ballistically, creating the Lieb-Robinson cone. The left panel shows the suppression of different elements of the propagator in time. The plot at the top shows the evolution of the maximum taken over the full lattice $\max_k |W_{75,k}(t)|$, where in the lower plot the maximum inside the inner region of the Lieb-Robinson cone (between the red dashed lines) is plotted. The maximum taken over the full lattice is reached for k in the wave front (indicated by the blue curve in the right panel) and the suppression goes as $t^{-1/3}$, while in the bulk of the cone, the suppression is proportional to $t^{-1/2}$. The suppression stabilizes, once the wave fronts collide.

For our proof of local relaxation towards a Gaussian state, we further assume that the quadratic Hamiltonian exhibits transport in the following sense:

Definition 2.—(Delocalizing transport) A quadratic Hamiltonian with propagator W on a $d_{\mathcal{L}}$-dimensional cubic lattice of volume V exhibits delocalizing transport with constants $C_{\mathrm{Trans}} > 0$, $\alpha_{\mathrm{Trans}} > d_{\mathcal{L}}/4$ and recurrence time $t_{\mathrm{Rec}} > 0$ if, for all $t \in (0, t_{\mathrm{Rec}}]$, we have that

$$\forall j, k: \; |W_{j,k}(t)| \leq C_{\mathrm{Trans}} \max\{t^{-\alpha_{\mathrm{Trans}}}, V^{-\alpha_{\mathrm{Trans}}}\}. \tag{4}$$

The intuition behind this definition is that an initially localized fermionic operator will spread over a large area, such that its component on a single localized operator is dynamically suppressed. In particular, such a suppression with $\alpha_{\mathrm{Trans}} = d_{\mathcal{L}}/3$ can be proven for quadratic hopping Hamiltonians (see the Supplemental Material [17] and also Fig. 1) and the critical Ising model. In finite dimensional systems, any nontrivial bound of the form (4) is eventually violated due to the recurrent nature of their dynamics. For quadratic hopping Hamiltonians, it can be shown that the recurrence time grows at least like $V^{6/7d_{\mathcal{L}}}$ with the system size.

Main result.—Our main result can be stated as follows:

Theorem 1.—(Gaussification in finite time) Consider a family of systems on cubic lattices of increasing volume V.

Let the initial states exhibit exponential clustering of correlations, and let the Hamiltonians be quadratic finite range and have delocalizing transport with the corresponding constants $\xi, C_{\mathrm{Clust}}, C_{\mathrm{Trans}}, \alpha_{\mathrm{Trans}}$ independent of V. Then for any local operator A on a fixed finite region and any $0 < \nu < 4\,\alpha_{\mathrm{Trans}} - d_{\mathcal{L}}$, there is a V independent constant C_{Total} such that for any $t \leq \min(t_{\mathrm{Rec}}, V)$

$$|\mathrm{tr}[A(t)\rho] - \mathrm{tr}[A(t)\rho_G]| \leq C_{\mathrm{Total}} t^{-4\alpha_{\mathrm{Trans}}+d_{\mathcal{L}}+\nu}. \quad (5)$$

Consequently, if the recurrence time t_{Rec} increases unboundedly as some function of V, then, given an error $\epsilon > 0$, there exists a relaxation time $t_{\mathrm{Relax}} > 0$ independent of the system size such that for all times $t \in [t_{\mathrm{Relax}}, t_{\mathrm{Rec}}]$ it holds that $|\mathrm{tr}[A(t)\rho] - \mathrm{tr}[A(t)\rho_G]| \leq \epsilon$.

The theorem states that for all times in the interval $[t_{\mathrm{Relax}}, t_{\mathrm{Rec}}]$ the expectation value of any local observable in the time evolved state $\rho(t)$ will agree up to an error ϵ with the expectation value in the Gaussian state $\rho_G(t)$, which has the same second moments as $\rho(t)$. With this, we find that the expectation values of all local observables can be approximated by a decomposition according to Wick's theorem and that it will be impossible to distinguish the true state ρ from the fermionic Gaussian state ρ_G by any local measurement on a fixed finite local region S. Note that since t_{Relax} is independent of the system size, but t_{Rec} increases with its volume, for any arbitrarily small ϵ, there always exists a system size such that $t_{\mathrm{Rec}} > t_{\mathrm{Relax}}$, and the interval where the theorem applies grows as a function of the system size.

We compare our general, rigorous, analytical result with a numerical simulation in Fig. 2 that shows an experimentally detectable signature of the Gaussification of a density-density correlator. The comparison reveals that our bound correctly reproduces the physical behavior in the sense that the true Gaussification dynamics follows a power-law. What is not correctly reproduced is the exponent of that power law, but we understand where the discrepancy between the observed t^{-1} decay and the $t^{-1/3+\nu}$ (for arbitrarily small ν) bound for $\alpha_{\mathrm{Trans}} = 1/3$ originates from: the reason is that the provable decay with $\alpha_{\mathrm{Trans}} = 1/3$ for the considered model roots in the slow decay of the matrix elements of the propagator at the wave front of the Lieb-Robinson cone. The elements in the bulk of the Lieb-Robinson cone can numerically be found to be suppressed as $t^{-1/2}$ leading to an effective $\alpha_{\mathrm{Trans}} = 1/2$ for the vast majority of matrix elements (see Fig. 1). Assuming this effective $\alpha_{\mathrm{Trans}} = 1/2$ in Theorem 1 leads to a suppression with t^{-1}.

The key steps in the proof, are based on three main physical ingredients: finite speed of propagation in lattice systems, homogeneous suppression of matrix elements of the propagator due to delocalizing transport, and exponential clustering of correlations in the initial state. The full proof with all details of the involved combinatorics can be found in the Supplemental Material [17].

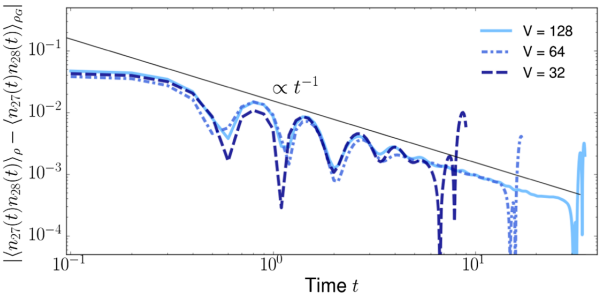

FIG. 2. Numerical study of the evolution of a nearest-neighbor density-density correlator for system sizes $V = 32, 64, 128$ under the quadratic hopping Hamiltonian $H = -\sum_j^V (f_j^\dagger f_{j+1} + f_{j+1}^\dagger f_j)$. The initial states are the ground states of the interacting spinless Fermi-Hubbard model $H_{\mathrm{FH}} = H + U\sum_j^V n_j n_{j+1} + \sum_j \omega_j n_j$ with $U = 2$, and weak on site disorder w_j drawn independently from a Gaussian distribution with variance $1/4$. For consistency, we have initially drawn 128 random numbers w_j and used the first V of them for different system sizes. All calculations were performed with periodic boundary conditions at half filling. The difference between the expectation values in the state ρ and its Gaussified version ρ_G of the density-density correlator between sites 27 and 28 as a function of time is suppressed approximately like t^{-1}, as indicated by the black line. At late times, due to the finite size of the system, recurrences occur, leading to an increase of the difference. Increasing the system size only shifts the recurrence time t_{Rec} but leaves the decay behavior unchanged. The visible oscillations depend on details of the model and initial state. The time evolution was performed by using Eq. (2).

Proof.—We expand the local operator A supported in a fixed finite region S in the basis of fermionic operators. To that end, let $\tilde{S} \coloneqq \{s_r\}$ for $r \in [2|S|] \coloneqq \{1, \ldots, 2|S|\}$ be the set of indices of all elements of the vector c with support in S, then

$$A(t) = \sum_{b_1,\ldots,b_{2|S|}=0}^{1} a_{b_1,\ldots,b_{2|S|}} c_{s_1}(t)^{b_1} \ldots c_{s_{2|S|}}(t)^{b_{2|S|}}. \quad (6)$$

Without loss of generality, we assume $\|A\| = 1$, such that $|a_{b_1,\ldots,b_{2m}}| \leq 1$. Thus,

$$|\mathrm{tr}[A\rho(t)] - \mathrm{tr}[A\rho_G(t)]| \leq 2^{2|S|} \max_{J\subset\tilde{S}} \left| \sum_{(k_j)_{j\in J}\in[2V]^{\times|J|}} \mathrm{tr}\left[\prod_{j\in J} W_{j,k_j}(t) c_{k_j}(\rho - \rho_G)\right]\right|. \quad (7)$$

Here and in the following, all products are meant to be performed in increasing order.

We assumed that the Hamiltonian has finite range interactions; i.e., there exists a fixed length l_0, such that $h_{j,k} = 0$ whenever $d(j,k) > l_0$, where $d(j,k) \coloneqq d(c_j, c_k)$. Such models satisfy Lieb-Robinson bounds [22], which in our setting can be stated as follows:

Lemma.—(Lieb-Robinson bound for quadratic systems [23]) For any quadratic fermionic Hamiltonians H with finite range interactions there exist constants $C_{\mathrm{LR}}, \mu, v > 0$ independent of the system size, such that its propagator W fulfills the bound

$$|W_{j,k}(t)| \leq C_{\mathrm{LR}} e^{\mu[v|t|-d(j,k)]}. \tag{8}$$

The Lieb-Robinson bound tells us that $c_j(t)$ and $c_k(t)$ essentially still have disjoint support as long as t is small enough such that $v|t| \ll d(j,k)$. We can hence restrict the sum in Eq. (7) to those k_j whose $\min_{s\in\tilde{S}} \mathrm{d}(k_j, s)$ is smaller than $(v + 2v_\epsilon)|t|$ for some fixed $v_\epsilon > 0$. The total contribution of the neglected terms can be bounded explicitly and, importantly, is independent of V and exponentially suppressed in $|v_\epsilon t|$.

For each of the remaining summands in Eq. (7), it is now important to keep track of the distribution of the indices k_j inside the cone. For this purpose, we define the Δ partition P_Δ of a subindex set $J \subset \tilde{S}$ and sequence of indices $(k_j)_{j\in J}$ as the unique decomposition of J into subsets (patches) p in the following way: the patches are constructed such that for any two subindices within any given patch p there is a connecting chain of elements from that patch in the sense that the distance between two consecutive c_{k_j} with $j \in p$ along that chain is not greater than Δ and the distance between any two $c_{k_j}, c_{k'_j}$ with j, j' from different patches is larger than Δ. For each patch p in the Δ partition of a given summand in Eq. (7), we define a corresponding operator

$$\hat{P}_p^{(k_j)_{j\in p}} := \prod_{j\in p} W_{j,k_j}(t) c_{k_j}. \tag{9}$$

We can then reorder the factors in Eq. (7) to write the product as a product over these operators. The exponential clustering of correlations (Definition 1) in the initial state allows us to factor the patches if we scale Δ suitably with $|t|$. Concretely, for $\sigma \in \{\rho, \rho_G\}$, the expectation values appearing in Eq. (7), which we denote by $\langle\cdot\rangle_\sigma$, can be approximated as follows:

$$\left\langle \prod_{p\in P_\Delta} \hat{P}_p^{(k_j)_{j\in p}} \right\rangle_\sigma \approx \prod_{p\in P_\Delta} \langle \hat{P}_p^{(k_j)_{j\in p}} \rangle_\sigma. \tag{10}$$

The error thereby introduced is exponentially suppressed with the ratio of patch distance to correlation length Δ/ξ.

It remains to bound the contribution from the factorized patches that are completely inside the Lieb-Robinson cone. Note that the right-hand side of Eq. (10) is nonzero only if all the patches are of even size, as ρ and ρ_G have an even particle number parity. Moreover, as the second moments of ρ and ρ_G are equal, the difference of the right-hand side for $\sigma = \rho$ and $\sigma = \rho_G$ vanishes whenever all patches have size 2. Hence, only partitions that contain at least one patch of size at least 4 contribute. The delocalizing transport of the Hamiltonian implies that the contribution from such larger patches however is dynamically suppressed. Whenever $|p| \geq 4$, it holds that

$$|\langle \hat{P}_p^{(k_j)_{j\in p}} \rangle_\sigma| \leq C_{\mathrm{Trans}}^4 t^{-4\alpha_{\mathrm{Trans}}} \tag{11}$$

as long as t is small enough given V. The influence of possible patches of size 2 in the same decomposition makes it necessary to bound the overall contribution with an involved recursive and combinatorial argument. However, effectively the dynamical suppression in Eq. (11) allows us to derive a bound that increases with the patch size Δ, as the number of possible patch-configurations grows with Δ, but is algebraically suppressed in time t. Choosing $\Delta = \max(1, t^{\nu/4d_{\mathcal{L}}})$ for some $0 < \nu < 4\alpha_{\mathrm{Trans}} - d_{\mathcal{L}}$, we obtain an at least algebraic suppression with t of all terms and thereby of the difference $|\mathrm{tr}(A(t)\rho) - \mathrm{tr}(A(t)\rho_G)|$. □

Physical implications and applications.—The Gaussification result presented above also has profound implications for the study of equilibration of quantum many-body systems. Whenever the second moments equilibrate, which is often observed [5,24–29], our results imply that the full reduced density matrix becomes stationary. The numerical study presented in Fig. 2 shows that the power law appearing in Theorem 1 is not an artifact of our proof strategy but reflects the underlying physics, that can moreover be observed in experiments. The quadratic models considered here constitute a "theoretical laboratory", in which the mechanisms of Gaussification and equilibration can be very precisely and quantitatively characterized, and all specifics of the processes laid out. This does not mean that the physics we address is very specific to quadratic Hamiltonians: we expect the fundamental mechanisms underlying the result—local relaxation due to transport and initial clustering of correlations—to be, the reason for relaxation in a wide classes of interacting models [30] and also classical ones [31]. The intuition, reminiscent of a quantum central limit theorem [32], that incommensurate influences of further and further separated regions lead to mixing and relaxation is then expected to still be valid. It is also important to stress that our main theorem equally applies to mixed initial states, such as thermal states, which are relevant in present day experiments with ultracold fermions [33–36].

Returning to the specifics of quadratic Hamiltonians, the result derived here can be interpreted in yet another way: it is reminiscent of the initial state converging towards a *generalized Gibbs ensemble* (GGE) [10,26,37] in the sense that the initial state becomes close to a Gaussian state, which is the maximum entropy state given the second moments. Different from a real GGE, the observables $\{I_\alpha\}$ held fixed while maximizing entropy can be time dependent, i.e., $\rho_G(t) = \exp(\sum_\alpha \lambda_\alpha I_\alpha(t))/\mathcal{Z}$. Here, $\{\lambda_\alpha\}$ are appropriately chosen Lagrange multipliers, $\mathcal{Z}$ the

partition function, and $\{I_\alpha(t)\}$ the number operators of the eigenmodes of γ. However, in the case of equilibrating second moments, all relevant I_α become time independent such that our theorem constitutes a proof of a convergence to a proper GGE in these cases. The same holds true for integrable spin models that can be mapped to the type of fermionic models considered here, complementing insights on bosonic systems [6,38].

Conclusion and outlook.—In this Letter, we have established an understanding of how systems quenched to noninteracting fermionic Hamiltonians locally converge to Gaussian states. Out of equilibrium dynamics is identified as having the tendency to bring systems locally in maximum entropy states given the second moments. This holds even if the initial state was far from being a Gaussian state, e.g., a ground state of a strongly interacting model. This is achieved based on just two natural assumptions: a form of delocalizing transport in the model and exponential clustering of correlations in the initial state. Otherwise, the initial state can be completely general. It is the hope that the present work will serve as a stepping stone to gain further insights into the relaxation dynamics of more complex quantum many-body systems and the consequences of the suppression of transport in, for example, localizing systems.

We acknowledge fruitful discussions with M. Cramer, M. M. Wolf, and P. Ćwikliński. We would like to thank the EU (RAQUEL, SIQS, AQuS, IP, QUIC), the ERC (TAQ, OSYRIS, QITBOX), the Templeton Foundation, the BMBF (Q.com), the DFG (EI 519/7-1, CRC 183), the Studienstiftung des Deutschen Volkes, MPQ-ICFO, the Spanish Ministry Project FOQUS (FIS2013-46768-P), MINECO (Severo Ochoa Grant No. SEV-2015-0522), Fundació Privada Cellex, the Generalitat de Catalunya (SGR 874 and 875), ICFOnest+ (FP7-PEOPLE-2013-COFUND), the EU's Marie Skłodowska-Curie Individual Fellowships programme under Grant Agreement No. 700140, and the COST Action MP1209 for support.

[1] A. Polkovnikov, K. Sengupta, A. Silva, and M. Vengalattore, Rev. Mod. Phys. **83**, 863 (2011).
[2] J. Eisert, M. Friesdorf, and C. Gogolin, Nat. Phys. **11**, 124 (2015).
[3] C. Gogolin and J. Eisert, Rep. Prog. Phys. **79**, 056001 (2016).
[4] I. Bloch, J. Dalibard, and S. Nascimbene, Nat. Phys. **8**, 267 (2012).
[5] S. Trotzky, Y.-O. Chen, A. Flesch, I. McCulloch, U. Schollwöck, J. Eisert, and I. Bloch, Nat. Phys. **8**, 325 (2012).
[6] M. Cramer, C. M. Dawson, J. Eisert, and T. J. Osborne, Phys. Rev. Lett. **100**, 030602 (2008).
[7] P. Reimann, Phys. Rev. Lett. **101**, 190403 (2008).
[8] N. Linden, S. Popescu, A. J. Short, and A. Winter, Phys. Rev. E **79**, 061103 (2009).
[9] A. J. Short and T. C. Farrelly, New J. Phys. **14**, 013063 (2012).
[10] M. Rigol, V. Dunjko, V. Yurovsky, and M. Olshanii, Phys. Rev. Lett. **98**, 050405 (2007).
[11] P. Reimann and M. Kastner, New J. Phys. **14**, 043020 (2012).
[12] A. S. L. Malabarba, L. P. Garcia-Pintos, N. Linden, T. C. Farrelly, and A. J. Short, Phys. Rev. E **90**, 012121 (2014).
[13] D. Pertot, A. Sheikhan, E. Cocchi, L. A. Miller, J. E. Bohn, M. Koschorreck, M. Köhl, and C. Kollath, Phys. Rev. Lett. **113**, 170403 (2014).
[14] M. B. Hastings and T. Koma, Commun. Math. Phys. **265**, 781 (2006).
[15] B. Nachtergaele and R. Sims, contribution to the XVth International Congress on Mathematical Physics New Trends in Mathematical Physics (2007).
[16] M. Kliesch, C. Gogolin, M. J. Kastoryano, A. Riera, and J. Eisert, Phys. Rev. X **4**, 031019 (2014).
[17] See Supplemental Material at http://link.aps.org/supplemental/10.1103/PhysRevLett.117.190602, for further details of the proof of the main argument and elaborates on applications in the study of spin chains, which includes Refs. [18–21].
[18] A. Kitaev, Ann. Phys. (Amsterdam) **321**, 2 (2006).
[19] E. Lieb, T. Schultz, and D. Mattis, Ann. Phys. (N.Y.) **16**, 407 (1961).
[20] J. H. van Lint and R. M. Wilson, *A Course in Combinatorics* (Cambridge University Press, Cambridge, United Kingdom, 1992).
[21] C. V. Kraus, M. M. Wolf, J. I. Cirac, and G. Giedke, Phys. Rev. A **79**, 012306 (2009).
[22] E. H. Lieb and D. W. Robinson, Commun. Math. Phys. **28**, 251 (1972).
[23] M. B. Hastings, Phys. Rev. Lett. **93**, 126402 (2004).
[24] A. Flesch, M. Cramer, I. P. McCulloch, U. Schollwöck, and J. Eisert, Phys. Rev. A **78**, 033608 (2008).
[25] P. Calabrese and J. Cardy, Phys. Rev. Lett. **96**, 136801 (2006).
[26] P. Calabrese, F. H. Essler, and M. Fagotti, J. Stat. Mech. (2012) P07022.
[27] I. Peschel and V. Eisler, J. Phys. A **42**, 504003 (2009).
[28] M. Fagotti and F. H. L. Essler, Phys. Rev. B **87**, 245107 (2013).
[29] S. Bhattacharyya, A. Das, and S. Dasgupta, Phys. Rev. B **86**, 054410 (2012).
[30] S. R. Manmana, S. Wessel, R. M. Noack, and A. Muramatsu, Phys. Rev. Lett. **98**, 210405 (2007).
[31] T. V. Dudnikova, A. Komech, and H. Spohn, J. Math. Phys. (N.Y.) **44**, 2596 (2003).
[32] R. L. Hudson, J. Appl. Probab. **10**, 502 (1973).
[33] U. Schneider, L. Hackermuller, J. P. Ronzheimer, S. Will, S. Braun, T. Best, I. Bloch, E. Demler, S. Mandt, D. Rasch, and A. Rosch, Nat. Phys. **8**, 213 (2012).
[34] M. F. Parsons, F. Huber, A. Mazurenko, C. S. Chiu, W. Setiawan, K. Wooley-Brown, S. Blatt, and M. Greiner, Phys. Rev. Lett. **114**, 213002 (2015).
[35] N. Strohmaier, Y. Takasu, K. Günter, R. Jördens, M. Köhl, H. Moritz, and T. Esslinger, Phys. Rev. Lett. **99**, 220601 (2007).
[36] E. Haller, J. Hudson, A. Kelly, D. A. Cotta, B. Peaudecerf, G. D. Bruce, and S. Kuhr, Nat. Phys. **11**, 738 (2015).
[37] A. Lazarides, A. Das, and R. Moessner, Phys. Rev. Lett. **112**, 150401 (2014).
[38] M. Cramer and J. Eisert, New J. Phys. **12**, 055020 (2010).

Supplementary material: Equilibration via Gaussification in fermionic lattice systems

M. Gluza,[1] C. Krumnow,[1] M. Friesdorf,[1] C. Gogolin,[2,3] and J. Eisert[1]

[1]*Dahlem Center for Complex Quantum Systems, Freie Universität Berlin, 14195 Berlin, Germany*
[2]*ICFO-Institut de Ciencies Fotoniques, Mediterranean Technology Park, 08860 Castelldefels (Barcelona), Spain*
[3]*Max-Planck-Institut für Quantenoptik, Hans-Kopfermann-Straße 1, 85748 Garching, Germany*

(Dated: September 24, 2016)

I. MAJORANA OPERATORS AND TIME EVOLUTION IN QUADRATIC FERMIONIC SYSTEMS

In this appendix, we formulate the Majorana operator description that allows to conveniently derive the operator governing transport in the system. We introduce the Majorana operators as

$$m_{2j-1} \coloneqq (f_j^\dagger + f_j)/\sqrt{2}, \tag{1}$$

$$m_{2j} \coloneqq \mathrm{i}\,(f_j^\dagger - f_j)/\sqrt{2}, \tag{2}$$

which are collected in a vector $m = (m_1, \ldots, m_{2V})$ [1]. The vector c of creation and annihilation operators used in the main text and m are related by the unitary transformation

$$\Omega \coloneqq \frac{1}{\sqrt{2}} \bigoplus_{j=1}^{V} \begin{pmatrix} 1 & 1 \\ -\mathrm{i} & \mathrm{i} \end{pmatrix}, \tag{3}$$

as $m = \Omega\, c$. The Majorana operators are Hermitian and satisfy the anti-commutation relations $\{m_j, m_k\} = \delta_{j,k}$ for $j, k \in [2V] \coloneqq \{1, \ldots, 2V\}$. The algebra generated by those operators constitutes a Clifford algebra. Linear transformations of the form

$$m'_j = \sum_{j,k=1}^{2V} O_{j,k}\, m_k, \quad O \in SO(2V) \tag{4}$$

transform a vector of legitimate Majorana operators to a new such vector.

The most general form of a Hamiltonian considered in this work can be written in terms of the Majorana operators as follows

$$H = \mathrm{i} \sum_{j,k=1}^{2V} m_j\, K_{j,k}\, m_k\ , \tag{5}$$

where $K = -K^T$ is real and anti-symmetric. It is straightforward to relate such Hamiltonians to the ones expressed in the form of the main text. The kernel K can be obtained form h via $K = -\mathrm{i}\,\Omega\, h\, \Omega^\dagger$.

Time evolution can be captured conveniently in the Majorana operator formulation. Using the Baker-Campbell-Hausdorff formula, that K is anti-symmetric, and the algebraic structure of the Majorana fermions, one arrives at the following expression for their time evolution in the Heisenberg picture

$$m_j(t) \coloneqq \mathrm{e}^{\mathrm{i}Ht} m_j \mathrm{e}^{-\mathrm{i}Ht} = \sum_{k=1}^{2V} (\mathrm{e}^{2tK})_{j,k}\, m_k = \sum_{k=1}^{2V} L_{j,k}(t)\, m_k, \tag{6}$$

where $L(t) \coloneqq \mathrm{e}^{2tK}$. Now notice that as the propagator defined in the main text is related to $L(t)$ via

$$W(t) = \Omega^\dagger\, L(t)\, \Omega \tag{7}$$

and hence

$$c_j(t) = \sum_{k=1}^{2V} W_{j,k}(t)\, c_k \tag{8}$$

as claimed in the main text.

Further, we introduce some general notation which we will use in the following. For any given operator A that is supported on a region S we had defined the set $\tilde{S} = \{s_1, \cdots, s_{2|S|}\}$ with $s_1 < s_2 < \ldots < s_{2|S|}$ the set of the indices of fermionic basis operators in S. We can expand A as

$$A = \sum_{b_1,\ldots,b_{2|S|}=0}^{1} a(\{s_r : b_r = 1\})\, c_{s_1}^{b_1} \ldots c_{s_{2|S|}}^{b_{2|S|}} \,, \tag{9}$$

with $a(\{s_r : b_r = 1\}) = a_{b_1,\ldots,b_{2|S|}}$. The sum in Eq. (9) goes over all possible configurations of fermionic basis operators on the region S. We can hence group the summands according to the subset J of indices from $\tilde{S}$ for which a given term actually contains a fermionic basis operator and write it as a sum

$$A = \sum_{J \subset \tilde{S}} a(J)\, A_J \,, \tag{10}$$

with

$$A_J \coloneqq \prod_{j \in J} c_j \,. \tag{11}$$

Here, and whenever such expressions appear in the following, we take the product over $j \in J$ in the ordered dictated by the ordering of the lattice sites. The time evolution of A is then given by $A(t) = \sum_{J \subset \tilde{S}} a(J)\, A_J(t)$ with

$$A_J(t) = \sum_{(k_j)_{j \in J} \in [2V]^{\times |J|}} \left(\prod_{j \in J} W_{j,k_j}(t)\, c_{k_j} \right) . \tag{12}$$

II. TRANSPORT

In this appendix we show that two prototypical example systems exhibit delocalizing transport as defined in Definition 2 in the main text: the fermionisation of the Ising model with appropriate initial states and the fermionic nearest neighbor hopping model. Our proofs closely follow along the lines of the investigation of the transport properties of the propagator presented in Ref. [2].

A. Spreading in the Ising model

We start by considering the 1D Ising model and show that it exhibits delocalizing transport at criticality. Its Hamiltonian for V sites is

$$H_{\mathrm{IS}} = -\sum_{j=1}^{V} X_j X_{j+1} - g \sum_{j=1}^{V} Z_j \,, \tag{13}$$

where X_j, Z_j are the Pauli matrices supported on site j and g is a real parameter. We adopt periodic boundary conditions. Invoking the Jordan-Wigner transformation [3], this spin system can be mapped to fermions, using the substitutions

$$Z_j \mapsto f_j f_j^\dagger - f_j^\dagger f_j = 1 - 2n_j \,, \tag{14}$$

$$S_j = \frac{1}{2}(X_j - \mathrm{i}Y_j) \mapsto \prod_{l<j} (1 - 2n_l) f_j \,, \tag{15}$$

$$S_j^\dagger = \frac{1}{2}(X_j + \mathrm{i}Y_j) \mapsto \prod_{l<j} (1 - 2n_l) f_j^\dagger \,, \tag{16}$$

where S_j is the spin annihilation operator associated with site j and $n_j = f_j^\dagger f_j$ the usual fermionic number operator. After this transformation, the Ising Hamiltonian takes the form

$$\begin{aligned} H_{\rm IS} &= -\sum_{j=1}^{V-1}(f_j^\dagger + f_j)(1-2n_j)(f_{j+1}^\dagger + f_{j+1}) - \prod_{j=1}^{V-1}(1-2n_j)(f_V^\dagger + f_V)(f_1^\dagger + f_1) - g\sum_{j=1}^{V}(1-2n_j) \\ &= -\sum_{j=1}^{V-1}(f_j^\dagger - f_j)(f_{j+1}^\dagger + f_{j+1}) + \prod_{j=1}^{V}(1-2n_j)(f_V^\dagger - f_V)(f_1^\dagger + f_1) - g\sum_{j=1}^{V}(1-2n_j). \end{aligned} \tag{17}$$

Using the Majorana operators introduced in Appendix I, we can rewrite the Hamiltonian as

$$H_{\rm IS} = \sum_{j=1}^{V-1} \mathrm{i}(m_{2j}m_{2j+1} - m_{2j+1}m_{2j}) - \mathrm{i}\prod_{j=1}^{V}(1-2n_j)(m_{2V}m_1 - m_1 m_{2V}) - \mathrm{i}g\sum_{j=1}^{V}(m_{2j}m_{2j-1} - m_{2j-1}m_{2j}). \tag{18}$$

As Theorem 1 would not be applicable otherwise, we restrict the discussion here to initial spin-states ρ which are mapped by the Jordan Wigner transformation to proper fermionic states respecting the parity super-selection rule. In that case, the parity operator $\prod_{j=1}^{V}(1-2n_j)$ will take a fixed value $\sigma = \pm 1$, depending on the parity of ρ. That is, depending on the parity sector of the state labeled by σ, $H_{\rm IS}$ is of the form

$$H^\sigma = \mathrm{i}\sum_{j,k=1}^{2V} m_j K^\sigma_{j,k} m_k \tag{19}$$

with

$$K^\sigma = \begin{pmatrix} 0 & g & & & & \sigma \\ -g & 0 & 1 & & & \\ & -1 & 0 & g & & \\ & & -g & 0 & 1 & \\ & & & -1 & 0 & \\ -\sigma & & & & & \ddots \end{pmatrix}. \tag{20}$$

In the following we consider the special case $g = 1$, corresponding to the critical Ising model.

Lemma 1 (Delocalizing transport in the critical Ising model)**.** *For the one-dimensional fermionic model given in Eqs.* (19) *and* (20) *corresponding to the critical Ising model, there is a constant $C_{\rm Trans} > 0$ such that for all $t \in (0, t_{\rm Rec}]$, with $t_{\rm Rec} = V^{6/7}$ the recurrence time, it holds that*

$$|W^\sigma_{j,k}(t)| \leq C_{\rm Trans} t^{-1/3} \,\forall j,k. \tag{21}$$

Proof. We diagonalize with K^σ using a modified discrete Fourier transform

$$U^\sigma_{k,x} = \frac{1}{\sqrt{2V}} \mathrm{e}^{\mathrm{i}\pi k x/2V} \mathrm{e}^{\mathrm{i}\pi(1+\sigma)(x+k)/4V} \tag{22}$$

in order to obtain its spectrum

$$\lambda^\sigma_k = 2\sin(\pi[k + (1+\sigma)/4]/V). \tag{23}$$

We then find for the propagator (see Eq. (6))

$$L^\sigma_{j,l}(t) = (e^{2tK^\sigma})_{j,l} = \frac{1}{2V}\sum_{k=1}^{2V} \mathrm{e}^{\mathrm{i}\pi[k+(1+\sigma)/4](l-j)/V} f(\pi[k+(1+\sigma)/4]/V), \tag{24}$$

with $f(\phi) = \mathrm{e}^{2\mathrm{i}t\sin(\phi)}$. The Fourier transform of $f(\phi)$ is given by $f(\phi) = \sum_{n=-\infty}^{\infty} f_n \mathrm{e}^{-\mathrm{i}n\phi}$ with the modes $f_n = J_n(2t)$ where J_n denotes the Bessel function of first kind. By partial integration we can upper bound the absolute value of the Fourier modes of f by

$$|f_n| = \frac{1}{2\pi n^2}\left|\int_0^{2\pi} \mathrm{e}^{\mathrm{i}n\phi}\frac{d^2}{d\phi^2}\mathrm{e}^{2\mathrm{i}t\sin(\phi)}d\phi\right| \leq 4\frac{|t|+|t|^2}{n^2}. \tag{25}$$

Inserting the Fourier decomposition of f into Eq. (24) yields

$$L^{\sigma}_{j,l}(t) = \frac{1}{2V}\sum_{n=-\infty}^{\infty}\sum_{k=1}^{2V} \mathrm{e}^{\mathrm{i}\pi[k+(1+\sigma)/4](l-j-n)/V} f_n = \sum_{p=-\infty}^{\infty} (-\sigma)^p f_{l-j+2pV}. \tag{26}$$

By the periodicity of the model, i.e. $L_{j,l}(t) = -\sigma L_{j-2V,l}(t) = -\sigma L_{j,l-2V}(t)$, we are save to assume w.l.o.g. $|j-l| \leq V$. Using the upper bound in Eq. (25) and upper bounding the resulting converging series for $|j-l| \leq V$ yields

$$|L^{\sigma}_{j,l}(t) - J_{l-j}(2t)| \leq \frac{8(|t|+|t|^2)}{4V^2}\sum_{p=1}^{\infty}\frac{1}{[(l-j)/2V+p]^2} \leq \pi^2\frac{|t|+|t|^2}{V^2}. \tag{27}$$

With the general upper bound on the Bessel function of first kind $J_n(x) \leq x^{-1/3}$ we conclude that for $L > 1$

$$|L^{\sigma}_{j,k}(t)| \leq 11\, t^{-1/3} \quad \forall j,k \tag{28}$$

for $t \in (0, t_{\mathrm{Rec}}]$ with $t_{\mathrm{Rec}} = V^{6/7}$. Due to the block structure of Ω in Eq.(7) it then follows directly that

$$|W^{\sigma}_{j,k}(t)| \leq 22\, t^{-1/3} \quad \forall j,k. \tag{29}$$

□

B. Transport in fermionic nearest neighbor hopping models in square lattices

We now turn to fermionic hopping models, i.e., systems whose Hamiltonian is a linear combination of terms of the form $f_j^\dagger f_k$. Instead of the general quadratic form in the form of the main text, the Hamiltonian can then be written as

$$H = \sum_{j,k=1}^{V} f_j^\dagger M_{j,k} f_k, \tag{30}$$

with M a real and symmetric matrix, i.e., $M = M^T$. The time evolution of fermionic annihilation operators in the Heisenberg picture is then given by

$$f_j(t) = \mathrm{e}^{\mathrm{i}Ht}\, f_j\, \mathrm{e}^{-\mathrm{i}Ht} = \sum_{k=1}^{V} N_{j,k}(t)\, f_k, \tag{31}$$

where $N(t) \coloneqq \mathrm{e}^{-\mathrm{i}Mt}$. To connect this to the notation used in the main text, note that with P the permutation matrix that acts as

$$(f_1, f_1^\dagger, \ldots, f_V, f_V^\dagger) = P(f_1, \ldots, f_V, f_1^\dagger, \ldots, f_V^\dagger). \tag{32}$$

The Hamiltonian from Eq. (30) can be written in the form of the main text by adding an appropriate constant and setting

$$h = \frac{1}{2} P\,(M \oplus -M)\, P^\dagger. \tag{33}$$

$N(t)$ is then related to $W(t)$, via

$$W(t) = P(N(t) \oplus N(t)^\dagger)P^\dagger. \tag{34}$$

We now consider the particularly important case of nearest neighbor hopping on a square lattice of spacial dimension $d_{\mathcal{L}}$ with V sites, periodic boundary conditions and hopping strength one. For convenience, we restrict the discussion to $V^{1/d_{\mathcal{L}}}$ even. Writing the Hamiltonian as in (30), the coupling matrix M of this model can be decomposed into a sum over the $d_{\mathcal{L}}$ different spatial directions as follows

$$M = \sum_{k=0}^{d_{\mathcal{L}}-1} \mathbb{1}^{\otimes k} \otimes M^{(1)} \otimes \mathbb{1}^{\otimes(d_{\mathcal{L}}-k-1)}, \tag{35}$$

with

$$M^{(1)} \coloneqq -\begin{pmatrix} 0 & 1 & & & 1 \\ 1 & 0 & 1 & & \\ & 1 & 0 & 1 & \\ & & 1 & 0 & \\ 1 & & & \ddots & \end{pmatrix} \in \mathbb{R}^{V^{1/d_{\mathcal{L}}} \times V^{1/d_{\mathcal{L}}}}. \tag{36}$$

For such models we can bound the spreading as follows:

Lemma 2 (Delocalizing transport in fermionic hopping models)**.** *For the fermionic nearest neighbor hopping model on a square lattice of spacial dimension $d_{\mathcal{L}}$ and V sites with $V^{1/d_{\mathcal{L}}}$ even and periodic boundary conditions there is a constant $C_{\mathrm{Trans}} > 0$, independent of the volume V, such that for all $t \in (0, t_{\mathrm{Rec}}]$, with $t_{\mathrm{Rec}} = V^{6/7d_{\mathcal{L}}}$ the recurrence time, it holds that*

$$\forall j,k \qquad |W_{j,k}(t)| \leq C_{\mathrm{Trans}}\, t^{-d_{\mathcal{L}}/3}. \tag{37}$$

Proof. From the structure of the Hamiltonian it follows that $N(t) = (\mathrm{e}^{-\mathrm{i}M^{(1)}t})^{\otimes d_{\mathcal{L}}}$. For $V^{1/d_{\mathcal{L}}}$ even we obtain that

$$-\mathrm{i}K^{\sigma}(t) = Q^{\dagger} M^{(1)}(t) Q \tag{38}$$

with $Q = \mathrm{diag}(1, i, -1, -i, 1, \ldots)$ where $\sigma = -1$ if $V^{1/d_{\mathcal{L}}}/2$ is even and $\sigma = 1$ otherwise. From the proof of Lemma 1 we then obtain for all $0 < t < t_{\mathrm{Rec}} = 2V^{6/7d_{\mathcal{L}}}$

$$\forall j,k \qquad |N_{j,k}(t)| \leq 2^{d_{\mathcal{L}}/3} 11^{d_{\mathcal{L}}} t^{-d_{\mathcal{L}}/3}. \tag{39}$$

This bound is inherited by W as N and W are related by a permutation of rows and columns. □

III. FERMIONIC GAUSSIAN STATES AND CLUSTERING OF CORRELATIONS

In this appendix, we provide some background on fermionic Gaussian states. We first demonstrate that they are the maximum entropy states given their correlation matrix. Moreover, we show that whenever a state has exponential clustering of correlations, then its Gaussified version also shows an exponential correlation decay.

A. Gaussian states as maximum entropy states

In this subsection, we show that fermionic Gaussian states are the maximum entropy states given the second moments of fermionic operators. This in particular highlights that the state to which we show apparent local convergence has the characteristic feature of generalized Gibbs ensembles (GGE) that it is the maximum entropy state given the expectation value of a set of observables, being the second moments here.

Lemma 3 (Gaussian states as maximum entropy states)**.** *For a given correlation matrix $\gamma \in \mathbb{C}^{2V \times 2V}$,*

$$\rho_G = \arg\max_{\rho} \left\{ S(\rho) : \gamma(\rho) = \gamma \right\}, \tag{40}$$

where the maximization is performed over all quantum states ρ and $\gamma(\rho)$ denotes the correlation matrix of a state ρ.

Proof. This statement follows immediately from the positivity of the quantum relative entropy. For an arbitrary state ρ and the Gaussian state ρ_G with the same correlation matrix, we have

$$0 \leq S(\rho \| \rho_G) = -S(\rho) - \mathrm{tr}(\rho \log(\rho_G)). \tag{41}$$

Since ρ_G is a Gaussian state, it can be written as $\rho_G = e^H$ for a suitable Hermitian operator H that is quadratic in the fermionic basis operators, which means that

$$\mathrm{tr}(\rho \log(\rho_G)) = \mathrm{tr}(\rho_G \log(\rho_G)) = -S(\rho_G), \tag{42}$$

from which the assertion follows. □

B. Clustering of correlations of Gaussified states

In this subsection we show that, given a state ρ that exhibits exponential clustering of correlation as defined in Definition 1, its Gaussified version ρ_G inherits the exponential clustering of correlations with a changed scaling of the pre-factor with the support of the considered operators. We prove this statement by means of Wick's theorem, which connects higher to second moments for general Gaussian states. Precisely, Wick's theorem can be stated as follows.

Lemma 4 (Wick's theorem [4])**.** *A Gaussian state ρ_G fulfills*

$$\mathrm{tr}[\prod_{k=1}^{n} c_{i_k}\rho_G] = \mathrm{Pf}(\gamma^c[i_1,\ldots,i_n])\,, \tag{43}$$

where

$$\gamma^c[i_1,\ldots,i_n]_{a,b} = \begin{cases} \mathrm{tr}(c_{i_a}c_{i_b}\rho_G) & \text{for } a<b,\\ -\mathrm{tr}(c_{i_b}c_{i_a}\rho_G) & \text{for } b<a,\\ 0 & \text{else.}\end{cases} \tag{44}$$

Given a state with exponential clustering of correlations also its Gaussified version will show clustering of correlations in following sense:

Lemma 5 (Weak clustering of correlations for Gaussified states)**.** *Let ρ be a state that exhibits exponential clustering of correlations according to Definition 1 with constants $C_{\mathrm{Clust}}, \xi > 0$, then for all operators A, B with $\|A\| = \|B\| = 1$ its Gaussified version ρ_G satisfies*

$$|\,\mathrm{tr}(\rho_G\,A\,B) - \mathrm{tr}(A\,\rho_G)\;\mathrm{tr}(B\,\rho_G)| \leq C_{\mathrm{Clust}}\,4^{|\,\mathrm{supp}(A)|+|\,\mathrm{supp}(B)|}(|\,\mathrm{supp}(A)|+|\,\mathrm{supp}(B)|)^{|\,\mathrm{supp}(A)|+|\,\mathrm{supp}(B)|}\mathrm{e}^{-\,\mathrm{d}(A,B)/\xi}. \tag{45}$$

Proof. Note that we can assume without loss generality $C_{\mathrm{Clust}}\mathrm{e}^{-\,\mathrm{d}(A,B)/\xi} \leq 1$ as otherwise the trivial bound $|\,\mathrm{tr}(\rho_G\,A\,B) - \mathrm{tr}(A\,\rho_G)\;\mathrm{tr}(B\,\rho_G)| \leq 2$ concludes the proof.

We decompose a general operator supported on $\mathrm{supp}(A)$ and $\mathrm{supp}(B)$ as in Eq. (10) into the fermionic operator-basis

$$A = \sum_{K\subset\mathrm{supp}(A)} a(K)\prod_{k\in K} c_k \tag{46}$$

and

$$B = \sum_{J\subset\mathrm{supp}(B)} b(J)\prod_{j\in J} c_j \tag{47}$$

correspondingly. From $\|A\| = 1 = \|B\|$ it follows that $|a(K)| \leq 1$ and $|b(J)| \leq 1$ for all J and K. Using the triangle inequality, we can therefore write

$$|\,\mathrm{tr}(\rho_G\,A\,B) - \mathrm{tr}(A\,\rho_G)\;\mathrm{tr}(B\,\rho_G)| \leq 2^{|\,\mathrm{supp}(A)\cup\mathrm{supp}(B)|}\max_{\substack{K\subset\mathrm{supp}(A),\\ J\subset\mathrm{supp}(B)}}\left|\mathrm{tr}(\rho_G\prod_{k\in K}c_k\prod_{j\in J}c_j) - \mathrm{tr}(\prod_{k\in K}c_k\,\rho_G)\;\mathrm{tr}(\prod_{j\in J}c_j\,\rho_G)\right|. \tag{48}$$

Let J' and K' be the sets for which the maximum is attained. Wick's theorem then allows us to write the expectation values in terms of second moments

$$|\,\mathrm{tr}(\rho_G\,A\,B) - \mathrm{tr}(A\,\rho_G)\;\mathrm{tr}(B\,\rho_G)| \leq 2^{|\,\mathrm{supp}(A)\cup\mathrm{supp}(B)|}|\,\mathrm{Pf}\,\gamma^c[(k)_{k\in K'},(j)_{j\in J'}] - \mathrm{Pf}\,\gamma^c[(k)_{k\in K'}]\;\mathrm{Pf}\,\gamma^c[(j)_{j\in J'}]|. \tag{49}$$

From the definition of γ^c in Eq. (44) it follows that $\gamma^c[(k)_{k\in K'},(j)_{j\in J'}]$ decomposes into blocks as follows

$$\gamma^c[(k)_{k\in K'},(j)_{j\in J'}] = \gamma^c[(k)_{k\in K'}]\oplus\gamma^c[(j)_{j\in J'}] + \begin{pmatrix} 0 & E\\ -E^T & 0\end{pmatrix}\,. \tag{50}$$

As E contains only second moments of which one operator is supported on $\mathrm{supp}(A)$ and the other on $\mathrm{supp}(B)$ we obtain from the exponential clustering of correlations of ρ that $|E_{a,b}| \leq C_{\mathrm{Clust}}\mathrm{e}^{-\,\mathrm{d}(A,B)/\xi}$. Expanding therefore the Pfaffians in Eq. (49) yields that each term either appears in both terms of the difference and cancels out or that it contains at least one element of E as a factor. Counting the number of terms in the expansion of the Pfaffians gives that the sum contains

$$(2[|\,\mathrm{supp}(A)|+|\,\mathrm{supp}(B)|]-1)!! \leq 2^{|\,\mathrm{supp}(A)|+|\,\mathrm{supp}(B)|}(|\,\mathrm{supp}(A)|+|\,\mathrm{supp}(B)|)^{|\,\mathrm{supp}(A)|+|\,\mathrm{supp}(B)|} \tag{51}$$

many terms which yields the final bound stated in the Lemma.

□

IV. DETAILS OF THE PROOF OF THEOREM 1

In this appendix we provide all the details of the proof of our main result Theorem 1. We proceed as follows: In Section IV A we bound the error introduced by truncating to the Lieb-Robinson cone. In Section IV B we introduce the necessary concepts and notation to then in Section IV C bound the error made by factorizing expectation values into a products of local contributions from different patches. In Section IV D we use the properties of delocalizing transport to show a bound on the remaining non-Gaussian contributions to the expectation value. Finally, in Section IV E, we assemble all the parts of the proof and state a more technical version of the main theorem.

A. Truncating to the Lieb-Robinson cone

We decompose a general operator supported in the region S according to Eq. (10). Without loss of generality we can assume that A is normalized, i.e., $\|A\| \leq 1$, which implies $|a(J)| \leq 1$ and so in the following we concentrate on the individual terms of the form given in Eq. (12). We will demonstrate that sums over time evolved fermionic operators in Eq. (12) can be truncated to an enlarged Lieb-Robinson cone up to an error that decays exponentially with time. Rather than summing over all possible index positions $k_j \in [2V]$ it is then sufficient to only sum over positions inside this enlarged Lieb-Robinson cone. We will require the following auxiliary lemma:

Lemma 6 (Norm bound on restricted sums of fermionic operators)**.** *Let $I \subset [2V]$ and $W \in U(2V)$ be unitary. Then for all $j \in [2V]$*

$$\left\| \sum_{k_j \in I} W_{j,k_j} c_{k_j} \right\| \leq 1 \, . \tag{52}$$

Proof. The proof can be carried out with straightforward norm estimates and using the normalisation of the two-point correlator γ. We begin with

$$\left\| \sum_{k_j \in I} W_{j,k_j} c_{k_j} \right\| = \sup_{\substack{|\psi\rangle \\ \||\psi\rangle\|=1}} \langle\psi| \sum_{r_j \in I} \overline{W}_{j,r_j} c^\dagger_{r_j} \sum_{k_j \in I} W_{j,k_j} c_{k_j} |\psi\rangle = \sup_{\substack{|\psi\rangle \\ \||\psi\rangle\|=1}} \sum_{r_j \in I} \sum_{k_j \in I} \overline{W}_{j,r_j} \langle\psi| c^\dagger_{r_j} c_{k_j} |\psi\rangle W_{j,k_j} \, . \tag{53}$$

We now rewrite this as a matrix multiplication on the index space

$$\left\| \sum_{k_j \in I} W_{j,k_j} c_{k_j} \right\| \leq \sup_{\gamma} \langle j| \overline{W} P_I \gamma P_I W^T |j\rangle \ , \tag{54}$$

where $|j\rangle$ is a vector on the index space, P_I denotes the projector onto the interval I and γ denotes fermionic correlation matrices. A straightforward norm estimate and using that $\|\gamma\| \leq 1$, as every fermionic mode can be occupied by at most one particle, gives

$$\left\| \sum_{k_j \in I} W_{j,k_j} c_{k_j} \right\| \leq \|\overline{W}\| \, \|P_I\| \, \|\gamma\| \, \|P_I\| \, \|W^T\| \leq 1 \, , \tag{55}$$

which concludes the proof. □

As introduced in the main text, we then denote by $\mathrm{d}(A,B)$ the shortest distance between the supports $\mathrm{supp}(A), \mathrm{supp}(B)$ of two operators A and B. For $k_1, k_2 \in [2V]$ we then define the distance $\mathrm{d}(k_1,k_2) := \mathrm{d}(c_{k_1}, c_{k_2})$. Note that d defines only a pseudometric on $[2V]$ as for $k_1, k_2 \in [2V]$ with $c_{k_1} = f_s$ and $c_{k_2} = f_s^\dagger$ we have $k_1 \neq k_2$ but $\mathrm{d}(k_1,k_2) = 0$.

Given a pseudometric, we define a ball around a set as follows.

Definition 1 (Ball around set)**.** *Given $l > 0$, a set M with pseudometric d and $J \subset M$, we define the l-ball $\mathcal{B}_l(J) \subset M$ around J by*

$$\mathcal{B}_l(J) = \{s \in M : \min_{j \in J} \mathrm{d}(j,s) \leq l\}. \tag{56}$$

With this, we define an enlarged Lieb-Robinson cone around a set of indices J with radius $(v + 2v_\epsilon)|t|$ for some $v_\epsilon > 0$ and bound the error made by restricting sums of the form given in Eq. (12) to this widened Lieb-Robinson cone:

Lemma 7 (Error made in restricting to widened Lieb-Robinson cone)**.** *Given a $d_{\mathcal{L}}$-dimensional cubic lattice system with a quadratic Hamiltonian H that satisfies a Lieb-Robinson bound of the form given in Lemma 2 of the main text with parameters $C_{\mathrm{LR}}, \mu, v > 0$. Let $v_\epsilon > 0$ and define for any set $J \subset [2V]$ the widened cone $\mathcal{C}(t) \coloneqq \mathcal{B}_{(v+2v_\epsilon)|t|}(J)$, then there exists a constant $\tilde{C}_{\mathrm{LR}}(d_{\mathcal{L}})$, such that*

$$\left\| \sum_{(k_j)_{j\in J} \notin \mathcal{C}(t)^{\times |J|}} \prod_{j\in J} W_{j,k_j}(t)\, c_{k_j} \right\| \leq \tilde{C}_{\mathrm{LR}}(d_{\mathcal{L}}) |J|^2 \mathrm{e}^{-\mu v_\epsilon |t|} \,. \tag{57}$$

Proof. We begin by splitting the sum according to whether the first index is inside the cone or not. All other indices are free if k_{j_1} is outside the cone, while at least one other index is outside the cone if k_{j_1} lies in it. Using Lemma 6, we obtain

$$\begin{aligned}
\left\| \sum_{(k_j)_{j\in J} \notin \mathcal{C}(t)^{\times |J|}} \prod_{j\in J} W_{j,k_j}(t)\, c_{k_j} \right\| &\leq \left\| \sum_{k_{j_1} \notin \mathcal{C}(t)} W_{j_1,k_{j_1}}(t)\, c_{k_{j_1}} \right\| \left\| \prod_{j\in J\setminus\{j_1\}} c_j(t) \right\| \\
&\quad + \left\| \sum_{k_{j_1} \in \mathcal{C}(t)} W_{j_1,k_{j_1}}(t)\, c_{k_{j_1}} \right\| \left\| \sum_{(k_j)_{j\in J\setminus\{j_1\}} \notin \mathcal{C}(t)^{\times |J|-1}} \prod_{j\in J\setminus\{j_1\}} W_{j,k_j}(t)\, c_{k_j} \right\| \\
&\leq \left\| \sum_{k_{j_1} \notin \mathcal{C}(t)} W_{j_1,k_{j_1}}(t)\, c_{k_{j_1}} \right\| + \left\| \sum_{(k_j)_{j\in J\setminus\{j_1\}} \notin \mathcal{C}(t)^{\times |J|-1}} \prod_{j\in J\setminus\{j_1\}} W_{j,k_j}(t)\, c_{k_j} \right\| .
\end{aligned} \tag{58}$$

The first term in the above equation now, due to Lemma 2 of the main text , satisfies

$$\begin{aligned}
\left\| \sum_{k_{j_1} \notin \mathcal{C}(t)} W_{j_1,k_{j_1}}(t)\, c_{k_{j_1}} \right\| &\leq C_{\mathrm{LR}} \sum_{l=(v+2v_\epsilon)\,|t|}^{V} |\mathcal{B}_{l+1}(J)\backslash\mathcal{B}_l(J)|\, \mathrm{e}^{\mu\,(v\,|t|-l)} \\
&\leq 2^{d_{\mathcal{L}}+1}\, d_{\mathcal{L}}\, |J|\, C_{\mathrm{LR}}\, \mathrm{e}^{\mu\, v\,|t|} \sum_{l=(v+2v_\epsilon)\,|t|}^{\infty} l^{d_{\mathcal{L}}-1}\, \mathrm{e}^{-\mu\, l} \,,
\end{aligned} \tag{59}$$

where we have used that the number $|\mathcal{B}_{l+1}(J)\backslash\mathcal{B}_l(J)|$ of points in the surface of a cone with radius l around J in a cubic lattice is bounded by $4\, d_{\mathcal{L}}\, |J|\, (2l)^{d_{\mathcal{L}}-1}$. Shifting the limits of the sum then yields

$$\left\| \sum_{k_{j_1} \notin \mathcal{C}(t)} W_{j_1,k_{j_1}}(t)\, c_{k_{j_1}} \right\| \leq \mathrm{e}^{-\mu\, v_\epsilon\, |t|}\, |J|\, 2^{d_{\mathcal{L}}+1}\, d_{\mathcal{L}}\, C_{\mathrm{LR}} \sum_{l=0}^{\infty} (l + (v+2v_\epsilon)|t|)^{d_{\mathcal{L}}-1}\, \mathrm{e}^{-\mu\,(l+v_\epsilon|t|)} \,. \tag{60}$$

We now define the time independent constant

$$\tilde{C}_{\mathrm{LR}}(d_{\mathcal{L}}) \coloneqq \sup_{t\in\mathbb{R}^+} 2^{d_{\mathcal{L}}+1}\, d_{\mathcal{L}}\, C_{\mathrm{LR}} \sum_{l=0}^{\infty} (l + (v+2v_\epsilon)|t|)^{d_{\mathcal{L}}-1}\, \mathrm{e}^{-\mu\,(l+v_\epsilon|t|)} \tag{61}$$

which can be written in terms so of the Hurwitz-Lerch-Phi function Φ (also known as Lerch transcendent)

$$\tilde{C}_{\mathrm{LR}}(d_{\mathcal{L}}) \coloneqq \sup_{t\in\mathbb{R}^+} 2^{d_{\mathcal{L}}+1}\, d_{\mathcal{L}}\, C_{\mathrm{LR}}\, \Phi(\mathrm{e}^{-\mu}, 1-d_{\mathcal{L}}, (v+2v_\epsilon)|t|)\mathrm{e}^{-\mu v_\epsilon|t|} \,. \tag{62}$$

Inserting the estimate into Eq. (58) and iteratively using the resulting inequality $|J|$-times gives the result as stated.

As argued above, the constant is directly related to the Hurwitz-Lerch-Phi function and can easily be explicitly evaluated for physical dimensions $d_{\mathcal{L}} = 1, 2, 3$. In one dimension, the constant takes the form

$$\tilde{C}_{\mathrm{LR}}(1) = 4\, C_{\mathrm{LR}}\, \frac{1}{1-\mathrm{e}^{-\mu}} \,. \tag{63}$$

□

B. Partitions: Tracking indices on the lattice

Using the result of Lemma 7 we can restrict the time evolution in Eq. (12) to the Lieb-Robinson cone at the cost of an exponentially suppressed error term. In this section we therefore look at

$$A_J^{LR}(t) \coloneqq \sum_{(k_j)_{j\in J} \in \mathcal{C}(t)^{\times |J|}} \left(\prod_{j\in J} W_{j,k_j}(t)\, c_{k_j} \right) , \tag{64}$$

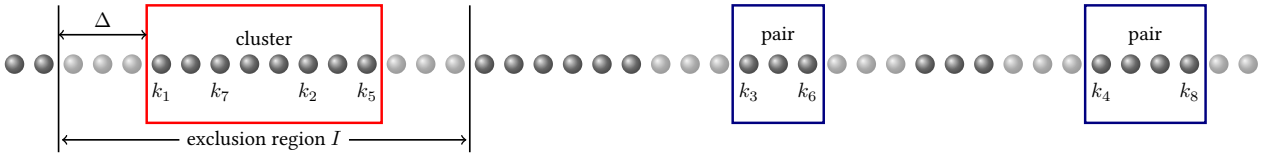

Figure 1. Illustration of a Δ-partition of a given index configuration with $\Delta = 3$ and $J = \{1, \dots, 8\}$. To the above configuration of the indices $k_1, \dots k_8$ we associate the Δ-partition $\{\{1, 2, 5, 7\}, \{3, 6\}, \{4, 8\}\}$ such that a patch of size four (a cluster) and two patches of size two (pairs) are formed. Around each patch exists an buffer region (shaded nodes) which separates different patches. For a given Δ-partition P we obtain all possible index configurations in $\mathcal{K}_P^M$ by placing the patches iteratively. A placed patch will hereby create an exclusion region consisting of the patch itself and the buffer region around it in which no further patch can be placed.

the restriction of a term of the form Eq. (12) to the widened Lieb-Robinson cone $\mathcal{C}(t) = \mathcal{B}_{(v+2v_\epsilon)|t|}(J)$. By grouping summands according to how close the respective indices k_j are on the lattice we will rewrite $A_J^{LR}(t)$ as a sum over partitions of the sub-index set J. This will later allow us to factorize certain expectation values using the exponential decay of correlations in the initial state.

We start by introducing some notation. Given a finite non-empty set J, a partition P of J is a set of non-empty subsets (patches) of J, whose union is J, i.e., $\overline{P} \coloneqq \bigcup_{p\in P} p = J$. We denote by $\pi_m(P) \coloneqq \{p \in P : |p| = m\}$ the subset of all patches in a partition with a given size m and by $\pi_{>m}(P) = \{p \in P : |p| > m\}$ that of all patches with size larger than m. We refer to patches of size two as pairs and patches of size at least four as clusters. Partitions will be called even, if all patches in it have an even size. We further denote by $\mathcal{P}(J) = \{P : P \text{ partition of } J\}$ the set of all partitions of J, and by $\mathcal{P}_m(J)$ and $\mathcal{P}_{>m}(J)$ the sets of all partitions into patches of size exactly equal to, or larger than m, respectively. Given two partitions P, Q of the set J we say that Q is a coarsening of P and write $Q > P$ if $\forall p \in P\, \exists q \in Q : p \subset q$ and $P \neq Q$.

Next we introduce the notion of a Δ-partition of the sub-index set J. To each configuration of indices $(k_j)_{j\in J}$, we assign a unique partition P of the subindices j such that all indices $(k_j)_{j\in p}$ with subindices that lie within one set p of the partition are connected by a path of steps with maximal length Δ and all indices k_j corresponding to subindices in two different sets of the partition lie more than a distance Δ apart.

Definition 2 (Δ-partition)**.** *Given a distance $\Delta > 0$, a finite set $J \subset \mathbb{N}$, a finite set M equipped with a pseudometric d, and a sequence of elements $(k_j)_{j\in J} \in M^{\times|J|}$. We define the Δ-partition $P_\Delta(J, (k_j)_{j\in J})$ to be the unique partition of J which fulfills (1) Each set in the partition is path connected by hops of length at most Δ in the sense that*

$$\forall p \in P_\Delta(J, (k_j)_{j\in J}) : \forall x, y \in p \exists z_1, \dots, z_N \in p : x = z_1, y = z_N \wedge \forall i \in [N-1] : \mathrm{d}(k_{z_i}, k_{z_{i+1}}) \leq \Delta. \tag{65}$$

(2) The different patches in the partition are separated by a distance larger than Δ in the sense that

$$\forall p \neq q \in P_\Delta(J, (k_j)_{j\in J}) : \forall x \in p, y \in q : \mathrm{d}(k_x, k_y) > \Delta. \tag{66}$$

In addition, we define a compact notation for index configurations distributed over the lattice such that their Δ-partition agrees with a given partition P.

Definition 3 (Index sets respecting Δ-partitions)**.** *Given a distance $\Delta > 0$, the set $[2V]$ of all sites on the lattice equipped with a pseudometric d, a sub-index set $M \subset [2V]$, and a partition $P \in \mathcal{P}(J)$. We denote the set of sequences contained in M whose Δ partitions is equal to P by*

$$\mathcal{K}_P^M \coloneqq \{(k_j)_{j\in\overline{P}} \in M^{\times|\overline{P}|} : P_\Delta(\overline{P}, (k_j)_{j\in\overline{P}}) = P\}. \tag{67}$$

The notation introduced above allows us to rewrite the sum over the indices $(k_j)_{j\in J}$ in Eq. (64) inside the cone by sorting them according to their associated Δ-partition.

$$\begin{aligned} A_J^{LR}(t) = \sum_{(k_j)_{j\in J}\in\mathcal{C}(t)^{\times|J|}} \left(\prod_{j\in J} W_{j,k_j}(t)\, c_{k_j}\right) &= \sum_{P\in\mathcal{P}(J)} \sum_{(k_j)_{j\in J}\in\mathcal{K}_P^{\mathcal{C}(t)}} \prod_{j\in J} W_{j,k_j}(t)\, c_{k_j} \\ &= \sum_{P\in\mathcal{P}(J)} \mathrm{sign}(P) \sum_{(k_j)_{j\in J}\in\mathcal{K}_P^{\mathcal{C}(t)}} \prod_{p\in P} \hat{P}_p^{(k_j)_{j\in p}}, \end{aligned} \tag{68}$$

where for each $p \in P$ we have introduced a patch operator $\hat{P}_p^{(k_j)_{j\in p}}$, defined by

$$\hat{P}_p^{(k_j)_{j\in p}} = \prod_{j\in p} W_{j,k_j}(t) c_{k_j}\ . \tag{69}$$

The $\mathrm{sign}(P)$ denotes the sign picked up from reordering the fermionic basis operators into the corresponding patches, where keeping the relative order of the operators inside each patch fix.

C. Factorizing expectation values

In the last section, we have developed the formalism to group indices on the lattice according to their distribution on the lattice and introduced the patch operators $\hat{P}_p^{(k_j)_{j\in p}}$. We now use the exponential clustering of correlations in the initial state to show that expectation values of products of such patch operators can be factorized into a product of expectation values of the individual patch operators up to a small error.

Lemma 8 (Factorizing expectation values in states with exponential clustering of correlations)**.** *Let ρ be a state that exhibits exponential clustering of correlations as defined in Definition 1 with system size independent parameters $C_{\mathrm{Clust}}, \xi > 0$. Let $J \subset [2V]$ and $P \in \mathcal{P}(J)$ be a partition of J. Then for any distance $\Delta > 0$ it holds that*

$$\sum_{(k_j)_{j\in J}\in\mathcal{K}_P^{\mathcal{C}(t)}} \left| \left\langle \prod_{p\in P} \hat{P}_p^{(k_j)_{j\in p}} \right\rangle_\rho - \prod_{p\in P} \langle \hat{P}_p^{(k_j)_{j\in p}} \rangle_\rho \right| \leq |J|^3 \, C_{\mathrm{Clust}} \, |\mathcal{C}(t)|^{|J|} \mathrm{e}^{-\Delta/\xi} \, . \tag{70}$$

Proof. We begin by factorizing out the contribution from the first patch $p_1 \in P$. Using Lemma 6 and the exponential clustering of the initial state, we find for a given $(k_j)_{j\in J} \in \mathcal{K}_P^{\mathcal{C}(t)}$

$$\left| \left\langle \prod_{p\in P} \hat{P}_p^{(k_j)_{j\in p}} \right\rangle_\rho - \langle \hat{P}_{p_1}^{(k_j)_{j\in p_1}} \rangle_\rho \left\langle \prod_{p\in P\setminus\{p_1\}} \hat{P}_p^{(k_j)_{j\in p}} \right\rangle_\rho \right| \leq |p_1| \, |\overline{P} \setminus p_1| \, C_{\mathrm{Clust}} \, \mathrm{e}^{-\Delta/\xi} \, . \tag{71}$$

Using the trivial bound $|p_1| \, |\overline{P} \setminus p_1| \leq |J|^2$, iterating the step above $|P| \leq |J|$ times and using that $|\mathcal{K}_P^{\mathcal{C}(t)}| \leq |\mathcal{C}(t)|^{|J|}$ yields the result as stated. □

From Lemma 5 follows that the same theorem applies to the Gaussified version of a state exhibiting clustering of correlations if we allow C_{Clust} to scale with the size of the support according to $C_{\mathrm{Clust}} \to C_{\mathrm{Clust}} 4^{|J|} |J|^{|J|}$.

D. Suppression of non-Gaussian contributions

In the last two sections we have bounded the error made in approximating expectation values of terms of the from given in Eq. (12) by certain sums of products of expectation values of patch operators. This allows us to bound the difference between the left and right hand side of

$$\mathrm{tr}[A(t)\,\rho) - \mathrm{tr}(A(t)\,\rho_G] \approx \sum_{J\subset\tilde{S}} a(J) \sum_{P\in\mathcal{P}(J)} \mathrm{sign}(P) \sum_{(k_j)_{j\in J}\in\mathcal{K}_P^{\mathcal{C}(t)}} \left(\prod_{p\in P} \langle \hat{P}_p^{(k_j)_{j\in p}} \rangle_\rho - \prod_{p\in P} \langle \hat{P}_p^{(k_j)_{j\in p}} \rangle_{\rho_G} \right) . \tag{72}$$

It is obvious that to the right hand side only partitions P in which all patches p are of even size can contribute, as ρ and ρ_G have an even particle number parity. Moreover, as the second moments of ρ and ρ_G are equal by definition, the difference between the products also vanishes whenever all patches have size exactly 2. Hence, every contributing term contains at least one patch of size at least 4. In the remainder of this section we now bound the contribution of such partitions to the right hand side of the above equation. The combinatorial nature of the problem makes this a tedious endeavor. The final result is summarized in the following lemma, which is the last result that we need before we can assemble all the parts of the proof in Section IV E.

Lemma 9 (Bounding contributions from partitions that contain large patches)**.** *Let ρ be a state exhibiting exponential clustering of correlations as defined in Definition 1 with system size independent parameters $C_{\mathrm{Clust}}, \xi > 0$ and ρ_G its Gaussified version. Let $\Delta \geq 1$, $J \subset [2V]$, and $P \in \mathcal{P}(J)$ be an even partition that contains a patch of size at least four (cluster), and $m \coloneqq |\pi_2(P)|$ many patches of size two (pairs). Given that the time evolution of the system is governed by a Hamiltonian showing delocalizing transport as defined in Definition 2 with parameters C_{Trans}, α_{Trans}, for all $t \in (0, \min(t_{\mathrm{Rec}}, V)]$ and $\sigma \in \{\rho, \rho_G\}$ it holds that*

$$\begin{aligned} R_P(J,m,t) &\coloneqq \left| \sum_{(k_j)_{j\in J}\in\mathcal{K}_P^{\mathcal{C}(t)}} \prod_{p\in P} \langle \hat{P}_p^{(k_j)_{j\in p}} \rangle_\sigma \right| \\ &\leq (|\mathcal{C}(t)|^{1/4} C_{\mathrm{Trans}} t^{-\alpha_{\mathrm{Trans}}} 2^{2d_{\mathcal{L}}} |J|^{d_{\mathcal{L}}} \Delta^{d_{\mathcal{L}}})^{|J|-2m} \\ &\quad \times \left[(1 + C_{\mathrm{Clust}} |\mathcal{C}(t)|^2 \mathrm{e}^{-\Delta/\xi}) + 2^{2d_{\mathcal{L}}|J|} |J|^{(d_{\mathcal{L}}+1)|J|+1} \sum_{r=0}^{|J|/2} (|\mathcal{C}(t)|^{1/4} C_{\mathrm{Trans}} t^{-\alpha_{\mathrm{Trans}}} \Delta^{d_{\mathcal{L}}})^{2r+4} \right]^m . \end{aligned} \tag{73}$$

Proof. In order to prove the above bound we separate the partition into a part containing only pairs and one containing the rest

$$P = \pi_2(P) \cup \pi_{>2}(P) \ . \tag{74}$$

For every given fixed position of the indices corresponding to clusters in $\pi_{>2}(P)$, the indices corresponding to the pairs are restricted to the set $K \coloneqq \mathcal{C}(t) \setminus \mathcal{B}_\Delta(\{k_j\}_{j\in\overline{\pi_{>2}(P)}})$, as all patches are separated by a distance larger than Δ. Thus, we can write

$$R_P(J,m,t) = \left| \sum_{(k_j)_{j\in\overline{\pi_{>2}(P)}}\in\mathcal{K}^{\mathcal{C}(t)}_{\pi_{>2}(P)}} \left[\left(\prod_{p\in\pi_{>2}(P)} \langle \hat{P}_p^{(k_j)_{j\in p}} \rangle_\sigma \right) \sum_{\substack{(k_j)_{j\in\overline{\pi_2(P)}}\in\mathcal{K}^{K}_{\pi_2(P)},\\ K\coloneqq\mathcal{C}(t)\setminus\mathcal{B}_\Delta(\{k_j\}_{j\in\overline{\pi_{>2}(P)}})}} \prod_{p\in\pi_2(P)} \langle \hat{P}_p^{(k_j)_{j\in p}} \rangle_\sigma \right] \right| . \tag{75}$$

The homogeneous suppression due to delocalizing transport for $t \in (0, \min(t_{\mathrm{Rec}}, V)]$ and $|\overline{\pi_{>2}(P)}| = |J| - 2m$ imply

$$\left\| \prod_{p\in\pi_{>2}(P)} \hat{P}_p^{(k_j)_{j\in p}} \right\| \leq (C_{\mathrm{Trans}} t^{-\alpha_{\mathrm{Trans}}})^{|J|-2m} \ . \tag{76}$$

Using this and the triangle inequality for the first sum in Eq. (75) we arrive at

$$R_P(J,m,t) \leq (C_{\mathrm{Trans}} t^{-\alpha_{\mathrm{Trans}}})^{|J|-2m} \sum_{(k_j)_{j\in\overline{\pi_{>2}(P)}}\in\mathcal{K}^{\mathcal{C}(t)}_{\pi_{>2}(P)}} \left| \sum_{\substack{(k_j)_{j\in\overline{\pi_2(P)}}\in\mathcal{K}^{K}_{\pi_2(P)},\\ K=\mathcal{C}(t)\setminus\mathcal{B}_\Delta(\{k_j\}_{j\in\overline{\pi_{>2}(P)}})}} \prod_{p\in\pi_2(P)} \langle \hat{P}_p^{(k_j)_{j\in p}} \rangle_\sigma \right| . \tag{77}$$

At this point, the inner sum still depends on the position of the clusters, as they create an exclusion region for the pairs (see Fig. 1). Taking the supremum over such exclusion regions decouples the sum. Then bounding the possible number of positions of the $|J| - 2m$ indices in the $|\pi_{>2}(P)|$ clusters by

$$|\mathcal{K}^{\mathcal{C}(t)}_{\pi_{>2}(P)}| \leq |\mathcal{C}(t)|^{|\pi_{>2}P|} (2^{2d_\mathcal{L}} |J|^{d_\mathcal{L}} \Delta^{d_\mathcal{L}})^{|J|-2m} \ , \tag{78}$$

gives

$$R_P(J,m,t) \leq |\mathcal{C}(t)|^{|\pi_{>2}(P)|} (C_{\mathrm{Trans}} t^{-\alpha_{\mathrm{Trans}}} 2^{2d_\mathcal{L}} |J|^{d_\mathcal{L}} \Delta^{d_\mathcal{L}})^{|J|-2m} \max_{I\subset\mathcal{C}(t)} \left| \sum_{(k_j)_{j\in\overline{\pi_2(P)}}\in\mathcal{K}^{\mathcal{C}(t)\setminus I}_{\pi_2(P)}} \prod_{p\in\pi_2(P)} \langle \hat{P}_p^{(k_j)_{j\in p}} \rangle_\sigma \right| \tag{79}$$

$$\leq (|\mathcal{C}(t)|^{1/4} C_{\mathrm{Trans}} t^{-\alpha_{\mathrm{Trans}}} 2^{2d_\mathcal{L}} |J|^{d_\mathcal{L}} \Delta^{d_\mathcal{L}})^{|J|-2m} \max_{M\subset J:|M|=2m} \max_{\substack{I\subset\mathcal{C}(t),\\ P\in\mathcal{P}_2(M)}} \left| \sum_{(k_j)_{j\in M}\in\mathcal{K}^{\mathcal{C}(t)\setminus I}_P} \prod_{p\in P} \langle \hat{P}_p^{(k_j)_{j\in p}} \rangle_\sigma \right| . \tag{80}$$

We now define

$$f(m,t) \coloneqq \max_{M\subset J:|M|=2m} \max_{\substack{I\subset\mathcal{C}(t),\\ P\in\mathcal{P}_2(M)}} \left| \sum_{(k_j)_{j\in M}\in\mathcal{K}^{\mathcal{C}(t)\setminus I}_P} \prod_{p\in P} \langle \hat{P}_p^{(k_j)_{j\in p}} \rangle_\sigma \right| \tag{81}$$

and apply an recursive argument to achieve a bound of the form

$$f(m,t) \leq C(m,t) \ . \tag{82}$$

a. Start of recursion: For the case of one pair ($m = 1$), by using Lemma 6, we can bound the appearing maximum as follows

$$f(1,t) = \max_{M\subset J:|M|=2}\max_{I\subset\mathcal{C}(t)}\left|\sum_{(k_j)_{j\in M}\in\mathcal{K}^{\mathcal{C}(t)\setminus I}_{\{M\}}}\langle\hat{P}^{(k_j)_{j\in M}}_M\rangle_\sigma\right| = \max_{M\subset J:|M|=2}\max_{I\subset\mathcal{C}(t)}\left|\sum_{\substack{k_{l_1},k_{l_2}\in\mathcal{C}(t)\setminus I,\\ \{l_1,l_2\}=M:\\ \mathrm{d}(k_{l_1},k_{l_2})\leq\Delta}}\langle\hat{P}^{(k_j)_{j\in M}}_M\rangle_\sigma\right| \tag{83}$$

$$\leq \max_{M\subset J:|M|=2}\max_{I\subset\mathcal{C}(t)}\left(\left|\sum_{\substack{k_{l_1},k_{l_2}\in\mathcal{C}(t)\setminus I,\\ \{l_1,l_2\}=M}}\langle\hat{P}^{(k_j)_{j\in M}}_M\rangle_\sigma\right| + \left|\sum_{\substack{k_{l_1},k_{l_2}\in\mathcal{C}(t)\setminus I,\\ \{l_1,l_2\}=M:\\ \mathrm{d}(k_{l_1},k_{l_2})>\Delta}}\langle\hat{P}^{(k_j)_{j\in M}}_M\rangle_\sigma\right|\right)$$

$$\leq \max_{M\subset J:|M|=2}\max_{I\subset\mathcal{C}(t)}(1+|\mathcal{C}(t)|^2 C_{\mathrm{Clust}}\mathrm{e}^{-\Delta/\xi}) \tag{84}$$

$$= 1+|\mathcal{C}(t)|^2 C_{\mathrm{Clust}}\mathrm{e}^{-\Delta/\xi}\ . \tag{85}$$

With this, we can move to setting up the recursion.

b. Setting up the recursion: To obtain a recursion formula for an upper bound $C(m,t)$ on $f(m,t)$ we now relax the condition that different pairs may not occupy close-by lattice regions. If we drop this constraint, the only remaining constraint is that paired indices k_l and $k_{l'}$ lie close to each other, i.e. $\mathrm{d}(k_l,k_{l'})\leq\Delta$. For any set $M\subset J$ with $|M|=2m$, set $I\subset\mathcal{C}(t)$, $P\in\mathcal{P}_2(M)$ Eq. (85) yields directly

$$\left|\prod_{p\in P}\sum_{(k_j)_{j\in p}\in\mathcal{K}^{\mathcal{C}(t)\setminus I}_{\{p\}}}\langle\hat{P}^{(k_j)_{j\in p}}_p\rangle_\sigma\right| \leq (1+C_{\mathrm{Clust}}|\mathcal{C}(t)|^2\mathrm{e}^{-\Delta/\xi})^m. \tag{86}$$

This leaves us with controlling the difference between the constrained and unconstrained pairs and yields

$$f(m,t)\leq\left(1+|\mathcal{C}(t)|^2 C_{\mathrm{Clust}}\mathrm{e}^{-\Delta/\xi}\right)^m + \max_{M\subset J:|M|=2m}\max_{\substack{I\subset\mathcal{C}(t),\\ P\in\mathcal{P}_2(M)}} g(M,P,I), \tag{87}$$

$$g(M,P,I) \coloneqq \left|\sum_{(k_j)_{j\in M}\in\mathcal{K}^{\mathcal{C}(t)\setminus I}_P}\prod_{p\in P}\langle\hat{P}^{(k_j)_{j\in p}}_p\rangle_\sigma - \prod_{p\in P}\sum_{(k_j)_{j\in p}\in\mathcal{K}^{\mathcal{C}(t)\setminus I}_{\{p\}}}\langle\hat{P}^{(k_j)_{j\in p}}_p\rangle_\sigma\right|. \tag{88}$$

In order to get the error under control, we need the notion of a coarsening of a partition defined above [5]. The key insight here is that the above difference between constrained and unconstrained pairs can be captured by considering all possible coarsening of the partition P

$$g(M,P,I) = \left|\sum_{\substack{Q\in\mathcal{P}(M):\\ Q>P}}\sum_{\substack{(k_j)_{j\in M}\in\mathcal{K}^{\mathcal{C}(t)\setminus I}_Q:\\ \forall\{l,l'\}\in P:\mathrm{d}(k_l,k_{l'})\leq\Delta}}\prod_{p\in P}\langle\hat{P}^{(k_j)_{j\in p}}_p\rangle_\sigma\right| \leq \sum_{w=0}^{m-2}\sum_{\substack{Q\in\mathcal{P}(M):\\ Q>P,|\pi_2(Q)|=w}}\left|\sum_{\substack{(k_j)_{j\in M}\in\mathcal{K}^{\mathcal{C}(t)\setminus I}_Q:\\ \forall\{l,l'\}\in P:\mathrm{d}(k_l,k_{l'})\leq\Delta}}\prod_{p\in P}\langle\hat{P}^{(k_j)_{j\in p}}_p\rangle_\sigma\right|, \tag{89}$$

where we have applied the triangle inequality and sorted the coarsenings by the numbers of pairs w they have. This is almost the original expression $R_P(J,m,t)$ which this lemma is trying to bound, with the exception that there is still a signature left of the fact that the clusters were created by joining pairs, such that consecutive indices have to be at most distance Δ apart in the

cluster. Following the same steps as above, one can show that

$$
\begin{aligned}
g(M,P,I) &\leq \sum_{w=0}^{m-2} \sum_{\substack{Q\in\mathcal{P}(M):\\ Q>P,|\pi_2(Q)|=w}} \left| \sum_{\substack{(k_j)_{j\in M}\in\mathcal{K}_Q^{\mathcal{C}(t)\setminus I}:\\ \forall\{l,l'\}\in P:\mathrm{d}(k_l,k_{l'})\leq\Delta}} \prod_{p\in P} \langle \hat{P}_p^{(k_j)_{j\in p}}\rangle_\sigma \right| \\
&\leq \sum_{w=0}^{m-2} \sum_{\substack{Q\in\mathcal{P}(M):\\ Q>P,|\pi_2(Q)|=w}} (C_{\mathrm{Trans}}t^{-\alpha_{\mathrm{Trans}}})^{2m-2w} \sum_{\substack{(k_j)_{j\in\overline{\pi_{>2}(P)}}\in\mathcal{K}^{\mathcal{C}(t)}_{\pi_{>2}(P)}\\ \forall\{l,l'\}\in P:\mathrm{d}(k_l,k_{l'})\leq\Delta}} \left| \sum_{\substack{(k_j)_{j\in\overline{\pi_2(P)}}\in\mathcal{K}^K_{\pi_2(P)},\\ K=\mathcal{C}(t)\setminus\mathcal{B}_\Delta(\{k_j\}_{j\in\overline{\pi_{>2}(P)}})}} \prod_{p\in\pi_2(P)} \langle \hat{P}_p^{(k_j)_{j\in p}}\rangle_\sigma \right| \\
&\leq \sum_{w=0}^{m-2} (2m)^{2m} (|\mathcal{C}(t)|^{1/4} C_{\mathrm{Trans}} t^{-\alpha_{\mathrm{Trans}}} 2^{2d_{\mathcal{L}}} |J|^{d_{\mathcal{L}}} \Delta^{d_{\mathcal{L}}})^{2m-2w} f(w,t) \;, \qquad (90)
\end{aligned}
$$

where we used that for a finite set M, we can upper bound the number of partitions of this set by $|\mathcal{P}(M)| \leq |M|^{|M|}$. Thus we obtain for the function $f(m,t)$ the following upper bound

$$
\begin{aligned}
f(m,t) &\leq \left(1+|\mathcal{C}(t)|^2 C_{\mathrm{Clust}} \mathrm{e}^{-\Delta/\xi}\right)^m + \sum_{w=0}^{m-2} |J|^{|J|} (|\mathcal{C}(t)|^{1/4} C_{\mathrm{Trans}} t^{-\alpha_{\mathrm{Trans}}} 2^{2d_{\mathcal{L}}} |J|^{d_{\mathcal{L}}} \Delta^{d_{\mathcal{L}}})^{2m-2w} f(w,t) \qquad (91) \\
&\leq \left(1+|\mathcal{C}(t)|^2 C_{\mathrm{Clust}} \mathrm{e}^{-\Delta/\xi}\right)^m + 2^{2d_{\mathcal{L}}|J|} |J|^{(d_{\mathcal{L}}+1)|J|} \sum_{w=0}^{m-2} (|\mathcal{C}(t)|^{1/4} C_{\mathrm{Trans}} t^{-\alpha_{\mathrm{Trans}}} \Delta^{d_{\mathcal{L}}})^{2m-2w} f(w,t) \\
&\leq \left(1+|\mathcal{C}(t)|^2 C_{\mathrm{Clust}} \mathrm{e}^{-\Delta/\xi}\right)^m + 2^{2d_{\mathcal{L}}|J|} |J|^{(d_{\mathcal{L}}+1)|J|} \sum_{r=0}^{|J|/2} (|\mathcal{C}(t)|^{1/4} C_{\mathrm{Trans}} t^{-\alpha_{\mathrm{Trans}}} \Delta^{d_{\mathcal{L}}})^{2r+4} \sum_{w=0}^{m-2} f(w,t) \\
&\leq \alpha^m + \delta \sum_{w=0}^{m-1} C(w,t) =: C(m,t) \;,
\end{aligned}
$$

where we overestimated by introducing the sum over r and adding the $m-1$ term to the second sum and have introduced the abbreviations

$$
\alpha = (1 + C_{\mathrm{Clust}} |\mathcal{C}(t)|^2 \mathrm{e}^{-\Delta/\xi}), \qquad (92)
$$

$$
\delta = 2^{2d_{\mathcal{L}}|J|} |J|^{(d_{\mathcal{L}}+1)|J|} \sum_{r=0}^{|J|/2} (|\mathcal{C}(t)|^{1/4} C_{\mathrm{Trans}} t^{-\alpha_{\mathrm{Trans}}} \Delta^{d_{\mathcal{L}}})^{2r+4} \;. \qquad (93)
$$

By now setting

$$
C(0,t) \coloneqq f(0,t) = 1, \qquad (94)
$$

$$
C(1,t) \coloneqq \alpha + \delta \geq \alpha \geq f(1,t), \qquad (95)
$$

$$
\forall m \geq 1: \quad C(m,t) = \alpha^m + \delta \sum_{w=0}^{m-1} C(w,t), \qquad (96)
$$

we have a recursively defined upper bound $C(m,t)$ on $f(m,t)$.

c. Solving the recursion: To resolve the recursion, we first show that

$$
\alpha C(m,t) \leq C(m+1,t) \;, \qquad (97)
$$

by relying on an induction. To begin with, we have

$$
\alpha\, C(0,t) = \alpha \leq \alpha + \delta = C(1,t) \;. \qquad (98)
$$

For the induction step, we use

$$\alpha\, C(m,t) = \alpha^{m+1} + \delta \sum_{w=0}^{m-1} \alpha\, C(w,t) \tag{99}$$

$$\leq \alpha^{m+1} + \delta \sum_{w=0}^{m-1} C(w+1,t) \tag{100}$$

$$\leq \alpha^{m+1} + \delta \sum_{w=0}^{m} C(w,t) = C(m+1,t)\ , \tag{101}$$

where we used the induction when moving from the first to the second line by relying on the fact that the sum only goes until $w = m-1$ and we added $\delta C(0,t) > 0$ in the last line. From this, we immediately know that $C(m,t)$ is monotonically increasing as a function of m, since $\alpha \geq 1$. This implies

$$C(m,t) \leq \alpha\, C(m,t) \leq C(m+1,t)\ . \tag{102}$$

This allows us to resolve the recursion by iteratively using this estimate as follows

$$\begin{aligned} C(m,t) &= \alpha^m + \delta \sum_{w=0}^{m-1} C(w,t) \\ &\leq \alpha^m + (m-1)\delta C(m-1,t) \\ &\leq \sum_{j=0}^{m} \alpha^{m-j}\delta^j \frac{m!}{(m-j)!} \\ &\leq \sum_{j=0}^{m} \alpha^{m-j}\delta^j \frac{m!}{(m-j)!}\frac{|J|^j}{j!} \\ &= (\alpha + |J|\delta)^m. \end{aligned} \tag{103}$$

For $f(m,t)$, we hence obtain

$$\begin{aligned} f(m,t) &\leq (\alpha + |J|\delta)^m \\ &= \left[(1 + C_{\mathrm{Clust}}|\mathcal{C}(t)|^2 \mathrm{e}^{-\Delta/\xi}) + |J| 2^{2d_{\mathcal{L}}|J|} |J|^{(d_{\mathcal{L}}+1)|J|} \sum_{r=0}^{|J|/2} (|\mathcal{C}(t)|^{1/4} C_{\mathrm{Trans}} t^{-\alpha_{\mathrm{Trans}}} \Delta^{d_{\mathcal{L}}})^{2r+4} \right]^m \end{aligned} \tag{104}$$

and for the original quantity considered in this lemma, this yields

$$\begin{aligned} R_P(J,m,t) \leq\ & (|\mathcal{C}(t)|^{1/4} C_{\mathrm{Trans}} t^{-\alpha_{\mathrm{Trans}}} 2^{2d_{\mathcal{L}}} |J|^{d_{\mathcal{L}}} \Delta^{d_{\mathcal{L}}})^{|J|-2m} \\ & \times \left[(1 + C_{\mathrm{Clust}}|\mathcal{C}(t)|^2 \mathrm{e}^{-\Delta/\xi}) + |J| 2^{2d_{\mathcal{L}}|J|} |J|^{(d_{\mathcal{L}}+1)|J|} \sum_{r=0}^{|J|/2} (|\mathcal{C}(t)|^{1/4} C_{\mathrm{Trans}} t^{-\alpha_{\mathrm{Trans}}} \Delta^{d_{\mathcal{L}}})^{2r+4} \right]^m , \end{aligned} \tag{105}$$

which concludes the proof. □

E. Overview of the proof of Theorem 1

Collecting all the results of the preceding sub-sections, we can now proof the following result, which directly implies theorem 1 in the main text.

Theorem (Gaussification in finite time)**.** *Let $C_{\mathrm{Clust}}, \xi, C_{\mathrm{Trans}} > 0$. Consider a family of systems on $d_{\mathcal{L}}$-dimensional cubic lattices of increasing volume V and let S be some fixed finite region of sites and $\alpha_{\mathrm{Trans}} > d_{\mathcal{L}}/4$. Let the corresponding initial states exhibit exponential clustering of correlations with constant C_{Clust} and correlation length ξ. Let the Hamiltonians of these systems be quadratic finite range and let them exhibit delocalizing transport with constants C_{Trans} and α_{Trans} and a recurrence time t_{Rec} increasing unboundedly as some function of the volume V. Then for any $\epsilon > 0$ there exists a relaxation time $t_{\mathrm{Relax}} > 0$ independent of the system size such that for all $t \in [t_{\mathrm{Relax}},\, t_{\mathrm{Rec}}]$ it holds that $\|\rho^S(t) - \rho^S_G(t)\|_1 \leq \epsilon$.*

Proof. To begin with we rewrite the one-norm as

$$\|\rho^S(t) - \rho_G^S(t)\|_1 = \sup_{A\in\mathcal{A}_S} \operatorname{tr}\left(A(t)(\rho-\rho_G)\right) \ , \tag{106}$$

and expand the operator A in the basis of fermionic operators

$$A(t) = \sum_{b_1,\dots,b_{2|S|}=0}^{1} a_{b_1,\cdots,b_{2|S|}}\, c_{s_1}(t)^{b_1}\dots c_{s_{2|S|}}(t)^{b_{2|S|}} \ . \tag{107}$$

Normalization of the operator $\|A\| = 1$ implies that all of the $2^{2|S|}$ coefficients satisfy $|a_{b_1,\cdots,b_{2m}}| \leq 1$, thus

$$\begin{aligned}\|\rho^S(t) - \rho_G^S(t)\|_1 &\leq 2^{2|S|}\max_{J\subset\tilde{S}}\left|\operatorname{tr}\Big(\prod_{j\in J} c_j(t)\,(\rho-\rho_G)\Big)\right| \\ &\leq 2^{2|S|}\max_{J\subset\tilde{S}}\left|\sum_{(k_j)_{j\in J}\in[2V]^{\times|J|}} \operatorname{tr}\Big(\prod_{j\in J} W_{j,k_j}(t)\,c_{k_j}\,(\rho-\rho_G)\Big)\right| .\end{aligned} \tag{108}$$

Using the Lieb-Robinson bound stated in Lemma 7, we can restrict the sum in the right hand side of the previous inequality to the Lieb-Robinson cone $\mathcal{C}(t)$. This leads to an error term that is exponentially suppressed in time t and we obtain

$$\|\rho^S(t) - \rho_G^S(t)\|_1 \leq 2^{2|S|}\max_{J\subset\tilde{S}}\left(\left|\sum_{(k_j)_{j\in J}\in[\mathcal{C}(t)]^{\times|J|}} \operatorname{tr}\Big(\prod_{j\in J} W_{j,k_j}(t)\,c_{k_j}\,(\rho-\rho_G)\Big)\right| + 2\tilde{C}_{\mathrm{LR}}(d_{\mathcal{L}})|J|^2\mathrm{e}^{-\mu v_\epsilon|t|}\right) . \tag{109}$$

We now reorder the terms in the sum according to how the indices k_j are distributed on the lattice. To that end, in Section IV B, we have introduced the concept of a Δ-partition. We turn the sum into a sum over all possible partitions $\mathcal{P}(J)$ and then, for each partition $P\in\mathcal{P}(J)$, sum over all possible ways $\mathcal{K}_P^{\mathcal{C}(t)}$ to distributed the indices over the lattice whose Δ-partition coincides with that given partition P. Partitions consist of patches and we collect the factors $W_{j,k_j}(t)\,c_{k_j}$ from the product over $j\in J$ into patch operators $\hat{P}_p^{(k_j)_{j\in p}}$ for each patch p, as defined in Eq. (69). Together with the triangle inequality this yields

$$\|\rho^S(t) - \rho_G^S(t)\|_1 \leq 2^{2|S|}\max_{J\subset\tilde{S}}\left(\sum_{P\in\mathcal{P}(J)}\left|\sum_{(k_j)_{j\in J}\in\mathcal{K}_P^{\mathcal{C}(t)}} \left(\langle\prod_{p\in P}\hat{P}_p^{(k_j)_{j\in p}}\rangle_\rho - \langle\prod_{p\in P}\hat{P}_p^{(k_j)_{j\in p}}\rangle_{\rho_G}\right)\right| + 2\tilde{C}_{\mathrm{LR}}(d_{\mathcal{L}})|J|^2\mathrm{e}^{-\mu v_\epsilon|t|}\right) . \tag{110}$$

Lemma 8 allows us to factor the expectation values with respect to ρ and using Lemma 5 its Gaussified version ρ_G into products of expectation values of the individual patch operators. This leads to an additional error term that grows polynomially with the size of the cone, but is exponentially suppressed in the minimal patch distance Δ, so that we get

$$\begin{aligned}\|\rho^S(t) - \rho_G^S(t)\|_1 \leq 2^{2|S|}\max_{J\subset\tilde{S}}\Bigg(\sum_{P\in\mathcal{P}(J)}\Bigg|\sum_{(k_j)_{j\in J}\in\mathcal{K}_P^{\mathcal{C}(t)}} \Big(\prod_{p\in P}\langle\hat{P}_p^{(k_j)_{j\in p}}\rangle_\rho - \prod_{p\in P}\langle\hat{P}_p^{(k_j)_{j\in p}}\rangle_{\rho_G}\Big)\Bigg| \\ + (1+2^{2|J|}|J|^{|J|})|J|^{|J|+3}C_{\mathrm{Clust}}|\mathcal{C}(t)|^{|J|}\mathrm{e}^{-\Delta/\xi} + 2\tilde{C}_{\mathrm{LR}}(d_{\mathcal{L}})|J|^2\mathrm{e}^{-\mu v_\epsilon|t|}\Bigg) .\end{aligned} \tag{111}$$

It is now apparent that partitions that contain at least one patch of odd size do not contribute to the sum as then the corresponding patch operator does not fulfill the parity super-selection rule. Likewise, partitions that contain only patches of size two do not contribute, as the expectation values of their patch operators are the same in ρ and ρ_G. It remains to bound the contribution from the remaining partitions. For these we cannot use cancellations between the parts coming from ρ and those coming from ρ_G, but instead bound them in absolute value. All these partitions contain at least one cluster of size at least four, which allows us to bound the corresponding term from the homogeneous suppression of the elements of the propagator implied by the delocalizing transport (see Definition 2). Doing this explicitly is tedious because of the interplay of contributions from the larger patches and those of size two, and the involved combinatorics of how the smaller patches can be distributed on the lattice. All this is done by first ordering contributions according to the number m of patches of size two they contain and then applying Lemma 9, which internally uses a recursive argument. It yields an upper bound on the absolute value of sums of the form $\sum_{(k_j)_{j\in J}\in\mathcal{K}_P^{\mathcal{C}(t)}}\prod_{p\in P}\langle\hat{P}_p^{(k_j)_{j\in p}}\rangle_\rho$ that grows with Δ but is algebraically suppressed with time t. Assuming $\Delta\geq 1$ this yields for

$t \leq \min(t_{\mathrm{Rec}}, V)$ the following bound

$$\begin{aligned}\|\rho^S(t) - \rho_G^S(t)\|_1 \leq 2^{2|S|}\Bigg[&2^{2|S|+1}|S|^{2|S|}\sum_{m=0}^{|S|}(2^{3d_{\mathcal{L}}}|S|^{d_{\mathcal{L}}}|\mathcal{C}(t)|^{1/4}C_{\mathrm{Trans}}t^{-\alpha_{\mathrm{Trans}}}\Delta^{d_{\mathcal{L}}})^{2m+4}\Bigg(1 + C_{\mathrm{Clust}}|\mathcal{C}(t)|^2\mathrm{e}^{-\Delta/\xi} \\ &+ 2^{2(3d_{\mathcal{L}}+1)|S|+1}|S|^{2|S|(d_{\mathcal{L}}+1)+1}\sum_{r=0}^{|S|}(|\mathcal{C}(t)|^{1/4}C_{\mathrm{Trans}}t^{-\alpha_{\mathrm{Trans}}}\Delta^{d_{\mathcal{L}}})^{2r+4}\Bigg)^{|S|} \\ &+ 8\tilde{C}_{\mathrm{LR}}(d_{\mathcal{L}})|S|^2\mathrm{e}^{-\mu v_\epsilon|t|} + 2^{8|S|+4}|S|^{4|S|+3}C_{\mathrm{Clust}}|\mathcal{C}(t)|^{2|S|}\mathrm{e}^{-\Delta/\xi}\Bigg]\,.\end{aligned} \tag{112}$$

Recalling that $|\mathcal{C}(t)| \leq 2|S|[2(v+2v_\epsilon)t+1]^{d_{\mathcal{L}}}$ and setting $v_\epsilon = v$ one realizes that by letting Δ grow in a suitable way with t, all terms are at least algebraically suppressed in t. More precisely, this happens for all $\Delta = \max(1, t^{\nu/4d_{\mathcal{L}}})$ with $0 < \nu < 4\alpha_{\mathrm{Trans}} - d_{\mathcal{L}}$. For large enough times the bound is then dominated by a power-law originating from the $m = 0$ term of the first sum. Eq. (112) in particular implies that there exists a constant C_{Total} that depends on ν, $|S|$, and the physical parameters of the Hamiltonian and initial state, but that is independent of the size of the total system, such that for all $t \leq \min(t_{\mathrm{Rec}}, V)$

$$\|\rho^S(t) - \rho_G^S(t)\|_1 \leq C_{\mathrm{Total}}\, t^{-4\alpha_{\mathrm{Trans}}+d_{\mathcal{L}}+\nu}. \tag{113}$$

Moreover, for every ϵ there exists a critical system size from which on the bound above becomes smaller than that ϵ for a suitable relaxation time $t_{\mathrm{Relax}} \leq \min(t_{\mathrm{Rec}}, V)$. The saturation of the delocalizing transport once t is equal to V implies a minimal value that bound can achieve for any given V. This sets the minimal system size for which $t_{\mathrm{Relax}} < t_{\mathrm{Rec}}$. □

[1] A. Kitaev, Ann. Phys. **321**, 2 (2006).
[2] M. Cramer and J. Eisert, New J. Phys. **12**, 055020 (2010).
[3] E. Lieb, T. Schultz, and D. Mattis, Ann. Phys. **16**, 407 (1961).
[4] C. V. Kraus, M. M. Wolf, J. I. Cirac, and G. Giedke, Phys. Rev. A **79**, 012306 (2009).
[5] J. H. van Lint and R. M. Wilson, *A course in combinatorics* (Cambridge University Press, 1992).

3

EQUILIBRATION TOWARDS GENERALIZED GIBBS ENSEMBLES IN NON-INTERACTING THEORIES

The previous chapter presented a step towards establishing a general derivation of equilibration in closed quantum systems. However, it also left certain questions unresolved which we will address here, at the same time showing how their answer amounts to essentially the completion of the research programme on equilibration dynamics following an interaction quench.

We will show that short-range translation invariant non-interacting Hamiltonians on a ring lead to coherent mixing that features the delocalizing transport property which we have previously identified to be the cornerstone of the Gaussification mechanism. In fact, for these models this property can be viewed as facilitating a notion of ergodicity matching the classical definition. Roughly, in a classical gas one would speak of ergodicity if the particles explore the whole available phase space which may be constrained, e.g., by the conserved energy shell. One way to interpret our result is that we achieve precisely that. The notion of phase space in quantum systems can take up various meanings depending on the context and it is beyond the scope of this work to facilitate a notion of ergodicity that matches all diverse settings that one would view as being 'ergodic' [134]. However for Gaussian systems, which are the focus of this chapter by virtue of the Gaussification theorem presented in the previous chapter, it is possible to have an intuition of what a notion of ergodicity should entail. First of all for Gaussian systems we should focus on second moments and the coupling matrix parametrizing the quadratic Hamiltonian in question. It is sometimes preferred to refer to working with Gaussian systems as single particle problems which stresses that the unitary evolution on the entire state is specified by the Green functions that would describe a single particle in the system and in the presence of more particles in the system there is only coherent mixing of the individual evolutions of particles not conditioned on the dynamics of the other particles. Hence, it seems instructive to focus on the properties of a single particle Green function that hint towards a notion of ergodicity. As the paper describes, for a lattice system the entries of single particle Green functions provably decay as a power law in time everywhere in space. That means that particles have to necessarily spread in space over time, i.e., even if in the beginning the particle was localized at a single lattice site over time then due to the coherent quantum evolution the particle behaves more as a dispersing wave packet than a well-defined particle localized in space and for long times one cannot tell where the particle was in the beginning once the wave-packet spreads across the entire system. When this happens we can conclude that the particle has explored its whole available space uniformly and as all the particles do the same we see that the system is an example of an ergodic system where all particles become uniformly distributed in the system over time.

On the technical side we prove rigorously that such spreading of wave-packets occurs for short-range translation invariant models on a lattice. Here the lattice appears to play an interesting role ensuring that even if some parts of the dispersion relation are approximately linear then there necessarily must also be parts which are non-linear. It is this latter part of the spectrum that is shown to lead to the dispersion of wave-packets. While this property is usually argued by the so-called stationary phase approximation we have employed techniques developed in analytical number theory that may be of interest in their own right as our bound allowed us to tackle evolution times that cannot be directly studied by asymptotic expansions. This is because the stationary phase approximation is usually employed by relating the lattice problem to integrals but at late times the oscillations become too rapid and the error committed by linking to integral expressions does not seem to admit a simple bound. In contrast by working exclusively in the lattice we were in a position to derive a result valid for extensively long times.

Secondly, we will discuss in great detail how non-translation invariant initial conditions come to equilibrate under translation-invariant Hamiltonians. This leads to a comprehensive understanding of counter-examples to equilibration, essentially due to the absence of spectral non-linearities and hence slow dephasing. Here, we uncover that viewing the covariance matrix in momentum space is crucial and show that in this formulation it is possible to identify which states will equilibrate rapidly. Specifically, we want that the long wave-length components of the current or density distributions in the system are not populated. Initial correlations at all other wave-lengths are not constrained by our assumptions and will dephase towards a steady-state so there is a lot of freedom of freely choosing the initial configurations only to find by means of our theorem that the system will equilibrate. Such independence of initial conditions is a hallmark feature of statistical mechanics.

Finally, we also contribute interesting insights to the general question concerning the question with conserved charges are relevant for parametrizing a generalized Gibbs ensemble? Clearly any projector $|E_k\rangle\langle E_k|$ onto a many-body eigenstate of the quench Hamiltonian is a conserved quantity. As there are exponentially many in the system size and they are non-local, such charges should be discarded by some physical argument. Moreover, even in the context of Gaussian systems, there are many non-local conserved quantities. For example for a translation invariant Hamiltonian the number operators of the momentum eigenmodes are not local and are made up of a sum over terms ranging over the whole system. We give evidence that it is enough to consider conserved quantities expressed in terms of local terms, whose range cannot substantially exceed the finite correlation length in the initial system. This in particular renders the generalized Gibbs ensembles, that we prove to be the equilibrium ensembles, to be only a slight generalization of ordinary Gibbs ensembles: They are again parametrized by local generalized thermodynamical potentials and there is only a small (intensive) number of them. If one wishes to not be conservative about the notion of thermal ensembles, e.g., positing that the state be thermal with respect to the Hamiltonian governing the dynamics, then the equilibrium ensembles that we uncover could be viewed as thermal. Indeed, historically in order to accommodate systems exchanging particle numbers grand canonical ensembles parametrized by the chemical potential in addition to the temperature have been considered. Our work shows the necessity of bringing such generalizations one step further due to precisely quantifiable memory effects. However, the number of new thermodynamical potentials is intensive so this step is in a way a natural adjustment of the thermodynamical description rather than a complete overhaul. Thus rather than viewing the generalized Gibbs ensembles to be exotic one could also conceivably view the equilibrium ensembles that we characterize as constituting a thermodynamical framework for the system after relaxation. In that sense we once more come to realize how marvelously flexible the thermodynamic framework turns out to be.

The work presented has reached a certain breadth and it is essentially possible to give a conclusive answer to specific questions of equilibration in the setting at hand. We find that it is not necessary to know the specific values of the initial correlations or of the couplings in the model and as long as our general physical assumptions are fulfilled we can rigorously bound the extent of fluctuations away from equilibrium proving that they are small and decay towards zero in time. At the same time, precisely the observations that allow us to characterize when equilibration does or does not occur allow to pose new exciting directions of future research about the dynamics of systems that are on the verge of not equilibrating.

3.1 FORMULATION OF THE PROBLEM

Following up on the work presented in the previous chapter our challenge was: Prove Gaussification and equilibration after an interaction quench based on physical properties only. Again one needs to be cautious about possible pitfalls when tackling this problem. Firstly, when relying on physical properties such as finite correlation length of the initial state or translation invariance of the quench Hamiltonian one does not work with a particular system but in a way tackles a whole class of models and initial configurations in a single analytical argument. Hence, while it is instructive to consider numerical examples one has to be careful to appropriately generalize the effects observed in calculations and formulate them as conjectures that then can be proven analytically. As the paper will demonstrate there are various counter-examples to equilibration even if Gaussification occurs. Intuitively, if the system is initialized with a distribution of particles involving eigen-modes with large wave-lengths, for example a half-occupied container, then equilibration will be obstructed by large-scale oscillations which persist as the dispersion of the relevant modes is negligible and there is no many-body scattering that would rearrange the mode occupation numbers. Given such observations one is faced with the challenge to formulate general properties that form a sufficient set of assumptions implying equilibration but at the same time the assumptions should not be constraining to set of instances that one can handle. Secondly, after ruling out configurations that are resilient to equilibration the aim is to provide an argument independent of the precise pattern of the initial correlations so that one can speak of the emergence of statistical mechanics at large and not for some particular initial configurations.

3.2 OUR RESULTS

Previous works have allowed to suspect that quite a general result is possible concerning the setting of an interaction quench. Specifically, we have identified the following general physical specification of systems for which equilibration can be proven.

Take a system of non-interacting fermions on a line described by a translation invariant (with periodic boundary conditions) short-ranged Hamiltonian. Assume that the couplings are generic such that there are no points with coinciding roots of the derivatives $E''(p) = E'''(p) = 0$ of the dispersion relation E. Initialize the system in a state with finite correlation length and non-resilient second moments (defined precisely in the paper in relation to linear parts of the spectrum). Then local equilibration occurs according to the following statement.

Theorem 2 (Emergence of statistical mechanics)**.** *There exist a constant relaxation time* t_0 *and a recurrence time* t_{Rec} *proportional to the system size such that for all times* $t \in [t_0, t_{\text{Rec}}]$ *the system locally equilibrates to a Gaussian generalized Gibbs ensemble* $\hat{\rho}^{(\text{eq})}$*, with*

$$|\langle \hat{A} \rangle_{\hat{\rho}(t)} - \langle \hat{A} \rangle_{\hat{\rho}^{(\text{eq})}}| \leqslant C t^{-\gamma}$$

for some $C, \gamma > 0$ *independent of the system size.*

This means that we can set $\epsilon = C t_0^{-\gamma}$ in Eq. (2.1.1) for $t_0 \leqslant t \leqslant t_{\text{Rec}}$ and hence the result shows equilibration to a generalized Gibbs ensemble.

3.3 THE IMPLICATIONS OF THE RESULT

The equilibrium ensemble $\hat{\rho}^{(\text{eq})}$ is a generalized Gibbs ensemble. Moreover, it is parametrized by an *intensive* number of generalized temperatures that scales with the correlation length ξ of the initial state and the thermodynamical potentials involved are exclusively local. These are two defining features of statistical mechanics and indeed are present in our equilibrium ensemble.

The novel feature beyond known non-interacting results [1, 76, 81, 135--139] is that for the first time we show equilibration over a reasonable time in a closed quantum system to occur *generically* within a *class* of models and initial states. Such ubiquitous validity is one of the defining features of statistical mechanics. Roughly speaking, in our case it occurs as a result of translation-invariance of the dynamics, even if the initial state is non-Gaussian and is not translation invariant, as long as it does not have unnatural initial correlations. Note that our argument does without the knowledge of the actual values of the couplings or specific initial configurations of the particles as long as these satisfy our general assumptions. This generality is a crucial feature of statistical mechanics and is to a large degree responsible for its success.

While strong results are possible even in the general interacting case [103, 104, 107, 109, 140--142], deriving a rigorous bound on the equilibration time of the type $\epsilon = O(t^{-\gamma})$ has been elusive so far even in the non-interacting case. By our result equilibration occurs via dynamics generated by non-interacting Hamiltonians according to a power-law in time.

In the main text, we give results for non-interacting fermions even though the same statements hold for non-interacting bosons with a little technical fine-print due to the local Hilbert space being unbounded, and one needs additional assumptions on the correlations as in Ref. [124].

In the paper we present an interesting scenario employing a super-lattice quench which is a possible way for a clear observation of a generalized Gibbs ensemble in an optical lattice experiment. For this, one should start with a thermal system in one-dimension with temperature low enough such that neighboring sites have a distinct correlation. Next, one should double-up the lattice via a quench and let the system evolve according to the nearest-neighbor hopping Hamiltonian in the new lattice. Our prediction is that a steady state will be reached where the nearest-neighbor currents will be missing but there will be other off-diagonal currents which will amount to about half the magnitude of the correlations between nearest-neighbor sites in the lattice prior to the quench. Such a state will be non-thermal because these have dominant nearest-neighbor correlations and we show that they will be missing. The same scenario can be considered when starting from a thermal state in presence of interactions. Ref. [13] presents a new tomographic method for reconstructing off-diagonal current correlations in optical lattices and hence provides a method for observing this effect in an optical lattice quantum simulator.

Finally, it turned out to be necessary to demand that the second-moments be non-resilient in order to prove our results. Engineering the violation of this property allows to construct cases where equilibration takes a long time to occur. The simplest example of a state without this property occurs when particles occupy half of the system and the other half is empty.

3.4 OPEN PROBLEMS

Problem 1. If Gaussification remains intact for a certain time even in the presence of interactions, to what extent does the state equilibrate?

Problem 2. We observed numerically that the steady states of initial thermal states of the Anderson insulator Hamiltonian often do not require non-trivial generalized Gibbs ensembles. Do most thermal Anderson insulators thermalize after quenching to the kinetic energy?

Problem 3. We proposed a way to realize the generalized Gibbs ensemble in an optical lattice quantum simulation experiment. How fast will the state thermalize in the presence of interactions?

Problem 4. Do resilient initial states eventually thermalize, e.g., on average due to a large effective dimension?

Problem 5. The analysis in the appendix shows that non-translation invariant steady states are in principle possible for initial states without a correlation length as a result of the band inversion symmetry $\omega_k = \omega_{L-k}$ where L is the number of sites. Can this effect be ruled out from occurring in physical systems or is it sufficiently robust to be observable?

SciPost Phys. 7, 038 (2019)

Equilibration towards generalized Gibbs ensembles in non-interacting theories

Marek Gluza[1], **Jens Eisert**[1,2,3] **and Terry Farrelly**[4⋆]

1 Dahlem Center for Complex Quantum Systems,
Freie Universität Berlin, 14195 Berlin, Germany
2 Department of Mathematics and Computer Science,
Freie Universität Berlin, 14195 Berlin, Germany
3 Helmholtz-Zentrum Berlin für Materialien und Energie, 14109 Berlin, Germany
4 Institut für Theoretische Physik, Leibniz Universität Hannover, 30167 Hannover, Germany

⋆ farreltc@tcd.ie

Abstract

Even after almost a century, the foundations of quantum statistical mechanics are still not completely understood. In this work, we provide a precise account on these foundations for a class of systems of paradigmatic importance that appear frequently as mean-field models in condensed matter physics, namely non-interacting lattice models of fermions (with straightforward extension to bosons). We demonstrate that already the translation invariance of the Hamiltonian governing the dynamics and a finite correlation length of the possibly non-Gaussian initial state provide sufficient structure to make mathematically precise statements about the equilibration of the system towards a generalized Gibbs ensemble, even for highly non-translation invariant initial states far from ground states of non-interacting models. Whenever these are given, the system will equilibrate rapidly according to a power-law in time as long as there are no long-wavelength dislocations in the initial second moments that would render the system resilient to relaxation. Our proof technique is rooted in the machinery of Kusmin-Landau bounds. Subsequently, we numerically illustrate our analytical findings by discussing quench scenarios with an initial state corresponding to an Anderson insulator observing power-law equilibration. We discuss the implications of the results for the understanding of current quantum simulators, both in how one can understand the behaviour of equilibration in time, as well as concerning perspectives for realizing distinct instances of generalized Gibbs ensembles in optical lattice-based architectures.

Received 17-07-2019
Accepted 29-08-2019
Published 26-09-2019
doi:10.21468/SciPostPhys.7.3.038

Check for updates

Contents

1 Introduction 3

2 Sufficient conditions for local equilibration to a generalized Gibbs ensemble 5
2.1 Notions of equilibration 5

2.2 Statement of the main result 5
2.3 Discussion of the main result 6

3 Class of physical systems considered 7
3.1 Non-interacting fermionic models 7
3.2 Constants of motion 9

4 Power-law equilibration 10
4.1 Strategy of the argument 10
4.2 Definition of non-resilient second moments 12
4.3 Equilibration of non-resilient second moments 13
4.4 Examples of non-resilient second moments 14
4.5 P-periodic initial density distributions and nearest neighbour hopping 15

5 Quasi-free ergodicity 16
5.1 Notions of ergodicity 16
5.2 Gaussification is generic 17

6 Proving Theorem 1 17

7 Numerical results 17
7.1 Quenches of the Anderson insulator to an ergodic translation invariant Hamiltonian 17
7.2 Realizing generalized Gibbs ensembles in optical lattices 20

8 Discussion and outlook 20

A Quasi-free propagators generated by non-interacting Hamiltonians 22
A.1 Bosonic and fermionic lattice models 22
A.2 Circulant matrices 25
A.3 Bessel function asymptotics 27

B Steady states and local conservation laws via circulant matrices 28

C Bound on oscillatory sums of sequences with compact Fourier representation 30

D Quasi-free ergodicity 37

E Equilibration of the covariance matrix 38

F Examples of non-resilient second moments 41
F.1 **m**-step periodic states 41
F.2 Random dislocations 41
F.3 Uniformly random currents 41
F.4 Resilient example: $P = L/2$ - periodic block calculation 42
F.5 Details of quenches from disordered to translation invariant models 43

References 43

1 Introduction

Over more than a century, it has become clear that the methods of statistical mechanics work incredibly well in a vast range of physical situations. But, to this day, a complete understanding of *why* this is the case remains elusive. Based on both experimental and theoretical work, a good deal of progress has already been made [1–6]. Nevertheless, the key objective, finding a set of physical assumptions from which we can demonstrate that quantum systems reach thermal equilibrium, has yet to be achieved. And there are exceptional cases where this simply does not occur, which typically involve the existence of locally conserved quantities.

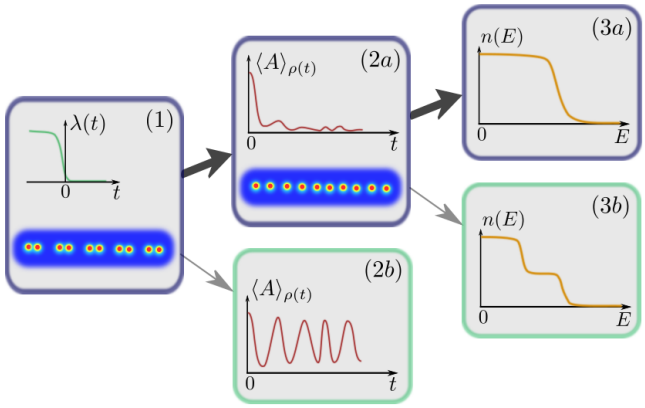

Figure 1: Thermalization and equilibration are often studied in a dynamical quench scenario, where a parameter in the Hamiltonian is suddenly quenched to zero, which knocks the system out of equilibrium (1). The subsequent process of (generalized) thermalization has two components. First, the system must relax to a steady state (2a) with respect to meaningful quantities. Exceptions to this are typically characterized by oscillations, as in (2b). Second, if equilibration occurs, the equilibrium state must be thermal (exemplified here by the Fermi-Dirac distribution in (3a)), or correspond to a generalized Gibbs ensemble (3b) in case further constants of motion are relevant.

The process whereby a system locally relaxes to a thermal state or a generalized Gibbs ensemble (which we call generalized thermalization) can be broken down into two components (see Fig. 1). The first is simply that it equilibrates, meaning the system spends most of the time locally close to some time-independent steady state. This should be true at least for large classes of important observables, e.g., local observables. A crucial aspect (sometimes overlooked) is that the equilibration time for this must be realistic: in experiments, we can observe physical systems relaxing over reasonable times only, which is something that needs to be appreciated. The second component in the case of thermalization is that the equilibrium steady state has no detailed memory of the initial state (beyond, e.g., temperature or chemical potential), namely it is a thermal state.

It has become clear, however, that some specific classes of physical systems do not equilibrate [7–10], at least over the times one can assess in the laboratory. Furthermore, some systems equilibrate but not to a thermal state, instead retaining some memory of the initial state [11–13]. A major distinction arises in this context between non-integrable systems, which indeed are expected to equilibrate to a thermal state, and integrable systems, which are expected not to fully thermalize, but to equilibrate to generalized Gibbs ensembles [14–20]. Many-body localized systems [11,21], in which disorder and interactions interplay in a subtle

manner, can be seen as being reminiscent of the latter systems, as instances of quantum systems which also do not thermalize. In both cases, local (or quasi-local) conserved quantities play a major role. Whenever initial states with inequivalent values of these conserved quantities are experimentally accessible, the resulting steady states will retain a memory of these differences that can be measured. A rigorous *dynamical derivation* of generalized thermalization must therefore overcome several difficulties arising from these observations: we must identify what properties most physical systems have that lead them to thermalize or relax to a generalized Gibbs ensemble.

There are several different theoretical approaches to this challenging long-standing problem. One is to focus on what can be proven for abstract quantum systems with as few assumptions as possible [4, 22–24]. In this case, powerful results have been found, though often without reproducing the relevant equilibration times [25–28]. Another approach is to use randomness to attack the problem [29–34]. Suggestions for the mechanism underlying the relatively fast process of equilibration in the general setting have been offered [35, 36], but a consensus together with more concrete estimates for equilibration times have yet to emerge.

A second approach is to build the analysis on specific physical settings (e.g., the Bose-Hubbard model in the free superfluid regime). But even here there is a dearth of results justifying why the observed times are so short in comparison to the general bounds. Some exceptions in specific cases are, amongst others, presented in Refs. [14, 37, 38]. In particular, studying quenches has been particularly rewarding [39]. In this context, numerical studies often provide useful insights [1–4, 40–48].

In this work, we first analyse quenches of lattice fermions (and – less explicitly – bosons) to non-interacing Hamiltonians. Our first main result is that they locally equilibrate quickly. Two tools we employ are the Kusmin-Landau bound [49] and fermionic Gaussification from Ref. [50]. The latter showed that non-interacting fermions on a lattice locally Gaussify, meaning the state becomes locally indistinguishable from a Gaussian state for relatively long times. However, this Gaussian state may be time dependent. Not only do we show that one of the assumptions of Ref. [50] is unnecessary for Gaussification, but we also show that the Gaussian state that the system approaches will be time independent. This is a proof of equilibration over realistic times for these models, and it also proves that the equilibrium state can be described by a *generalized Gibbs ensemble (GGE)*.

In fact, our work can be seen as a comprehensive rigorous proof of a convergence to generalized Gibbs ensembles, bringing the program initiated in Refs. [14, 19, 51, 52] to an end, by widely generalizing the previous results, while keeping the discussion fully rigorous. We then turn to discussing the question of whether one does indeed need the extra degrees of freedom of a GGE (as opposed to simply a thermal state). We show numerically that initial states corresponding to thermal states of an Anderson insulator equilibrate after quenching the on-site disorder to a thermal state (or grand canonical state), except in cases with highly correlated noise. In this latter case, the equilibrium state must be described by a GGE. It is easy to see that if one has strongly inhomogeneous initial conditions, the equilibration times can be of the order of the system size, see, e.g., Ref. [38]. Finally, we consider some possibilities for realizing distinct instances of generalized Gibbs ensembles in optical lattices and systematically studying their stability in the presence of interactions.

2 Sufficient conditions for local equilibration to a generalized Gibbs ensemble

2.1 Notions of equilibration

A quantum system locally equilibrates if, for all times t between some relaxation time t_0 and some recurrence time t_R, the state at time t is practically indistinguishable from the time-averaged state $\hat{\varrho}^{(\mathrm{eq})}$ with respect to local observables [4]. In other words, the extent of non-equilibrium fluctuations is bounded by some small $\epsilon > 0$ such that for every local observable $\hat{A}$ we have

$$|\langle\hat{A}\rangle_{\hat{\varrho}(t)} - \langle\hat{A}\rangle_{\hat{\varrho}^{(\mathrm{eq})}}| \leq \epsilon \tag{1}$$

for all $t \in [t_0, t_R]$, where $\langle\hat{A}\rangle_{\hat{\varrho}} = \mathrm{tr}[\hat{\varrho}\hat{A}]$. Clearly, whenever a system equilibrates, the equilibrium state must be the infinite time average

$$\hat{\varrho}^{(\mathrm{eq})} = \lim_{T\to\infty} \frac{1}{T}\int_0^T \mathrm{dt}\,\hat{\varrho}(\mathrm{t})\,. \tag{2}$$

While it is highly plausible that systems equilibrate, it is significantly more challenging to identify the equilibration time $t_0 > 0$. When equilibration does indeed occur, a most natural question is how to precisely characterize this equilibrium state. Statistical physics is built upon the assumption that systems equilibrate to a thermal state. The thermal (or Gibbs) state of a quantum system with Hamiltonian $\hat{H}$ is defined to be

$$\hat{\varrho}^{(\beta,\mu)} = \frac{e^{-\beta(\hat{H}-\mu\hat{N})}}{\mathrm{tr}[e^{-\beta(\hat{H}-\mu\hat{N})}]}, \tag{3}$$

where $\beta > 0$ is the inverse temperature, which fixes the value of the expected energy, μ is the chemical potential, which determines the expected particle number, and $\hat{N}$ is the particle number operator. We say that a system with initial state $\hat{\varrho}$ *thermalizes* locally if during the evolution generated by $\hat{H}$ it equilibrates in the sense defined above and if $\hat{\varrho}^{(\mathrm{eq})}$ is locally indistinguishable from the thermal state of $\hat{H}$ (for some value of β and μ). For the case of non-interacting, quasi-free models, thermal states of quadratic Hamiltonians are called Gaussian or quasi-free and are the target equilibrium ensemble upon quenches to quasi-free dynamics.

2.2 Statement of the main result

Our main result is the following. Take a system of non-interacting fermions on a line described by a translation invariant (with periodic boundary conditions) short-ranged Hamiltonian. Assume that the couplings are generic such that there are no points with coinciding roots of the derivatives $E''(p) = E'''(p) = 0$ of the dispersion relation E. Initialize the system in a state with finite correlation length and non-resilient second moments (defined presently). Then local equilibration occurs according to the following statement.

Theorem 1 (Emergence of statistical mechanics)**.** *There exist a constant relaxation time t_0 and a recurrence time t_R proportional to the system size such that for all times $t \in [t_0, t_R]$ the system locally equilibrates to a Gaussian generalized Gibbs ensemble, with*

$$|\langle\hat{A}\rangle_{\hat{\varrho}(t)} - \langle\hat{A}\rangle_{\hat{\varrho}^{(\mathrm{eq})}}| \leq C t^{-\gamma} \tag{4}$$

for some $C, \gamma > 0$ independent of the system size. That is, we can set $\epsilon = C t_0^{-\gamma}$ in Eq. (1) for $t_0 \leq t \leq t_R$.

The equilibrium ensemble $\hat{\varrho}^{(\mathrm{eq})}$ is a generalized Gibbs ensemble. Moreover, it is parametrized by an *intensive* number of generalized temperatures that scales with the correlation length ξ of the initial state and the thermodynamical potentials involved are exclusively local. These are two defining features of statistical mechanics and indeed are present in our equilibrium ensemble. We argue this by invoking the Jaynes' principle of looking for the maximum entropy state given expectation values of quantities of interest. In our case, these are the tunnelling currents $\hat{I}_z$ (defined in detail below) which are quadratic operators, e.g., $\hat{I}_0$ is the mean on-site particle density and $\hat{I}_1$ corresponds to the nearest-neighbour tunnelling. Since the equilibrium ensemble is Gaussian we can also use the property that characterizes these states, namely that they are the maximum entropy states given fixed second moments [50]. Hence fixing the values $\langle \hat{I}_z \rangle$ is a way of specifying a Gaussian state. Say that $\epsilon = C t_0^{-1/6}$ is our desired experimental resolution, and deviations from equilibrium should not be larger than this number. Then within that precision we neglect all the currents with range significantly above the correlation length $z > z_\xi \approx \xi \ln(\epsilon^{-1})$ and aim at reproducing in the equilibrium ensemble $\hat{\varrho}^{(\mathrm{eq})}$ the values of the relevant conserved quantities obtained from the initial state

$$I_z = \langle \hat{I}_z \rangle_{\hat{\varrho}(0)} = \langle \hat{I}_z \rangle_{\hat{\varrho}^{(\mathrm{eq})}} \tag{5}$$

for $z \leq z_\xi$. This condition is met by setting the state to be parametrized as

$$\hat{\varrho}^{(\mathrm{eq})} = Z^{-1} e^{-\sum_{z=0}^{z_\xi} \lambda_z \hat{I}_z} , \tag{6}$$

where $Z > 0$ ensures normalization and λ_z are Lagrange multipliers. Note that for fixed $\epsilon > 0$, e.g., determined by the experimental resolution of the apparatus, only an *intensive* number of generalized temperatures λ_z significantly contributes to the parametrization of this ensemble. It remains to argue that for $z \geq z_\xi$ all correlation functions are smaller than the desired resolution ϵ. By the result in Ref. [53], any one-dimensional thermal state of the type (6) has exponentially decaying correlations with a correlation length bounded by some ξ_A. Hence indeed we recover asymptotically $\langle \hat{I}_z \rangle_{\hat{\varrho}_G^{(\mathrm{eq})}} \sim C_{\mathrm{Clust}} e^{-z/\xi_A} \ll \epsilon$. Here we can identify the chemical potential as $\mu = \lambda_0$ and oftentimes $\beta = \lambda_1$, e.g., in the case of the nearest-neighbour hopping quench Hamiltonian. If we find that $\sum_{z=0}^{z_\xi} \lambda_z \hat{I}_z = \beta \hat{H} + \mu \hat{N}$ where $\hat{H}$ is exactly the quench Hamiltonian and $\hat{N}$ the particle number of operator then we would say that the equilibrium ensemble is *thermal*. Whenever this is not the case then one concludes that relaxation towards a *generalized Gibbs ensemble* (GGE) has taken place.

2.3 Discussion of the main result

The novel feature beyond known non-interacting results [14, 19, 42, 50–52, 54–57] is that for the first time we show equilibration over a reasonable time in a closed quantum system to occur *generically* within a *class* of models and initial states. Such ubiquitous validity is one of the defining features of statistical mechanics. Roughly speaking, in our case it occurs as a result of translation-invariance of the dynamics, even if the initial state is non-Gaussian and is not translation invariant, as long as it does not have unnatural initial correlations. Note that our argument does without the knowledge of the actual values of the couplings or specific initial configurations of the particles as long as these satisfy our general assumptions. This generality is a crucial feature of statistical mechanics and is to a large degree responsible for its success.

Throughout the work, it will be our goal to give intuition that grounds the proof of this result. Let us begin by explaining how equilibration can fail or is physically implausible if any of the ingredients of Theorem 1 is relaxed and therefore other assumptions become necessary. By our result equilibration occurs via dynamics generated by non-interacting Hamiltonians: while

strong results are possible even in the general interacting case [24,25,28,38,58–60], deriving a rigorous bound on the equilibration time of the type $\epsilon = O(t^{-\gamma})$ has been elusive so far. In fact, it may be impossible on grounds of quantum computational complexity [61–64] because equilibrated time-evolution is concomitant to converging results of a quantum algorithm and often the runtime should be longer than polynomial [65].

In the main text, we will present the results for non-interacting fermions even though same statements hold for non-interacting bosons with a little technical fine-print due to the local Hilbert space being unbounded, and one needs additional assumptions on the correlations in Ref. [51]. Concerning geometry, we consider a ring configuration, mostly for the clarity of the argument while of course thermodynamics should not change by the choice of boundary conditions. However, in higher dimensions additional complications could occur as the group velocity, i.e., the derivative of the dispersion relation could vanish along curves instead of separated points [66], but certainly our techniques should generalize when supplemented with additional assumptions that exclude such technical issues. One of the core physical assumptions enabling sufficient scrambling of the initial conditions is translation invariance of the Hamiltonian. Relaxing it, one can find that particles do not propagate and without mixing ergodicity breaks down and with it relaxation. As a prime example, the Anderson insulator model [67] is a non-translation invariant Hamiltonian where equilibration is obstructed due to localization.

Long-ranged non-interacting models can actually violate causality [68,69]. That is to say, if equilibration occurs, then one would need to develop an entirely new intuition for its mechanisms. Here, we assume a short-ranged local Hamiltonian which is already enough to ensure effective causality by means of the Lieb-Robinson bound [70–74]. By additional technical calculation, it should be possible to extend the results to couplings that asymptotically decay exponentially. Note that we consider a closed system described by a static Hamiltonian. If we relax the condition on exponentially decaying correlations then one can consider as the initial state a state evolved backwards to extensively long times which suddenly would acquire "out of nowhere" non-equilibrium dynamics while the system should be expected to be equilibrated.

Finally, it has turned out to be necessary to demand that second-moments of the fermionic state be non-resilient. The simplest example of a state without this property occurs when particles occupy half of the system and the other half is empty. Then for any short-ranged Hamiltonian by the Lieb-Robinson bound it will take extensive times for the particles to even explore the system and equilibration to occur. This property will be precisely stated below in the form of a definition after the necessary notation has been introduced. Summarizing this discussion, trying to establish equilibration one can encounter numerous obstructions, some of them are fundamental difficulties and some are rather technical. In this work we identify precise conditions, mostly concerning locality of couplings and correlations, which are physically very natural and general, and at the same time are sufficient to establish local equilibration with time-scales for a closed quantum system.

3 Class of physical systems considered

3.1 Non-interacting fermionic models

We denote fermionic annihilation operators by $\hat{f}_x$ and will discuss bosons in the appendix. The annihilation operators obey the canonical anti-commutation relations $\{\hat{f}_x, \hat{f}_y^\dagger\} = \hat{f}_x\hat{f}_y^\dagger + \hat{f}_y^\dagger\hat{f}_x = \delta_{x,y}$. Note that any fermionic initial state satisfies the parity superselection rule [75,76], meaning physical states can never involve a superposition of even and odd numbers of fermions. More precisely, we assume that the density operator $\hat{\varrho}$ commutes

with $(-1)^{\hat{N}}$, where $\hat{N} = \sum_{x=1}^{L} \hat{N}_x$ is the total number operator with $\hat{N}_x = \hat{f}_x^\dagger \hat{f}_x$.

A non-interacting fermionic model conserving particle number is characterized by a quadratic Hamiltonian of the form

$$\hat{H}(h) = \sum_{x,y=1}^{L} h_{x,y} \hat{f}_x^\dagger \hat{f}_y \,, \tag{7}$$

where $h = h^\dagger \in \mathbb{C}^{L\times L}$ is the coupling matrix for a finite system size L. By a linear transformation of the fermionic operators preserving the anti-commutation relations, any such Hamiltonian can be brought into diagonal form. Whenever the system is translation invariant then h is *circulant*, and so h can be diagonalized by a discrete Fourier transform. Throughout, we make the assumption that $h \in \mathbb{R}^{L\times L}$ is real, translation invariant and has range R, that is $J_z := h_{1,1+z}$ vanishes for $z > R$ and hence we consider the hopping models of the form

$$\hat{H}(h) = J_0 + \sum_{z=1}^{R} J_z \sum_{x=1}^{L} \hat{f}_x^\dagger \hat{f}_{x+z} + \text{h.c.} \,. \tag{8}$$

By this, we can define the dispersion relation $E : \mathbb{R} \to \mathbb{R}$ as

$$E(p) = J_0 + 2\sum_{z=1}^{R} J_z \cos(pz) \tag{9}$$

and evaluating at $p_k = 2\pi k/L$ we can write the eigenvalues of h as $\omega_k = E(p_k)$ for any finite system size $L > 2R$. Here $E(p)$ is analytic and its derivative can be used to express the dispersion gaps, e.g., $\omega_{k+1} - \omega_k = E'(\tilde{p}_k)2\pi/L$ for some $\tilde{p}_k \in [p_k, p_{k+1}]$ by the mean value theorem. It will be useful to define $J_{\max} = \max_{z=1,\ldots,R} |J_z|$. The Heisenberg evolution of mode operators reads

$$\hat{f}_x(t) = e^{it\hat{H}(h)} \hat{f}_x e^{-it\hat{H}(h)} = \sum_{y=1}^{L} G^*_{x,y}(t) \hat{f}_y \,, \tag{10}$$

where $G^*(t) = e^{-ith}$ is the *propagator* given by

$$G_{x,y}(t) = \frac{1}{L} \sum_{k=1}^{L} e^{i\omega_k t + 2\pi i k(x-y)/L} \tag{11}$$

in the translation invariant case, see Appendix A. The *covariance matrix* is defined as the collection of second moments of a state $\hat{\varrho}$, given by

$$\Gamma_{x,y} = \langle \hat{f}_x^\dagger \hat{f}_y \rangle_{\hat{\varrho}} \,. \tag{12}$$

Observe that physically only the operator $\hat{\Gamma}_{x,y} = \hat{f}_x^\dagger \hat{f}_y$ is not Hermitian and hence not an observable. However, its real and imaginary parts defined as $2\text{Re}[\hat{\Gamma}_{x,y}] = \hat{f}_x^\dagger \hat{f}_y + \hat{f}_y^\dagger \hat{f}_x$ and $2\text{Im}[\hat{\Gamma}_{x,y}] = -i(\hat{f}_x^\dagger \hat{f}_y - \hat{f}_y^\dagger \hat{f}_x)$ are physical observables. Hence, their expectation values can be measured individually in a physical system and then one obtains

$$\Gamma_{x,y} = \frac{1}{2}\langle \hat{f}_x^\dagger \hat{f}_y + \hat{f}_y^\dagger \hat{f}_x \rangle_{\hat{\varrho}} + \frac{i}{2}\langle -i(\hat{f}_x^\dagger \hat{f}_y - \hat{f}_y^\dagger \hat{f}_x) \rangle_{\hat{\varrho}} \,. \tag{13}$$

Note that we consider states with no pairing correlations: $\langle \hat{f}_x^\dagger \hat{f}_y^\dagger + \text{h.c} \rangle = 0$. Our methods can be generalized to that case as well [77,78], but this complicates the presentation. Using (10) we see that the covariance matrix at time t is

$$\Gamma(t) = G(t)\Gamma G(t)^\dagger \,. \tag{14}$$

Of particular relevance for us will be fermionic Gaussian states, which are completely specified by their second moments and Wick's theorem for higher-order correlation functions [77].

To prove many of our results later, we will require that the initial state has exponential decay of correlations, meaning there exist positive constants $C_{\text{Clust}}, \xi > 0$ such that correlations decay like

$$|\langle \hat{A}\hat{B}\rangle_{\hat{\varrho}} - \langle \hat{A}\rangle_{\hat{\varrho}}\langle \hat{B}\rangle_{\hat{\varrho}}| \leq s(\hat{A})s(\hat{B})C_{\text{Clust}}e^{-d/\xi} , \tag{15}$$

where $\hat{A}$ and $\hat{B}$ are observables acting non-trivially only on lattice regions separated by a distance d with sizes $s(\hat{A})$ and $s(\hat{B})$ respectively. For simplicity, we have chosen $\|\hat{A}\| = \|\hat{B}\| = 1$, where $\|\cdot\|$ is the operator norm.

3.2 Constants of motion

What are the relevant constants of motion for translation invariant dynamics? The most obvious candidate consists of momentum occupation numbers

$$\hat{n}_k = \frac{1}{L}\sum_{x,y=1}^{L} e^{2\pi i k(y-x)/L}\hat{f}_x^\dagger \hat{f}_y . \tag{16}$$

Another set of conserved quantities are the *current* operators

$$\hat{I}_z(\eta) = \frac{1}{L}\sum_{x=1}^{L} e^{i\eta}\hat{f}_x^\dagger \hat{f}_{x+z} + \text{h.c.} , \tag{17}$$

where η can in sometimes be interpreted as coming from a magnetic field via Peierls substitution. These are indeed conserved quantities, which follows because they are linear combinations of the momentum occupation numbers. The following two extreme cases are important $\hat{I}_z(\eta = 0) = (2/L)\sum_{k=1}^{L}\cos(2\pi kz/L)\hat{n}_k$, cf. e.g. [79] and for $\hat{I}_z(\eta = \pi/2) = -(2/L)\sum_{k=1}^{L}\sin(2\pi kz/L)\hat{n}_k$. For the latter type of currents to be *present* it is necessary that the covariance matrix as defined above is not real.

The current operators allow us to judge how many conserved quantities are really necessary to describe the steady state with finite experimental resolution ϵ. Due to the exponential decay of correlations Eq. (15), we have $|\langle \hat{I}_z\rangle| \leq C_{\text{Clust}}e^{-z/\xi}$, and so $|\langle \hat{I}_z\rangle| \leq \epsilon$ for $z \geq \xi \ln(C_{\text{Clust}}/\epsilon)$. So there are only $z \sim \xi$ non-negligible values of $\langle \hat{I}_z\rangle$ which constitute the only relevant local conserved quantities. Thus, whenever equilibration occurs, then the equilibrium ensembles of any set of non-local momentum occupation numbers $\{\langle \hat{n}_k\rangle\}$ with the same current content will agree.

For initial states $\hat{\varrho}(0)$ with short range correlations we prove in the appendix, assuming minimal degeneracy of the dispersion relation ω_k, that the steady-state obtained from the infinite-time average $\Gamma^{(\infty)}_{x,y}$ is translation invariant up to a small parameter

$$\left|\Gamma^{(\infty)}_{x,y} - \Gamma^{(\text{eq})}_{x,y}\right| \leq C_I L^{-1} , \tag{18}$$

where C_I is independent of the system size. We can define the equilibrium values by a real-space *average*

$$\Gamma^{(\text{eq})}_{x,y} = \frac{1}{L}\sum_{z=1}^{L}\Gamma_{x+z,y+z} . \tag{19}$$

We then can find the Peierls angle by setting $\eta_z = \arg[\Gamma^{(\text{eq})}_{1,z}]$. By this, we find that our target equilibrium ensemble has matrix elements which agree with the *initial* expectation value of the conserved operator

$$I_{|x-y|} = \Gamma^{(\text{eq})}_{x,y} = \cos(\eta_{|x-y|})\langle \hat{I}_{|x-y|}(0)\rangle_{\hat{\varrho}(0)} + i\sin(\eta_{|x-y|})\langle \hat{I}_{|x-y|}(\pi/2)\rangle_{\hat{\varrho}(0)} . \tag{20}$$

Here and throughout whenever x, y are positions on the chain then $|x-y|$ is meant in the sense of the distance on the ring geometry. Note that due to the average the equilibrium covariance matrix and hence also $\hat{\varrho}_G^{(\mathrm{eq})}$ will be translation invariant which implies that the current operators can be evaluated by a strictly local measurement. For example if the initial covariance matrix is real then $\eta = 0$ and we have

$$I_{|x-y|} = \langle \hat{I}_{|x-y|} \rangle_{\hat{\varrho}_G^{(\mathrm{eq})}} = \langle \hat{f}_x^\dagger \hat{f}_y \rangle_{\hat{\varrho}_G^{(\mathrm{eq})}} + \mathrm{h.c.}\,, \tag{21}$$

where x, y can be chosen arbitrarily as long as their separation is $d = |x-y|$.

4 Power-law equilibration

4.1 Strategy of the argument

Our goal in this section is to bound how quickly time-evolved second moments $t \mapsto \Gamma_{x,y}(t)$ relax towards the time-averaged value. The culmination of this is a bound of the form

$$\left| \Gamma_{x,y}(t) - \Gamma_{x,y}^{(\mathrm{eq})} \right| \leq C_\Gamma t^{-\gamma}\,, \tag{22}$$

where $C_\Gamma, \gamma > 0$ are constants independent of the system size. Let us begin by defining the decomposition of the covariance matrix Γ into its currents $\Gamma^{(d)}$ with entries

$$\Gamma_{x,y}^{(d)} = \Gamma_{x,y}\delta_{x,y+d}\,, \tag{23}$$

where we use the convention $\delta_{a,b+L} = \delta_{a,b}$. Intuitively, one can find $\Gamma^{(d)}$ by picking out bands from Γ parallel to the diagonal and we will show that each band equilibrates individually to the conserved current value I_d using that the evolution is linear in the bands $\Gamma(t) = \sum_{d=-\lfloor (L+1)/2 \rfloor + 1}^{\lfloor L/2 \rfloor} \Gamma^{(d)}(t)$. Now we expand $\Gamma^{(d)}$ via the discrete Fourier transform

$$\Gamma_{z+d,z} = \sum_{n=1}^{L} \mathcal{X}_n^{(d)} e^{2\pi i n z/L}\,. \tag{24}$$

Here $\mathcal{X}_n^{(d)}$ are defined implicitly by the inverse discrete Fourier transform and the most important one is

$$\mathcal{X}_{n=L}^{(d)} = \frac{1}{L}\sum_{x=1}^{L} \Gamma_{x,x+d} = \Gamma_{x,y}^{(\mathrm{eq})}\,, \tag{25}$$

which is the equilibrium value. After a technical calculation we obtain

$$\Gamma_{x,y}^{(d)}(t) = \sum_{n=1}^{L} \mathcal{X}_n^{(d)} e^{2\pi i n(x-d)/L} f_n(t)\,, \tag{26}$$

with

$$f_n(t) = \frac{1}{L}\sum_{k=1}^{L} e^{i(\omega_{(k+n)} - \omega_k)t + 2\pi i s(x-y-d)/L}\,. \tag{27}$$

This step is of crucial importance. We have separated out a dynamical function f_n which, when it decays, does so independent of the initial state – or colloquially speaking, it scrambles the initial state. To prove our result, we show in Appendix C that f_n dephases in time

$$|f_n(t)| \leq C_\# \left(\frac{n\pi}{L}\right) t^{-\gamma}\,, \tag{28}$$

with some constant $\gamma > 1/(6R+6)$. Here, one should note that $C_\#(n\pi/L)$ will be constant in time but could depend on the system size. Indeed for $n \approx 1$ we will have $C_\#(n\pi/L) \sim L^2$. However, we will see that this is not an artefact of the technique that we use to obtain the bound (28) – points n with constant larger than some threshold $C_\#(n\pi/L) > C_{\text{th}}$ are *resilient points* where f_n dephases slowly and will be discussed in detail below. In the end $C_\#$ has a simple form and it does not scale in the system size for very many natural initial configurations.

In order to derive the bound from Eq. (28), we will study the *phase function* $\Phi_{t,\alpha} : [0, 2\pi) \to \mathbb{R}$ defined as

$$\Phi_{t,\alpha}(p) = Dp - 4t \sum_{z=1}^{R} J_z \sin(z\alpha) \sin(zp + z\alpha) \,. \tag{29}$$

Choosing $D = 2\pi(x - y + d)/L$ and $\alpha = \pi n/L$ we have

$$f_n(t) = \frac{1}{L} \sum_{k=1}^{L} e^{i\Phi_{t,\alpha}(2\pi k/L)} \,. \tag{30}$$

This relation (30) is called an exponential sum and its dephasing is instrumental for the state to dephase itself. In order to bound it, we make use of the *Kusmin-Landau technique* [49]. This powerful machinery allows to arrive at quantitative bounds as opposed to intuitive estimates obtained from stationary phase approximations [80, 81]. The crux of this method is, however, similar – dephasing is determined by the *gaps* of ω or specifically by the first derivative of Φ. By analyzing the dispersion relation E, we find a lower bound to the gaps by appropriate Taylor expansions. The bound is then determined by the values of the derivatives of Φ at points that one could view as stationary points. We define

$$\mathcal{S}_\alpha^{(1)} = \{p \in [0, 2\pi] \text{ s.t. } \Phi'_{t,\alpha}(p) = 0\} \,, \tag{31}$$

and correspondingly

$$\mathcal{S}_\alpha^{(2)} = \{p \in [0, 2\pi] \text{ s.t. } \Phi''_{t,\alpha}(p) = 0\} \tag{32}$$

for the second derivative. Due to the finite range R of the Hamiltonian, there are at most $2R+2$ stationary points, which we prove in the appendix. While in the appendix we prove a more general statement, here we discuss the generic case only where we assume that there are no points such that $\Phi''_{t,\alpha}(p) = \Phi'''_{t,\alpha}(p) = 0$. Hence, for any first order root $r \in \mathcal{S}^{(1)}$ we either have $\Phi''_{t,\alpha}(r) \neq 0$ or $\Phi'''_{t,\alpha}(r) \neq 0$. For the Taylor expansion we want to take the value of the minimal derivative that does not vanish at r so we take $\kappa_r = 1$ if $\Phi''_{t,\alpha}(r) \neq 0$ and otherwise we set $\kappa_r = 2$. In Appendix C we show a more general statement, but in the generic case we simply have

$$\gamma = 1/3 \tag{33}$$

and

$$C_\#(\alpha) = 6(2R+1) \max\{1, 8R^4 J_{\max}/M_\alpha^2\} \,, \tag{34}$$

where we define the minimal derivative value used for lower bounding dephasing through a Taylor expansion

$$M_\alpha = \frac{1}{t} \min\left\{ \min_{r \in \mathcal{S}^{(1)}} \left| \Phi_{t,\alpha}^{(\kappa_r+1)}(r) \right|, \min_{r \in \mathcal{S}^{(2)}} \left| \Phi'''_{t,\alpha}(r) \right|^2 \right\} \,. \tag{35}$$

Note that this constant is time independent hence the time scaling is governed by the smallest next order derivative which does not vanish at a stationary point.

Hence, as proved in Appendix C, we obtain a bound on the dephasing of the form (28), which is a huge simplification as the bound is now encoded in the minimal value of derivatives at stationary points which is a sparse set. As an example, let us study M_α of $\hat{H}(h)$ with only one non-trivial coupling value $J_1 \neq 0$. Then we have the simplification

$$\Phi'_{t,\alpha}(p) = D - 2tJ_1 \sin(\alpha)\cos(p+\alpha)\,. \tag{36}$$

Then we find that $\mathcal{S}^{(1)}$ has at most 2 roots and we should evaluate the value of the second derivative at these points

$$\Phi''_{t,\alpha}(p) = 2tJ_1 \sin(\alpha)\sin(p+\alpha)\,. \tag{37}$$

Now, we notice that for $n \approx 0$ we have $\alpha = n\pi/L \approx 0$ which means that $M_\alpha \sim \alpha \sim L^{-1}$ and hence $C_\# \sim L^2$ becomes size dependent. In this case $C_\#$ can be independent of the system size only if n is a significant fraction of L. However, inspecting (27) for $\alpha = n\pi/L \approx 0$ we find that it will in fact not dephase for the same reason that our bound yields a large $C_\#(\alpha)$ constant as we have

$$f_n(t) \approx \frac{1}{L}\sum_{k=1}^{L} e^{2\pi i k(x-y+d)/L} \tag{38}$$

for times $t \ll L$. Therefore we would need times t scaling in the system size for dephasing to even set in – this is an effect that we call *resilience*.

4.2 Definition of non-resilient second moments

Choosing the initial state such that Γ has substantial $\mathcal{X}_n^{(d)}$ around a resilient point will render the covariance matrix resilient against equilibration. This should be expected and has been discussed in the literature [2] with the simplest example being a system with a linear dispersion relation. By Eq. (9) we see that generically we will find regions in momentum space where the dispersion relation is indeed approximately linear and populating the initial state with quasiparticles from these regions will obstruct dephasing. More generally, resilience to equilibration can be characterized within the framework of resource theories [82]. Here, we have enough structure to be able to phrase a sufficient condition for correlations to be non-resilient using the above intuition.

Definition 2 (Non-resilient second moments). *For a threshold constant $C_{\text{th}} > 0$ independent of the system size L we call points in*

$$\mathcal{R} = \{\alpha \in (0,\pi)\ s.t.\ C_\#(\alpha) \geq C_{\text{th}}\} \tag{39}$$

resilient. If for all d there exist constants $C_{RS}, C_{NRS} > 0$ independent of the system size such that the distribution $\mathcal{X}$ has little weight at resilient points

$$\sum_{\frac{n\pi}{L}\in\mathcal{R}} \left|\mathcal{X}_n^{(d)}\right| \leq C_{RS}L^{-1} \tag{40}$$

and is bounded outside

$$\sum_{\frac{n\pi}{L}\notin\mathcal{R}} \left|\mathcal{X}_n^{(d)}\right| \leq C_{NRS}\,, \tag{41}$$

then we say that the correlations Γ are non-resilient second moments at the level C_{th}.

The crucial mathematical feature of this definition that is needed to ensure equilibration is the system size independence of the constants such that constants derived in further bounds are also system size independent. Notice that in the definition of $\mathcal{R}$ we exclude $\alpha = \pi$ which corresponds to $\Gamma^{(\mathrm{eq})}_{x,x+d} = I_d = \mathcal{X}^{(d)}_{n=L}$ which is a constant of motion. In the following we will bound the deviation from equilibrium $|\Gamma_{x,y}(t) - \Gamma^{(\mathrm{eq})}_{x,y}|$ and hence this definition can be thought of as defining initial conditions that are non-resilient to equilibration towards *translation invariant* steady states.

4.3 Equilibration of non-resilient second moments

We can easily see that with this definition, we can give a bound as to how fast individual currents (26) relax as long using the bound (28) where now we have the promise that $C_{\#} \leq C_{\mathrm{th}}$. Indeed, at the resilient points we can use a trivial upper bound $|f_n(t)| \leq 1$, to obtain

$$\left|\Gamma^{(d)}_{x,y}(t) - I_d \delta_{x,y+d}\right| \leq C_{\mathrm{RS}} L^{-1} + C_{\mathrm{NRS}} C_{\mathrm{th}} t^{-\gamma} \tag{42}$$

$$\leq C^{(d)}_{\Gamma} t^{-\gamma}\,, \tag{43}$$

where in the second line we used $t \leq t_R = \Theta(L)$. By the decay of correlations only currents with range of the order of the correlation length $d_\xi(t) = \xi \ln(t^\gamma)$ will be relevant. In the appendix we show using the unitarity of the propagator that

$$\sum_{d=d_\xi(t)}^{\lfloor L/2 \rfloor} \left|\Gamma^{(d)}_{x,y}(t)\right| \leq \frac{C_{\mathrm{Clust}}}{1 + e^{-1/\xi}} t^{-\gamma}\,, \tag{44}$$

and hence one easily arrives at a bound for fluctuations of the covariance matrix entries away from equilibrium

$$\begin{aligned}\left|\Gamma_{x,y}(t) - \Gamma^{(\mathrm{eq})}_{x,y}\right| &\leq \sum_{d=-\lfloor (L+1)/2 \rfloor + 1}^{\lfloor L/2 \rfloor} \left|\Gamma^{(d)}_{x,y}(t) - I_d \delta_{x,y+d}\right| \\ &\leq C_\Gamma t^{-\tilde{\gamma}},\end{aligned} \tag{45}$$

where C_Γ is obtained by appropriately collecting the system size independent constants and $\tilde{\gamma} \approx \gamma$ is chosen such that $\ln(t^\gamma) t^{-\gamma} \leq t^{-\tilde{\gamma}}$ for all times of interest $t_0 \leq t \leq t_R$. The following proposition encapsulating these ideas is proven in full detail in Appendix E.

Proposition 3 (Equilibration of second moments)**.** *Consider a fermionic system with initially exponentially decaying correlations and non-resilient second moments* Γ*. Then there exist a constant relaxation time* t_0 *and a recurrence time* $t_R = \Theta(L)$ *such that, for all* $t \in [t_0, t_R]$*,*

$$\left|\Gamma_{x,y}(t) - \Gamma^{(\mathrm{eq})}_{x,y}\right| \leq C_\Gamma t^{-\gamma}\,, \tag{46}$$

where $C_\Gamma, \gamma > 0$ *are constants.*

As we will see, this general bound must have $\gamma \leq 1/2$ by giving a specific example with a tight relaxation scaling via the Bessel function asymptotics. On the other hand, we have that the exponent is lower bounded due to $\gamma \geq 1/(6R) - \varepsilon$ for any $\varepsilon > 0$, as explained in Appendix E.

4.4 Examples of non-resilient second moments

As the simplest example of non-resilient second moments, consider the covariance matrix $\Gamma^{(0,1)}$ of the charge-density wave corresponding to the Fock state vector $|0,1,0,1,\ldots\rangle$ which will equilibrate under the nearest-neighbour model. More generally, if there is no shift symmetry of the dispersion relation any P-periodic configuration of currents will be non-resilient for intensive P not scaling in the system size, see Appendix F. This continues to hold true even in the presence of sparse defect sites at random points. This is the most important case and captures the intuition about what physically one should expect to be necessary for equilibration, namely that the mass distribution (and concomitantly currents) are already distributed over the system, albeit with possibly intensive random configurations at microscopic scales.

On the other hand, a P-periodic state with extensive P will be resilient and not relax towards a translation invariant steady state according to a power-law. Specifically, second moments of the form $\Gamma_{x,x} = 1$ for $x \leq L/2$ and all other entries vanishing are resilient. Intuitively this is a block of particles over an extensive part of the system and is resilient because by the Lieb-Robinson bound one would need to wait to extensively long times for the current to become evenly distributed. Such a covariance matrix would violate our definition of non-resilient second moments already on the level of $\mathcal{X}_n^{(d)}$, see Appendix F. Let us finally remark that the definition of non-resilient second moments has a linear structure and mixtures of different P-periodic covariance matrices $\Gamma^{(P)}$ are again non-resilient, as long as the weights decay fast enough, i.e.,

$$\Gamma^{(\mathrm{Mixt})} = \sum_P a_P \Gamma^{(P)} \tag{47}$$

can be non-resilient for various weights a_P.

If we would like to quantify the resilience in the generic case, we may neglect physical constraints on the covariance matrix and choose $\Gamma_{x,y}^{(\mathrm{rnd})} \in [a,b]$ uniform at random. In this case, we will indeed find non-resilience on average $\mathbb{E}[\mathcal{X}_n^{(d)}] = (a+b)\delta_{n,L}/2$. However, the fluctuations are rather large as we find $\mathrm{Var}[\mathcal{X}_n^{(d)}] = (a-b)^2/(12L)$, so drawing a random selection from the uniform distribution will often yield a significant number of the L-many harmonics to be of the order $(X_n^{(d)})^2 \sim \mathrm{Var}[\mathcal{X}_n^{(\mathrm{rnd},d)}] \sim L^{-1}$ which is too large and could lead to resilience. Yet, constructing a mixture of such matrices can smoothen the distribution and so for $\Gamma = \sum_{k=1}^K \Gamma^{(\mathrm{rnd}:k)}/K$, we should find $\mathcal{X}_n^{(d)} \approx \mathbb{E}[\mathcal{X}_n^{(d)}]$ up to fluctuations decaying $K^{-1/2}$, i.e., one can get closer to the average behaviour which is non-resilient. Observe, that by Eq. (27) dephasing could also occur if the Fourier weights $\mathcal{X}_n^{(d)}$ are larger than what we allow for in Definition 2 if they fluctuate uniformly on the scale where $f_n(t)$ does not change strongly. Later, in order to discuss equilibration of a random selection of second moments, which are physically admissible and have a finite correlation length, we will discuss thermal states of the Anderson insulator – numerically we indeed find equilibration in that case too.

Finally, note that our definition of non-resilient second moments characterizes initial states that equilibrate to translation invariant steady states. However, it is important to note that non-translation invariant steady states can also occur – due to possible shift symmetries of the dispersion relation such that we have $\omega_k = \omega_{k+n}$ for all $k = 1,\ldots,L$. The simplest example is to notice that $\omega_k = \omega_{k+L/2}$ for the next-nearest-neighbour model so then $f_{L/2}(t) = \mathtt{const}$. In this case, our definition of non-resilient second moments excludes any Γ which has significant $\mathcal{X}_n^{(d)}$ for $n \approx L/2$ via the condition on the $C_\#(n\pi/L) \leq C_{\mathrm{th}}$ constant. These are very special cases, see Fig. 2 and we have chosen to study equilibration exclusively towards translation invariant steady states. Notably, the nearest-neighbour model has no shift symmetry hence only states with long-range dislocations, or a population of long-wavelength quasiparticles are being excluded by the definition of non-resilience.

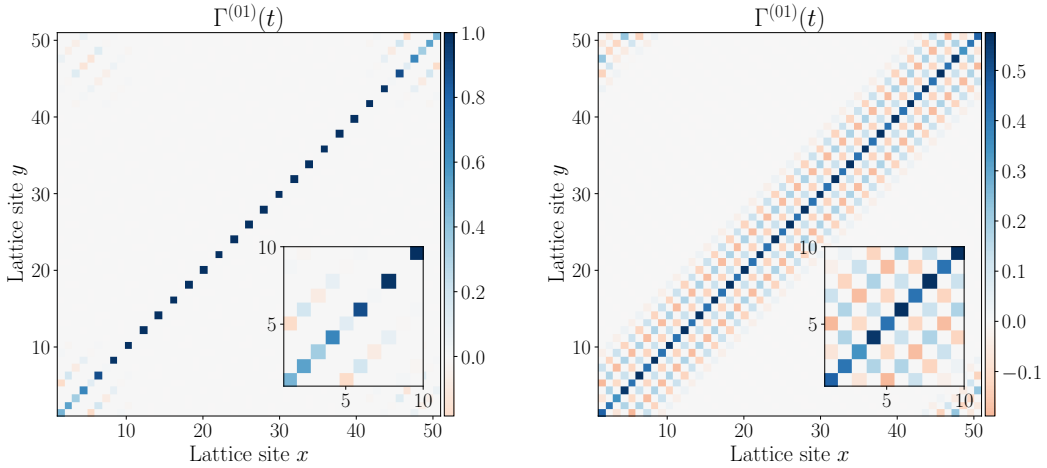

Figure 2: Covariance matrix of a charge-density wave $\Gamma^{(0,1)}$ which corresponds to the Fock state vector $|0,1,0,1,\ldots\rangle$ has varying equilibration behaviour depending on the locality of the Hamiltonian and the system size parity. For the next-nearest-neighbour model the system in this special initial state splits up into two independent sub-lattices and is in an exact steady state whenever the system size L is even. However, for odd L the symmetry of the density distribution is incommensurate with the system size and there is necessarily a defect of the type $|\ldots,0,1,0,0,1,\ldots\rangle$ or $|\ldots,1,0,1,1,0,1,\ldots\rangle$ around which the charge-density wave pattern starts becoming homogeneous. Note, that away from the defect point the charge-density wave looks locally like a steady state of the Hamiltonian and one can prove by the LR bounds that the middle region will remain unaffected for extensively long times. The left plot shows $\Gamma^{(0,1)}(t=1.5)$ after a quench to the next-nearest-neighbour model (the inset throughout shows the sub-block of the first 10 sites). On the other hand, if we quench to the nearest-neighbour model then there is no transient symmetry present and the charge-density wave is completely non-resilient and homogeneously tends towards equilibrium as seen in the right plot for the same initial state.

4.5 P-periodic initial density distributions and nearest neighbour hopping

A specifically instructive case is to study the situation in which the initial state is such that the covariance matrix is diagonal with a P-periodic structure, and the system is quenched to evolve via the nearest neighbour hopping model. This means that the density distribution repeats every P sites in that $\Gamma_{x,x} = \Gamma_{x+P,x+P}$ for all x. It is one of the strengths of our result that we need not care about the structure within the block because any such distribution for an intensive P is non-resilient. The steady state will be translation invariant and diagonal with the second moments given by $\Gamma^{(\mathrm{eq})}_{x,y} = \delta_{x,y}/F$ where $1/F$ is the filling ratio. For example, if the initial covariance matrix was $\Gamma^{(1,0)} = \mathrm{diag}(1,0,1,0,\ldots)$, then we have half-filling $1/F = 1/2$ and for $\Gamma^{(1,0,0)} = \mathrm{diag}(1,0,0,1,0,0\ldots)$ we get $1/F = 1/3$. When considering the evolution under a nearest-neighbour fermionic hopping Hamiltonian, and such initial conditions, we find that the propagator follows a law $O(t^{-1/2})$ in time, as laid out in Appendix A.3, dictated by the asymptotics of Bessel functions of the first kind. This decay is inherited by the actual correlation decay, in that for any P-periodic initial condition, one finds that

$$|\Gamma_{x,y}(t) - \Gamma^{(\mathrm{eq})}_{x,y}| = O(t^{-1/2}) \tag{48}$$

for all x, y. It is also interesting to note that the resulting steady states can be seen as an *infinite temperature Gibbs state* at a specific chemical potential which imposes the value of the

total particle number. Specifically, one finds for the equilibrium covariance matrices

$$\Gamma^{(\mathrm{eq})}_{x,y} = \frac{1}{1+e^{-\mu}}\delta_{x,y}\ , \tag{49}$$

from which one can obtain the value of the chemical potential in explicit form $\mu = -\ln(F-1)$ for any x, y due to translation invariance.

5 Quasi-free ergodicity

5.1 Notions of ergodicity

One of the key questions of statistical mechanics is what precise properties of the Hamiltonian governing the dynamics can be held responsible for the emergence of aspects of quantum statistical mechanics. In classical mechanics it results from sufficient transport properties which is evident already in Boltzmann's H-Theorem. In the quantum regime for free systems, a notion with similar operational meaning can also be identified, namely that propagators decay quickly, which holds with surprising generality and can be interpreted as a lower bound to particle transport.

Theorem 4 (Free fermionic ergodicity)**.** *Let $t \mapsto G(t)$ be the propagator for a non-interacting translation invariant fermionic Hamiltonian $\hat{H}(h)$ which is off-diagonal on the one-dimensional real-space lattice. Then for all times t between a relaxation time $t_0 = O(1)$ up until a recurrence time $t_R = \Theta(L)$ the propagator obeys*

$$|G_{x,y}(t)| \leq C t^{-\gamma}\ , \tag{50}$$

where $C, \gamma > 0$ are constants. We can take $\gamma = 1/3$, provided there are no points p such that $E''(p) = E'''(p) = 0$ which is true for generic models.

We can interpret Theorem 4 as proving free-particle ergodicity for these models. This notion of ergodicity is motivated by the classical notion of ergodicity, which states that an ergodic system essentially explores the whole available phase space, and it does so homogeneously. In free systems, we have to respect the linear constraint in the relation (10) at all times and given that, the suppression (50) allows to show that the particles must spread over the lattice. Indeed unitarity of the propagator $\sum_{y=1}^{L} |G_{x,y}(t)|^2 = 1$ implies that a particle initially at site x must occupy at least $O(t^{2\gamma})$ sites. If for most sites the bound is not tight, then the particle must have spread to an even larger region. Indeed, whenever the spatial separation $d = x - y$ is far away from a ballistic wavefront, typically found in free translation invariant systems, then our proof can be used to obtain $\gamma = 1/2$ which would imply that the particle spreads homogeneously over a region of size $O(t)$. Note that our bound is independent of d and hence $\gamma = 1/3$ is necessary and reflects the scaling at the wavefront [50]. Conversely, in localized systems such as Anderson insulators, particles cannot spread freely and typically $|G_{x,y}(t)| \leq Ce^{-|x-y|/\ell_0}$ which together with the unitarity of the propagator can be used to show that $\sum_{x=y-\ell_0}^{y+\ell_0} |G_{x,y}(t)| > O(1)$ for all times, i.e., particles cannot spread by more than the localization length ℓ_0. The proof of Theorem 4 is given in Appendix D and is again based on Kusmin-Landau inequality [49]. It could be also of general interest as a method for deriving error-bars for stationary phase arguments in field theory. Note that one can explicitly calculate the relaxation time and the recurrence time, t_0 and t_R, using only the dispersion relation.

5.2 Gaussification is generic

Combining the above results with insights from Ref. [50] lead to a remarkably strong result. Ref. [50] presented results on how non-interacting fermionic quantum systems that show delocalizing transport would "Gaussify", that is, turn to a quantum state that is Gaussian to an arbitrarily good approximation in time. However, Theorem 4 shows precisely this: Non-interacting one-dimensional models generically exhibit delocalizing transport. We hence arrive at a statement of a rigorous convergence to a generalized Gibbs ensemble with enormous generality. When stating this Gaussification theorem, we define the state $\hat{\varrho}_G(t)$ to be a Gaussian state with the same covariance matrix as $\hat{\varrho}(t)$.

Theorem 5 (Fermionic generic Gaussification)**.** *Consider the initial fermionic state $\hat{\varrho}(0)$ with exponential decay of correlations and a non-interacting translation-invariant post-quench Hamiltonian with dispersion relation $E(p)$ such that there are no points with $E''(p) = E'''(p) = 0$ for any p. Then there exist a constant relaxation time t_0 and a recurrence time $t_R = \Theta(L)$ such that, for all $t \in [t_0, t_R]$,*

$$|\langle \hat{A} \rangle_{\hat{\varrho}(t)} - \langle \hat{A} \rangle_{\hat{\varrho}_G(t)}| \leq C t^{-1/6} \,, \tag{51}$$

where $C > 0$.

6 Proving Theorem 1

In this section we collect all our findings that lead to the statement of Theorem 1. Within the setting described above the two crucial ingredients are an initial state featuring exponentially decaying correlations and the quench Hamiltonian being translation invariant. By Theorem 5, we have that at a sufficiently large time any local correlation function can be approximated by the value obtained from the Gaussified state. That is, it suffices to take the second moments Γ of the initial state $\hat{\varrho}(0)$, evolve them according to the quench Hamiltonian and evaluate $\langle \hat{A} \rangle_{\hat{\varrho}(t)}$ by appropriately employing Wick's theorem for $\Gamma(t)$. We hence find equilibration $\langle \hat{A} \rangle_{\hat{\varrho}(t)} \approx \texttt{const}$ if $\Gamma(t) \approx \texttt{const}$ is time independent. This is already the case if we perform the quench starting from a translation-invariant non-Gaussian state because then the covariance matrix Γ is also translation invariant and so $\Gamma(t) = \Gamma(0)$ because $\partial_t \Gamma(t) = i[h, \Gamma(t)] = 0$. For such cases Gaussification is sufficient for equilibration [50]. However, thanks to Proposition 3 we obtain a much more general statement. Namely, any non-resilient covariance matrix will equilibrate. This result applies to very natural initial conditions that can dramatically deviate from a homogenous configuration. The relaxation takes the form of a power law $O(t^{-1/6})$ determined by the Gaussification times. This, however, is an artifact of our rigorous uniform bounds – one should expect the calculation for a special configuration from Refs. [42, 54] to be generic $O(t^{-1/2})$. A proof of such a behaviour being the standard time-scale may be possible but would involve a significantly more detailed treatment of the wavefront which is responsible for our scalings not being tight as compared to the behaviour in the bulk of the Lieb-Robinson cone [50].

7 Numerical results

7.1 Quenches of the Anderson insulator to an ergodic translation invariant Hamiltonian

As a numerical illustration, in this section, we discuss the situation arising from starting in the thermal state of a disordered Anderson insulator, initially not translation invariant, followed

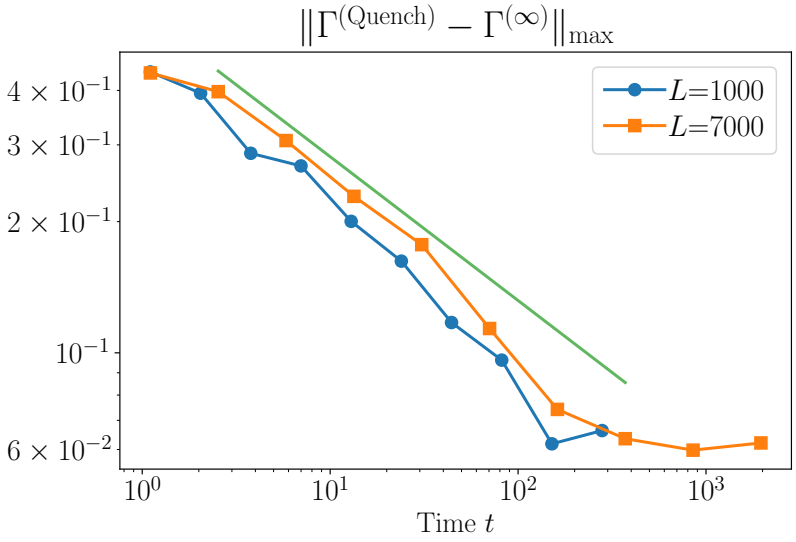

Figure 3: We have sampled a thermal state of the Anderson insulator $\Gamma^{(\mathrm{Quench})}$ for system sizes $L = 1000, 7000$ at $\beta = 1$ and $w = 5$ as an example of a strongly disordered initial condition. We find that after switching off the on-site disorder the ensuing non-equilibrium evolution under the nearest-neighbour hopping model leads to relaxation towards the infinite-time average $\Gamma^{(\infty)}$ which is indeed quantified in the functional form by a power-law in time $\|\Gamma^{(\mathrm{Quench})} - \Gamma^{(\infty)}\|_{\max} \sim t^{-\alpha}$. The green line is a guide to the eye scaling as $\sim t^{-1/3}$. At some point, the power-law relaxation must level off either due to finite system size, with the ultimate small parameter being $\epsilon \sim t_{\mathrm{R}}^{-\alpha} \sim L^{-\alpha}$, or due to the specific quasiparticle content $\mathcal{X}^{(d)}$.

by a quench to a perfectly translation invariant ergodic hopping Hamiltonian. Needless to say, the equilibrium states emerging are once again generalized Gibbs ensembles and Gaussian states: It is interesting to note, however, that they resemble fully thermal states with high probability to a rather good approximation.

To be specific, as a starting point we choose an initial covariance matrix which is not translation invariant and has a finite correlation length. A natural way of assigning such initial conditions is to consider a Gibbs state of the Anderson insulator with Hamiltonian

$$\hat{H}_\xi = \sum_{x=1}^{L} \left(\hat{f}_{x+1}^\dagger \hat{f}_x + \hat{f}_x^\dagger \hat{f}_{x+1} + \xi_x \hat{f}_x^\dagger \hat{f}_x \right), \tag{52}$$

where the noise is uniformly distributed in the interval $\xi_x \in [-w, w]$ for $w > 0$. We study the quench consisting in switching off the disorder, i.e., setting $\xi_x = 0$ for all x. Following a numerical calculation, the quenched state $\Gamma^{(\mathrm{Quench})}(t) = \Gamma^{(\beta,\mathrm{Anderson})}(t)$ can be seen to become largely homogeneous for sufficiently long duration of the evolution, see Fig 3. As a measure of equilibration, we make use of the max norm distance

$$\|\Gamma^{(1)} - \Gamma^{(2)}\|_{\max} = \max_{x,y} \left| \Gamma^{(1)}_{x,y} - \Gamma^{(2)}_{x,y} \right| \tag{53}$$

between two covariance matrices $\Gamma^{(1)}, \Gamma^{(2)}$. Whenever $\|\Gamma^{(1)} - \Gamma^{(2)}\|_{\max}$ is small, a large fidelity between the two states is implied [83, 84]. Fig. 3 provides further substance to the above established rigorous insights, in that a significant part of the equilibration is indeed governed by a power-law by comparing $\Gamma^{(\mathrm{Quench})}(t)$ to the infinite time average $\Gamma^{(\infty)}$. To further elaborate on this setting, we discuss the features of the equilibrium state, see Fig. 4. We begin by

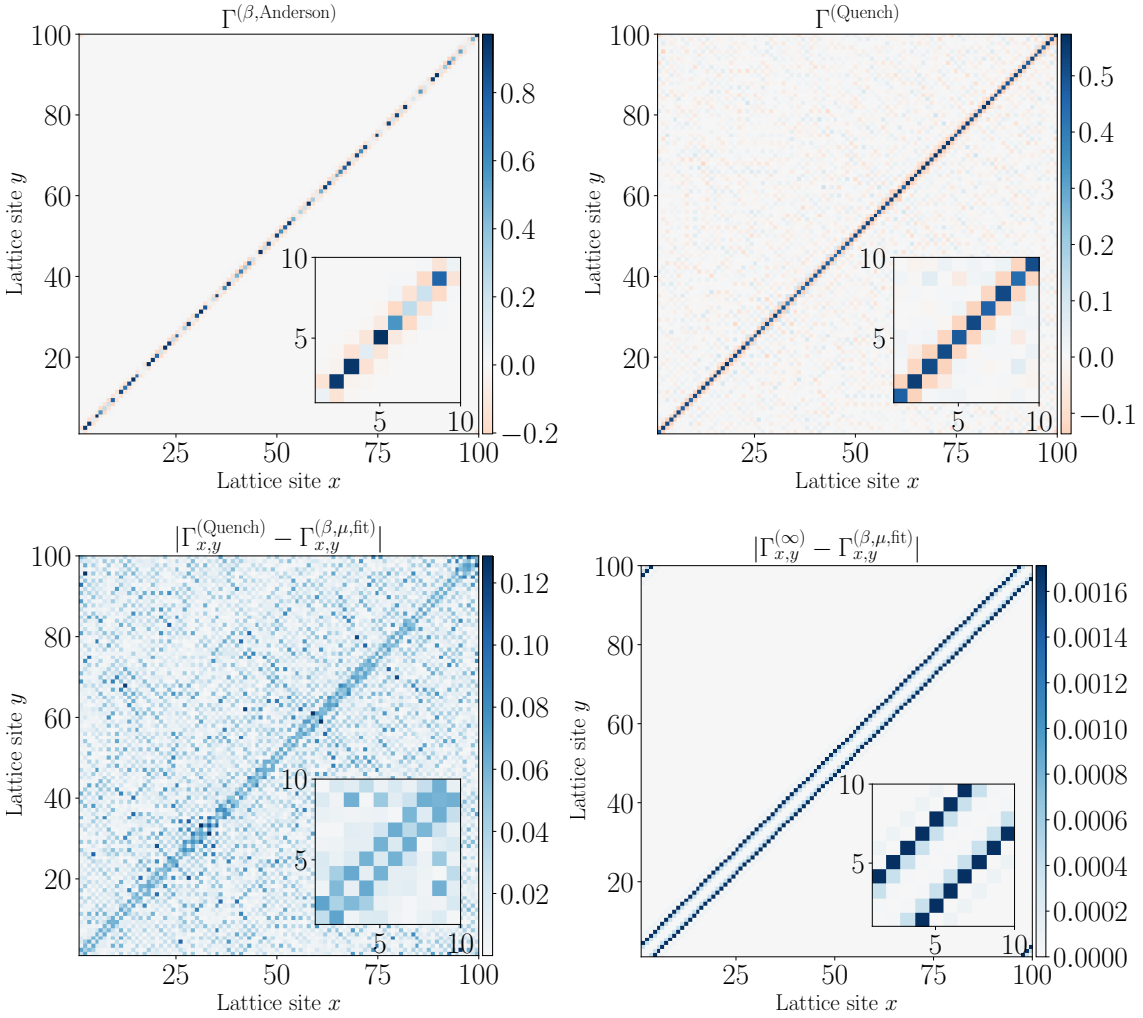

Figure 4: A system initially in a thermal state of an Anderson insulator $\Gamma^{(\beta,\mathrm{Anderson})}$ with $\beta = 1$ and $w = 5$ (top-left) can be quenched to translation invariant evolution by switching off the on-site disorder which results in approximate translation invariance $\Gamma^{(\mathrm{Quench})} = \Gamma^{(\beta,\mathrm{Anderson})}(t = L/4)$ (top-right). This can be quantified with a comparison to the thermal state of nearest-neighbour hopping $\Gamma^{(\beta,\mu,\mathrm{fit})}$ obtained from fitting over the temperature β and chemical potential μ (bottom-left). While deviations are seen the inverse system size $L^{-1} = 10^{-2}$ is not a stringent small parameter. However if equilibration occurs for larger systems, then it will be towards the infinite time average $\Gamma^{(\infty)}$ which looks thermal at already small system sizes (bottom-right) and this property is retained when going towards the thermodynamical limit.

investigating the difference between the quenched state $\Gamma^{(\mathrm{Quench})}(t)$ and a fit to a thermal covariance matrix $\Gamma^{(\beta,\mu,\mathrm{fit})}$ of the quench Hamiltonian obtained from fitting over the temperature β and chemical potential μ. We find that the discrepancy is already diminished for $L = 100$ and $|\Gamma^{(\mathrm{Quench})}_{x,y}(t) - \Gamma^{(\infty)}_{x,y}|$ is homogeneously distributed. For the infinite time average we have $\|\Gamma^{(\infty)} - \Gamma^{(\beta,\mu,\mathrm{fit})}\|_{\max} \approx 10^{-3}$ as the distance to the Gibbs state. The upshot of the findings is that due to a concentration of measure effect, the resulting generalized Gibbs ensembles are with high probability close to an actual Gibbs state, with stray fluctuations being detected. We discuss further details of this argument in Appendix F.5.

7.2 Realizing generalized Gibbs ensembles in optical lattices

Ultra-cold atoms trapped in optical lattices [85] have proven to be an excellent platform for studying relaxation phenomena [86,87] in instances of quantum simulators [88–90], because the system is well isolated from the environment during the evolution and one can prepare with high-level of control states that have very visible non-equilibrium dynamics after the quench. Here we hint that with the present techniques that have been used in various settings one can prepare two different initial states that will equilibrate to two different steady states which are easily distinguishable – despite the Hamiltonian governing the dynamics being the same in both cases. This is expected to be possible at least for intermediate times in instances of *prethermalization*, before interaction effects will lead to a genuine full thermalization. The first steady state would be one obtained from simply letting the gas equilibrate on the lattice. For the second type of the steady state, we would prepare the initial state in the same way and perform the quench by suddenly doubling the lattice by adding in-between sites, exploiting optical *super-lattices*, similar to the situation described in Ref. [86]. In that situation the initial covariance matrix will feature a checker-board pattern with only the odd sites being occupied and currents being non-zero only between odd sites, see Fig. 5. Note that the specific details of how the doubling is performed are not important as long as the initial state preparation will feature a charge-density wave pattern – however it is absolutely crucial for our example that the charge-density wave is also present in the current structure. The quench then consists in allowing for tunneling between all sites. By our analytical result, the density pattern which is a $P = 2$-periodic block structure will equilibrate to a uniform distribution at each site. The same, again, will occur for each current individually. Usually, the nearest-site tunnelling current will be the strongest so if we had $I_1 = \langle \hat{I}_1 \rangle$ before the doubling then the current will equilibrate to $I_1/2$ after the doubling of the lattice. However, the surprise value lies in the fact that this will be the next-nearest-neighbour current I_2' in the new lattice, and in the steady state the final nearest-neighbour current should not be present $I_1' \approx 0$. That is, after the quench, one will observe that there are only currents in the system in multiples of two sites, cf. Fig. 5. This is a non-trivial observation, because the sites that have been un-occupied immediately after the doubling will become occupied and there will be currents flowing out of them to the next-nearest sites, i.e., the neighbouring initially un-occupied sites. In contrast, in the steady state there will be no tunnelling between the nearest-neighbour sites which is unintuitive as the Hamiltonian is nearest-neighbour showcasing peculiar memory effects that can be obtained with quenches to quasi-free evolution. Realizing such a setup in gases where interactions can be controlled by a Feshbach resonance would also allow to study how nearest-neighbour currents can be generated by many-body scattering, an effect not present in a non-interacting Hamiltonian [91–94].

8 Discussion and outlook

In this work, we have established a widely applicable and very general situation in which the convergence to generalized Gibbs ensembes can be proven. Specifically, we have shown in large generality that for large classes of natural initial conditions, local expectation values of systems relaxing under unitary dynamics generated by non-interacting Hamiltonians take the values of translation invariant genaralized Gibbs ensembles. The emerging steady state is parametrized by thermodynamical potentials whose number is intensive, namely of the order of the initial correlation length in units of the lattice spacing. Our assumption is that the quadratic Hamiltonian is translation invariant which leads to homogeneous spreading of particles on the lattice, a generic effect which we describe as a possible notion of ergodicity for quasi-free quantum systems. We have given numerical examples illustrating our rigorous

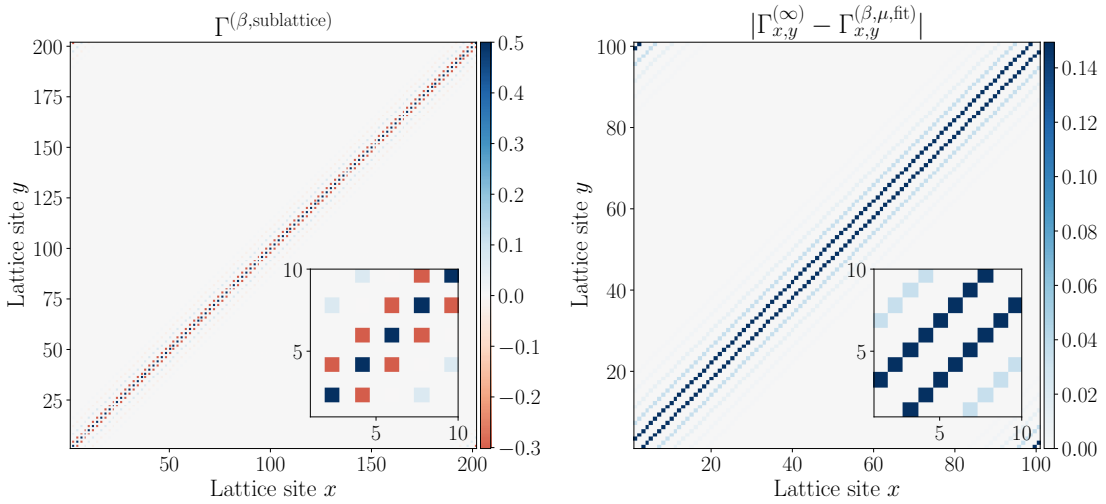

Figure 5: A system initially in a thermal state of the nearest-neighbour hopping Hamiltonian (left) on a sub-lattice can be quenched to translation invariant evolution which results in approximate translation invariance as one relaxes towards the steady state in finite time. The special initial condition results in the absence of nearest-neighbour currents on the whole lattice in the infinite time average (right). The best fit to a thermal state is given by an infinite temperature state with the corresponding filling ratio and strongly deviates from the steady state $\Gamma^{(\infty)}$. This is despite the density distribution becoming homogenous because the state deviates from the thermal ensemble by the absence of the nearest-neighbour current I'_1 and the presence of the next-nearest neighbour tunnelling I'_2. Note that there are particles and currents present on the initially unoccupied sub-lattice too. This showcases a general approach to creating initial conditions that demand a description in terms of a GGE by exploiting the existence of memory in terms of conserved local currents.

statements and explain how to observe non-trivial generalized Gibbs ensembles in, e.g., an optical lattice experiment.

Specifically, we saw that locally the memory of initial, possibly non-Gaussian, correlations is lost via the process of Gaussification, which relies only on finite correlation length in the initial state. Hence, even if the initial state preparation involves intricate interactions, a quench to quasi-free evolution will lead to a loss of memory of these initial strong correlations, and the state will obey Wick's theorem up to an error decaying algebraically in time. Such states (i.e., Gaussian) are determined only by their covariance matrix which we show to equilibrate. A necessary condition for this was that the initial current and density distributions did not have large-scale structure (which may still equilibrate, but only after a time of the order of the system size [38]). Thus, we derived a rapid polynomial time-scale for equilibration (which is independent of the system size). More precisely, the deviation from equilibrium of any normalized local correlation function is bounded by $\epsilon = O(t^{-\gamma})$, and the scaling is functionally tight, which we showed numerically.

The goal of our work was to show that it is possible to make rigorous statements concerning the dynamical emergence of statistical mechanics in mean-field models. For this reason we had to leave several aspects of the subject unanswered. Within our setting we have not discussed in detail the possibility of the infinite-time dephasing leading to steady states which are non-translation invariance due to degeneracy of the dispersion relation, and the proof of Lemma 11 in the appendix hints at that. It would also be interesting to understand in more detail if

Gaussification is possible for Green's functions which have only very weak quasi-free ergodicity, i.e., $|G_{x,y}(t)| = O(t^{-\gamma})$ for $\gamma < 1/4$ for a significant number of entries x, y. If the argument in Ref. [50] is optimal then one should observe for $\gamma < 1/4$ a temporal persistence of deviations from Wick's theorem for quenches of non-Gaussian states.

Concerning the question of adding small interactions one would expect the GGE examples that we have given to eventually thermalize. Understanding the dynamical stability of the GGE description is important for applications, e.g., work extraction protocols [95] but also is instrumental for our conceptual understanding of the emergence of thermalization. Above, we have hinted at an open problem of characterizing the structure of dephased states as being thermal in light of computational complexity and that an interesting approach would be to first make progress concerning high-temperature quenches.

Note added

Upon completion of this manuscript, a preprint presenting closely related results appeared [96]. Our work puts significantly more emphasis on including rigorous error bounds, whereas Ref. [96] stresses more the physical intuition underlying the phenomena observed. The methods are also somewhat different (though related in spirit), as Ref. [96] uses stationary phase approximations, while we employ the machinery of Kusmin-Landau bounds.

Acknowledgements

We gratefully acknowledge insightful discussions with M. Friesdorf, C. Krumnow, C. Gogolin, M. Goihl and T. J. Osborne.

Funding information We thank the ERC (TAQ), the DFG (CRC 183, EI 519/14-1, EI 519/7-1, FOR 2724), and the Templeton Foundation for support. This work has also received funding from the European Union's Horizon 2020 research and innovation programme under grant agreement No 817482 (PASQUANS).

A Quasi-free propagators generated by non-interacting Hamiltonians

A.1 Bosonic and fermionic lattice models

In this section we will derive the propagator representation from the main text. All statements concern quasi-free Hamiltonians conserving the total particle number.

Fermions. A fermionic annihilation operator acting on mode x is denoted by $\hat{f}_x$. These operators obey the canonical anti-commutation relations $\{\hat{f}_x, \hat{f}_y^\dagger\} = \hat{f}_x\hat{f}_y^\dagger + \hat{f}_y^\dagger\hat{f}_x = \delta_{x,y}$ and $\{\hat{f}_x, \hat{f}_y\} = \{\hat{f}_x^\dagger, \hat{f}_y^\dagger\} = 0\}$. Quasifree fermionic Hamiltonians conserving the particle number are of the form

$$\hat{H}(h) = \sum_{x,y}^{L} h_{x,y}\hat{f}_x^\dagger\hat{f}_y \,, \tag{54}$$

where $h = h^\dagger \in \mathbb{C}^{L\times L}$ is the coupling matrix for a finite system size L.

Lemma 6 (Fermionic propagator). *We have*

$$\hat{f}_x(t) = e^{it\hat{H}(h)}\hat{f}_x e^{-it\hat{H}(h)} = \sum_{y=1}^{L} G^*_{x,y}(t)\hat{f}_y \ , \tag{55}$$

where propagator is given by $G^*(t) = e^{-ith}$.

Proof. We begin by noticing that $\hat{f}_x(t)$ is differentiable and take a time-derivative obtaining

$$\partial_t \hat{f}_x(t) = i\hat{H}(h)\hat{f}_x(t) - i\hat{f}_x(t)\hat{H}(h) \tag{56}$$

$$= i[\hat{H}(h), \hat{f}_x(t)], \tag{57}$$

which is the Heisenberg equation of motion. We further notice that

$$\partial_t \hat{f}_x(t) = i\ e^{it\hat{H}(h)}\ [\hat{H}(h),\ \hat{f}_x\ ]\ e^{-it\hat{H}(h)}\ , \tag{58}$$

which means that we need to evaluate the commutator at $t = 0$. Next, we calculate the commutator

$$[\ \hat{f}_y^\dagger \hat{f}_z,\ \hat{f}_x\ ] = \hat{f}_y^\dagger [\ \hat{f}_z,\ \hat{f}_x\ ] + [\ \hat{f}_y^\dagger,\ \hat{f}_x\ ]\hat{f}_z \tag{59}$$

$$= 2\hat{f}_y^\dagger \hat{f}_z \hat{f}_x + 2\hat{f}_y^\dagger \hat{f}_x \hat{f}_z - \delta_{x,y}\hat{f}_z \tag{60}$$

$$= -\delta_{x,y}\hat{f}_z\ , \tag{61}$$

which gives by linearity

$$[\hat{H}(h),\ \hat{f}_x] = -\sum_{y,z=1}^{L} h_{y,z}\delta_{x,y}\hat{f}_z \tag{62}$$

$$= -\sum_{z=1}^{L} h_{x,z}\hat{f}_z\ . \tag{63}$$

This allows us to write the above Heisenberg equation of motion explicitly as

$$\partial_t \hat{f}_x(t) = -i\sum_{y=1}^{L} h_{x,y}\hat{f}_y\ . \tag{64}$$

This is a system of L linearly coupled ordinary differential equations and is solved by

$$\hat{f}_x(t) = \sum_{y=1}^{L} G^*_{x,y}(t)\hat{f}_y\ , \tag{65}$$

where $G^*(t) = e^{-ith} \in U(L)$. Indeed, this becomes apparent if one considers a vector $\hat{f} = (\hat{f}_1, \ldots, \hat{f}_L)^\top$ then we get in vector notation

$$\partial_t\ \hat{f}(t) = -ih\ \hat{f}(t) \quad \Leftrightarrow \quad \hat{f}(t) = e^{-ith}\ \hat{f} = G^*(t)\ \hat{f}\ . \tag{66}$$

□

Bosons. Bosonic operators $\hat{b}$ obey the canonical commutation relations $[\hat{b}_x, \hat{b}_y^\dagger] = \hat{b}_x\hat{b}_y^\dagger - \hat{b}_y^\dagger\hat{b}_x = \delta_{x,y}$ and $[\hat{b}_x, \hat{b}_y] = [\hat{b}_x^\dagger, \hat{b}_y^\dagger] = 0$. Quasifree bosonic Hamiltonians conserving the particle number are of the form

$$\hat{H}(h) = \sum_{x,y}^{L} h_{x,y}\hat{b}_x^\dagger\hat{b}_y \ , \tag{67}$$

where $h = h^\dagger \in \mathbb{C}^{L\times L}$ is again the coupling matrix for a finite system size L.

Lemma 7 (Bosonic propagator)**.** *We have*

$$\hat{b}_x(t) = e^{it\hat{H}(h)}\hat{b}_x e^{-it\hat{H}(h)} = \sum_{y=1}^{L} G^*_{x,y}(t)\hat{b}_y \ , \tag{68}$$

where the propagator is given by $G^*(t) = e^{-ith}$.

Proof. Again, the Heisenberg equation of motion is

$$\partial_t \hat{b}_x(t) = i[\hat{H}(h),\ \hat{b}_x(t)] \tag{69}$$

and it suffices to evaluate the commutator at $t = 0$. We have

$$[\hat{b}_y^\dagger\hat{b}_z,\ \hat{b}_x] = [\hat{b}_y^\dagger,\ \hat{b}_x]\hat{b}_z \tag{70}$$

$$= -\delta_{x,y}\hat{b}_z \, , \tag{71}$$

which gives by linearity

$$\partial_t \hat{b}_x(t) = -i\sum_{y=1}^{L} h_{x,y}\hat{b}_y \ . \tag{72}$$

This is again a system of L linearly coupled ordinary differential equations with the solution

$$\hat{b}_x(t) = \sum_{y=1}^{L} G^*_{x,y}(t)\hat{b}_y \ , \tag{73}$$

where $G = e^{-ith} \in U(L)$. Here, we have used the general correspondence

$$\partial_t\ \hat{b}(t) = -ih\ \hat{b}(t) \quad \Leftrightarrow \quad \hat{b}(t) = e^{-ith}\ \hat{b} \tag{74}$$

for the vector $\hat{b} = (\hat{b}_1, \ldots, \hat{b}_L)^\top$.

□

Translation invariance. Let us consider

$$\hat{H}(h) = \sum_{x,y}^{L} h_{x,y}\hat{a}_x^\dagger\hat{a}_y \ , \tag{75}$$

where $\hat{a}$ stands either for $\hat{f}$ in the case of fermions or $\hat{b}$ for bosons and $h = h^\dagger \in \mathbb{C}^{L\times L}$ is the coupling matrix for a finite system size L. The above two paragraphs have shown that

$$\hat{a}_x(t) = e^{it\hat{H}(h)}\hat{a}_x e^{-it\hat{H}(h)} = \sum_{y=1}^{L} G^*_{x,y}(t)\hat{a}_y \ . \tag{76}$$

In this paragraph we will be interested in translation invariant Hamiltonians.

Lemma 8 (Translation invariant propagator). *Let h be real translation invariant couplings with hopping amplitudes J_k. The propagator is given by*

$$G^*_{x,y}(t) = \frac{1}{L}\sum_{k=1}^{L} e^{-i\omega_k t + 2\pi i k(x-y)/L}, \tag{77}$$

where $\omega_k = J_0 + 2\sum_{z=1}^{\lfloor L/2\rfloor} J_z \cos(2\pi k z/L)$.

Proof. A translation invariant model has couplings which satisfy $h_{x,y} = h_{x+z,y+z}$ with periodic boundary conditions. Below we recall that such matrices are called circulant and are diagonalized by a discrete Fourier transform. Hence we can write

$$h_{x,y} = \frac{1}{L}\sum_{k=1}^{L} \omega_k e^{2\pi i k(x-y)/L}, \tag{78}$$

with ω_k as above which is obtained by an explicit calculation using Fourier modes. Using the formula $G(t) = e^{-ith}$, we hence get

$$G^*_{x,y}(t) = \frac{1}{L}\sum_{k=1}^{L} e^{-i\omega_k t + 2\pi i k(x-y)/L} \tag{79}$$

for the propagator. □

A.2 Circulant matrices

In this section we gather some basic facts about circulant matrices, leading up to the characterization that these are exactly the matrices diagonalizable by a discrete Fourier transformation. Additionally we describe simple formulas for the spectrum in the general case and for periodic boundary conditions. We begin by giving a precise definition of a circulant matrix.

Definition 9 (Circulant matrix). *A matrix $h \in \mathbb{C}^{L\times L}$ is called circulant if*

$$h_{x,y} = h_{x+z,y+z} \tag{80}$$

for any $x, y, z = 1, \ldots, L$ [1] *and we use modulo-L indices i.e. $h_{x+L,\cdot} = h_{x,\cdot}$ and $h_{\cdot,y+L} = h_{\cdot,y}$.*

The name comes from the fact that in a circulant matrix the k-th row is a circulant shift of the first row by $k-1$ steps to the right. That, is if $(J_0, J_1, \ldots, J_{L-1})$ is the first row then the second is $(J_{L-1}, J_0, \ldots, J_{L-2})$, the third $(J_{L-2}, J_{L-1}, J_0, \ldots, J_{L-3})$ and altogether

$$\begin{pmatrix} J_0 & J_1 & J_2 & \ldots & J_{L-1} \\ J_{L-1} & J_0 & J_1 & \ldots & J_{L-2} \\ & & \ddots & & \\ J_2 & \ldots & J_{L-1} & J_0 & J_1 \\ J_1 & \ldots & J_{L-2} & J_{L-1} & J_0 \end{pmatrix}. \tag{81}$$

We see that it is enough to know the vector of (hopping) amplitudes $J_z = h_{1,1+z}$ for $z = 1, \ldots, L-1$ to describe the whole matrix h. A translation invariant Hamiltonian $H(h)$ has a couplings matrix which is circulant but also Hermitian. This means that $J_{L-1} = J_1^*$, $J_{L-2} = J_2^*$ and in general $J_{L-z} = J_z^*$. In that case $J_0, J_1, \ldots, J_{\lfloor L/2\rfloor}$ are necessary to parametrize the matrix.

[1] z could have smaller range but it doesn't harm

Lemma 10 (Circulant matrices and discrete Fourier transforms). *A matrix h is circulant if and only if it is diagonalized by a discrete Fourier transform. For $k = 1, \ldots, L$ the eigenvectors are*

$$\psi_k = \frac{1}{\sqrt{L}}\left(\phi_k, \phi_k^2, \ldots, \phi_k^{L-1}, 1\right)^\top, \tag{82}$$

where $\phi_k = e^{2\pi i k/L}$ and the corresponding eigenvalue read

$$\lambda_k(h) = J_0 + \sum_{z=1}^{L-1} J_z e^{2\pi i z k/L} \,. \tag{83}$$

An important case is when the Hamiltonian couplings are real in addition to being circulant matrices and then we have

$$\lambda_k(h = h^\top = h^*) = J_0 + \sum_{z=1}^{\lfloor L/2 \rfloor} 2J_z \cos(2\pi z k/L) \,. \tag{84}$$

In the most general translation invariant case, which is relevant for the case of conserved quantities if the initial covariance matrix was not purely real, we have

$$\lambda_k(h = h^\dagger) = J_0 + 2\sum_{z=1}^{\lfloor L/2 \rfloor} \Re[J_z e^{2\pi i z k/L}] \,. \tag{85}$$

Here we have used translation invariance which in general reads $J_z = J_{L-z}^*$. As an example consider

$$\hat{I}_{z=1}(\eta = \pi/2) = \frac{1}{L}\sum_{x=1}^{L}(i\hat{f}_x^\dagger \hat{f}_{x+1} - i\hat{f}_{x+1}^\dagger \hat{f}_x) \,, \tag{86}$$

for which we have $\lambda_k = 2\Re[J_{z=1}e^{2\pi i z k/L}] = (2/L)\Re[ie^{2\pi i z k/L}] = -(2/L)\sin(2\pi z k/L)$.

Proof. To show the first direction, we will show that $\psi_{k'}^\dagger(h\psi_k) = \lambda_k(h)\delta_{k',k}$. We have

$$\psi_{k'}^\dagger(h\psi_k) = L^{-1}\sum_{x,y=1}^{L} h_{x,y} e^{\frac{2\pi i}{L}(ky - k'x)} \tag{87}$$

$$= L^{-1}\sum_{x,z=1}^{L} h_{x,x+z} e^{\frac{2\pi i}{L}(k-k')x} e^{\frac{2\pi i}{L}kz} \tag{88}$$

$$= L^{-1}\sum_{z=1}^{L} h_{1,1+z} e^{\frac{2\pi i}{L}kz} \sum_{x=1}^{L} e^{\frac{2\pi i}{L}(k-k')x} \tag{89}$$

$$= \sum_{z=1}^{L} h_{1,1+z} e^{\frac{2\pi i}{L}kz} \delta_{k,k'} \,, \tag{90}$$

which is by definition of $\lambda_k(h)$ what we were looking for. For the converse direction, we must show that a rotation by the discrete Fourier transform matrix of a spectrum λ yields a circulant

matrix. We do this by checking the defining property

$$\tilde{h}_{x,y} = \left(\sum_{k=1}^{L} \lambda_k \psi_k \psi_k^\dagger\right)_{x,y} \tag{91}$$

$$= L^{-1} \sum_{k=1}^{L} \lambda_k e^{2\pi i k(x-y)/L} \tag{92}$$

$$= L^{-1} \sum_{k=1}^{L} \lambda_k e^{2\pi i k(x+z-y-z)/L} \tag{93}$$

$$= \tilde{h}_{x+z,y+z}\,. \tag{94}$$

Thus, the matrix $\tilde{h}$ is circulant. □

A.3 Bessel function asymptotics

A particularly insightful situation is the special case of a nearest-neighbour fermionic hopping Hamiltonian, setting $J_0 = 0$ and $J_1 = 1$. In this situation, we simply obtain

$$\omega_k = 2\cos(2\pi k/L)\,, \tag{95}$$

and hence

$$G^*_{x,y}(t) = \frac{1}{L}\sum_{k=1}^{L} e^{-2i\cos(2\pi k/L)t + 2\pi i k(x-y)/L} \tag{96}$$

for the propagator. In the limit of large L, this can be seen as a Riemann sum approximation [54] to the integral

$$\tilde{G}^*_{x,y}(t) = \frac{1}{2\pi}\int_0^{2\pi} d\phi\, e^{-2i\cos(\phi)t} e^{i\phi(x-y)} = i^{x-y}\mathcal{J}_{x-y}(-2t)\,, \tag{97}$$

where $\mathcal{J}_l : \mathbb{R} \to \mathbb{R}$ is the Bessel function of the first kind. The error in this approximation can be bounded from above as

$$|G^*_{x,y}(t) - i^{x-y}\mathcal{J}_{x-y}(-2t)| \leq \frac{\pi|x-y-2t|}{L}\,. \tag{98}$$

These Bessel functions satisfy

$$|\mathcal{J}_{x-y}(-2t)| = O(t^{-1/2}) \tag{99}$$

for all x, y. That is to say, in this situation, one gets an equilibration following a $O(t^{-1/2})$ behaviour. This feature of the propagator is actually inherited by the actual correlation decay. In fact, a stronger statement can be made: $O(t^{-1/2})$ is not only an upper bound for $|\mathcal{J}_{x-y}(-2t)|$, but there cannot be a tighter uniform bound in the form of a power law. The asymptotics of Bessel functions [97] can be captured as

$$J_{x-y}(\tau) = \left(\frac{2}{\pi\tau}\right)^{1/2}\cos\left(\tau - \frac{(x-y)\pi}{2} - \frac{\pi}{4}\right) + O(|\tau|^{-1})\,, \tag{100}$$

for $\tau > 0$, showing that no tighter uniform power law bound can exist.

B Steady states and local conservation laws via circulant matrices

Now we prove that dephasing under Hamiltonians that are only minimally degenerate leads to steady states with $\Gamma^{(\mathrm{eq})}_{x,y} \approx \langle \hat{I}_{|x-y|} \rangle$ where as in the main text we take the index arithmetic to be modulo L.

Lemma 11 (Steady state covariance matrices as approximately circulant matrices)**.** *Consider a state with covariance matrix Γ and exponentially decaying correlations. For any $\hat{H}(h)$ with dispersion relation satisfying $\omega_k = \omega_{k'}$ only for $k = k'$, or $k = L - k'$ where $k' > k$ the steady state is approximately a circulant matrix with entries*

$$|\Gamma^{(\mathrm{eq})}_{x,y} - \langle \hat{I}_{|x-y|} \rangle| = O(L^{-1}) \,. \tag{101}$$

In particular, this holds true for the nearest-neighbour hopping model with dispersion relation $\omega_k = \cos(2\pi k/L)$.

Proof. Let us consider the action of the dephasing map on the initial covariance matrix $\Gamma^{(\mathrm{eq})} = \lim_{T\to\infty} \frac{1}{T} \int_0^T \Gamma(t)$ for two sites x, y which reads

$$\Gamma^{(\mathrm{eq})}_{x,y} = \lim_{T\to\infty} \frac{1}{T} \int_0^T \Gamma_{x,y}(t) \tag{102}$$

$$= \lim_{T\to\infty} \frac{1}{T} \int_0^T \sum_{x',y'=1}^{L} G_{x,x'}(t) \Gamma_{x',y'} G^*_{y',y}(t) \tag{103}$$

$$= L^{-2} \sum_{x',y'=1}^{L} \Gamma_{x',y'} \sum_{k,k'=1}^{L} \left(\lim_{T\to\infty} \frac{1}{T} \int_0^T e^{(-i\omega_k t + i\omega_{k'})t} \right) e^{\frac{2\pi i}{L}(k(x-x') - k'(y-y'))} \tag{104}$$

$$= L^{-2} \sum_{x',y'=1}^{L} \Gamma_{x',y'} \sum_{k,k'=1}^{L} \delta_{\omega_k,\omega_{k'}} e^{\frac{2\pi i}{L}(k(x-x') - k'(y-y'))} \,. \tag{105}$$

Next, we will use the assumption concerning the minimal degeneracy of the dispersion relation which gives

$$\Gamma^{(\mathrm{eq})}_{x,y} = L^{-2} \sum_{x',y'=1}^{L} \Gamma_{x',y'} \sum_{k,k'=1}^{L} \delta_{k,k'} e^{\frac{2\pi i}{L}(k(x-x') - k'(y-y'))} \tag{106}$$

$$+ L^{-2} \sum_{x',y'=1}^{L} \Gamma_{x',y'} \sum_{k,k'=1}^{L} \delta_{k,L-k'}(1-\delta_{k,k'}) e^{\frac{2\pi i}{L}(k(x-x') - k'(y-y'))} \,. \tag{107}$$

We notice that the condition $k = k'$ gives

$$\delta_{x-y,x'-y'} = L^{-1} \sum_{k=1}^{L} e^{\frac{2\pi i}{L} k(x-x'-y+y')} \,. \tag{108}$$

The other condition $k = L - k'$ also leads to simplification but one needs to be careful to observe that for L even we may obtain $k = L - k'$ and $k = k' = L/2$ and such terms are already included in the previous sum. Additionally, $k' = L$ gives no solution to $k = L - k'$ and so together we

have

$$\Gamma^{(\mathrm{eq})}_{x,y} = L^{-1} \sum_{x',y'=1}^{L} \Gamma_{x',y'} \delta_{x-y,x'-y'} \tag{109}$$

$$+ L^{-2} \sum_{x',y'=1}^{L} \Gamma_{x',y'} \sum_{k,k'=1}^{L-1} \delta_{k,L-k'} e^{\frac{2\pi i}{L}(k(x-x')-k'(y-y'))} \tag{110}$$

$$- L^{-2} \sum_{x',y'=1}^{L} \Gamma_{x',y'} \sum_{k,k'=1}^{L-1} \delta_{k,L-k'} \delta_{k,k'} e^{\frac{2\pi i}{L}(k(x-x')-k'(y-y'))} \,. \tag{111}$$

Here we identify the first line to give a current expectation value $\langle \hat{I}_{|x-y|} \rangle$. The inner sum in second line gives $L\delta_{x+y-x'-y'} - 1$ and the third is either 0 or can be bounded from above

$$\left| \Gamma^{(\mathrm{eq})}_{x,y} - \langle \hat{I}_{|x-y|} \rangle \right| \leq L^{-1} \sum_{x',y'=1}^{L} |\Gamma_{x',y'}| \delta_{x+y-x'-y'} + 2L^{-2} \sum_{x',y'=1}^{L} |\Gamma_{x',y'}| \,. \tag{112}$$

Finally, we make use of the exponential decay of correlations $|\Gamma_{x,x+z}| \leq C_{\mathrm{Clust}} e^{-z/\xi}$, obtaining

$$L^{-2} \sum_{x',y'=1}^{L} |\Gamma_{x',y'}| \leq L^{-2} \sum_{z=0}^{L} \sum_{x=1}^{L} |\Gamma_{x,x+z}| \leq L^{-1} C_{\mathrm{Clust}} \sum_{z=0}^{\infty} e^{-z/\xi} \tag{113}$$

$$\leq \frac{C_{\mathrm{Clust}}}{1 - e^{1/\xi}} L^{-1} \,. \tag{114}$$

Employing a similar bound for the first term we obtain

$$\left| \Gamma^{(\mathrm{eq})}_{x,y} - \langle \hat{I}_{|x-y|} \rangle \right| \leq C_I L^{-1} \,. \tag{115}$$

□

Lemma 12 (Relevant currents)**.** *Consider a state with covariance matrix* Γ *and exponentially decaying correlations parametrized by the correlation length* $\xi > 0$*. Then for any time* t *we have*

$$|\Gamma^{(d)}_{x,y}(t)| \leq C_{\mathrm{Clust}} e^{-d/\xi} \,. \tag{116}$$

Proof. After a technical calculation using the definition of $\Gamma^{(d)}$ we find

$$\left| \Gamma^{(d)}_{x,y}(t) \right| = \left| \sum_{z,w=1}^{L} G_{x,w}(t) \Gamma_{z+d,z} \, \delta_{w,z+d} G^{*}_{y,z}(t) \right| \tag{117}$$

$$\leq \max_{z=1,\ldots,L} \left| \Gamma_{z,z+d} \right| \left(\sum_{w=1}^{L} \left| G(t)_{x,w} \right|^2 \right)^{1/2} \left(\sum_{z=1}^{L} \left| G_{y,z}(t) \right|^2 \right)^{1/2} \tag{118}$$

$$= \max_{z=1,\ldots,L} \left| \Gamma_{z,z+d} \right| \tag{119}$$

$$\leq C_{\mathrm{Clust}} e^{-d/\xi} . \tag{120}$$

The second line follows from the inequality

$$|\langle v | A | w \rangle| \leq \|A\| \sqrt{\langle v|v \rangle} \sqrt{\langle w|w \rangle} \,, \tag{121}$$

where we are thinking of $\Gamma_{z,z+d} \, \delta_{w,z+d}$ as a matrix, with operator norm given by $\max_z \left| \Gamma_{z,z+d} \right|$. The third line follows because $G(t)$ is a unitary matrix, so its rows and columns are orthonormal vectors. In the last line, we have used the definition of exponentially decaying correlations. □

C Bound on oscillatory sums of sequences with compact Fourier representation

We would like to prove a general bound on oscillatory sums of the type appearing in the main text where the phase sequence can be decomposed in a Fourier series with bounded number of harmonics. Specifically, we define a smooth phase function $\Phi_t : [0, 2\pi] \to \mathbb{R}$ of the form

$$\Phi_t(p) = dp + t\sum_{z=1}^{R} J_z \cos(zp + \alpha_z) \,, \tag{122}$$

where $t, d, J_1, \ldots, J_R, \alpha_1, \ldots \alpha_R \in \mathbb{R}$ with $J \neq 0$. It will be convenient to define

$$\Phi(p) = \sum_{z=1}^{R} J_z \cos(zp + \alpha_z) \,, \tag{123}$$

which plays, e.g., the role of a dispersion relation and we have $\Phi_t^{(\kappa)} = t\Phi^{(\kappa)}$ for all higher-order derivatives $\kappa > 1$. If we additionally define $p_k = 2\pi k/L$, then the sequence of interest will be

$$\varphi_k = \Phi_t(p_k) \,, \tag{124}$$

for $k = 1, \ldots, L$, where L as in the main text stands for the system size. Note that our results become non-trivial for $L \geq t_0$ where t_0 is the relaxation time which dependents only on J_z. Physically, it is always given that L is asymptotically large giving a uniform small parameter, so for system sizes of interest our requirements should be fulfilled. Mathematically all our statements remain correct by defining $[t_0, t_R] = \emptyset$ if $t_0 \geq t_R$ but it should be stressed that when L is large enough we obtain a very non-trivial bound with $t_0 < t_R$.

Before we state our main theorem of this section, let us make the following definitions. We will use the Kusmin-Landau bound and the role of stationary points will be taken by the roots of Φ_t' denoted by

$$\mathcal{S}^{(1)} = \{p \in [0, 2\pi] \text{ s.t. } \Phi_t'(p) = 0\} \tag{125}$$

and the extremal points of the group velocity Φ_t'

$$\mathcal{S}^{(2)} = \{p \in [0, 2\pi] \text{ s.t. } \Phi_t''(p) = 0\} \,. \tag{126}$$

The former set of points are exactly the points of vanishing group velocity while for the latter the band curvature vanishes. Let us make additionally the following definition useful for Taylor expansions around roots $r \in \mathcal{S} = \mathcal{S}^{(1)} \cup \mathcal{S}^{(2)}$. In general for $r \in \mathcal{S}$ we define

$$\kappa_r \geq 1 \tag{127}$$

to be the minimal integer such that for $r \in \mathcal{S}^{(a)}$ where $a = 1, 2$ the $(\kappa_r + a)$'th derivative does not vanish $|\Phi_t^{(\kappa_r + a)}(r)| \neq 0$. Additionally,

$$\kappa_0 = \max_{r \in \mathcal{S}} \kappa_r \tag{128}$$

will set the scaling of the final bound in the following theorem.

Theorem 13 (Dephasing bound). *There exist a constant relaxation time t_0 and a recurrence time $t_R = \Theta(L)$ such that, for all $t \in [t_0, t_R]$ we obtain the bound*

$$\frac{1}{L}\left|\sum_{k=1}^{L} e^{i\varphi_k}\right| \leq C_{\#} t^{-\gamma} \,, \tag{129}$$

where

$$C_{\#} = 6(2R+1)\max\left\{1, \min_{r\in\mathcal{S}^{(2)}} \frac{\left|\Phi^{(\kappa_r+2)}(r)\right|}{2C^{(3)}_{max}\,\kappa_r!}, \max_{r\in\mathcal{S}^{(2)}} \frac{8\,(\kappa_r!)^2\,C^{(3)}_{max}}{\left|\Phi^{(\kappa_r+2)}(r)\right|^2}, \max_{r\in\mathcal{S}^{(1)}} \frac{4\,\kappa_r!}{\left|\Phi^{(\kappa_r+1)}(r)\right|}\right\} \tag{130}$$

and $\gamma = 1/(3\kappa_0) > 1/(6R)$ *are constants. We can take* $\gamma = 1/3$*, provided there are no repeated roots* $\Phi_t''(p) = \Phi_t'''(p) = 0$ *which holds true in the generic case.*

This theorem will for example allow us to bound

$$|G_{x,y}(t)| = \frac{1}{L}\left|\sum_{k=1}^{L} e^{i\omega_k t + 2\pi i k d/L}\right| \leq C_{\#}\, t^{-\alpha} \tag{131}$$

or

$$|f_n(t)| = \frac{1}{L}\left|\sum_{s=1}^{L} e^{i(\omega_{(s+n)}-\omega_s)t + 2\pi i s(x-y-d)/L}\right| \leq C_{\#}(\tfrac{n\pi}{L})\, t^{-\alpha}\,, \tag{132}$$

as a function of time and with constants expressed in the analytic properties of Φ_t. The following lemma attributed to Kusmin and Landau [49] will be our key tool.

Lemma 14 (Kusmin-Landau bound)**.** *Suppose* $(\varphi_n)_{n\in\{1,\dots,N\}}$ *are real numbers and suppose the gaps* $\delta_n = (\varphi_{n+1} - \varphi_n)$ *for* $n \in \{1,\dots,N-1\}$ *are (i) increasing* $\delta_n \geq \delta_{n-1}$ *and (ii) each gap satisfies* $\delta_n \in [\lambda, 2\pi - \lambda]$ *with* $\lambda > 0$*. Then we have*

$$\left|\sum_{n=1}^{N} e^{i\varphi_n}\right| \leq \cot(\lambda/4) \leq \frac{2\pi}{\lambda}\,, \tag{133}$$

where the second inequality follows from $\cos(x) \leq 1$ *and* $\sin(x) \geq 2x/\pi$ *for* $x \in [0, \pi/2]$*.*

To apply Lemma 14, we need to understand the discrete Kusmin gaps defined by

$$\delta_k = \varphi_{k+1} - \varphi_k\,, \tag{134}$$

and show that they are separated from 0 and 2π by some $\lambda > 0$ on a constant number of intervals where they are also monotonous. Because $\varphi_k = \Phi_t(p_k)$ we can use the mean value theorem obtaining

$$\delta_k = \frac{2\pi}{L}\Phi_t'(\tilde{p}_k) \tag{135}$$

for some $\tilde{p}_k \in [p_k, p_{k+1}]$ and $2\pi/L$ is the size of the interval to which we apply the theorem. We denote the summation domain by

$$\mathcal{D} = \{1, 2, \dots, L\} \tag{136}$$

and collect the corresponding $\tilde{p}_k$ points in

$$\mathcal{I} = \{\tilde{p}_k : k = 1, \dots, L-1\}\,. \tag{137}$$

Observe, that by the mean-value relation (135) the Kusmin gaps are monotonous on some $\mathcal{I}_r \subset \mathcal{I}$ if Φ_t' is monotonous on $\overline{\mathcal{I}}_r = \mathrm{conv}(\mathcal{I}_r)$. By using the mapping $k \mapsto \tilde{p}_k$, we can define intervals in $\mathcal{D}$ associated to any subset $\mathcal{I}_r \subseteq \mathcal{I}$ defining $\mathcal{D}_r = \{k \in \mathcal{D} \text{ s.t. } \tilde{p}_k \in \mathcal{I}_r\}$. We want to divide $\mathcal{D}$ into intervals where δ are monotonous. After an elementary application of the triangle inequality, to each such region we want to apply the Kusmin-Landau bound. It is important to notice that their number is bounded above by the maximal coupling range R according to the following lemma.

Lemma 15 (Roots). *The function $\Omega : [0, 2\pi] \to \mathbb{C}$ defined by*

$$\Omega(p) = a_0 + \sum_{z=1}^{R} (a_z e^{ipz} + b_z e^{-ipz}) \,, \tag{138}$$

where $a_j, b_j \in \mathbb{C}$ has at most $2R$ roots as long as $a \neq 0$ or $b \neq 0$.

Proof. Define a complex polynomial $Y : \mathbb{C} \to \mathbb{C}$ by $Y(u) = a_0 u^R + \sum_{z=1}^{R} a_z u^{z+R} + \sum_{z=1}^{R} b_z u^{R-z})$ and observe that it is not identically zero and has degree at most $2R$ and hence at most $2R$ roots. Further, note that when restricted to the unit circle S_1 in the complex plane we have $Y(e^{ip}) = e^{iRp}\Omega(p)$ for any $p \in [0, 2\pi]$. From this we see that whenever $\Omega(p) = 0$ for some $p \in [0, 2\pi]$ then $u = e^{ip}$ is a root of Y because the multiplicative prefactor e^{ip} does not remove any roots. Thus the number of roots of Ω cannot exceed the number of roots of Y which is upper bounded by $2R$. □

Corollary 16 (Number of roots of phase functions). *The phase function Φ_t and all its derivatives Φ_t', Φ_t'' etc. have at most $2R$ roots.*

As we can easily check without loss of generality we can assume that $\Phi_t'(0) = \Phi_t'(2\pi) = 0$ and hence the interior between consecutive extremal points in $\mathcal{S} = \mathcal{S}^{(1)} \cup \mathcal{S}^{(2)}$ defines at most $4R+2$ intervals where $\Phi_t'(p)$ and $\Phi_t''(p)$ have a fixed sign. Specifically, we define these intervals as the points in $\mathcal{I}$ that lie between two consecutive roots from $\mathcal{S}$ and denote them by $\mathcal{I}_r \subset \mathcal{I}$ and note that r ranges from 1 to some $R_0 \leq 4R + 2$. If, e.g., $\Phi_t(p) = \cos(p)$, then $R = 1$ and we have $R_0 = 4$ regions. We now establish condition *i)* of the Kusmin-Landau Lemma which concerns monotonicity.

Lemma 17 (Monotonicity). *Let $r < r_2$ be two consecutive points belonging to $\mathcal{S}$. Then the Kusmin-Landau gaps δ_k are monotonous for all points k corresponding to the interval $\mathcal{I}_r = \mathcal{I} \cap [r, r_2]$.*

Proof. Between r and r_2 the first derivative of the phase function Φ_t' must be non-zero or otherwise there would be an intermediate root which is not possible as r and r_2 are consecutive. There is also no intermediate root of the second derivative Φ_t'' so it must have a fixed sign on the interior of the interval hence the derivative Φ_t' is either weakly increasing or decreasing and so the Kusmin-Landau gaps δ_k must be monotonous. □

It will be useful to observe that any κ_r can be bounded by the range R.

Lemma 18 (Bounds from the range). *We have $\kappa_0 \leq 2R$.*

Proof. Consider again the non-zero polynomial Y associated to Φ_t' or Φ_t'' as described above. Then Y has degree at most $\deg(Y) \leq 2R$ and because $J \neq 0$ we have that $\Phi_t \neq \texttt{const}$ and so $Y \neq 0$. Now, if we had that $Y(z_0) = Y'(z_0) = \ldots = Y^{(2R)}(z_0) = 0$ then, for any z by Taylor expansion, we would find

$$Y(z) = \sum_{n=0}^{2R} \frac{Y^{(n)}(z_0)}{n!} (z - z_0)^n = 0 \,. \tag{139}$$

Thus, for $Y(e^{ip}) \neq 0$ to be true at some point e^{ip} then $Y^{(n)}(z_0) \neq 0$ must be true for some $n \leq 2R$. □

With this definition we can further set the constants

$$t_0 := \max\left\{1, \max_{r\in\mathcal{S}^{(2)}}\left|\frac{1}{\kappa_r+1}\frac{\Phi^{(\kappa_r+3)}(r)}{\Phi^{(\kappa_r+2)}(r)}\right|^{3\kappa_r}, \max_{r\in\mathcal{S}^{(1)}}\left|\frac{1}{\kappa_r+1}\frac{C_{\max}^{(\kappa_r+2)}}{\Phi^{(\kappa_r+1)}(r)}\right|^{3\kappa_r}, \left(\frac{C_0+1}{\min_{q,r\in\mathcal{S}}|q-r|}\right)^{2R+2}\right\} \tag{140}$$

and

$$t_{\mathrm{R}} = \frac{L}{4\max\{C_{\max}^{(1)}, C_1\}}. \tag{141}$$

This quantity is finite and independent of L by the above remark and definition of κ_r, and because the numerator can be upper bounded by

$$C_{\max}^{(\kappa)} = \sum_{z=1}^{R} z^{\kappa}|J_z| \leq R^{\kappa+1}\max_z|J_z|\,. \tag{142}$$

Furthermore, we define the time-independent constant

$$C_0 = \min_{r\in\mathcal{S}^{(2)}}\frac{\left|\Phi^{(\kappa_r+2)}(r)\right|}{2C_{\max}^{(3)}k_r!}\,. \tag{143}$$

We will now show that, after removing a small amount of points close to the border from each of the intervals $\mathcal{I}_r$, for the remaining points the Kusmin gaps will be lower and upper bounded. More precisely we define the two scalings that we shall use

$$p_t = C_0 t^{-1/3} \text{ and } q_t = t^{-1/(3\kappa_r)}\,. \tag{144}$$

Proof of Theorem 13. Let us use the elementary observation that

$$\frac{1}{L}\left|\sum_{k=1}^{L}e^{i\varphi_k}\right| = \frac{1}{L}\left|\sum_{k=1}^{L}e^{i\varphi_{k+a}}\right| \tag{145}$$

for any a together with the fact that our phase function is always periodic up to a constant

$$\Phi_t(p-r) = \Phi_t(p) - dr\,. \tag{146}$$

Observing that in the absolute value of the total sum any constant term in Φ_t drops out, we may assume that $\Phi_t'(0) = 0$ without loss of generality. Then using that the cosine functions are 2π periodic we also find that $\Phi_t'(2\pi) = 0$. With this step we reduced the total sum to a sum over the intervals $\mathcal{I}_r$ where the boundary points are appropriate roots.

Consider $r \in \mathcal{S}$ and the corresponding interval $\mathcal{I}_r$. Without loss of generality we may assume that $\Phi_t'(r) < \Phi_t'(r_2)$ and hence our task is to lower bound the Kusmin gaps around r. (If on $\mathcal{I}_r$ the gaps are negative then we can simply lower bound $\Phi_t'^{(-)} = -\Phi_t'$, while in the case $\Phi_t'(r) > \Phi_t'(r_2)$ we would have to lower bound the Kusmin gaps around r_2 which can be done the same way). By the monotonicity lemma, this assumption implies $\Phi_t'' > 0$ on $\mathcal{I}_r$.

Step 1: Restrict $\mathcal{I}_r$ to $\mathcal{I}_r \cap \mathcal{S}_t^c$ where

$$\mathcal{S}_t^c = [0,2\pi)\backslash\{q\in[0,2\pi) \text{ s.t. } |r-q| \leq p_t + q_t \text{ for all } r\in\mathcal{S}\}\,, \tag{147}$$

such that $\delta_k \geq \lambda$ for

$$\lambda = \frac{2\pi C_1}{L} t^{1/3} \tag{148}$$

and

$$C_1 = \tfrac{1}{4} \min \left\{ \min_{r\in\mathcal{S}^{(1)}} \frac{\left|\Phi^{(\kappa_r+1)}(r)\right|}{\kappa_r!}, \min_{r\in\mathcal{S}^{(2)}} \frac{\left|\Phi^{(\kappa_r+2)}(r)\right|}{\kappa_r!} C_0 \right\} . \tag{149}$$

Step 1, case 1: $r \in \mathcal{S}^{(1)}$.
In this step, we expand around r, to obtain

$$\Phi_t'(r+q_t) = \frac{\Phi_t^{(\kappa_r+1)}(r)}{\kappa_r!} q_t^{\kappa_r} + \frac{\Phi_t^{(\kappa_r+2)}(\tilde{q})}{(\kappa_r+1)!} q_t^{\kappa_r+1}, \tag{150}$$

where the Lagrange error term in the first line is evaluated at some $\tilde{q} \in [r, r+q_t]$. We will show that for $t \geq t_0$ we have

$$\Phi_t^{(\kappa_r+1)}(r) \geq \frac{\Phi_t^{(\kappa_r+2)}(\tilde{q})}{\kappa_r+1} q_t \,, \tag{151}$$

which implies

$$\Phi_t'(r+q_t) \geq \frac{1}{2} \frac{\Phi_t^{(\kappa_r+1)}(r)}{\kappa_r!} q_t^{\kappa_r} \,. \tag{152}$$

We have that $\Phi_t'(p) > 0$ so by Eq. (150) we infer using (151) that $\Phi_t^{(\kappa_r+1)}(r) > 0$ and hence we have a non-trivial lower bound of the form

$$\Phi_t'(r+q_t) \geq \lambda_r = \frac{1}{2} \frac{\Phi_t^{(\kappa_r+1)}(r)}{\kappa_r!} t^{-1/3} = \frac{1}{2} \frac{\Phi^{(\kappa_r+1)}(r)}{\kappa_r!} t^{2/3} \tag{153}$$

and observe that $2\pi\lambda_r/L \geq \lambda$. It thus remains to show (151) which follows easily noticing that we can make q_t sufficiently small using $t \geq t_0$. This condition is implied by finding that

$$\Phi^{(\kappa_r+1)}(r) \geq \frac{C_{\max}^{(\kappa_r+2)}}{\kappa_r+1} t^{-1/(3\kappa_r)} \,, \tag{154}$$

which is equivalent to

$$t \geq \left(\frac{1}{\kappa_r+1} \frac{C_{\max}^{(\kappa_r+2)}}{\Phi^{(\kappa_r+1)}(r)} \right)^{3\kappa_r} . \tag{155}$$

This can be shown to be true by invoking the definition of t_0.

Step 1, case 2: $r \in \mathcal{S}^{(2)}$.
Expanding around $r+q_t$ we obtain

$$\Phi_t'(r+q_t+p_t) = \Phi_t'(r+q_t) + \Phi_t''(r+q_t)p_t + \tfrac{1}{2}\Phi_t'''(\tilde{q})p_t^2 \,, \tag{156}$$

where the Lagrange error term in the first line is evaluated at some $\tilde{q} \in [r+q_t, r+q_t+p_t]$. Note that we choose q_t and p_t small enough such that there is no repeated roots at this step. Because $\Phi_t'(r+q_t) \geq 0$

$$\Phi_t'(r+q_t+p_t) \geq \Phi_t'(r+p_t+q_t) - \Phi_t'(r+q_t) \tag{157}$$

$$\geq \Phi_t''(r+q_t)p_t + \tfrac{1}{2}\Phi_t'''(\tilde{q})p_t^2 \,. \tag{158}$$

We will show below that

$$\Phi_t''(r+q_t) \geq \Phi_t'''(\tilde{q})p_t, \tag{159}$$

which directly implies

$$\Phi_t'(r+q_t+p_t) \geq \tfrac{1}{2}\Phi_t''(r+q_t)p_t\ . \tag{160}$$

We next continue to expand $\Phi_t''(r+q_t)$ around r using the Taylor expansion

$$\Phi_t''(r+q_t) = \frac{\Phi_t^{(\kappa_r+2)}(r)}{\kappa_r!}q_t^{\kappa_r} + \frac{1}{2}\frac{\Phi_t^{(\kappa_r+3)}(\tilde{q})}{(\kappa_r+1)!}q_t^{\kappa_r+1}, \tag{161}$$

where the last term is the Lagrange error term, so $\tilde{q}\in[r,r+q_t]$ and $\kappa_r\geq 1$ was defined above. We check that q_t is sufficiently small such that $\left|\Phi_t^{(\kappa_r+2)}(r)\right| \geq \left|\frac{\Phi_t^{(\kappa_r+3)}(r)}{\kappa_r+1}q_t\right|$. Indeed, using $t\geq t_0$ leads to

$$q_t^{-1} = t^{1/(3\kappa_r)} \geq t_0^{1/(3\kappa_r)} \geq \frac{1}{\kappa_r+1}\left|\frac{\Phi_t^{(\kappa_r+3)}(r)}{\Phi_t^{(\kappa_r+2)}(r)}\right|\ , \tag{162}$$

which after a simple rearrangement leads to that observation. This in turn implies that

$$\Phi_t''(r+q_t) \geq \frac{1}{2}\frac{\Phi_t^{(\kappa_r+2)}(r)}{\kappa_r!}q_t^{\kappa_r}\ . \tag{163}$$

Note that this is a non-trivial bound as due to the monotonicity on $\mathcal{I}_r$ we have $\Phi_t''>0$ and so $\Phi_t^{(\kappa_r+2)}(r)$ cannot be negative because the other term on the right hand side of (161) would be too small to make the whole right hand side positive. We are now in the position to check that condition (159) is satisfied which is implied by showing

$$\frac{1}{2}\frac{\Phi^{(\kappa_r+2)}(r)}{\kappa_r!}q_t^{\kappa_r} \geq C_{\max}^{(3)}p_t\ , \tag{164}$$

$$\frac{1}{2}\frac{\Phi^{(\kappa_r+2)}(r)}{\kappa_r!}t^{-1/3} \geq C_{\max}^{(3)}C_0 t^{-1/3}\ , \tag{165}$$

which is equivalent to

$$C_0 \leq \frac{\Phi^{(\kappa_r+2)}(r)}{2\kappa_r!C_{\max}^{(3)}}\ , \tag{166}$$

again using $\Phi_t^{(\kappa_r+2)}(r)\geq 0$ we find that this is true by comparing to the definition (143). With this result we obtain the lower bound (160) and explicitly inserting the time dependence arrive at

$$\Phi_t'(r+q_t+p_t) \geq \lambda_r = \frac{1}{4\kappa_r!}\Phi_t^{(\kappa_r+2)}(r)C_0t^{-2/3} = \frac{1}{4\kappa_r!}\Phi^{(\kappa_r+2)}(r)C_0t^{1/3}\ , \tag{167}$$

where again we find $2\pi\lambda_r/L\geq\lambda$, as desired.

Step 1 summary: Using (135) we obtain the following uniform bound lower bound $\delta_k\geq\lambda$ for $k\in\mathcal{I}_r\cap\mathcal{S}_t^c$ and any $r\in\mathcal{S}$.

Step 2: Upper bound $|\delta_k|\leq 2\pi-\lambda$. We show this by the bound

$$|\delta_k| \leq \frac{2\pi}{L}\max_{p\in[0,2\pi)}\left|\Phi_t'(p)\right| \leq \frac{2\pi}{L}(tC_{\max}^{(1)}+|d|)\ . \tag{168}$$

Note that we can always take $|d| \leq L/2$. To see this, suppose that, e.g., $L > d = x - y > L/2$. Then we can replace x by $x' = x + L$, which does not affect the propagator, but now we have $|x' - y| \leq L/2$. A similar trick works if $x - y < -L/2$. So we can upper bound $2\pi|d|/L$ by π, and we

$$|\delta_k| \leq \frac{2\pi t C^{(1)}_{\max}}{L} + \pi\,. \tag{169}$$

Next, we make use of Eq. (141) to see that

$$\frac{2\pi t C^{(1)}_{\max}}{L} + \lambda \leq \frac{2\pi t C^{(1)}_{\max}}{L} + \frac{2\pi}{L} C_1 t \leq \pi\,, \tag{170}$$

which implies

$$|\delta_k| \leq 2\pi - \lambda\,. \tag{171}$$

Hence for each $\mathcal{I}_r$ we can apply the Kusmin bound for times $t_0 \leq t \leq t_R$.

Step 3: Use the Kusmin-Landau lemma and obtain the final bound.
Summing up the discarded contribution and taking into account the bound on the number of the monotonous intervals we obtain the bound

$$\frac{1}{L}\left|\sum_{k=1}^{L} e^{i\varphi_k}\right| \leq (4R+2)\left[\frac{p_t + q_t}{\pi} + C_1^{-1} t^{-1/3}\right] \leq C_{\#}\, t^{-1/(3\kappa_0)}\,, \tag{172}$$

where we have used that there are at most $4R+2$ Kusmin-Landau intervals that we restrict each at the edges by fewer than $L2(p_t+q_t)/\pi$ points and where the last term is the Kusmin-Landau bound. Inspecting the definition of C_1 we find that

$$C_1^{-1} = 4\max\left\{\max_{r\in\mathcal{S}^{(1)}} \frac{\kappa_r!}{\left|\Phi^{(\kappa_r+1)}(r)\right|}, 2C^{(3)}_{\max} \max_{r\in\mathcal{S}^{(2)}} \frac{(\kappa_r!)^2}{\left|\Phi^{(\kappa_r+2)}(r)\right|}^2\right\}. \tag{173}$$

Here, we have put the absolute values such that the bound in this form remains valid for monotonously growing and decreasing intervals. Hence, the constant $C_{\#}$ reads

$$C_{\#} := 6(2R+1)\max\left\{1, \min_{r\in\mathcal{S}^{(2)}} \frac{\left|\Phi^{(\kappa_r+2)}(r)\right|}{2C^{(3)}_{\max}\kappa_r!}, \max_{r\in\mathcal{S}^{(2)}} \frac{8\,(\kappa_r!)^2\, C^{(3)}_{\max}}{\left|\Phi^{(\kappa_r+2)}(r)\right|^2}, \max_{r\in\mathcal{S}^{(1)}} \frac{4\kappa_r!}{\left|\Phi^{(\kappa_r+1)}(r)\right|}\right\}. \tag{174}$$

Generic case. Let us finally remark on the generic case assuming there are no points for which $\Phi''(p) = \Phi'''(p) = 0$. For $r \in \mathcal{S}^{(1)}$ we can set $\kappa_r = 1$ whenver $\Phi''(r) \neq 0$. If $\Phi'(r) = \Phi''(r) = 0$ then in the generic case we will have $\Phi'''(r) \neq 0$ which would yield $\kappa_r = 2$ but then our bound would be dominated by $q_t = t^{-1/6}$ which we can improve. Instead expanding in q_t we expand in $w_t = t^{-1/3}$ obtaining the equation

$$\Phi_t'(r + w_t) = \frac{\Phi_t'''(r)}{2} w_t^2 + \frac{\Phi_t^{(3)}(\tilde{q})}{6} w_t^3\,. \tag{175}$$

As only the expansion length has changed we would find along the same arguments the lower bound

$$\Phi_t'(r + w_t) \geq \lambda_r = \frac{\Phi_t'''(r)}{4} w_t^2 = \frac{\Phi_t'''(r)}{4} t^{1/3}\,. \tag{176}$$

Therefore we are removing $\sim t^{-1/3}$ points and $\lambda^{-1} \sim t^{-1/3}$ also so the terms contributed from this case will have the scaling $\sim t^{-1/3}$. For $r \in \mathcal{S}^{(2)}$ we set $\kappa_r = 1$ and directly get the lower bound (148) also with the scaling $\sim t^{-1/3}$.

□

In the main text, we have stated that $C_\#$ can in fact to be taken in a simpler form in the generic case where we have no points such that $\Phi_t''(r) = \Phi_t'''(r) = 0$. This means that $C_0 \leq 1$. If $\kappa_r = 1$ then nothing changes in our expansions. For $r \in \mathcal{S}^{(1)}$ also $\kappa_r = 2$ is possible. In this case, inspecting Eq. (175) we find that find that $\Phi_t'''(r)/4$ is the contribution to the C_1 constant instead of $\Phi_t''(r)/2$. This means that altogether we can define

$$M = \frac{1}{4}\min\left\{\min_{r\in\mathcal{S}^{(1)}}\left|\Phi^{(\kappa_r+1)}(r)\right|, \min_{r\in\mathcal{S}^{(2)}}\left|\Phi^{(3)}(r)\right|^2\right\}, \tag{177}$$

which leads us to the simplified constant

$$C_\# = 6(2R+1)\max\left\{1, \frac{8C^{(3)}_{\max}}{M^2}\right\}. \tag{178}$$

Finally, it is worth mentioning that one can go beyond this setting by breaking up the gaps into those in the window $[\lambda, 2\pi-\lambda]$ and those in the window $[2\pi+\lambda, 4\pi-\lambda]$. Then we can apply the Kusmin bound to terms in each window separately. One can shift the gaps in $[2\pi+\lambda, 4\pi-\lambda]$ by making the substitution $a_n \mapsto a_n - 2\pi n$, which leads to $\delta_n \mapsto \delta_n - 2\pi$. Because we have only shifted a_n by multiples of 2π, this does not affect the exponential sum. After this shift, δ_n are in the interval $[\lambda, 2\pi-\lambda]$, and we can apply the Kusmin bound. This way, we would get bounds on equilibration valid for times after t_R. One could continue this process further with windows $[2n\pi+\lambda, 2(n+1)\pi-\lambda]$ for $n \in \mathbb{N}$, as long as the number of windows is small compared to L. It would be interesting to see if this patch-working of the Kusmin-Landau method for long times breaks down at the Poincare recurrence time which is much longer than the finite size revival time.

D Quasi-free ergodicity

For clarity we restate the theorem from the main text.

Theorem 19 (Free fermionic ergodicity). *Let $t \mapsto G(t)$ be the propagator for a non-interacting translation invariant fermionic Hamiltonian $\hat{H}(h)$ which is off-diagonal on the one-dimensional real-space lattice. Then for all times t between a relaxation time $t_0 = O(1)$ up until a recurrence time $t_R = \Theta(L)$ the propagator obeys*

$$|G_{x,y}(t)| \leq C t^{-\gamma}, \tag{179}$$

where $C, \gamma > 0$ are constants. We can take $\gamma = 1/3$, provided there are no points p such that $E''(p) = E'''(p) = 0$ which is true for generic models.

Proof of theorem: Quasi-free ergodicity. As was explained in the main text we need to formulate a phase function such that it evaluates to the phases of the propagator. This is achieved by

$$\Phi_t(p) = dp + t\sum_{z=1}^{R} J_z \cos(zp) + J_0, \tag{180}$$

which evaluates to

$$\varphi_k = \Phi_t(p_k) = t\omega_k + 2\pi dk/L \tag{181}$$

for $p = 2\pi/L$ and $d = x - y$. By Theorem 13, we hence find the bound with $C_\#$ given in Eq. (174) being system size independent as the couplings are fixed. The relaxation and recurrence times t_0 and t_R are given implicitly by the constraints in the proof of Theorem 13. The generic behaviour of the exponent $\gamma = 1/(3\kappa_0)$ is obtained for $\kappa_0 = 1$ which is attained at the wavefront of the nearest-neighbour hopping model [50]. □

E Equilibration of the covariance matrix

In this section we will bound the deviations of the time evolved second moments $\Gamma(t)$ from the equlibrium covariance matrix $\Gamma^{(\mathrm{eq})}$ defined in Eq. (19) by a uniform real-space average of the local current densities.

Proposition 20 (Equilibration of second moments)**.** *Consider a fermionic system with initially exponentially decaying correlations and non-resilient second moments* Γ*. Then there exist a constant relaxation time* t_0 *and a recurrence time* $t_R = \Theta(L)$ *such that, for all* $t \in [t_0, t_R]$*,*

$$\left|\Gamma_{x,y}(t) - \Gamma^{(\mathrm{eq})}_{x,y}\right| \leq C_\Gamma t^{-\gamma}, \tag{182}$$

where $C_\Gamma, \gamma > 0$ *are constants.*

Proof. Our goal is to bound how quickly $\Gamma_{x,y}(t)$, where $\Gamma(t) = G(t)\Gamma G(t)^\dagger$, relaxes towards the equilibrium values. First notice that these equal a real-space average where the value depends only on the separation $d = \min\{|x-y|, |x-y+L|, |x-y-L|\}$. Let us define the decomposition of Γ into its currents, that is $\Gamma = \sum_{d=-\lfloor (L+1)/2\rfloor+1}^{\lfloor L/2\rfloor} \Gamma^{(d)}$ with entries

$$\Gamma^{(d)}_{x,y} = \Gamma_{x,y}\delta_{x,y+d}\,, \tag{183}$$

where we use the convention $\delta_{a,b+L} = \delta_{a,b}$. The evolution is linear, so

$$\Gamma(t) = \sum_{d=-\lfloor (L-1)/2\rfloor+1}^{\lfloor L/2\rfloor} \Gamma^{(d)}(t)\,, \tag{184}$$

where we define

$$\Gamma^{(d)}_{x,y}(t) := \left(G(t)\Gamma^{(d)}G(t)^\dagger\right)_{x,y} = \sum_{z,w}^{L} G_{x,w}(t)\Gamma^{(d)}_{w,z}G^*_{y,z}(t) \tag{185}$$

$$= \sum_{z,w=1}^{L} G_{x,w}(t)\Gamma_{w,z}\delta_{w,z+d}G^*_{y,z}(t) \tag{186}$$

$$= \sum_{z=1}^{L} G_{x,z+d}(t)\Gamma_{z+d,z}G^*_{y,z}(t)\,. \tag{187}$$

Our target equilibrium ensemble has matrix elements given by

$$\Gamma^{(\mathrm{eq})}_{x,y} = \sum_{d=-\lfloor (L+1)/2\rfloor+1}^{\lfloor L/2\rfloor} I_d\delta_{x,y+d}\,, \tag{188}$$

where specifically the value equilibrium values read

$$I_d = \frac{1}{L}\sum_x \Gamma_{x,x+d}\,. \tag{189}$$

If the initial covariance matrix is real then this is exactly the d-th current in the initial state. Otherwise, one has to consider also the 'complex' currents as discussed above. With these definitions, we obtain the bound

$$\left|\Gamma_{x,y}(t) - \Gamma^{(\mathrm{eq})}_{x,y}\right| \leq \sum_{d=-\lfloor (L+1)/2\rfloor+1}^{\lfloor L/2\rfloor} \left|\Gamma^{(d)}_{x,y}(t) - I_d\delta_{x,y+d}\right| \tag{190}$$

by using the triangle inequality. After these steps organizing the notation, we will present a first non-trivial bound showing that in the above sum only the currents with $d \leq d_\xi(t)$ contribute significantly. This is natural because of the exponentially decaying correlations so denoting the correlation length as ξ it suffices to use Lemma 12 with

$$d_\xi(t) = \xi \ln(t^{1/(3\kappa_0)}) \,, \tag{191}$$

where κ_0 is a positive constant which is indpendent of the system size and will be defined below. Then the currents $d > d_\xi(t)$ will negligibly contribute to $\|\Gamma(t) - \Gamma^{(\mathrm{eq})}\|_{\max}$ for sufficiently large $t > t_0$. So we consider $d \leq d_\xi(t)$. Now we expand $\Gamma^{(d)}$ via the discrete Fourier transform

$$\Gamma_{z+d,z} = \sum_{n=1}^{L} \mathcal{X}_n^{(d)} e^{2\pi i n z/L} \,. \tag{192}$$

Then we have that

$$\Gamma_{x,y}^{(d)}(t) = \sum_{z=1}^{L} G_{x,z+d}(t) G_{y,z}^*(t) \Gamma_{z+d,z} = \sum_{n=1}^{L} \mathcal{X}_n^{(d)} \sum_{z=1}^{L} G_{x,z+d}(t) G_{y,z}^*(t) e^{2\pi i n z/L} \,. \tag{193}$$

Recall the definition of the propagator

$$G_{x,y}(t) = \frac{1}{L} \sum_{k=1}^{L} \exp(i\omega_k t + 2\pi i k(x-y)/L) \,, \tag{194}$$

by which we get

$$\Gamma_{x,y}^{(d)}(t) = \frac{1}{L^2} \sum_{n=1}^{L} \mathcal{X}_n^{(d)} \sum_{r,s=1}^{L} \sum_{z=1}^{L} e^{i\omega_r t + 2\pi i r(x-z-d)/L} e^{-i\omega_s t - 2\pi i s(y-z)/L} e^{2\pi i n z/L} \tag{195}$$

$$= \frac{1}{L^2} \sum_{n=1}^{L} \mathcal{X}_n^{(d)} \sum_{r,s=1}^{L} e^{i(\omega_r - \omega_s)t + 2\pi i(rx - sy - rd)/L} \sum_{z=1}^{L} e^{2\pi i z(-r+s+n)/L} \,. \tag{196}$$

Next, we use

$$\sum_{z=1}^{L} e^{2\pi i z(-r+s+n)/L} = L \sum_{\mu \in \mathbb{Z}} \delta_{-r+s+n,\mu L} \,, \tag{197}$$

applying it to the sum over r while summing over s, n. Then we find that $-r+s+n = \mu L$ has solutions with either $\mu = 0$ or $\mu = 1$ but not at the same time because of the variable range $r, s, n \in [L]$. Indeed, we always have $2 \leq s+n \leq 2L$ and so we have the unique solutions $r = s+n$ for $s+n \leq L$ and $r = s+n-L$ for $s+n \geq L$. Thus, using $\omega_{k+\mu L} = \omega_k$ which follows by inspecting the definition in Eq. (84) we get

$$\Gamma_{x,y}^{(d)}(t) = \frac{1}{L} \sum_{n=1}^{L} \mathcal{X}_n^{(d)} e^{2\pi i n(x-d)/L} \sum_{s=1}^{L} e^{i(\omega_{(s+n)} - \omega_s)t + 2\pi i s(x-y-d)/L} \tag{198}$$

$$= \sum_{n=1}^{L} \mathcal{X}_n^{(d)} e^{2\pi i n(x-d)/L} f_n(t) \,. \tag{199}$$

In the last line, we have defined

$$f_n(t) := \frac{1}{L} \sum_{s=1}^{L} e^{i(\omega_{(s+n)} - \omega_s)t + 2\pi i s(x-y-d)/L} \,. \tag{200}$$

The equilibrium currents will be uniform so we need to bound

$$\left|\Gamma^{(d)}_{x,y}(t) - I_d\delta_{x,y+d}\right| = \left|\sum_{n=1}^{L-1}\mathcal{X}^{(d)}_n e^{2\pi i n z/L} f_n(t)\right| , \tag{201}$$

because

$$I_d = \mathcal{X}^{(d)}_L . \tag{202}$$

As we have observed in the main text, we have

$$\omega_{(k+n)} - \omega_k = \sum_{z=1}^{R} K_z \sin\left(\frac{2\pi z k}{L} + \frac{\pi n z}{L}\right) , \tag{203}$$

with $K_z = -4J_z \sin(\pi z n/L)$. In order to use the dephasing bound from theorem 13, we define

$$\Phi_t(p) = -4t\sum_{z=1}^{R} J_z \sin(\alpha z)\sin(zp + z\alpha) + p(x-y-d) \tag{204}$$

and by evaluating with $\alpha = \pi n/L$ and $p_k = 2\pi k/L$, we have

$$\varphi_k = \Phi_t(p_k) = (\omega_{(k+n)} - \omega_k)t + 2\pi i k(x-y-d)/L . \tag{205}$$

We hence obtain the bound

$$|f_n(t)| \leq C_{\#}(\alpha) t^{-1/(3\kappa_0)} , \tag{206}$$

where now $C_{\#}$ depends on the derivatives of (204) evaluated at roots and we indicate the dependance on α as for $\alpha \approx 0$ the constant would not be system size independent. As long as K_z have no stray dependence on L these values are constant numbers in the system size so we can scale up the system size and get a non-trivial bound. All this is secured by using the assumption of non-resilient correlations which leads to

$$\begin{aligned}\left|\Gamma^{(d)}_{x,y}(t) - I_d\delta_{x,y+d}\right| &= \sum_{\substack{n=1\\ n\pi/L\in\mathcal{R}}}^{L-1}\left|\mathcal{X}^{(d)}_n\right| + \sum_{\substack{n=1\\ n\pi/L\notin\mathcal{R}}}^{L-1}\left|\mathcal{X}^{(d)}_n\right| |f_n(t)| && (207)\\ &\leq C_{\mathrm{RS}} L^{-1} + C_{\mathrm{NRS}} C_{\mathrm{th}} t^{-1/(3\kappa_0)} && (208)\\ &\leq (C_{\mathrm{RS}} + C_{\mathrm{NRS}} C_{\mathrm{th}}) t^{-1/(3\kappa_0)} , && (209)\end{aligned}$$

where we have used $L^{-1} \leq t^{-1/(3\kappa_0)}$, which holds true for $t \leq t_R = \Theta(L)$. We now finalize the total bound by

$$\begin{aligned}\left|\Gamma_{x,y}(t) - \Gamma^{(\mathrm{eq})}_{x,y}\right| &\leq 2d_\xi(t) \max_{|d|\leq d_\xi(t)}\left|\Gamma^{(d)}_{x,y}(t) - \Gamma^{(\mathrm{eq})}_{x,y}\right| + \frac{C_{\mathrm{Clust}}}{1+e^{-1/\xi}} t^{-1/3\kappa_0} && (210)\\ &\leq \tfrac{1}{2} C_\Gamma \ln(t^{1/(3\kappa_0)}) t^{-1/(3\kappa_0)} + \frac{C_{\mathrm{Clust}}}{1+e^{-1/\xi}} t^{-1/3\kappa_0} , && (211)\end{aligned}$$

where we have defined

$$C_\Gamma := \max\left\{4\xi(C_{\mathrm{RS}} + C_{\mathrm{NRS}} C_{\mathrm{th}}), \frac{2C_{\mathrm{Clust}}}{1+e^{-1/\xi}}\right\} . \tag{212}$$

Observe that $\kappa_0 \leq 2R$. Thus, for sufficiently large t we have for some $\varepsilon > 0$ the final bound

$$\|\Gamma(t) - \Gamma^{(\mathrm{eq})}\|_{\max} = \max_{x,y}\left|\Gamma_{x,y}(t) - \Gamma^{(\mathrm{eq})}_{x,y}\right| \leq C_\Gamma t^{-1/(3\kappa_0)+\varepsilon} . \tag{213}$$

□

F Examples of non-resilient second moments

F.1 m-step periodic states

Suppose $\Gamma_{z+d,z}$ is m-step periodic, with $\ell = L/m \in \mathbb{N}$, so that $\Gamma_{z+d+m,z+m} = \Gamma_{z+d,z}$. We get

$$\mathcal{X}_n^{(d)} = L^{-1} \sum_{z=0}^{L-1} \Gamma_{z+d,z} e^{-2\pi i n z/L} \tag{214}$$

$$= L^{-1} \sum_{u=0}^{m-1} \sum_{v=0}^{L/m-1} \Gamma_{u+vm+d,u+vm} e^{-2\pi i n(u+vm)/L} \tag{215}$$

$$= \left(\frac{1}{m} \sum_{u=0}^{m-1} \Gamma_{u+d,u} e^{-2\pi i n u/L} \right) \left(\frac{m}{L} \sum_{v=0}^{L/m-1} e^{-2\pi i n v m/L} \right) \tag{216}$$

$$= \left(\frac{1}{m} \sum_{u=0}^{m-1} \Gamma_{u+d,u}\, e^{-2\pi i n u L} \right) \left(\sum_{\alpha=0}^{m-1} \delta_{n,\alpha\ell} \right) . \tag{217}$$

So all $\mathcal{X}_n^{(d)}$ are vanishing, except those with with $n = \alpha\ell$, where $\alpha \in \{0, \ldots, m-1\}$.

F.2 Random dislocations

Suppose $\Gamma^{(d)}$ can be decomposed as $\Gamma^{(d)} = \Gamma^{(d,NR)} + \Gamma^{(d,SR)}$ where $\Gamma^{(d,NR)}$ is non-resilient and $\Gamma^{(d,NR)}$ has sparse support. Then $\Gamma^{(d)}$ is again non-resilient. This follows trivially as for the sparse part the Fourier transform is bounded by the inverse system size

$$|\mathcal{X}_n^{(d)}| \leq L^{-1} \sum_{z=0}^{L-1} |\Gamma_{z+d,z}^{(d,SR)}| \leq \frac{S}{L} , \tag{218}$$

where $S = O(1)$ is the number of the sparse entries in $\Gamma^{(d,SR)}$.

F.3 Uniformly random currents

Take $\Gamma_{z+d,z} \in [a, b]$ to be uniformly and independently distributed. Then $\Gamma^{(d)}$ is non-resilient. Indeed, we find that on average, we have

$$\mathbb{E}[\mathcal{X}_n^{(d)}] = \frac{1}{L} \sum_{z=1}^{L} \mathbb{E}[\Gamma_{z+d,z}] e^{-2\pi i n z/L} \tag{219}$$

$$= \frac{a+b}{2} L^{-1} \sum_{z=0}^{L-1} e^{-2\pi i n z/L} \tag{220}$$

$$= \frac{a+b}{2} \delta_{n,L} . \tag{221}$$

We furthermore calculate the second moment using

$$\mathbb{E}[\Gamma_{x,y}^2] = \frac{a^2 + ab + b^2}{3} \tag{222}$$

to get

$$\mathbb{E}[|\mathcal{X}_n^{(d)}|^2] = \frac{1}{L^2}\sum_{z,s=1}^{L}\mathbb{E}[\Gamma_{z+d,z}\Gamma_{s+d,s}]e^{-2\pi i n(s-z)/L} \tag{223}$$

$$= \frac{1}{L^2}\sum_{\substack{z,s=1\\ z\neq s}}^{L}\mathbb{E}[\Gamma_{z+d,z}\Gamma_{s+d,s}]e^{-2\pi i n(s-z)/L} + \frac{1}{L^2}\sum_{z=1}^{L}\mathbb{E}[\Gamma_{z+d,z}^2] \tag{224}$$

$$= \frac{a^2+2ab+b^2}{4L^2}\left(\sum_{z,s=1}^{L}e^{-2\pi i n(s+z)/L} - L\right) + \frac{a^2+ab+b^2}{3L} \tag{225}$$

$$= \mathbb{E}[\mathcal{X}_n^{(d)}]^2 + \frac{(a-b)^2}{12L}\,, \tag{226}$$

and hence the variance reads

$$\mathrm{Var}[\mathcal{X}_n^{(d)}] = \frac{(a-b)^2}{12L}\,. \tag{227}$$

By Chebyshev's inequality

$$\mathbb{P}\left(\left|\mathcal{X}_n^{(d)} - \mathbb{E}[\mathcal{X}_n^{(d)}]\right| \geq K\right) \leq \frac{\mathrm{Var}[\mathcal{X}_n^{(d)}]}{K^2}\,, \tag{228}$$

we obtain that

$$\left|\mathcal{X}_n^{(d)} - \mathbb{E}[\mathcal{X}_n^{(d)}]\right| \leq KL^{-1/2}\,, \tag{229}$$

with probability greater than $1-(CK)^{-2}$.

F.4 Resilient example: $P = L/2$ - periodic block calculation

Say L is even and we have a state with

$$\langle \hat{f}_x^\dagger \hat{f}_x\rangle = \begin{cases} 1, & x < L/2 \\ 0, & x \geq L/2\,. \end{cases} \tag{230}$$

Then all currents with $d \neq 0$ vanish and we should calculate the Fourier transform of the diagonal of the covariance matrix namely

$$\mathcal{X}_n^{(d)} = \sum_{k=1}^{L/2-1} e^{2\pi i n k/L} = \begin{cases} \frac{1-e^{i\pi n}}{1-e^{i\pi}} = 1, & n \text{ is odd} \\ 0, & n \text{ is even}\,. \end{cases} \tag{231}$$

Therefore there is no chance that we can get a non-trivial bound of the form

$$\left|\Gamma_{x,y}(t) - \Gamma_{x,y}^{(\mathrm{eq})}\right| \leq \sum_{n=1}^{L}\left|\mathcal{X}_n^{(d)}\right||f_n(t)|\,, \tag{232}$$

because it will scale with the system size as $\sim LC_{\mathrm{th}}t^{-\gamma}/2$ due to the number of non-trivial harmonics.

F.5 Details of quenches from disordered to translation invariant models

In this section, we provide more details on the discussion of the simularity of averaged generalized Gibbs ensembles with thermal ensembles. In this context, it is useful to discuss the exact quench state $\Gamma^{(\mathrm{Quench})}(t)$ and the infinite-time average $\Gamma^{(\infty)}$ on the level of quasiparticle occupation numbers in momentum space. For the quenched state these stay constant for all times due to unitarity and we have checked that typically there are initially fluctuations around the idealized Fermi-Dirac distribution but a Fermi edge can be observed. However, in order to obtain the infinite time average we apply a dephasing channel which as it is not unitary does change the occupation numbers despite conserving the relevant local currents. In that case we have noticed a much smoother quasiparticle number distribution, resembling much closer the thermal Fermi-Dirac distribution. Additionally we noticed that for the same model with the noise uniformly distributed in $[0, w]$ the resulting equilibrium state is not thermal, but additionally considering a chemical potential leads to agreement. These observations suggest that the equilibration process that we have discussed analytically leads to a thermal steady state for the particular selection of initial states discussed here which are thermal states of a Hamiltonian with the same tunnelling range as the quench Hamiltonian. It appears to be an interesting question whether we can in general expect GGEs which are simply thermal steady-states in the natural case occurring in many physical instances where the kinetic energy is an inherent property of the system over which we have little control and we prepare thermal initial states by controlling only the on-site potential by external forces.

A peculiarity stemming from quasi-free integrability is that it is enough to have access to only one translation invariant quench Hamiltonian to prepare thermal states of any other translation invariant model just by assigning the initial correlation content. In particular being able to tune the correlation length is a crucial ingredient, but the initial correlations need not be translation invariant or even Gaussian, as we have discussed above. Thanks to the Gaussification result, one can also use many-body interactions to tune close to a phase transition in order to increase the correlation length even if the state obtained will be non-Gaussian. Indeed we have a proof of equilibration to a Gaussian state but now the steady state may acquire an unusually large correlation length for a thermal state of the quench Hamiltonian. This "one to rule them all" result shows that the properties of the equilibrated state may be unrelated to the range of the dynamics, which is slightly at odds with the usual approach to inferring microscopic properties of various materials. It would be interesting to see whether experiments measuring only conductivity or other linear response properties could be adversarily tricked to indicate always different dynamical models by getting different states as input while the true Hamiltonian is always merely the nearest neighbour model. Such interactive experiments may be possible with existing quantum simulation technologies [85]. On the other hand if precise microscopic measurements are limited, then observing just the fundamental qualitative properties such as the formation of the Fermi edge which determines solid state properties should be a generic feature independent of the memory effect due to integrability. As there is only few trailblazing works concerning what happens to a GGE in the presence of weak interactions [91–94], it would be exciting to study this systematically in optical lattices experimentally.

References

[1] J. Eisert, M. Friesdorf and C. Gogolin, *Quantum many-body systems out of equilibrium*, Nat. Phys. **11**, 124 (2015), doi:10.1038/nphys3215.

[2] A. Polkovnikov, K. Sengupta, A. Silva and M. Vengalattore, *Colloquium: nonequilib-*

rium dynamics of closed interacting quantum systems, Rev. Mod. Phys. **83**, 863 (2011), doi:10.1103/RevModPhys.83.863.

[3] J. Goold, M. Huber, A. Riera, L. del Rio and P. Skrzypczyk, *The role of quantum information in thermodynamics—a topical review*, J. Phys. A **49**, 143001 (2016), doi:10.1088/1751-8113/49/14/143001.

[4] C. Gogolin and J. Eisert, *Equilibration, thermalisation, and the emergence of statistical mechanics in closed quantum systems*, Rep. Prog. Phys. **79**, 056001 (2016), doi:10.1088/0034-4885/79/5/056001.

[5] T. Mori, T. N. Ikeda, E. Kaminishi and M. Ueda, *Thermalization and prethermalization in isolated quantum systems: a theoretical overview*, J. Phys. B: At. Mol. Opt. Phys. **51**, 112001 (2018), doi:10.1088/1361-6455/aabcdf.

[6] A. M. Kaufman, M. E. Tai, A. Lukin, M. Rispoli, R. Schittko, P. M. Preiss and M. Greiner, *Quantum thermalization through entanglement in an isolated many-body system*, Science **353**, 794 (2016), doi:10.1126/science.aaf6725.

[7] T. Kinoshita, T. Wenger and D. S. Weiss, *A quantum newton's cradle*, Nature **440**, 900 (2006), doi:10.1038/nature04693.

[8] H. Bernien, S. Schwartz, A. Keesling, H. Levine, A. Omran, H. Pichler, S. Choi, A. S. Zibrov, M. Endres, M. Greiner, V. Vuletić and M. D. Lukin, *Probing many-body dynamics on a 51-atom quantum simulator*, Nature **551**, 579 (2017), doi:10.1038/nature24622.

[9] C. J. Turner, A. A. Michailidis, D. A. Abanin, M. Serbyn and Z. Papić, *Weak ergodicity breaking from quantum many-body scars*, Nat. Phys. **14**, 745 (2018), doi:10.1038/s41567-018-0137-5.

[10] C. Li, T. Zhou, I. Mazets, H. Stimming, Z. Zhu, Y. Zhai, W. Xiong, X. Zhou, X. Chen and J. Schmiedmayer, *Dephasing and relaxation of bosons in 1D: Newton's Cradle revisited* (2018), arXiv:1804.01969v1.

[11] M. Schreiber, S. S. Hodgman, P. Bordia, H. P. Lüschen, M. H. Fischer, R. Vosk, E. Altman, U. Schneider and I. Bloch, *Observation of many-body localization of interacting fermions in a quasi-random optical lattice*, Science **349**, 842 (2015), doi:10.1126/science.aaa7432.

[12] T. Langen, S. Erne, R. Geiger, B. Rauer, T. Schweigler, M. Kuhnert, W. Rohringer, I. E. Mazets, T. Gasenzer and J. Schmiedmayer, *Experimental observation of a generalized Gibbs ensemble*, Science **348**, 207 (2015), doi:10.1126/science.1257026.

[13] D. A. Abanin, E. Altman, I. Bloch and M. Serbyn, *Colloquium: Many-body localization, thermalization, and entanglement*, Rev. Mod. Phys. **91**, 021001 (2019), doi:10.1103/RevModPhys.91.021001.

[14] M. Cramer, C. M. Dawson, J. Eisert and T. J. Osborne, *Exact relaxation in a class of nonequilibrium quantum lattice systems*, Phys. Rev. Lett. **100**, 030602 (2008), doi:10.1103/PhysRevLett.100.030602.

[15] M. Rigol, V. Dunjko and M. Olshanii, *Thermalization and its mechanism for generic isolated quantum systems*, Nature **452**, 854 (2008), doi:10.1038/nature06838.

[16] M. Rigol, V. Dunjko, V. Yurovsky and M. Olshanii, *Relaxation in a completely integrable many-body quantum system: An ab initio study of the dynamics of the highly excited states of 1D lattice hard-core bosons*, Phys. Rev. Lett. **98**, 050405 (2007), doi:10.1103/PhysRevLett.98.050405.

[17] J.-S. Caux and F. H. L. Essler, *Time evolution of local observables after quenching to an integrable model*, Phys. Rev. Lett. **110**, 257203 (2013), doi:10.1103/PhysRevLett.110.257203.

[18] L. Vidmar and M. Rigol, *Generalized gibbs ensemble in integrable lattice models*, J. Stat. Mech. 064007 (2016), doi:10.1088/1742-5468/2016/06/064007.

[19] P. Calabrese, F. H. Essler and M. Fagotti, *Quantum quench in the transverse field ising chain: I. time evolution of order parameter correlators*, J. Stat. Mech. P07016 (2012), doi:10.1088/1742-5468/2012/07/p07016.

[20] B. Wouters, J. De Nardis, M. Brockmann, D. Fioretto, M. Rigol and J.-S. Caux, *Quenching the anisotropic Heisenberg chain: Exact solution and generalized Gibbs ensemble predictions*, Phys. Rev. Lett. **113**, 117202 (2014), doi:10.1103/PhysRevLett.113.117202.

[21] D. A. Huse, R. Nandkishore and V. Oganesyan, *Phenomenology of fully many-body-localized systems*, Phys. Rev. B **90**, 174202 (2014), doi:10.1103/PhysRevB.90.174202.

[22] H. Tasaki, *From quantum dynamics to the canonical distribution: general picture and a rigorous example*, Phys. Rev. Lett. **80**, 1373 (1998), doi:10.1103/PhysRevLett.80.1373.

[23] P. Reimann, *Foundation of statistical mechanics under experimentally realistic conditions*, Phys. Rev. Lett. **101**, 190403 (2008), doi:10.1103/PhysRevLett.101.190403.

[24] N. Linden, S. Popescu, A. J. Short and A. Winter, *Quantum mechanical evolution towards thermal equilibrium*, Phys. Rev. E **79**, 061103 (2009), doi:10.1103/PhysRevE.79.061103.

[25] A. J. Short and T. C. Farrelly, *Quantum equilibration in finite time*, New J. Phys. **14**, 013063 (2012), doi:10.1088/1367-2630/14/1/013063.

[26] P. Reimann and M. Kastner, *Equilibration of isolated macroscopic quantum systems*, New J. Phys. **14**, 043020 (2012), doi:10.1088/1367-2630/14/4/043020.

[27] S. Goldstein, T. Hara and H. Tasaki, *Time scales in the approach to equilibrium of macroscopic quantum systems*, Phys. Rev. Lett. **111**, 140401 (2013), doi:10.1103/PhysRevLett.111.140401.

[28] A. S. Malabarba, L. P. García-Pintos, N. Linden, T. C. Farrelly and A. J. Short, *Quantum systems equilibrate rapidly for most observables*, Phys. Rev. E **90**, 012121 (2014), doi:10.1103/PhysRevE.90.012121.

[29] L. Masanes, A. Roncaglia and A. Acín, *Complexity of energy eigenstates as a mechanism for equilibration*, Phys. Rev. E **87**, 032137 (2013), doi:10.1103/PhysRevE.87.032137.

[30] F. G. S. L. Brandão, P. Ćwikliński, M. Horodecki, P. Horodecki, J. K. Korbicz and M. Mozrzymas, *Convergence to equilibrium under a random Hamiltonian*, Phys. Rev. E **86**, 031101 (2012), doi:10.1103/PhysRevE.86.031101.

[31] M. Cramer, *Thermalization under randomized local Hamiltonians*, New J. Phys. **14**, 053051 (2012), doi:10.1088/1367-2630/14/5/053051.

[32] Vinayak and M. Žnidarič, *Subsystem dynamics under random Hamiltonian evolution*, J. Phys. A **45**, 125204 (2012), doi:10.1088/1751-8113/45/12/125204.

[33] C. Ududec, N. Wiebe and J. Emerson, *Information-theoretic equilibration: the appearance of irreversibility under complex quantum dynamics*, Phys. Rev. Lett. **111**, 080403 (2013), doi:10.1103/PhysRevLett.111.080403.

[34] P. Reimann, *Typical fast thermalization processes in closed many-body systems*, Nat. Commun. **7**, 10821 (2016), doi:10.1038/ncomms10821.

[35] H. Wilming, M. Goihl, C. Krumnow and J. Eisert, *Towards local equilibration in closed interacting quantum many-body systems* (2017), arXiv:1704.06291.

[36] T. R. de Oliveira, C. Charalambous, D. Jonathan, M. Lewenstein and A. Riera, *Equilibration time scales in closed many-body quantum systems*, New J. Phys. **20**, 033032 (2018), doi:10.1088/1367-2630/aab03b.

[37] L. P. García-Pintos, N. Linden, A. S. L. Malabarba, A. J. Short and A. Winter, *Equilibration time scales of physically relevant observables*, Phys. Rev. X **7**, 031027 (2017), doi:10.1103/PhysRevX.7.031027.

[38] T. Farrelly, *Equilibration of quantum gases*, New J. Phys. **18**, 073014 (2016), doi:10.1088/1367-2630/18/7/073014.

[39] F. H. L. Essler and M. Fagotti, *Quench dynamics and relaxation in isolated integrable quantum spin chains*, J. Stat. Mech. 064002 (2016), doi:10.1088/1742-5468/2016/06/064002.

[40] M. Rigol, V. Dunjko, V. Yurovsky and M. Olshanii, *Relaxation in a completely integrable many-body quantum system: An ab initio study of the dynamics of the highly excited states of 1D lattice hard-core bosons*, Phys. Rev. Lett. **98**, 050405 (2007), doi:10.1103/PhysRevLett.98.050405.

[41] M. Rigol, *Quantum quenches and thermalization in one-dimensional fermionic systems*, Phys. Rev. A **80**, 053607 (2009), doi:10.1103/PhysRevA.80.053607.

[42] M. Cramer, A. Flesch, I. McCulloch, U. Schollwöck and J. Eisert, *Exploring local quantum many-body relaxation by atoms in optical superlattices*, Phys. Rev. Lett. **101**, 063001 (2008), doi:10.1103/PhysRevLett.101.063001.

[43] P. R. Zangara, A. D. Dente, E. J. Torres-Herrera, H. M. Pastawski, A. Iucci and L. F. Santos, *Time fluctuations in isolated quantum systems of interacting particles*, Phys. Rev. E **88**, 032913 (2013), doi:10.1103/PhysRevE.88.032913.

[44] M. Eckstein, M. Kollar and P. Werner, *Interaction quench in the Hubbard model: Relaxation of the spectral function and the optical conductivity*, Phys. Rev. B **81**, 115131 (2010), doi:10.1103/PhysRevB.81.115131.

[45] J.-S. Bernier, R. Citro, C. Kollath and E. Orignac, *Correlation dynamics during a slow interaction quench in a one-dimensional bose gas*, Phys. Rev. Lett. **112**, 065301 (2014), doi:10.1103/PhysRevLett.112.065301.

[46] E. J. Torres-Herrera, D. Kollmar and L. F. Santos, *Relaxation and thermalization of isolated many-body quantum systems*, Phys. Scr. 014018 (2015), doi:10.1088/0031-8949/2015/t165/014018.

[47] L. F. Santos and E. J. Torres-Herrera, *Nonequilibrium quantum dynamics of many-body systems* (2017), arXiv:1706.02031.

[48] A. Khodja and J. Gemmer, *Effect of short-range order on transport in one-particle tight-binding models*, Phys. Rev. E **88**, 042103 (2013), doi:10.1103/PhysRevE.88.042103.

[49] L. Mordell, *On the Kusmin-Landau inequality for exponential sums*, Acta Arith. **4**, 3 (1958).

[50] M. Gluza, C. Krumnow, M. Friesdorf, C. Gogolin and J. Eisert, *Equilibration via gaussification in fermionic lattice systems*, Phys. Rev. Lett. **117**, 190602 (2016), doi:10.1103/PhysRevLett.117.190602.

[51] M. Cramer and J. Eisert, *A quantum central limit theorem for non-equilibrium systems: exact local relaxation of correlated states*, New J. Phys. **12**, 055020 (2010), doi:10.1088/1367-2630/12/5/055020.

[52] P. Calabrese, F. H. Essler and M. Fagotti, *Quantum quench in the transverse-field ising chain*, Phys. Rev. Lett. **106**, 227203 (2011), doi:10.1103/PhysRevLett.106.227203.

[53] H. Araki, *Gibbs states of a one dimensional quantum lattice*, Commun. Math. Phys. **14**, 120 (1969), doi:10.1007/BF01645134.

[54] A. Flesch, M. Cramer, I. McCulloch, U. Schollwöck and J. Eisert, *Probing local relaxation of cold atoms in optical superlattices*, Phys. Rev. A **78**, 033608 (2008), doi:10.1103/PhysRevA.78.033608.

[55] M. Fagotti and F. H. Essler, *Reduced density matrix after a quantum quench*, Phys. Rev. B **87**, 245107 (2013), doi:10.1103/PhysRevB.87.245107.

[56] S. Sotiriadis, *Memory-preserving equilibration after a quantum quench in a one-dimensional critical model*, Phys. Rev. A **94**, 031605 (2016), doi:10.1103/PhysRevA.94.031605.

[57] S. Sotiriadis and P. Calabrese, *Validity of the GGE for quantum quenches from interacting to noninteracting models*, J. Stat. Mech. P07024 (2014), doi:10.1088/1742-5468/2014/07/p07024.

[58] A. J. Short, *Equilibration of quantum systems and subsystems*, New J. Phys. **13**, 053009 (2011), doi:10.1088/1367-2630/13/5/053009.

[59] T. Farrelly, F. G. Brandão and M. Cramer, *Thermalization and return to equilibrium on finite quantum lattice systems*, Phys. Rev. Lett. **118**, 140601 (2017), doi:10.1103/PhysRevLett.118.140601.

[60] E. Ilievski, J. De Nardis, B. Wouters, J.-S. Caux, F. H. Essler and T. Prosen, *Complete generalized Gibbs ensembles in an interacting theory*, Phys. Rev. Lett. **115**, 157201 (2015), doi:10.1103/PhysRevLett.115.157201.

[61] M. A. Nielsen and I. L. Chuang, *Quantum Computation and Quantum Information: 10th Anniversary Edition*, Cambridge University Press (2010), doi:10.1017/CBO9780511976667 .

[62] T. J. Osborne, *Hamiltonian complexity*, Rep. Prof. Phys. **75**, 022001 (2012), doi:10.1088/0034-4885/75/2/022001.

[63] S. Gharibian, Y. Huang, Z. Landau, S. W. Shin *et al.*, *Quantum hamiltonian complexity*, Found. Tr. Th. Comp. Sc. **10**, 159 (2014), doi:10.1561/0400000066.

[64] M. R. Dowling and M. A. Nielsen, *The geometry of quantum computation*, Quant. Inf. Comp. **8**, 861 (2008).

[65] B. M. Terhal and D. P. DiVincenzo, *Problem of equilibration and the computation of correlation functions on a quantum computer*, Phys. Rev. A **61**, 022301 (2000), doi:10.1103/PhysRevA.61.022301.

[66] E. Witten, *Three lectures on topological phases of matter*, Riv. Nuovo Cimento **39**, 313 (2016), doi:10.1393/ncr/i2016-10125-3.

[67] P. W. Anderson, *Absence of diffusion in certain random lattices*, Phys. Rev. **109**, 1492 (1958), doi:10.1103/PhysRev.109.1492.

[68] P. Richerme, Z.-X. Gong, A. Lee, C. Senko, J. Smith, M. Foss-Feig, S. Michalakis, A. V. Gorshkov and C. Monroe, *Non-local propagation of correlations in quantum systems with long-range interactions*, Nature **511**, 198 (2014), doi:10.1038/nature13450.

[69] J. Eisert, M. van den Worm, S. R. Manmana and M. Kastner, *Breakdown of quasilocality in long-range quantum lattice models*, Phys. Rev. Lett. **111**, 260401 (2013), doi:10.1103/PhysRevLett.111.260401.

[70] E. H. Lieb and D. W. Robinson, *The finite group velocity of quantum spin systems*, In *Statistical Mechanics*, Springer (1972), doi:10.1007/978-3-662-10018-9_25.

[71] B. Nachtergaele and R. Sims, *Lieb-Robinson bounds and the exponential clustering theorem*, Commun. Math. Phys. **265**, 119 (2006), doi:10.1007/s00220-006-1556-1.

[72] M. B. Hastings and T. Koma, *Spectral gap and exponential decay of correlations*, Commun. Math. Phys. **265**, 781 (2006), doi:10.1007/s00220-006-0030-4.

[73] M. Cramer, A. Serafini and J. Eisert, *Locality of dynamics in general harmonic quantum systems* (2008), arXiv:0803.0890.

[74] M. Kliesch, C. Gogolin and J. Eisert, *Lieb-Robinson bounds and the simulation of time-evolution of local observables in lattice systems*, In *Many-Electron Approaches in Physics, Chemistry and Mathematics*, Springer (2014), doi:10.1007/978-3-319-06379-9_17.

[75] G. C. Wick, A. S. Wightman and E. P. Wigner, *The intrinsic parity of elementary particles*, Phys. Rev. **88**, 101 (1952), doi:10.1103/PhysRev.88.101.

[76] J. Earman, *Superselection rules for philosophers*, Erkenntnis **69**, 377 (2008), doi:10.1007/s10670-008-9124-z.

[77] V. Bach, E. H. Lieb and J. P. Solovej, *Generalized Hartree-Fock theory and the Hubbard model*, J. Stat. Phys. **76**, 3 (1994), doi:10.1007/BF02188656.

[78] C. V. Kraus and J. I. Cirac, *Generalized Hartree–Fock theory for interacting fermions in lattices: numerical methods*, New J. Phys. **12**, 113004 (2010), doi:10.1088/1367-2630/12/11/113004.

[79] P. Barmettler and C. Kollath, *Impact of local integrals of motion to metastable non-equilibrium states* (2013), arXiv:1312.5757.

[80] A. S. Buyskikh, M. Fagotti, J. Schachenmayer, F. Essler and A. J. Daley, *Entanglement growth and correlation spreading with variable-range interactions in spin and fermionic tunneling models*, Phys. Rev. A **93**, 053620 (2016), doi:10.1103/PhysRevA.93.053620.

[81] L. Cevolani, G. Carleo and L. Sanchez-Palencia, *Spreading of correlations in exactly solvable quantum models with long-range interactions in arbitrary dimensions*, New J. Phys. **18**, 093002 (2016), doi:10.1088/1367-2630/18/9/093002.

[82] R. Gallego, H. Wilming, J. Eisert and C. Gogolin, *What it takes to avoid equilibration*, Phys. Rev. A **98**, 022135 (2018), doi:10.1103/PhysRevA.98.022135.

[83] S. Bravyi, *Lagrangian representation for fermionic linear optics*, Quantum Inf. and Comp. **5**, 216 (2005), arXiv:quant-ph/0404180.

[84] L. Banchi, S. L. Braunstein and S. Pirandola, *Quantum fidelity for arbitrary gaussian states*, Phys. Rev. Lett. **115**, 260501 (2015), doi:10.1103/PhysRevLett.115.260501.

[85] I. Bloch, J. Dalibard and W. Zwerger, *Many-body physics with ultracold gases*, Rev. Mod. Phys. **80**, 885 (2008), doi:10.1103/RevModPhys.80.885.

[86] S. Trotzky, Y.-A. Chen, A. Flesch, I. P. McCulloch, U. Schollwöck, J. Eisert and I. Bloch, *Probing the relaxation towards equilibrium in an isolated strongly correlated one-dimensional Bose gas*, Nat. Phys. **8**, 325 (2012), doi:10.1038/nphys2232.

[87] U. Schneider, L. Hackermüller, J. P. Ronzheimer, S. Will, S. Braun, T. Best, I. Bloch, E. Demler, S. Mandt, D. Rasch and A. Rosch, *Fermionic transport and out-of-equilibrium dynamics in a homogeneous Hubbard model with ultracold atoms*, Nat. Phys. **8**, 213 (2012), doi:10.1038/nphys2205.

[88] J. I. Cirac and P. Zoller, *Goals and opportunities in quantum simulation*, Nat. Phys. **8**, 264 (2012), doi:10.1038/nphys2275.

[89] I. Bloch, J. Dalibard and S. Nascimbene, *Quantum simulations with ultracold quantum gases*, Nat. Phys. **8**, 267 (2012), doi:10.1038/nphys2259.

[90] A. Acín et al., *The quantum technologies roadmap: a European community view*, New J. Phys. **20**, 080201 (2018), doi:10.1088/1367-2630/aad1ea.

[91] B. Bertini, F. H. Essler, S. Groha and N. J. Robinson, *Prethermalization and thermalization in models with weak integrability breaking*, Phys. Rev. Lett. **115**, 180601 (2015), doi:10.1103/PhysRevLett.115.180601.

[92] M. Moeckel and S. Kehrein, *Interaction quench in the Hubbard model*, Phys. Rev. Lett. **100**, 175702 (2008), doi:10.1103/PhysRevLett.100.175702.

[93] M. Moeckel and S. Kehrein, *Real-time evolution for weak interaction quenches in quantum systems*, Ann. Phys. **324**, 2146 (2009), doi:10.1016/j.aop.2009.03.009.

[94] M. Moeckel and S. Kehrein, *Crossover from adiabatic to sudden interaction quenches in the hubbard model: prethermalization and non-equilibrium dynamics*, New J. Phys. **12**, 055016 (2010), doi:10.1088/1367-2630/12/5/055016.

[95] M. Perarnau-Llobet, A. Riera, R. Gallego, H. Wilming and J. Eisert, *Work and entropy production in generalised gibbs ensembles*, New J. Phys. **18**, 123035 (2016), doi:10.1088/1367-2630/aa4fa6.

[96] C. Murthy and M. Srednicki, *On relaxation to gaussian and generalized Gibbs states in systems of particles with quadratic Hamiltonians*, Phys. Rev. E **100**, 012146 (2019), doi:10.1103/PhysRevE.100.012146.

[97] M. Abramowitz and I. A. Stegun, *Handbook of mathematical functions: with formulas, graphs, and mathematical tables*, Courier Corporation (1965), ISBN:0486612724.

4

QUANTUM READ-OUT FOR COLD ATOMIC QUANTUM SIMULATORS

The sophistication of the state-of-the-art quantum simulators is immense. However, this may go unnoticed as they allow to observe a wealth of physical effects which are emergent and so can in principle be studied without a detailed knowledge of the experimental implementation. Therefore, before we will discuss the specific insights they have to offer let us shortly discuss how quantum simulation experiments with cold atoms come about.

Achieving a large amount of quantum coherence is highly non-trivial and a result of efforts and insights that came over many years. By using merely our daily experience it is hard to asses the challenges one must face for typical atomic lengths and velocities so in order to put the setting into perspective one can ask: How hard would it be to stop a sandstorm, catch in midair thousands of tiny rocketing bullets and eventually condense them into a fluid state? This could well be a scene from an action movie, however this is essentially what the experimental group of Jörg Schmiedmayer at TU Vienna is doing (repeating every few seconds when taking data) in their quantum simulation studies of ultra-cold atoms [143, 144].

They remove the influence of the surrounding laboratory air by operating at high vacuum. By running an electric current through a rubidium crystal they obtain single atom vapors that escape the solid state by having a huge kinetic energy and shoot like bullets through the vacuum chamber. In a setup the size of a large coffee machine the rubidium atoms travel initially with the speed of hundreds of meters per second but are held still within a centimeter-sized trap using laser and Doppler cooling. Then the magneto-optically trapped gas cools down even more and undergoes Bose-Einstein condensation. After moving to yet another trap, essentially levitating against the gravity forces, the gas is brought close to the so-called Atom Chip. Here a thin golden wire thanks to excellent thermal conductance transmits more current than would be enough to quench a superconductor of the same diameter. The magnetic field induced by this enormous current is powerful enough to allow to squeeze a three dimensional droplet of a Bose-Einstein condensate so strongly that the gas effectively becomes one-dimensional. This happens when all the atoms are in the ground state of the transverse trapping field, i.e., are transversally as localized as the Heisenberg uncertainty principle allows and effectively the only available direction of propagation is the longitudinal motion. Thanks to these extreme forces and control capabilities we get access to a one-dimensional quantum many-body system and can study its physics and dynamics.

This short description of the setup is useful to keep in mind how sophisticated the experimental system is which otherwise could go unnoticed when dealing with data. As discussed in detail in the appendix of the presented paper the output of measurements are phase profiles of the ultra-cold one-dimensional Bose gas. They are obtained by performing matter-wave interferometry of two adjacent gases and are extracted from the spatial distribution of the atoms [145, 146]. The outcomes of such measurements can be linked through theoretical modelling to correspond to the projective measurement of the quantum phase operator at different positions along of the quasi-condensates. From these single-shot outcomes full counting statistics of the interacting Bose gas can be studied and by forming appropriate statistical estimators correlation functions become accessible. This has allowed for a number of diverse physical observations [44, 55--57, 147, 148] in a setting which just half a century earlier was restricted to exclusively the theoretical domain [149].

The gradient of the phase operator can be physically interpreted as a velocity operator. In a typical setting there is no overall velocity (tunelling) between the two one-dimensional gases interfered together. Hence, the local expectation value of the phase gradient operator typically is trivial. However, the second moments reveal information about the kinetic energy in the system. The modelling of the experiment is based on the physical reasoning that an ultra-cold one-dimensional gas behaves as a hydrodynamic system and upon small disturbances it hosts wave-like excitations. The second moment of the phase is related to the kinetic energy of these wave-packets. However, there is another contribution to the energy of the system which captures the physical intuition that a substantial wave-packet is created by a higher energy input than is required for a smaller wave-packet. This energy is related to density fluctuations of the gas which are canonically conjugate to the phase. Specifically the local second moments of the density fluctuation operator must be assessed.

With just the interferometric data this second contribution to the overall energy cannot be accessed directly. The paper presented here resolves this issue by theoretically and practically establishing a tomographic read-out method

allowing to recover information about density fluctuations based on out-of-equilibrium dynamics of the phase. This in turn enables the study of new challenging physical questions that were so far out of reach.

The results presented were obtained in collaboration with the experimental group of Jörg Schmiedmayer at TU Vienna who experimentally control to a high degree Bose-Einstein condensates. The theoretical description of the system is set up using bosonic fields, $\hat{\varphi}(z)$ and $\delta\hat{\rho}(z)$, which represent phonons and will be referred to as phase and density fluctuation fields respectively. They are the only degrees of freedom relevant at the temperatures considered and have a bosonic character $[\hat{\varphi}(z), \delta\hat{\rho}(z')] = i\delta(z-z')$ where z, z' are two positions along of the one-dimensional gas.

The effective Hamiltonian of the system is quadratic and reads

$$\hat{H} = \int_0^L dz \left[\frac{\hbar^2 n_{GP}}{4m} (\partial_z \hat{\varphi})^2 + g\delta\hat{\rho}^2 \right] ,$$

where L is the length of the system, $\hbar$ is the reduced Planck constant, n_{GP} is the mean density of the gas which can be obtained theoretically by calculating the ground-state of the Gross-Pitaevskii equation, m is the mass of the atoms and g is the interaction strength related to the s-wave scattering of the atoms. As alluded to above we have two terms, one related to the velocities of the wave-packets $\hat{v} = \partial_z \hat{\varphi}$ and one to how much density fluctuations they typically carry $\delta\hat{\rho}$. This Hamiltonian is the effective model of many one-dimensional systems belonging to the class of Tomonaga-Luttinger liquids, for example electrons in a nano-wire [150, 151].

The eigenmodes of such a Hamiltonian can be found by performing an appropriate Bogoliubov transformation and generically will transform the Hamiltonian into a form comprised of independent Harmonic oscillators

$$\hat{H} = \sum_{k>0} \hbar\omega_k (\hat{\phi}_k^2 + \hat{\rho}_k^2) + g\hat{\rho}_0^2 .$$

Here ω is the spectrum which should be expected to be discrete due to trapping. The eigenmodes are non-local in terms of the real-space fields and e.g. in the homogeneous case we have for $k > 0$

$$\hat{\phi}_k = \sqrt{2}L \int_0^L dz \cos(2\pi k/L)\hat{\varphi}(z) \quad \text{and} \quad \hat{\rho}_k = \sqrt{2}L \int_0^L dz \cos(2\pi k/L)\delta\hat{\rho}(z) .$$

Finally, $\hat{\rho}_0$ denotes the overall density fluctuation canonically conjugate to the phase zero-mode which is removed from the data as opposed to the $k > 0$ modes.

The crucial insight allowing us to set up the reconstruction method is that the density and phase fluctuation fields are quadratures after transforming to momentum space, mathematically identical to the study of photons in quantum optics. The experimental setup considered allows natively to only measure the moments of the phase fluctuations. In order to assess the energy of the system, or access more refined information about the correlations present in the system, one must perform tomography. See Fig. 4.1 for an overview of the approach allowing to resolve the task formulated in the following subsection.

4.1 FORMULATION OF THE PROBLEM

The experiment gives access to the measurement of the second moments of the referenced relative phase fluctuations [44, 57, 144--146] between two adjacent gases

$$\Phi(z, z', t) = \langle (\hat{\varphi}(z,t) - \hat{\varphi}(z_0,t))(\hat{\varphi}(z',t) - \hat{\varphi}(z_0,t)) \rangle .$$

What are the second moments $\mathcal{Q}(z, z', t) = \langle \delta\hat{\rho}(z)\delta\hat{\rho}(z') \rangle$ of the relative density fluctuations in the system?

In the same system a series of experimental observations has been made. What further insights are possible experimentally?

4.2 OUR RESULT

By means of a tomographic reconstruction we have indirectly measured the density fluctuations. This has been done in momentum space, but using a specific form of the presumed eigenmode single-particle wave-functions and hence information about correlations is available in real space. This allows to reconstruct correlations between modes but

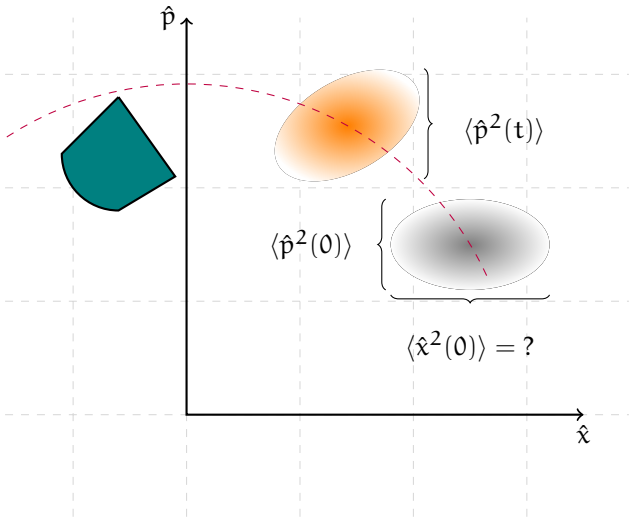

Figure 4.1: **Tomography for continuous field quantum simulators.** In many instances, only one type of measurement is possible while the expectation value of a canonically conjugated observable is inaccessible. Nevertheless, one can attempt an indirect measurement making use of harmonic evolution. The figure illustrates the phase space of a bosonic mode with canonically commuting bosonic observables $[\hat{x}, \hat{p}] = i\hbar$. Using a pulse of harmonic evolution generated by the Hamiltonian $\hat{H} = \frac{1}{2}\hbar\omega(\hat{x}^2 + \hat{p}^2)$ one finds that the fluctuations of the $\hat{p}$ quadrature include information about the fluctuations of $\hat{x}$ by means of the formula $\langle\hat{p}^2(t)\rangle = \cos^2(\omega t)\langle\hat{p}^2(0)\rangle + \sin^2(\omega t)\langle\hat{x}^2(0)\rangle$. In our case the tomography must be performed simultaneously for many modes with different momentum k based on phase information in real space which reveals information about the density fluctuations. Note that in the experiment the phase space distributions will be elliptical due to squeezing but will not be displaced from the origin which was added for the sake of clarity in this illustrative sketch.

also the expectation values of the phononic quasiparticle occupation numbers $n_k(t) = \frac{1}{2}\langle\hat{\phi}_k^2(t) + \hat{\rho}_k^2(t)\rangle - \frac{1}{2}$ can be studied. This information is momentum- and time-resolved and opens a new window into the physics in the quantum simulator which is a capability unparalleled in materials sharing the same effective description.

4.3 THE IMPLICATIONS OF THE RESULT

The method allows to study various physical effects related to dynamics of correlation functions. The paper demonstrates that inquiries into *coherent recurrences* of dynamics in the system become possible adding to the understanding of the details of this effect. The method opens a pathway towards studying phononic *quasiparticle decay* dynamics in a momentum and time resolved fashion. The publication shows results in a case when quasipacticle occupation numbers should be constants of motion effectively verifying the theoretical model in an experiment. Realizing an experimental setting where the quasiparticle occupation numbers would undergo a visible rearrangement would be an exciting prospect, e.g., one could study *Beliavin damping* for which theoretical calculations are notoriously hard.

One possibility of realizing such a physical effect, which may be explored in the future, is to tomographically investigate states influenced by the *sine-Gordon interactions*. The idea is that one would like to study non-equilibrium dynamics in the presence of a tunnel coupling giving rise to non-Gaussian correlations. At any desired point in time, one could perform a quench of the tunnel coupling rendering the system effectively non-interacting and perform tomography. For varying starting times the occupation numbers of phonons can be expected to be different as they cease to be conserved under sine-Gordon interactions.

The method presented gives access to non-commuting observables and future *entanglement* studies become possible. Entanglement of Gaussian states is well researched due to the importance of the subject in quantum optics. In principle, the entanglement detection methods from that field can directly be applied to the reconstructed state. However one must take extra care in this particular study as one aims at reconstructing a very refined information: Are the correlations in the system quantum or classical? To answer this question one must make sure that the finite experimental resolution does not modify the data which is the input to the tomography in such a

way that introduces additional correlations. That is to say, the tomographic method presented here must be studied together with details of the experimental measurement protocol in order to avoid out false-positives, i.e., a situation where tomography indicates entanglement but only due to resolution artifacts and the system is in reality not be entangled. However, this technical issue is the only obstacle to applying the method presented here for monitoring entanglement dynamics.

In addition to monitoring various features of correlations the tomography method presented here allows to measure energy and entropy dynamics which makes possible future studies of quantum thermodynamical operations. Specifically, as we can perform the complete callorimetry in the system by phonon counting we could measure phononic heat flow rates. At any given time the entropy of the system with covariance matrix Γ is upper bounded by the entropy of the Gaussian state with the same covariance matrix. Hence an upper bound on entropy production can be estimated by quasiparticle tomography and will be a good approximation to the entropy in the system whenever higher order connected correlation functions are negligible.

The latter can be directly measured and were the subject of our subsequent studies of the dynamical emergence of Gaussian correlations [12] and the tomographic method presented was employed during the proceeding of our investigations. The code developed to implement numerical reconstructions was the base for subsequent studies of quantum field thermal machines [14] where this type of tomography is also expected to be an important way of inquiry into the operation of the system.

4.4 OPEN PROBLEMS

Problem 1. Investigate further the stability of the method in the presence of statistical and systematic noise. Can systematic noise appear under the specific measurement resolution model relevant to the experimental setup?

Problem 2. The reconstructions for data taken in the presence of a 'harmonic' trap seem to be less reliable than for the 'box' trap. Is this issue theoretical or experimental (e.g. longitudinal breathing of the mean gas density)?

Problem 3. Implement the reconstruction method as presented here but based on in-situ data of density fluctuations, as proposed in Ref. [14].

COMMUNICATIONS PHYSICS

ARTICLE

https://doi.org/10.1038/s42005-019-0273-y OPEN

Quantum read-out for cold atomic quantum simulators

M. Gluza[1], T. Schweigler[2], B. Rauer[2], C. Krumnow[1], J. Schmiedmayer[2] & J. Eisert[1]*

Quantum simulators allow to explore static and dynamical properties of otherwise intractable quantum many-body systems. In many instances, however, the read-out limits such quantum simulations. In this work, we introduce an innovative experimental read-out exploiting coherent non-interacting dynamics. Specifically, we present a tomographic recovery method allowing to indirectly measure the second moments of the relative density fluctuations between two one-dimensional superfluids, which until now eluded direct measurements. Applying methods from signal processing, we show that we can reconstruct the relative density fluctuations from non-equilibrium data of the relative phase fluctuations. We employ the method to investigate equilibrium states, the dynamics of phonon occupation numbers and even to predict recurrences. The method opens a new window for quantum simulations with one-dimensional superfluids, enabling a deeper analysis of their equilibration and thermalization dynamics.

[1] Dahlem Center for Complex Quantum Systems, Freie Universität Berlin, 14195 Berlin, Germany. [2] Vienna Center for Quantum Science and Technology, Atominstitut, TU Wien, Stadionallee 2, 1020 Vienna, Austria. *email: jense@zedat.fu-berlin.de

Quantum simulators offer entirely new perspectives of assessing the intriguing physics of quantum many-body systems in and out of equilibrium. They are experimental setups allowing to probe properties of complex quantum systems under unprecedented levels of control[1–3], beyond the possibilities of classical simulations. Among other platforms, experiments with ultra-cold atoms involving large particle numbers or even continuous quantum fields have been particularly insightful[4–14].

And yet, key questions remain open for a highly unexpected reason: the read-out of state-of-the-art quantum simulators is limited. In one-dimensional (1D) superfluids, for example, one can probe the dynamics of equilibration[4] occurring in the presence of an effective light-cone[5] and leading to generalized Gibbs ensembles[6]. The excellent experimental control over that system allowed to observe coherent recurrences in the dynamics of a system of thousands of atoms[8]. However, in that particular setup, further quantifying the recent observations is currently obstructed because only phase quadratures but not canonically conjugate density fluctuations can be measured. On the contrary, if both quadratures could be measured, and hence if genuine quantum read-out was possible, then studies of intricate questions on the role of interactions, or entanglement dynamics after a quench, could become possible.

This situation is by no means an exception: In fact, in any quantum simulation platform, read-out prescriptions are always restricted in one way or another, which constitutes a crucial bottleneck towards studying intricate physical questions. For cold atoms in optical lattices, akin to the development which will be laid out in this work, innovations such as the quantum gas microscope[15–17] directly opened up the path towards studying exciting physical phenomena[9–14]. Sophisticated read-out methods are therefore highly desirable and key to a platform.

In this work, we show that quenching a single global parameter in the system can enable a genuine quantum read-out and even allow for state reconstructions. We hence open a new 'window' into a quantum simulator for which so far—as is common in quantum simulation—only incoherent, or 'classical', read-out was natively possible.

Tomography of many-body systems is typically limited due to the number of necessary observables and complexity of control. However, often for large systems, the observed dynamics can be described by an effective free field theory capturing the dynamics by means of modes which are long-lived, i.e., not over-damped. We shall demonstrate that observing their dynamics can already suffice to perform reconstructions of the relevant correlation functions for many-body systems. The basic principle is that non-equilibrium evolution can mix 'quadratures' (non-commuting operators describing the dynamics of a mode) in such a way that consistency of observed correlations implies constraints regarding the unobserved ones. We will show that they can be quantitatively reconstructed.

Specifically, in this work, we set out to introduce a novel method of tomographic read-out for quantum simulators, by combining known quantum dynamics and available measurements to obtain more information. Related ideas of exploiting known random or deterministic unitary dynamics to get access to otherwise inaccessible types of measurements have been theoretically explored[18–23]. However, closest in spirit are tomographic methods in quantum optics where a harmonic rotation in phase space allows to measure two canonically conjugated quadratures by a detector sensitive to only one of them, and hence perform a 'quantum measurement'.

Here, we consider this basic idea in a genuine multi-mode setting and demonstrate a practical application of the method to 1D superfluids. We acquire data at different times for many modes at the same time and make use of semi-definite programming techniques for achieving reconstructions insusceptible to noise. After introducing our new recovery method, we explore the physics of 1D superfluids studying the properties of quench dynamics and its initial conditions. We use the quantum read-out information concerning both density and phase fluctuations in momentum space to fit the temperature and the global tunnel coupling parameter of the initial state preparation. Concerning out-of-equilibrium dynamics, we are able to predict recurrences by relying solely on data taken at times away from the recurrence occurrence, demonstrating that the system is coherent throughout the evolution. Finally, we monitor dynamics of phonon occupation numbers constraining their growth over an extensive observation time giving further experimental evidence for the validity of the effective model. The successful functioning of our method demonstrates an excellent agreement of the experiment with the theory of elementary excitations of 1D superfluid[24,25]. Our approach is based on very general and ubiquitous ingredients, hence the framework that we establish can be expected to be in a natural way applicable to various quantum simulators.

Results

The system considered. In order to apply our read-out method in practice, we will consider the setting of two adjacent 1D Bose gases realized with ultra-cold atoms. Their low-energy relative fluctuations in phase and density, $\hat{\varphi}$ and $\delta\hat{\rho}$, are described by the effective Hamiltonian[8,25]

$$\hat{H} = \int_{-R_{1D}}^{R_{1D}} \mathrm{d}z \left[\frac{\hbar^2 n_{GP}(z)}{4m} (\partial_z \hat{\varphi}(z))^2 + g(z) \delta\hat{\rho}(z)^2 + \frac{\hbar^2}{4m n_{GP}(z)} (\partial_z \delta\hat{\rho}(z))^2 \right], \tag{1}$$

with m being the atomic mass and n_{GP} the average density profile defined by the ground state of a 1D Gross-Pitaevskii (GP) equation. The Hamiltonian describes phonons which are the elementary density-phase excitations, satisfying bosonic commutation relations $[\delta\hat{\rho}(z), \hat{\varphi}(z')] = \mathrm{i}\delta(z - z')$. The corresponding operators are defined within the atomic cloud whose spatial extension R_{1D} is given by the support of n_{GP}. Experimentally, one can engineer the density profile n_{GP} through the trapping potential. This determines the density–density interaction strength, which is functionally dependent on the density profile, $g(z) = g[n_{GP}(z)]$[8,26] (see Supplementary Note 1). For typical experimental parameters, the last term in Eq. (1) has less importance than the first two[27], which together make up the Luttinger model. In the Supplementary Note 1, we describe a general numerical scheme for obtaining approximate eigenfunctions of $\hat{H}$ for any n_{GP} of interest. For a constant density profile, this model gives a linear spectrum and oscillatory eigenfunctions —which is qualitatively also the case for Eq. (1) even with small GP profile inhomogeneities.

As the excitations are confined within the finite atomic cloud, their spectrum $\{\omega_k, k = 1, 2, \ldots\}$ is discrete[28]. We denote eigenmode operators of phase and density fluctuations by $\hat{\phi}_k$ and $\delta\hat{\rho}_k$, respectively, and use their corresponding wave functions $f_k^{\rho}, f_k^{\phi} \in C^2([-R_{1D}, R_{1D}])$ to decompose the real-space fields as

$$\hat{\varphi}(z) = \sum_{k=0}^{\infty} f_k^{\phi}(z)\hat{\phi}_k, \quad \delta\hat{\rho}(z) = \sum_{k=0}^{\infty} f_k^{\rho}(z)\delta\hat{\rho}_k. \tag{2}$$

Note that here we have $[\delta\hat{\rho}_k, \hat{\phi}_{k'}] = \mathrm{i}\delta_{k,k'}$ where $\delta_{k,k'}$ is the Kronecker symbol in contrast to the Dirac delta in the commutation relations of the real-space fields above. Written in terms of the eigenmode degrees of freedom $\hat{\phi}_k$ and $\delta\hat{\rho}_k$, the Hamiltonian

becomes diagonal

$$\hat{H} = \frac{1}{2}\sum_{k=1}^{\infty} \hbar\omega_k(\delta\hat{\rho}_k^2 + \hat{\phi}_k^2) + g_0\hat{\rho}_0^2 . \quad (3)$$

Here $\hat{\rho}_0$ does not contribute to the visible dynamics because it is conjugate to the global phase which carries no energy and is removed from the data. We shall refer to the eigenmode operators as quadratures as they constitute a discrete set of bosonic observables, which harmonically rotate and do not mix between different modes as can be directly seen from their time evolution within the Heisenberg-picture

$$\hat{\phi}_k(t) = \cos(\omega_k t)\hat{\phi}_k - \sin(\omega_k t)\delta\hat{\rho}_k . \quad (4)$$

In the method presented below, we will make use of approximate eigenmodes obtained from the eigenfunctions of a spatial discretization of the considered model which, for simplicity, we will continue to denote by $\hat{\phi}_k, \delta\hat{\rho}_k$ and f_k^ρ, f_k^ϕ—see the Supplementary Note 1 for a more detailed discussion. Let us stress that by the time evolution in Eq. (4) density fluctuations, which are not accessible by direct measurements, are dynamically mixed into the observed phase sector which is the foundation to our reconstruction approach.

Quadrature tomography. In this section, we turn to describing the reconstruction procedure, exploiting the known and efficiently tractable Hamiltonian dynamics on the one hand and ideas of reconstruction and signal processing on the other. This gives rise to a practical and versatile method of reconstructing correlation functions of a type inaccessible to direct measurement. The atom chip experiment[29] which we are considering here, measures referenced correlation functions of the relative phase through matter-wave interferometry[7,8,22,30–32]

$$\Phi(z,z',t) = \langle(\hat{\varphi}(z,t) - \hat{\varphi}(z_0,t))(\hat{\varphi}(z',t) - \hat{\varphi}(z_0,t))\rangle . \quad (5)$$

Here we chose to reference the phase with respect to the middle of the system $z_0 = 0$ μm, which removes from the data the global phase canonically conjugate to $\hat{\rho}_0$.

We aim to reconstruct the second moments of the initial state of the quadratures $\hat{r} = (\hat{\phi}_1, \ldots, \hat{\phi}_\mathcal{N}, \delta\hat{\rho}_1, \ldots, \delta\hat{\rho}_\mathcal{N})^T$ of the $\mathcal{N}$ lowest lying eigenmodes of $\hat{H}$ satisfying bosonic commutation relations $[\hat{r}_k, \hat{r}_{k'}] = \mathrm{i}\Omega_{k,k'}$ with $\Omega = \begin{pmatrix} 0 & \mathbb{1}_\mathcal{N} \\ -\mathbb{1}_\mathcal{N} & 0 \end{pmatrix}$. For this, we define the covariance matrix of the initial state as the collection of second moments

$$V_{j,k} = \frac{1}{2}\langle\{\hat{r}_j, \hat{r}_k\}\rangle = \frac{1}{2}\langle\hat{r}_j\hat{r}_k + \hat{r}_k\hat{r}_j\rangle . \quad (6)$$

It is important to note that a matrix V constitutes a collection of physically admissible second moments if and only if the matrix $\mathcal{Q}(V) = V + \frac{1}{2}\mathrm{i}\Omega \geqslant 0$ is positive-semidefinite, i.e., has non-negative eigenvalues. This condition reflects the Heisenberg uncertainty principle of canonically conjugated observables[33]. It will be convenient to use the notation

$$V = \begin{pmatrix} V^{\phi\phi} & V^{\phi\rho} \\ V^{\rho\phi} & V^{\rho\rho} \end{pmatrix}. \quad (7)$$

Note that here we include the interest in both type of correlations, not only those related to phase fluctuations. Altogether, V allows to provide a Gaussian description of the full unknown state of the system whose validity can be verified by measuring vanishing higher-order connected correlation functions[7]. In this work, we will consider initial states that are approximately Gaussian and under this assumption determining V yields a full state reconstruction. For non-Gaussian initial states, the method presented in the following can still reconstruct the second moments V, but will not provide specific information on the higher moments.

Using the decomposition into eigenmodes in Eq. (2), we obtain for the observable second moments defined in Eq. (5)

$$\Phi(z,z',t) = \sum_{j,k=1}^{\mathcal{N}} f_{z,z'}^{j,k} V_{j,k}^{\phi\phi}(t), \quad (8)$$

where $f_{z,z'}^{j,k} = (f_j^\phi(z) - f_j^\phi(z_0))(f_k^\phi(z') - f_k^\phi(z_0))$. Note that we have introduced the cut-off $\mathcal{N}$ in the summation over the eigenmodes, anticipating that higher energy modes will have a negligible contribution in the measured signal either because they carry too much energy to or due to finite real-space resolution in the experiment.

Next, we exploit that the time evolution of the Hamiltonian in Eq. (3) does not mix quadrature operators of different eigenmodes as stated in Eq. (4) which gives

$$V(t) = G_t V G_t^T \quad \text{for} \quad G_t = \begin{pmatrix} C_t & -S_t \\ S_t & C_t \end{pmatrix}, \quad (9)$$

where $C_t = \mathrm{diag}\,(\cos(\omega_k t), k = 1, \ldots, \mathcal{N})$ and $S_t = \mathrm{diag}(\sin(\omega_k t), k = 1, \ldots, \mathcal{N})$.

As summarized in Fig. 1, we now have all ingredients needed for quantum read-out. Specifically, based on the relations (8) and (9), we can recover the density correlations through a least-squares recovery problem. For this, we collect all measured values of $\Phi(z,z',t_i)$ at different points z and z' and times t_i in a vector b. Furthermore, we define a linear map $\mathcal{A}(\tilde{V})$ which, given some trial covariance matrix $\tilde{V}$, outputs the values of $\Phi(z,z',t_i)$ sorted as in b via Eq. (8). The time-evolution is implemented using Eq. (9) such that only the covariance matrix of the initial state is used to fit the observed data. If W denotes a weighting matrix, then $W(\mathcal{A}(\tilde{V}) - b)$ is the vector of the weighted least-squares residues. The covariance matrix optimally fitting the data is then given by the solution to the following optimization problem

$$\begin{aligned} \Theta &= \min_{\tilde{V}} \; \| W\mathcal{A}(\tilde{V}) - Wb\|_2, \\ \text{subject to} \quad & \mathcal{Q}(\tilde{V}) = \tilde{V} + \frac{1}{2}\mathrm{i}\Omega \succcurlyeq 0. \end{aligned} \quad (10)$$

The first line implements the minimization of the length $\|\cdot\|_2$ of the vector of weighted least-squares residues and the condition in the second line ensures that V is a physical covariance matrix. The

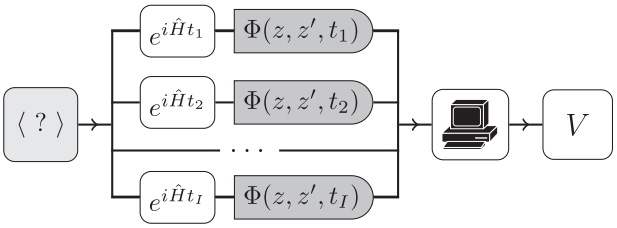

Fig. 1 Recovery procedure. How can we measure correlation functions of the elementary excitations in superfluids? We first note that the Hamiltonian in the system $\hat{H}$ (1) is decoupled on the level of momentum space operators $\{\hat{\phi}_k, \delta\hat{\rho}_k\}$ involving multiple modes rotating at different frequencies (3). Measurements of real-space continuum fields $\{\hat{\varphi}(z,t)\}$ yield the referenced two-point correlation functions $\Phi(z,z',t)$ defined in Eq. (5). In this work, by means of sophisticated post-processing using tools from signal processing, we are able to recover from real-space data taken at equidistant measurement times the full covariance matrix V (6) of the non-local eigenmodes of the Hamiltonian. This approach is general and can be applied to any other system in which quenches to non-interacting multi-mode Hamiltonians are available.

optimal solution to this convex quadratic problem with a semi-definite constraint yields the covariance matrix V of the initial state with a minimal value of Θ. The optimization can be performed efficiently and reliably numerically with standard methods for semi-definite programming. We use the package `cvx`[34], see the Supplementary Note 2 for more details on the implementation. The most basic idea of an algorithm solving (10) is to repeatedly take a steepest-descent step towards minimizing the least-squares residue and impose $\mathcal{Q}(V) \succcurlyeq 0$. Standard convex optimization packages like `cvx` solve such a problem in a more sophisticated way ensuring numerical accuracy and converge in a matter of seconds. In the implementation, we chose a diagonal weighting matrix W with entries $\sigma[\Phi(z,z',t_i)]^{-1}$, where $\sigma[\Phi(z,z',t_i)]$ denotes the standard deviation of each measured value. This weighting allows to put more emphasis on more precise values and yields with this a more reliable scheme as we find that $\Phi(z,z',t)$ grows typically for increasing spatial separations $|z-z'|$ but $\Phi(z,z',t)/\sigma[\Phi(z,z',t)] \approx \mathtt{const}$.

Note that the above idea and in fact the whole framework of quantum read-out formulated here is independent of the dimensionality of the Hamiltonian and can be applied, e.g., in two dimensions. There is also no restriction to continuum systems so lattice models can be treated similarly.

Experimental data analysis. Let us consider the state preparation procedure used in the recent experiment[8] where recurrent dynamics has been observed. Given an estimate of the average number of atoms per gas $N_{\mathrm{Avg}} \simeq 3400$ and the shape of the experimental box-like potential, we can numerically obtain the average density profile $n_{\mathrm{GP}}(z)$ from the GP equation. This specifies the Hamiltonian $\hat{H}$ (1) with $R_{\mathrm{1D}} \simeq 25\ \mu$m. Hence, we have the full information necessary to compute the eigenmode wave functions needed for the reconstruction procedure in Eq. (8). The number of relevant wave functions $\mathcal{N} \approx 10$ can be upper bounded by considering the finite resolution of the interference images. In our case, the phase fluctuations $\Phi(z,z',t)$ defined in Eq. (5) can be measured at points z, z' spaced by the pixel size of the camera $\delta \approx 2\ \mu$m[32]. In addition, other effects including diffraction limit the resolution. The measured values can be related to theoretical continuum predictions by implementing a real-space cut-off via a Gaussian convolution with standard-deviation $\sigma \approx 3.5\ \mu$m (see Supplementary Note 2).

Initially the two adjacent gases whose relative phase fluctuations we are studying are strongly coupled. Hence, the state preparation is to a good approximation governed by

$$\hat{H}_{\mathrm{Ini}} = \hat{H} + J \int_{-R_{\mathrm{1D}}}^{R_{\mathrm{1D}}} \mathrm{d}z\, n_{\mathrm{GP}}(z)\hat{\varphi}(z)^2, \tag{11}$$

where the tunnel coupling term of strength J is pulling the relative phase field to zero (i.e., $\langle\cos(\hat{\varphi})\rangle \simeq 1$). The initial state can be expected to be a low-temperature thermal state of $\hat{H}_{\mathrm{Ini}}$. Following that preparation, the system is quenched by suddenly turning off the tunnel coupling. Experimentally, this is realized by separating the two gases over a time of 2 ms until J drops to zero. The middle of this ramp defines the initial time $t = 0$ ms and the subsequent evolution under the Hamiltonian $\hat{H}$ (1) is measured in steps $\Delta t = 2.5$ ms.

Based on the data from this initial dynamics, we can reconstruct the initial state at $t = 0$ ms. In Fig. 2a, we plot the reconstructed

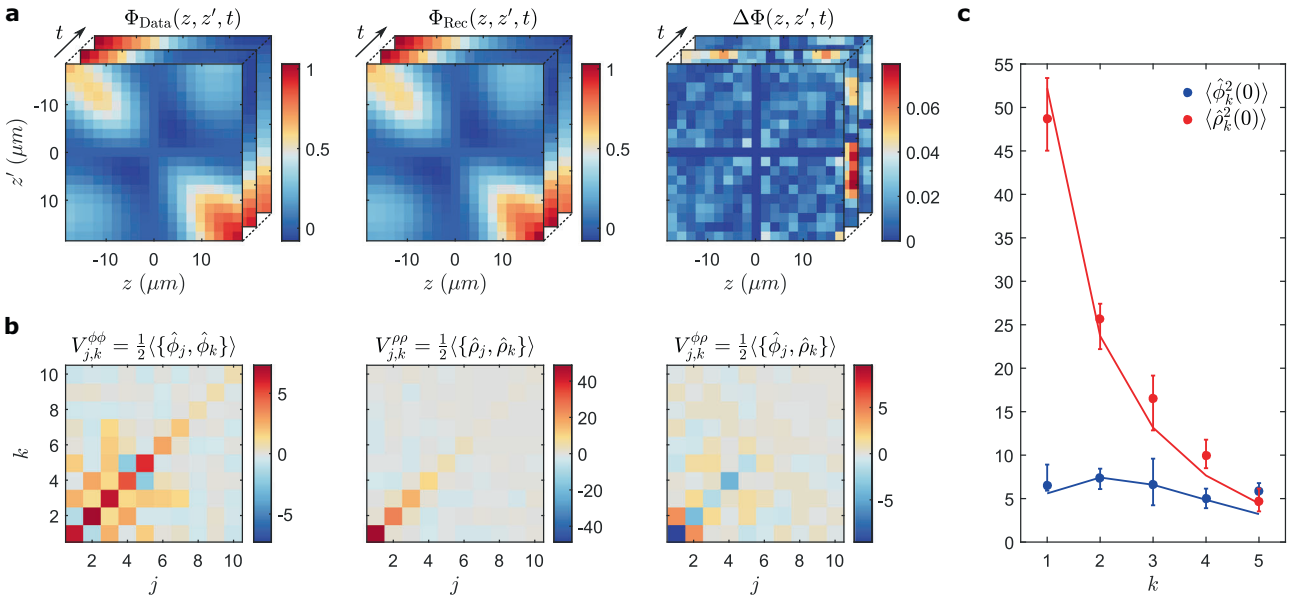

Fig. 2 Initial state reconstruction. Reconstruction of the full initial state right after decoupling at $t = 0$ ms based on the phase correlations measured during the dephasing dynamics immediately after the quench ($t = 1$, 3.5, 6, 8.5, 11 and 13.5 ms). **a** Comparison of the measured phase correlations $\Phi_{\mathrm{Data}}(z,z',t)$ to the reconstructed ones Φ_{Rec}. The time slice presented in the foreground corresponds to $t = 1$ ms. We find that the reconstruction yields good agreement with the data, evidenced by the respective weighted difference to the data $\Delta\Phi = |\Phi_{\mathrm{Data}} - \Phi_{\mathrm{Rec}}|/\sigma[\Phi_{\mathrm{Data}}]$ (right). **b** Reconstructed covariance matrix V of the initial state at $t = 0$ for the eigenmodes $j, k = 1, \ldots, 10$. From left to right, the reconstructed phase-phase $V^{\phi\phi}$, density-density $V^{\rho\rho}$ and phase-density correlations $V^{\phi\rho}$ are plotted. The correlations $V^{\phi\phi}$ and $V^{\rho\rho}$ are close to diagonal in the numerically obtained wave functions $f^{\phi}_{k'}$ indicating that the eigenmodes of the system are well captured. For an initial thermal state of the Hamiltonian (11), the cross-correlations should vanish $V^{\phi\rho} \equiv 0$, here we find a small contribution. Note that the influence of higher-energy modes is suppressed by the limited spatial resolution in the experiment (see Supplementary Note 2). **c** Comparison of the diagonal elements of $V^{\phi\phi}$ (blue bullets) and $V^{\rho\rho}$ (red bullets) at $t = 0$ with the predictions for a thermal state of the pre-quench Hamiltonian given in (11) (solid lines). The error bars correspond to the 80% confidence intervals obtained from a bootstrap analysis[35]. The thermal predictions are corrected for the suppression due to the finite imaging resolution, see Supplementary Note 2 and ref. [32]. We find the correlations of the first five modes to agree well with a thermal state at $T = 52$ nK and $J = 2\pi \times 1.1$ Hz obtained by a combined least-squares fit of $\langle\hat{\phi}^2_k\rangle$ and $\langle\delta\hat{\rho}^2_k\rangle$. The strong suppression of the higher mode signals by the imaging renders a meaningful comparison impossible.

phase correlations, showing good agreement with the measured values signifying the consistency of our method. The corresponding covariance matrix of the full initial state is shown in Fig. 2b. Most importantly, note that we are indeed able to infer density fluctuations of the form $\langle \delta\hat{\rho}_j \delta\hat{\rho}_k \rangle$. Using the mode transformation from Eq. (2), this information from the eigenmode-space can be also translated to real-space. However, many physical properties of the initial state can be directly extracted from the eigenmode correlations. We firstly observe that the blocks $V^{\phi\phi}$ and $V^{\rho\rho}$ are close to being diagonal. Hence, we find that the collective modes of the system are well captured by the numerically obtained wave functions f_k^{ϕ}. This supports the expectation that the initial state is thermal with respect to the pre-quench Hamiltonian (11). As the eigenmode wave functions are not strongly affected by the quench for the chosen trap geometry (see Supplementary Note 3), if the system was thermal with respect to the initial Hamiltonian, the reconstructed state should remain diagonal even when expressed in terms of the wave functions of the quench Hamiltonian.

On the other hand, we remark that allowing for off-diagonal correlations and cross correlations in V is necessary for an accurate reconstruction as otherwise the comparison in Fig. 2a is significantly worse. One reason for their presence can be small deviations between the assumed eigenmodes and the true eigenmodes of the system, e.g., due to pre- or post-quench trapping potential imperfections not included in the GP profile. Another reason could be that the initial state is genuinely out of thermal equilibrium, which would be interesting from the quantum information perspective in the context of the resource theory of coherence[36,37].

Independent of these subtleties, our read-out method allows us to study how the energy is distributed in the system based on the measured out-of-equilibrium phase fluctuations. We now have access to the phonon occupation numbers given by $n_k = \frac{1}{2}\langle \hat{\phi}_k^2 + \delta\hat{\rho}_k^2 \rangle - \frac{1}{2}$ and can study energy expectation values $\langle \hat{H} \rangle = \sum_{k=1}^{\mathcal{N}} \omega_k n_k$ with $\hat{H}$ given in Eq. (1). More specifically, we can check from the observed data if the energy is distributed among the modes in a thermal way. The gas is prepared in a double well trap with large tunnel coupling and we expect the prepared state to be thermal with respect to the Hamiltonian (11). Based on Fig. 2b, we find that the reconstructed initial state shows significant suppression of the phase fluctuations which are an order of magnitude smaller than the density fluctuations. This is consistent with the initial energetic penalty on phase fluctuations. In Fig. 2c, we show the quantitative comparison of the reconstructed second moments $\langle \hat{\phi}_k^2 \rangle$ and $\langle \delta\hat{\rho}_k^2 \rangle$ compared to the thermal theory with the Hamiltonian (11). Due to the finite imaging resolution, we are only able to resolve the lowest-lying eigenmodes. We find that their second moments agree with a thermal distribution of the coupled Hamiltonian (11). On the other hand, we also observed that the reconstructed initial state does not agree with the experimental state before the start of the decoupling ramp, as it leads to weaker phase locking than what was measured. This hints at the finite decoupling ramp having a significant influence on the correlations observed in the quench dynamics despite the tunnel coupling decreasing exponentially in the height of the barrier that is being ramped-up. The reconstruction hence extracts an effective initial state of the dynamics. If the physics of the initial Hamiltonian is of particular interest, then this effect might be diminished by performing a faster quench to the free system. On the other hand, let us remark that the physics of quenches of this type is key to the observation of generalized Gibbs ensembles in the considered setup[6]. In general, it is difficult to model the complete process of state preparation theoretically as it involves a strongly correlated phase of the sine-Gordon model out of equilibrium[7] and our method could offer new experimental insights.

Recurrent dynamics. With the reconstruction of the full state of the system, also its evolution beyond the interval of input times can be calculated. Propagating the covariance matrix V forward or backward in time via (9) allows us to pre- and redict the system's dynamics. In ref. [8], this dynamics was visualized and quantified through the correlator

$$C(|z - z'|, t) = \langle \cos(\hat{\varphi}(z,t) - \hat{\varphi}(z',t)) \rangle . \tag{12}$$

The phase-locked initial state corresponds to $C \approx 1$ independent of the longitudinal separation $\bar{z} = |z - z'|$. In Fig. 3a, we show $C(\bar{z}, t)$ obtained from the experimental data. Due to a linear dispersion relation and an equally spaced spectrum, the involved modes start to rephase after the inital dephasing dynamics leading to partial recurrences of the initial state[8]. Figure 3b–d shows how this rephasing dynamics can be predicted from the reconstructed states. For the reconstruction based on the initial dephasing dynamics, for example, we obtain a good qualitative prediction of the recurrences (red interval). Quantitative agreement is lost over time due to interaction effects between the modes. These interactions are mediated by higher-order terms beyond the effective model assumed in (1) and can therefore not be captured[25]. Nevertheless, the reconstruction method is robust enough such that we can obtain an accurate short-time prediction even using data that are seemingly fully dephased, i.e., where $C(\bar{z}, t)$ is nearly indistinguishable from the correlations of a thermal state of the quench Hamiltonian $\hat{H}$ (blue interval). However, in some cases (green interval), we find that statistical fluctuations can lead to large error bars, an effect reproduced by numerical simulations (see Supplementary Note 3). Note also that the last two intervals were intentionally chosen to be short, including only seemingly dephased data between the recurrences. They cover $I = 5$ input times, during which the slowest eigenmode performs only about a quarter of a rotation. Therefore, the influence of the finite statistical sample size is more severe in these reconstructions.

Phonon occupation dynamics. Besides providing new insights into the state preparation, access to the full covariance matrix can enable entirely new ways of exploring the effects of interactions. The effective model given in (1) is obtained in a perturbative expansion of the Lieb-Liniger Hamiltonian up to second order[25]. For long evolution times, however, the dynamics can also be affected by the neglected terms that, e.g., can give rise to effects such as Beliaev-Landau damping[25]. It is challenging to obtain the rates of such processes by numerical calculations as interacting bosonic dynamics are notoriously difficult to treat and various approximations are necessary[38–41]. Therefore, it would be interesting to use the atom chip experiments to measure the damping rates and compare with theoretical predictions to validate different methods.

Here we show how the recovery method described above can be used to investigate these higher-order processes. To that end, we perform the recovery procedure for different input intervals of length $I = 8$, with varying starting points. For each interval, we obtain an estimate of the central moments of phase and density fluctuations, $\langle \hat{\phi}_k^2(t) \rangle$ and $\langle \delta\hat{\rho}_k^2(t) \rangle$, and calculate the phonon occupation numbers $n_k(t) = \frac{1}{2}\langle \hat{\phi}_k^2(t) + \delta\hat{\rho}_k^2(t) \rangle - \frac{1}{2}$. Scanning the starting point of the input interval through the measurement times allows us to investigate the dynamics of these observables, as shown in Fig. 4. The interval length is chosen long enough such that the slowest eigenmode picks up enough dynamical phase to ensure a stable reconstruction. At the same time, it is chosen

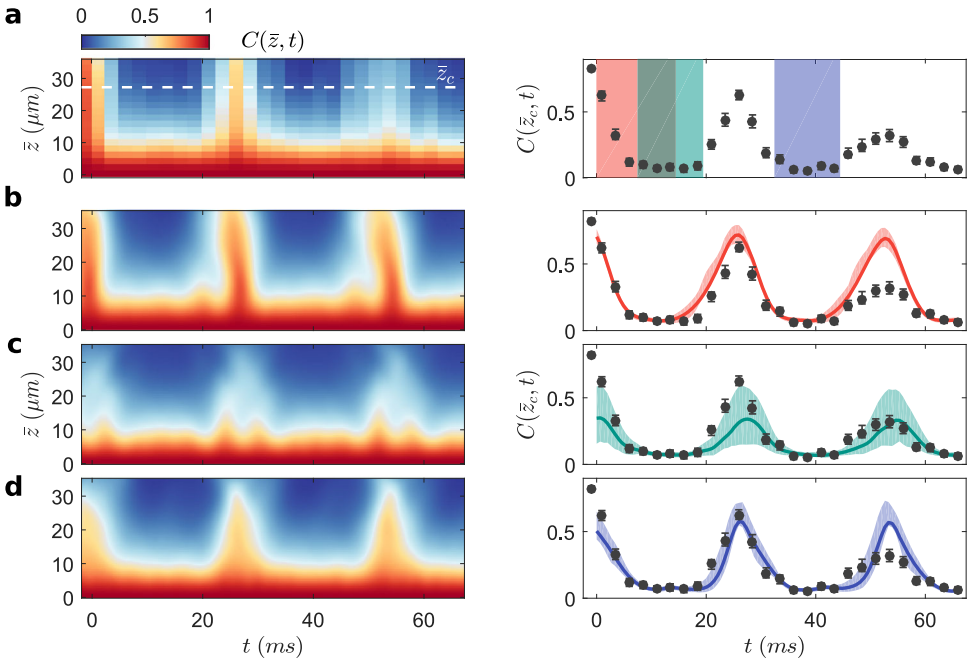

Fig. 3 Dynamical predictions. a Measured phase correlations $C(\bar{z},t)$ shown together with a cut at $\bar{z}_c = 27.25$ μm. Using this experimental dataset, we have performed reconstructions based on input data from a given time window (indicated by red, green and blue intervals) and we calculated the phase correlation functions $C(\bar{z},t)$ capturing the full spatio-temporal dynamics by evolving the reconstructed states to times beyond the input intervals. **b** The full spatio-temporal dynamics based on input data indicated by the red interval together with the cut at $\bar{z}_c$, which shows the quantitative comparison to the measured data. The red-coloured curve corresponds to the propagation of the reconstructed state based on initial times. **c** Similarly, we show the full spatio-temporal dynamics and a cut at $\bar{z}_c$ obtained from the reconstructed state based on seemingly dephased data after the quench (green interval). **d** Likewise, based on the times between the first and second recurrences (blue interval), we are able to obtain a reliable reconstruction. While the dynamical prediction based on the initial dephasing dynamics works well, the reconstructions based on data taken in between the recurrences is limited by the finite sample size (green interval)—an effect reproduced by numerical simulations (see Supplementary Note 3). Note that the quantitative discrepancy at times far away from input intervals is due to terms of higher order not captured by the effective theory of Eq. (1). The shaded area around the curves, as well as the error bars of the data, indicate 80% confidence intervals obtained from a bootstrap analysis[35].

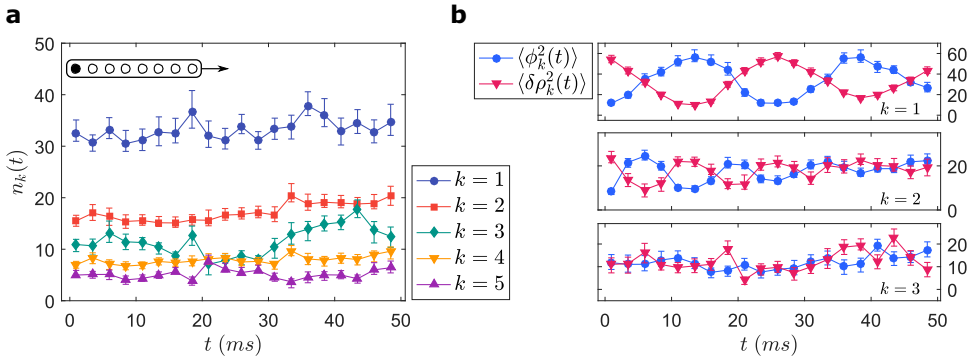

Fig. 4 Phonon occupation dynamics. a Phonon occupation numbers $n_k(t)$ of the first five modes $k = 1, \ldots, 5$ as a function of time t. Each point is based on a reconstruction with an input interval $\{t, t+\Delta t, \ldots, t+7\Delta t\}$ of length $l = 8$, illustrated by the black box in the upper left corner. For the ideal mean-field model, n_k should be a constant of motion. **b** Time-resolved central moments of the phase and density fluctuations in momentum space $\langle\hat{\phi}_k^2(t)\rangle$ and $\langle\delta\hat{\rho}_k^2(t)\rangle$ for the first three modes $k = 1, 2, 3$. We observe a gradual decay of the oscillation amplitude reflecting the apparent irreversible equilibration present in the system. The error bars indicate the 80% confidence intervals obtained from a bootstrap analysis[35]. The lines connecting the data points are a guide to the eye.

short enough such that interactions between the modes do not influence the reconstruction.

The occupation numbers n_k are constants of motion of $\hat{H}$. In Fig. 4a, we show their reconstructed dynamics for the five lowest eigenmodes. We find that overall the occupation numbers do not vary strongly and stay almost constant. This is expected as perturbations to the quench Hamiltonian should be negligible, and in any case they are irrelevant in the sense of the renormalization group. Note, however, that for different measurements with other system sizes, we find indications of a trend of slowly increasing mode occupations (see Supplementary Note 4). While the dynamics of occupation numbers is constant, Fig. 4b shows how at the same time the individual modes rotate between phase and density fluctuations. We find that this dynamics is clearly damped. This hints that the source of the recurrence damping observed in Fig. 3a and ref. [8] is a loss of the initial quadrature 'squeezing' $\langle\hat{\phi}_k^2(0)\rangle/\langle\delta\hat{\rho}_k^2(0)\rangle \ll 1$ within each mode k rather than changes in their occupations.

Our method makes it possible to extract mode-resolved damping rates of the collective excitations: In the future, using

smaller time steps Δt and possibly non-equidistant measurement times should allow to study also higher modes and test theoretical predictions concerning the dynamics under perturbations to the non-interacting effective model.

Discussion

We have formulated and demonstrated the functioning of a new quantum read-out method for quantum simulators where we reconstruct the second moments of pairs of conjugated observables by measuring at different times only one of them. The developed scheme allows us to reliably reconstruct the covariance matrix of non-local low-energy excitations of a 1D superfluid based on experimental data from an atom chip experiment which makes phase measurements but does not directly access density fluctuations.

We found several interesting insights into the physics of the system. Firstly, the strong energetic penalty on phase fluctuations present during the state preparation is reflected in the reconstructed correlations as there are significantly less phase than density fluctuations. The reconstructed state is almost diagonal, which underlines that the eigenmodes before and after the quench are closely related and on a higher level demonstrates that the effective theory captures the relevant degrees of freedom of the system. A fit to a thermal model for the initial state allowed us to estimate the temparature and the effective tunnel coupling in the state preparation. In the considered setting, recurrences of the system have been recently observed[8], which are due to an approximately linear spectrum of the phonons. We have demonstrated that our method can take input data from times when the system is seemingly dephased in order to predict recurrences by evolving the reconstructed covariance matrix in time, strongly underlining the predictive power of the obtained recovery scheme. Finally, we have studied the occupation numbers of the eigenmodes over time and obtained strong constraints on the rate of their growth. We have reconstructed the contribution of phase and density fluctuations over time and found that their oscillations are damped. We expect that a quantitative experimental assessment of possible reasons of the deviations from the non-interacting effective model will become possible by following the lines of this work.

Our work paves the way towards new intriguing experiments by giving access to quadrature operators which can be used as the basic ingredients for many quantum information processing protocols[42–44]. The method presented offers a novel window into quantum simulators, allowing to assess initial states, notions of entanglement and various other quantities previous read-out schemes did not allow for. It is our hope that our new quantum read-out method will enable exciting insights into the physics of ultra-cold superfluids, but also due to its generality that it will become a versatile tool used in state-of-the art quantum technologies allowing to fully use the power of the existing quantum simulation platforms[45].

Note added. After the completion of the manuscript, we became aware of similar developments in the discrete setting of optical lattices with applications to topological band insulators[22,23,46]—it would be interesting to also include there our ideas of using semi-definite constraints ensuring that the reconstructed covariance matrix is physical and the recovery stable.

Data availability

Data are available upon reasonable request.

Code availability

Code is available upon reasonable request.

Received: 19 August 2019; Accepted: 8 November 2019;
Published online: 17 January 2020

References

1. Bloch, I., Dalibard, J. & Nascimbene, S. Quantum simulations with ultracold quantum gases. *Nat. Phys.* **8**, 267 (2012).
2. Cirac, J. I. & Zoller, P. Goals and opportunities in quantum simulation. *Nat. Phys.* **8**, 264 (2012).
3. Blatt, R. & Roos, C. F. Quantum simulations with trapped ions. *Nat. Phys.* **8**, 277 (2012).
4. Gring, M. et al. Relaxation and pre-thermalization in an isolated quantum system. *Science* **337**, 1318 (2012).
5. Hofferberth, S., Lesanovsky, I., Fischer, B., Schumm, T. & Schmiedmayer, J. Non-equilibrium coherence dynamics in one-dimensional bose gases. *Nature* **449**, 324–327 (2007).
6. Langen, T. et al. Experimental observation of a generalised gibbs ensemble. *Science* **348**, 207–211 (2015).
7. Schweigler, T. et al. Experimental characterization of a quantum many-body system via higher-order correlations. *Nature* **545**, 323 (2017).
8. Rauer, B. et al. Recurrences in an isolated quantum many-body system. *Science* **360**, 307 (2018).
9. Endres, M. et al. Observation of correlated particle-hole pairs and string order in low-dimensional mott insulators. *Science* **334**, 200 (2011).
10. Trotzky, S. et al. Probing the relaxation towards equilibrium in an isolated strongly correlated one-dimensional Bose gas. *Nat. Phys.* **8**, 325 (2012).
11. Ronzheimer, J. P. et al. Expansion dynamics of interacting bosons in homogeneous lattices in one and two dimensions. *Phys. Rev. Lett.* **110**, 205301 (2013).
12. Schreiber, M. et al. Observation of many-body localization of interacting fermions in a quasi-random optical lattice. *Science* **349**, 842 (2015).
13. Cheneau, M. et al. Light-cone-like spreading of correlations in a quantum many-body system. *Nature* **481**, 484–7 (2012).
14. Kaufman, A. M. et al. Quantum thermalization through entanglement in an isolated many-body system. *Science* **353**, 794 (2016).
15. Sherson, J. F. et al. Single-atom-resolved fluorescence imaging of an atomic Mott insulator. *Nature* **467**, 68–72 (2010).
16. Bakr, W. S. et al. Probing the superfluid-to-mott insulator transition at the single-atom level. *Science* **329**, 547–550 (2010).
17. Weitenberg, C. et al. Single-spin addressing in an atomic Mott insulator. *Nature* **471**, 319–324 (2011).
18. Merkel, S. T., Riofrio, C. A., Flammia, S. T. & Deutsch, I. H. Random unitary maps for quantum state reconstruction. *Phys. Rev. A* **81**, 032126 (2010).
19. Ohliger, M., Nesme, V. & Eisert, J. Efficient and feasible state tomography of quantum many-body systems. *New J. Phys.* **15**, 015024 (2013).
20. Elben, A., Vermersch, B., Dalmonte, M., Cirac, J. I. & Zoller, P. Renyi entropies from random quenches in atomic Hubbard and spin models. *Phys. Rev. Lett.* **120**, 050406 (2018).
21. Barthel, T. & Lu, J. Fundamental limitations for measurements in quantum many-body systems. *Phys. Rev. Lett.* **121**, 080406 (2018).
22. Hauke, P., Lewenstein, M. & Eckardt, A. Tomography of band insulators from quench dynamics. *Phys. Rev. Lett.* **113**, 045303 (2014).
23. Ardila, L. A. P., Heyl, M., & Eckardt, A. Measuring the single-particle density matrix for fermions and hard-core bosons in an optical lattice. *Phys. Rev. Lett.* **121**, 260401 (2018).
24. Cazalilla, M. A. Bosonizing one-dimensional cold atomic gases. *J. Phys. B* **37**, S1 (2004).
25. Mora, C. & Castin, Y. Extension of Bogoliubov theory to quasicondensates. *Phys. Rev. A* **67**, 053615 (2003).
26. Salasnich, L., Parola, A. & Reatto, L. Effective wave equations for the dynamics of cigar-shaped and disk-shaped bose condensates. *Phys. Rev. A* **65**, 043614 (2002).
27. Stringari, S. Collective excitations of a trapped bose-condensed gas. *Phys. Rev. Lett.* **77**, 2360 (1996).
28. Messiah, A. *Quantum Mechanics* Vol. I (North Holland Publishing, Amsterdam, 1958).
29. Folman, R. et al. Controlling cold atoms using nanofabricated surfaces: atom chips. *Phys. Rev. Lett.* **84**, 4749–4752 (2000).
30. Schumm, T. et al. Matter-wave interferometry in a double well on an atom chip. *Nat. Phys.* **1**, 57–62 (2005).
31. van Nieuwkerk, Y. D., Schmiedmayer, J. & Essler, F. H. L. Projective phase measurements in one-dimensional bose gases. *SciPost Phys.* **5**, 046 (2018).
32. Schweigler, T. *Correlations And Dynamics of Tunnel-coupled One-Dimensional Bose Gases.* Ph.D. thesis, TU Wien (2019).

33. Simon, R., Mukunda, N. & Dutta, B. Quantum-noise matrix for multimode systems: $u(n)$ invariance, squeezing, and normal forms. *Phys. Rev. A* **49**, 1567 (1994).
34. Grant, M. & Boyd, S. CVX: Matlab software for disciplined convex programming, version 2.1, http://cvxr.com/cvx (2014).
35. Efron, B. & Tibshirani, R. Bootstrap methods for standard errors, confidence intervals, and other measures of statistical accuracy. *Statist. Sci.* **1**, 54–75 (1986).
36. Lami, L. et al. Gaussian quantum resource theories. *Phys. Rev. A* **98**, 022335 (2018).
37. Streltsov, A., Adesso, G. & Plenio, M. B. Colloquium: quantum coherence as a resource. *Rev. Mod. Phys.* **89**, 041003 (2017).
38. Mazets, I. E. & Mauser, N. J. Integer partition manifolds and phonon damping in one dimension. Preprint at https://arxiv.org/abs/1804.01374 (2018).
39. Polkovnikov, A. Phase space representation of quantum dynamics. *Ann. Phys.* **325**, 1790–1852 (2010).
40. Huber, S., Buchhold, M., Schmiedmayer, J. & Diehl, S. Thermalization dynamics of two correlated bosonic quantum wires after a split. *Phys. Rev. A* **97**, 043611 (2018).
41. Kukuljan, I., Sotiriadis, S. & Takacs, G. Correlation functions of the quantum sine-Gordon model in and out of equilibrium. *Phys. Rev. Lett.* **121**, 110402 (2018).
42. Weedbrook, C. et al. Gaussian quantum information. *Rev. Mod. Phys.* **84**, 621 (2012).
43. Eisert, J. & Plenio, M. B. Introduction to the basics of entanglement theory in continuous-variable systems. *Int. J. Quant. Inf.* **1**, 479–506 (2003).
44. Schnabel, R. Squeezed states of light and their applications in laser interferometers. *Phys. Rep.* **684**, 1 (2017).
45. Acin, A. et al. The European quantum technologies roadmap. *New J. Phys.* **20**, 080201 (2018).
46. Tarnowski, M. et al. Characterizing topology by dynamics: Chern number from linking number. *Nat. Commun.* **10**, 1728 (2019).

Acknowledgements

We thank C. Riofrio, F. Essler, I. Mazets and A. Steffens for useful discussions and comments. This work has been supported by the ERC (TAQ, QuantumRelax), the European Commission (AQuS), the German DFG (FOR 2724, CRC 183, EI 519/14-1, 519/9-1, EI 519/7-1), the Templeton Foundation, the FQXi, the Austrian Science Fund (FWF) through the doctoral program CoQuS (W1210) (T.S., B.R.) and the SFB 1225 ISOQUANT financed by the DFG and the FWF. This work has also received funding from the European Union's Horizon 2020 research and innovation programme under grant agreement No. 817482 (PASQuanS).

Author contributions

M.G. formulated and implemented the method following the suggestion of J.S. with contributions of T.S., B.R. and C.K. under the supervision of J.E. B.R., T.S. and J.S. performed the experiment and obtained the data. All authors contributed to the writing of the manuscript.

Competing interests

The authors declare no competing interests.

Additional information

Supplementary information is available for this paper at https://doi.org/10.1038/s42005-019-0273-y.

Correspondence and requests for materials should be addressed to J.E.

Reprints and permission information is available at http://www.nature.com/reprints

Publisher's note Springer Nature remains neutral with regard to jurisdictional claims in published maps and institutional affiliations.

Supplementary Information: Quantum read-out for cold atomic quantum simulators

SUPPLEMENTARY NOTE 1: CALCULATING THE EIGENMODES

In this section we describe in detail how we obtain the eigenmodes of the quench Hamiltonian which can be viewed as a CFT in curved space-time background whenever the GP profile is not homogeneous. In this case, a discretization of fields allows to approximate the low-lying eigenmodes of the continuum Hamiltonian by the eigenmodes of a Hamiltonian involving a finite number of degrees of freedom which are the average fields in a given discretization cell. We then show how to diagonalize the coarse-grained Hamiltonian numerically taking into account that the quench Hamiltonian has a zero-mode. Finally, we describe how to use the numerically obtained wavefunctions for finitely many modes as an approximation to the corresponding eigenmodes in the continuum limit.

The Hamiltonian describing the quench dynamics is functionally parametrized by the GP profile $n_{\rm GP}$. Due to transverse broadening of the wave functions [1] the density-density interaction is functionally dependent on the GP profile and reads

$$g(z) = \hbar\omega_\perp a_s(2+3a_s n_{\rm GP}(z))/(1+2a_s n_{\rm GP}(z))^{3/2} \tag{1}$$

where $\omega_\perp$ is the radial trapping frequency and a_s is the scattering length [2]. Hence, by knowing the GP profile, we know the Hamiltonian and so we can find the eigenmodes. Here we show how to do this even if the GP profile is not homogeneous $n_{\rm GP} \neq \texttt{const}$

A. Discretization of fields

We want to find approximations to the wave functions and eigenmodes discussed above by discretizing the interval $[-R_{1\rm D}, R_{1\rm D}]$ into N pixels, each of size $2R_{1\rm D}/N$. Fixing N, for $l = 1, \ldots, N+1$ the coordinates of the discretization lattice read $z_l = -R_{1\rm D} + 2R_{1\rm D}\frac{l-1}{N}$ and we define discretization pixels which are the closed intervals $p_l = [z_l, z_{l+1}]$ for $l = 1, \ldots, N$. We then introduce the discretized operators as the integration of the field operators via

$$\hat{\varphi}_l^{(N)} = \frac{1}{\Delta z}\int_{p_l} {\rm d}z\, \hat{\varphi}(z), \tag{2}$$

$$\delta\hat{\varrho}_l^{(N)} = \frac{1}{\Delta z}\int_{p_l} {\rm d}z\, \delta\hat{\varrho}(z), \tag{3}$$

with $\Delta z := |p_l| = 2R_{1\rm D}/N$. Following Refs. [3, 4], these discretized operators yields a vector of canonical coordinates

$$\hat{Q} = (\hat{\varphi}_1^{(N)}, \ldots \hat{\varphi}_N^{(N)}, \delta\hat{\varrho}_1^{(N)} \ldots \delta\hat{\varrho}_N^{(N)})^T, \tag{4}$$

satisfying the bosonic canonical commutation relations $[\hat{Q}_j, \hat{Q}_k] = {\rm i}\Omega_{j,k}/\Delta z$ where $\Omega = \left(\begin{smallmatrix} 0 & \mathbb{1}_N \\ -\mathbb{1}_N & 0 \end{smallmatrix}\right)$. as can be verified easily. Observe that the right-hand side will yield a Dirac delta in the continuum limit $N \to \infty$. The discretization of the effective model will be a quadratic operator in the discretized modes $\hat{\varphi}_l^{(N)}$ and $\delta\hat{\varrho}_l^{(N)}$ which can be efficiently diagonalized using single particle transformations only as we want to explain below in the next section.

B. Decoupling of the effective model using symplectic transformations

Using the general notation of quadratures $\hat{Q}$, we consider quadratic Hamiltonians of the form

$$\hat{H}_N = \tfrac{1}{2}\hat{Q}^T H \hat{Q} = \tfrac{1}{2}\sum_{j,k=1}^{2N} H_{j,k}\hat{Q}_j\hat{Q}_k, \tag{5}$$

where $H = H^\top \in \mathbb{R}^{2N\times 2N}$ are the couplings We will assume that H is positive semi-definite, i.e., $H \succeq 0$ and that there is no coupling between the phases and densities in the effective model and all Hamiltonians considered in this work will have this property. In this case the couplings H will be block diagonal and we will use the decomposition

$$H = \begin{pmatrix} H_\phi & 0 \\ 0 & H_\rho \end{pmatrix} = H_\phi \oplus H_\rho \,. \tag{6}$$

To discretize the integral we define the geometric mean $\eta_l = (n_{\mathrm{GP}}(z_l) n_{\mathrm{GP}}(z_{l+1}))^{1/2}$ for $l = 1\ldots, N$ which gives

$$\hat{H} \approx \Delta z \sum_{l=1}^{N-1} \frac{\hbar^2 \eta_l}{4m} \left(\frac{\hat{\varphi}_l^{(N)} - \hat{\varphi}_{l+1}^{(N)}}{\Delta z} \right)^2 + \Delta z \sum_{l=1}^{N} g(z_l) \delta\hat{\varrho}_l^{(N)2} + \Delta z \sum_{l=1}^{N-1} \frac{\hbar^2}{4m\eta_l} \left(\frac{\delta\hat{\varrho}_l^{(N)} - \delta\hat{\varrho}_{l+1}^{(N)}}{\Delta z} \right)^2 \tag{7}$$

$$= \Delta z \sum_{l=1}^{N-1} \left[\frac{\hbar^2 \eta_l}{4m} \left(\frac{\hat{Q}_l - \hat{Q}_{l+1}}{\Delta z} \right)^2 \right] + \Delta z \sum_{l=1}^{N} g(z_l) \hat{Q}_{l+N}^2 + \Delta z \sum_{l=1}^{N-1} \left[\frac{\hbar^2}{4m\eta_l} \left(\frac{\hat{Q}_{l+N} - \hat{Q}_{l+1+N}}{\Delta z} \right)^2 \right] \tag{8}$$

$$:= \hat{H}_N \,. \tag{9}$$

From this we read off

$$H_\phi = \frac{\hbar^2}{2m\Delta z} \begin{pmatrix} \eta_1 & -\eta_1 & & & \\ -\eta_1 & \eta_1+\eta_2 & -\eta_2 & & \\ & & \ddots & & \\ & & -\eta_{N-2} & \eta_{N-2}+\eta_{N-1} & -\eta_{N-1} \\ & & & -\eta_{N-1} & \eta_{N-1} \end{pmatrix}, \tag{10}$$

$$H_\rho = 2\Delta z \begin{pmatrix} g(z_1) & & & \\ & g(z_2) & & \\ & & \ddots & \\ & & & g(z_N) \end{pmatrix} + \frac{\hbar^2}{2m\Delta z} \begin{pmatrix} \eta_1^{-1} & -\eta_1^{-1} & & & \\ -\eta_1^{-1} & \eta_1^{-1}+\eta_2^{-1} & -\eta_2^{-1} & & \\ & & \ddots & & \\ & & -\eta_{N-2}^{-1} & \eta_{N-2}^{-1}+\eta_{N-1}^{-1} & -\eta_{N-1}^{-1} \\ & & & -\eta_{N-1}^{-1} & \eta_{N-1}^{-1} \end{pmatrix}. \tag{11}$$

Depending on the detail of the simulation $g(z) \approx g(0)$ can be taken constant or H_ρ may include the pressure term as discussed above with a similar discretization scheme. With this notation, we obtain

$$\hat{H}_N = \tfrac{1}{2} \hat{x}^\top (H_\phi \oplus H_\rho) \hat{x} \approx \hat{H} \,. \tag{12}$$

Starting from a set of canonical coordinates $\hat{Q}$ then $\hat{r} = S\hat{Q}$ for $S \in \mathbb{R}^{2N\times 2N}$ will again denote a vector of canonically commuting operators if S is symplectic, i.e., it fulfills

$$S\,\Omega\,S^T = \Omega \tag{13}$$

which can be seen by explicitly checking that $\hat{r}$ again fulfills $[\hat{r}_j, \hat{r}_k] = \mathrm{i}\Omega_{j,k}/\Delta z$.

In view of diagonalizing the Hamiltonians of interest, it is important to note that matrices of the form $S = Q \oplus Q$ for any orthogonal $Q \in O(N)$ as well as $S = A \oplus A^{-1}$ for any invertible $A \in GL(N, \mathbb{R})$ that is symmetric, i.e., $A^T = A$ are both symplectic matrices and that the inverse as well as the product of symplectic matrices are again symplectic. We can then diagonalize Hamiltonians of the form as given in Eq. (5) under the assumption that H_ρ is invertible. This property allows us to define a symplectic matrix

$$S_1 = \begin{pmatrix} (H_\rho)^{1/2} & 0 \\ 0 & (H_\rho)^{-1/2} \end{pmatrix} \tag{14}$$

such that

$$S_1^T H S_1 = ((H_\rho^T)^{1/2} H_\phi (H_\rho)^{1/2}) \oplus \mathbb{1}_N \,. \tag{15}$$

The matrix of the phase couplings in the new coordinates reads $\tilde{H}_\phi = (H_\rho^T)^{1/2} H_\phi (H_\rho)^{1/2}$ and is again real and symmetric such that it can be diagonalized by an orthogonal transformation $Q \in O(N)$ with $\tilde{H}_\phi = Q\Sigma Q^T$. Here, Σ is diagonal and we assume

that all zero eigenvalues are sorted to the first $N_0 \geq 0$ positions, i.e., $\Sigma = 0_{N_0} \oplus \tilde{\Sigma}$ with $\tilde{\Sigma} \succ 0$ diagonal and we define the eigenfrequencies ω via $\tilde{\Sigma}^{1/2} = \mathrm{diag}(\omega_{N_0+1}, \ldots, \omega_N)$. With the diagonal matrix $\Sigma_\phi = \mathbb{1}_{N_0} \oplus \tilde{\Sigma}$ and the transformation

$$S_2 = \begin{pmatrix} Q_\phi & 0 \\ 0 & Q_\phi \end{pmatrix} \begin{pmatrix} \Sigma_\phi^{-1/4} & 0 \\ 0 & \Sigma_\phi^{1/4} \end{pmatrix} \tag{16}$$

we obtain

$$S_2^T S_1^T H S_1 S_2 = (0_{N_0} \oplus \tilde{\Sigma}^{1/2}) \oplus (\mathbb{1}_{N_0} \oplus \tilde{\Sigma}^{1/2}) \, . \tag{17}$$

That is, in the canonical coordinates $(\hat{\phi}_1^{(N)}, \ldots \hat{\phi}_N^{(N)}, \delta\hat{\rho}_1^{(N)} \ldots \delta\hat{\rho}_N^{(N)})^T = \hat{r} = \sqrt{\Delta z}(S_1 S_2)^{-1}\hat{Q}$ we have that the Hamiltonian in Eq. (5) takes the form

$$\hat{H}_N = \tfrac{1}{2}\sum_{j=1}^{N_0}\big(\delta\hat{\rho}_j^{(N)}\big)^2 + \tfrac{1}{2}\sum_{j=N_0+1}^{N}\omega_j\big(\big(\delta\hat{\rho}_j^{(N)}\big)^2 + \big(\hat{\phi}_j^{(N)}\big)^2\big), \tag{18}$$

such that $\hat{\phi}_j^{(N)} \approx \hat{\phi}_j$ and $\delta\hat{\rho}_j^{(N)} \approx \delta\hat{\rho}_j$ as $\hat{H} \approx \hat{H}_N$. We will therefore not distinguish between $\hat{\phi}_j^{(N)}$ and $\hat{\phi}_j$ and $\delta\hat{\rho}_j^{(N)}$ and $\delta\hat{\rho}_j$ outside of this section.

C. Discrete approximations

With this, we can read off the discrete approximation to the wave functions f_k^ϕ and f_k^ρ relating $\hat{\phi}^{(N)}$ and $\hat{\varphi}^{(N)}$ or correspondingly $\delta\hat{\rho}^{(N)}$ $\delta\hat{\varrho}^{(N)}$ as the rows of $S = S_1 S_2$ which is of block structure, i.e.,$S = S^\phi \oplus S^\rho$. Specifically we find

$$f_k^\phi(z_k) \approx \sqrt{\Delta z}^{-1} S^\phi_{j+N_0,k} \tag{19}$$

and

$$f_k^\rho(z_k) \approx \sqrt{\Delta z}^{-1} S^\rho_{j+N_0,k} \, . \tag{20}$$

Note that when relating $\hat{\phi}^{(N)}$ and $\hat{\varphi}^{(N)}$ or $\delta\hat{\rho}^{(N)}$ and $\delta\hat{\varrho}^{(N)}$ we included a factor $\sqrt{\Delta z}$. The inclusion of this factor allows to change the commutation relations from $[\delta\hat{\varrho}_j^{(N)}, \hat{\varphi}_k^{(N)}] = i\delta_{j,k}/\Delta z \to i\delta(z_j - z_k)$ to $[\delta\hat{\rho}_j^{(N)}, \hat{\phi}_k^{(N)}] = i\delta_{j,k} \to i\delta_{j,k}$ as one would expect from the discrete canonical eigenmodes of the system. Let us furthermore observe that the relation to the real-space correlators are given by

$$\langle\hat{\varphi}(z_j)\hat{\varphi}(z_k)\rangle \approx \langle\hat{\varphi}_j^{(N)}\hat{\varphi}_k^{(N)}\rangle = \Delta z^{-1}\sum_{j',k'=1}^{N} S^{-1}_{j,j'}S^{-1}_{j,j'}\langle\hat{\phi}_{j'}^{(N)}\hat{\phi}_{k'}^{(N)}\rangle, \tag{21}$$

where we exploited that S has a block-diagonal structure and the inverse scaling in the discretization step Δz should be noted.

SUPPLEMENTARY NOTE 2: DETAILED FORMULATION OF THE RECOVERY PROCEDURE

In this section, we describe the data analysis and formulate the reconstruction procedure with additional details. As described in Refs. [1, 5, 6] through matter-wave interferometry phase profiles φ of the superfluid can be measured. After the two superfluids were coupled with tunneling strength $J \approx 3.5\,\mathrm{Hz}$ for sufficiently long times, the separation potential is increased rapidly in about $1\,\mathrm{ms}$. The end of the ramp defines the initial time $t_0 = 0\,\mathrm{ms}$ for the quench evolution that follows. The gas can then be held for a specific time t which defines the time during which the system evolves under the quench Hamiltonian in Eq. (1). Here we focus on the referenced second moments obtained from the profiles, for which the corresponding physical observable is

$$\Phi(z, z', t) = \langle[\hat{\varphi}(z,t) - \hat{\varphi}(z_0,t)][\hat{\varphi}(z',t) - \hat{\varphi}(z_0,t)]\rangle \, , \tag{22}$$

where z_0 denotes a fixed reference point in the system.

For each hold time t about $n_{\mathrm{Sample}} \approx 200$ phase profiles were obtained, this number is limited by the stability of the setup, but can be increased if fewer hold times are considered in total. Supplementary Figure 2 shows an example of two of many phase

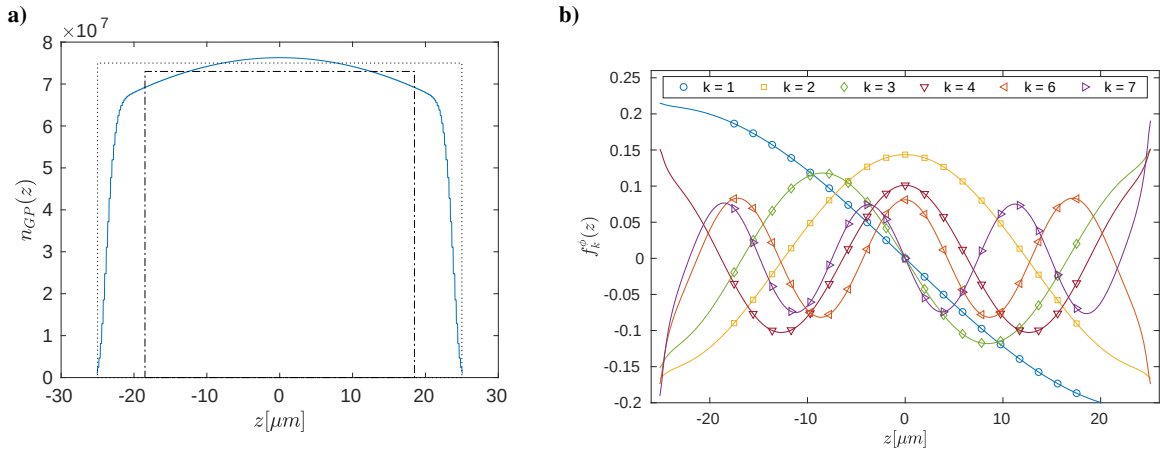

Supplementary Figure 1. **a)** We show the Gross-Pitaevskii profile $n_{\rm GP}$ reflecting the setting of the experiment where the box trapping potential is finite and is superposed with an additional weak harmonic potential both of these features lead to $n_{\rm GP}$ not being perfectly homogeneous. The dotted rectangle indicates a region of width $50\,\mu$m such that at the edges the profile amounts to 5% of the peak density. The dashed-dotted region corresponds to the window where data is typically taken – here the profile is relatively homogeneous. **b)** We plot low-lying eigenmode functions taking the values $f_j^\phi(z_k) \approx \sqrt{\Delta z}^{-1} S_{j,k}^\phi$ which show oscillatory behavior similar to the analytical solution to the Luttinger liquid model that can be obtained for the homogeneous profile.

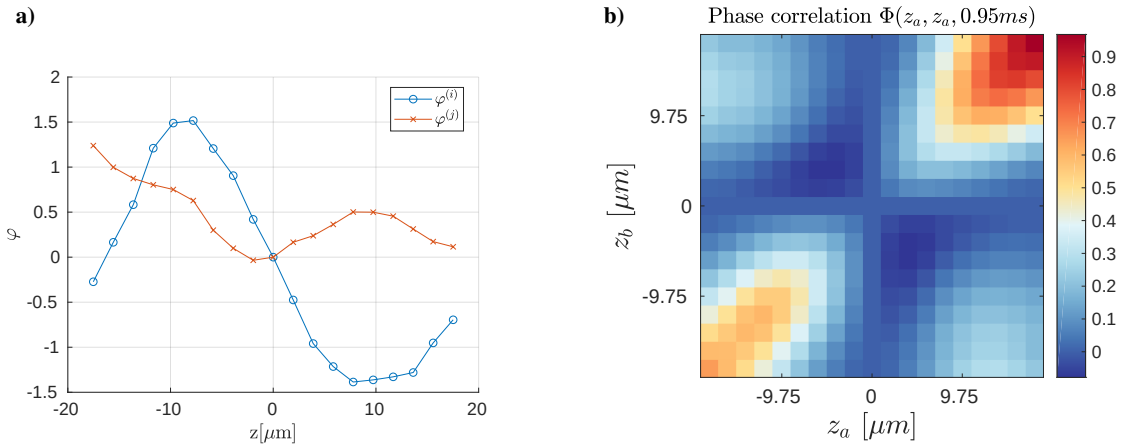

Supplementary Figure 2. **a)** We plot an example of two arbitrarily chosen referenced phase profiles $\varphi^{(i)}$ and $\varphi^{(j)}$ obtained in the experiment referenced to the center of the considered portion of the cloud. **b)** We show an example of the measured values of $\tilde{\Phi}(z_a, z_b, t)$ extracted from $n_{\rm Sample} \approx 200$ profiles. The referenced second moments vanish trivially if z_a or z_b equals the reference point and increase with increasing distance to z_0.

profiles used in the analysis. In the data analysis, data from $N_p = 19$ central pixels is used which corresponds to about 60% of the cloud as each pixel has size $\ell = 1.95\,\mu$m, so the total size observed is about $37\,\mu$m. The positions of the pixels are

$$z_a = (a - 10)\ell \tag{23}$$

and the reference point is chosen as $z_0 = 0\,\mu$m, i.e., in the middle of the cloud. We consider referenced second moments here, as by this we are able to consistently remove any offset phase between two different measured profiles. In practice we subtract at each pixel a the central phase profile value $\varphi^{(i)}(z_0)$. The experimental estimate for Eq. (22) is then

$$\Phi_{\rm est}(z_a, z_b, t) = \frac{1}{n_{\rm Sample}} \sum_{i=1}^{n_{\rm Sample}} \big(\varphi^{(i)}(z_a) - \varphi^{(i)}(z_0)\big)\big(\varphi^{(i)}(z_b) - \varphi^{(i)}(z_0)\big)\,. \tag{24}$$

In terms of the eigenmodes this reads

$$\Phi(z_a, z_b, t) = \frac{1}{2} \sum_{j,k=1}^{\mathcal{N}} (f_j^\phi(z_a) - f_j^\phi(z_0))(f_k^\phi(z_b) - f_k^\phi(z_0))\, \langle\{\hat{\phi}_j(t), \hat{\phi}_k(t)\}\rangle := \sum_{j,k=1}^{N} f_{j,k}^{a,b} V_{j,k}^{\phi\phi}(t)\,. \tag{25}$$

Using the expressions for the time evolution, we get

$$\begin{aligned}\Phi(z_a,z_b,t) = &\sum_{j,k=1}^{\mathcal{N}} f_{j,k}^{a,b}\big(\cos(E_j t)\cos(E_k t)V_{j,k}^{\phi\phi} + \sin(E_j t)\sin(E_k t)V_{j,k}^{\rho\rho}\big) \\ &- \sum_{j,k=1}^{\mathcal{N}} (f_{j,k}^{a,b} + f_{k,j}^{a,b})\cos(E_j t)\sin(E_k t)V_{j,k}^{\phi\rho}\ .\end{aligned} \tag{26}$$

It must be noted that the measured value at a pixel z_a does not exactly reflect the value of the field $\hat{\varphi}(z_a)$ but rather a *convolution* of the field with a Gaussian function, i.e., it probes the value averaged over a patch of specific characteristic length. More precisely, the experiment allows us only access to measurements of

$$\tilde{\hat{\varphi}}(z_a) = \frac{\int_{-R_{1\mathrm{D}}}^{R_{1\mathrm{D}}} \mathrm{d}z'\ e^{-\frac{(z'-z_a)^2}{2\sigma^2}}\hat{\varphi}(z')}{\int_{-R_{1\mathrm{D}}}^{R_{1\mathrm{D}}} \mathrm{d}z'\ e^{-\frac{(z'-z_a)^2}{2\sigma^2}}} \tag{27}$$

and we define the correspondingly convoluted wave function

$$\tilde{f}_j^{\phi}(z_a) = \frac{\int_{-R_{1\mathrm{D}}}^{R_{1\mathrm{D}}} \mathrm{d}z' e^{-\frac{(z'-z_a)^2}{2\sigma^2}} f_j^{\phi}(z')}{\int_{-R_{1\mathrm{D}}}^{R_{1\mathrm{D}}} \mathrm{d}z' e^{-\frac{(z'-z_a)^2}{2\sigma^2}}}\ . \tag{28}$$

For the considered experimental setup we find the estimation $\sigma \approx 3\,\mu\mathrm{m}$. In order to include the convolution in the reconstruction it then suffices to use the convoluted wave functions and set

$$\tilde{\Phi}(z_a,z_b,t) = \frac{1}{2}\sum_{j,k=1}^{\mathcal{N}} (\tilde{f}_j^{\phi}(z_a) - \tilde{f}_j^{\phi}(z_0))(\tilde{f}_k^{\phi}(z_b) - \tilde{f}_k^{\phi}(z_0))\ \langle\{\hat{\phi}_j(t),\hat{\phi}_k(t)\}\rangle := \sum_{j,k=1}^{N} \tilde{f_{j,k}^{a,b}} V_{j,k}^{\phi\phi}(t)\ . \tag{29}$$

D. Recovery procedure

In the implementation, we vectorize the covariance matrix V such that each block is a vector, i.e., $v^{\phi\phi} = \mathrm{vec}(V^{\phi\phi})$ etc. and define $v = v^{\phi\phi} \oplus v^{\phi\rho} \oplus v^{\rho\rho} \in \mathbb{R}^{3\mathcal{N}^2}$ and use the notation $v = \mathrm{vec}(V)$. Formula (26) shows that for each input (z_a, z_b, t) we can find a vector $w \in \mathbb{R}^{3\mathcal{N}^2}$ such that $\Phi(z_a,z_b,t) = w^T v$. For a fixed time t_{i_k} we then collect the from the measured data extracted second moments $\Phi_{\mathrm{est}}(z_a,z_b,t_i)$ in a vector $b_k \in \mathbb{R}^{N_p^2}$ and construct the corresponding vectors w and collect them as rows in a matrix $A_k \in \mathbb{R}^{N_p^2 \times 3\mathcal{N}^2}$. Doing this for all n times $t_{i_1},\ldots,t_{i_n}$ which are used for the reconstruction as input, we then stack all b_k and A_k into a large vector b matrix A correspondingly, i.e.,

$$A = \begin{bmatrix} A_1 \\ \vdots \\ A_n \end{bmatrix}\ , \quad b = \begin{bmatrix} b_1 \\ \vdots \\ b_n \end{bmatrix}\ . \tag{30}$$

We furthermore define at each time step a diagonal matrix $W \in \mathbb{R}^{N_p^2 \times N_p^2}$ which contains the inverse statistical errors of the experimental measurement of the second moments $W^{(k)}_{(a,b),(a,b)} = 1/\sigma_{\mathrm{est}}(\Phi(z_a,z_b,t_k))$ and collect all $W^{(k)}$ in on large block-diagonal matrix W in order to define a more uniform target function for the optimization. With this definition we aim at minimizing the vector Hilbert Schmidt-norm

$$\Theta = \|WA\,\mathrm{vec}(V) - Wb\|_2 \tag{31}$$

subject to the semi-definite constraint

$$V + \tfrac{1}{2}i\Omega \succeq 0\ , \tag{32}$$

where in the main text we have introduced the notation $\mathcal{A}(V) = A\,\mathrm{vec}(V)$. The numerical reconstruction has been implemented with use of the `cvx` package. The standard theory of semi-definite programming shows that there is always a unique solution v_{Opt} to this optimization problem. Unfolding the vectorization yields the reconstructed covariance matrix V_{Opt}.

As a final remark, it is interesting to note that positivity constraints (imposing that the density operator is positive semi-definite) similar to the Heisenberg constraint (reflecting the Heisenberg uncertainty principle as a semi-definite constraint) characterizing bosonic covariance matrices can significantly increase stability of least squares reconstructions [7]. In fact, wide classes of recoveries with a positivity constraint [7] can be interpreted as compressed sensing schemes [8]. In this context, is important to stress that the semi-definite constraint $V+\frac{1}{2}i\Omega \succeq 0$ readily implies that $V > 0$, so that V is strictly positive, so that the constraint of Ref. [7] is readily enforced. Hence, it is interesting to see that much of the intuition on the positive cone for density operators carries over to the Heisenberg cone for covariance matrices. Further explorations of seeing our scheme as a compressed sensing scheme will be left to future work.

SUPPLEMENTARY NOTE 3: SIMULATION OF THE RECONSTRUCTION PROCEDURE

Various aspects of the reconstruction can be modeled by considering a thermal state of the effective Hamiltonian of the strongly coupled condensates as discussed in the main text. Thermal correlations in the discretized model can be obtained either by considering the exact formulas from Refs. [9, 10] or by classical phase approximation [11]. In the following we consider the latter and study the effects of finite sample size and finite measurement resolution. We denote the real-space phase fluctuation functions by

$$(\Gamma^{\phi\phi})_{a,b} = \langle \hat{\varphi}(z_a)\hat{\varphi}(z_b)\rangle \tag{33}$$

and in classical field approximation we can calculate these via $\Gamma^{\phi\phi} \approx (H_\phi(J \neq 0))^{-1}/k_B T$ [11]. Together with the correlations for density fluctuations, we can propagate these under the quench Hamiltonian. Supplementary Figure 3 shows the correlations $\Gamma^{\phi\phi}$ and additionally the effect of the referencing which removes the running phase, of the convolution which comes from the measurement resolution and finally discretization due to a finite amount of pixels.

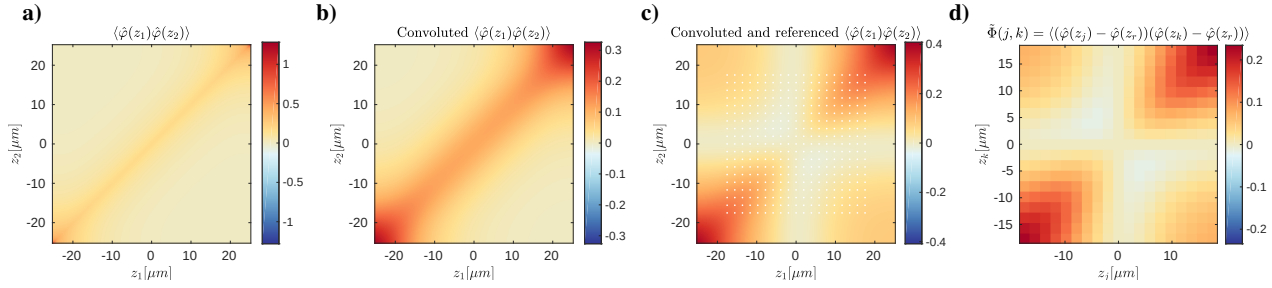

Supplementary Figure 3. Phase correlations in real-space: **a)** direct values, **b)** convoluted correlations, **c)** convoluted and referenced correlations (pixel positions indicated by white dots) and finally **d)** the convoluted referenced observable evaluated at pixel positions.

E. Influence of finite sample size

At each time the phase correlations can be used as a positive matrix parametrizing a (classical) Gaussian distribution from which single-shot random profiles can be sampled. After convolution these can be seen to correspond to the direct observable of the interferometry which is useful to assess the systematic imperfections of our procedure. Here we study two possible aspects. By resampling with $n_{\mathrm{Sample}} = 200$ and $n_{\mathrm{Sample}} = 2000$ we study the sensitivity of our reconstructions to statistical fluctuations in the experiment. Secondly, we study the real-space correlations and the convolution of these to see how finite measurement resolution impacts the information that can be obtained from our procedure.

We have simulated the $\hat{H}_N$ for $N = 400$ and $J/\hbar = 2\pi \times 3.5\,\mathrm{Hz}$ obtaining the correlation functions of the thermal state at $T = 40\,\mathrm{nK}$. Using the phase-phase correlation functions at different times we have resampled the profiles. After referencing the profiles the resampled phase-phase correlation functions were obtained. We then perform a recovery at the times indicated in Supplementary Figure 4 which shows that finite sample size of about 200 experimental runs for each time constrains the possibility of recovering the phase locking in its full extent.

F. Influence of finite measurement resolution

The measured phase fluctuations at a given pixel are in fact a convolution which spreads into the neighboring pixels too. Its primary effect is introducing a frequency cutoff, as the higher modes oscillate quickly and are averaged out. The secondary

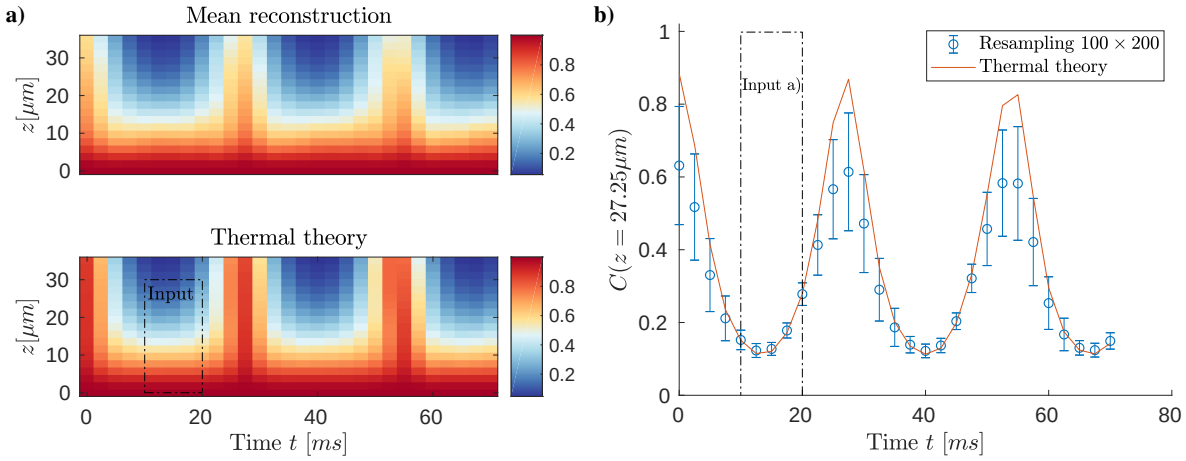

Supplementary Figure 4. We present the results of 100 reconstructions obtained based on 200 phase profiles sampled from the thermal state of the state preparation Hamiltonian with a phase coupling $J/\hbar = 2\pi \times 3.5\,\mathrm{Hz}$ and $T = 40\,\mathrm{nK}$. **a)** We show the averaged correlator C as was done in the main text (the input window corresponds to the input region a) in Fig. 3 in the main text). We find that the height of the reconstructed revivals based on estimators with sample size $n_{\mathrm{Sample}} = 200$ is significantly lower than for the exact correlations obtained as an ensemble average from the thermal state. **b)** We present a cut at $z = 27.25\,\mu\mathrm{m}$ for the thermal state (in red) and the reconstructions from the resampled data (blue points) where the error-bars indicate the standard deviation of the 100 reconstructions. This uncertainty analysis shows than based on a single sample of $n_{\mathrm{Sample}} = 200$ profiles available experimentally the heights of the reconstructed revivals may fluctuate strongly. The large standard deviation for points at the revival indicate that both large and small revival heights can be obtained depending on random fluctuations of the sampled phase profiles.

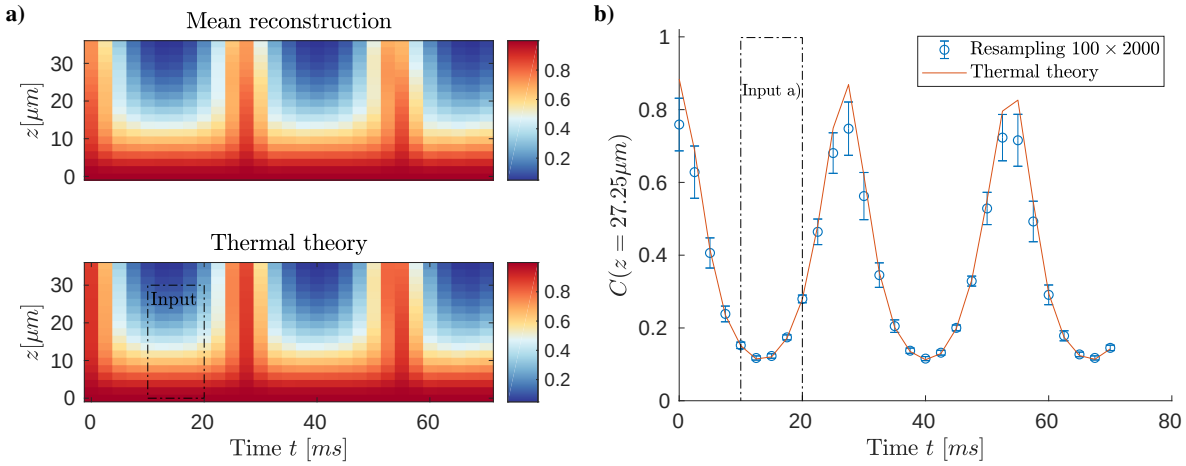

Supplementary Figure 5. A simulation of the reconstruction as above with increased sample size $n_{\mathrm{Sample}} = 2000$ for which the estimators of the two-point correlation functions based on the sampled phase profiles should be close to the true values. We find that our method can very reliably reconstruct the state **a)**, including revival heights **b)** with error bars indicating standard deviation of 100 realizations, and hence identify the finite sample size in the experiment $n_{\mathrm{Sample}} = 200$ as the main source of inaccuracy of our reconstructions.

effect is introducing non-universal additional artifacts into the correlations that come from the convolution and are a feature of the measurement setup. We consider the thermal real-space covariance matrix. It is diagonal in the eigenmodes of the initial strongly coupled Hamiltonian, see Supplementary Figure 6a. The convolution introduces however new correlations that are not present in the state and are an artifact of the coarse-graining, Supplementary Figure 6b. If we consider the post-quench Hamiltonian, the modes change slightly due to the non-homegenous GP profile and the covariance matrix is slightly off-diagonal in these modes Supplementary Figure 6c. After the convolution again a cut-off is introduced, but also additional stray artifacts, Supplementary Figure 6d.

Thus, the convolution will introduce in an uncontrolled way additional artifacts at different times and hence the measured real-space second moments of phases will have a discrepancy incorporated by the finite measurement resolution. This explains why in the data analysis, and the resampling simulation above, a perfect reconstruction is impossible. We conclude that the

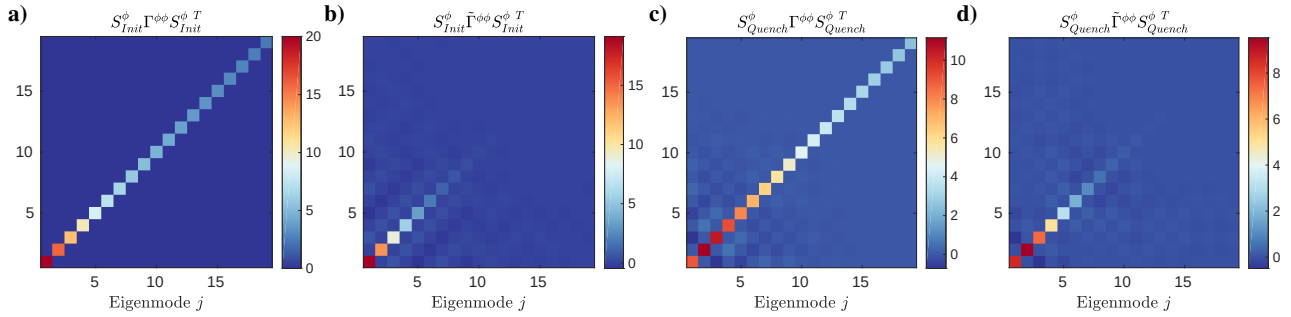

Supplementary Figure 6. Real space correlations after rotating into the eigenmode space. **a)** We plot the rotation of the real space covariance matrix $\Gamma^{\phi\phi}_{j,k} = \langle\hat{\varphi}(z_j)\hat{\varphi}(z_k)\rangle$ defined at discretization pixels rotated into the eigenmode space S^{ϕ}_{Init} of the initial Hamiltonian. On all plots we show the lowest-lying eigenmodes and do not show the zero-energy mode considering only the eigenmodes relevant in the experiment. **b)** We plot the Gaussian convolution of $\Gamma^{\phi\phi}$ denoted by $\tilde{\Gamma}^{\phi\phi}$ which takes into account the finite measurement resolution in the eigenmode space of the initial Hamiltonian. Observe, that in both cases we obtain diagonal matrices, but the convolution introduces a cut-off for resolving the occupation of the higher modes. **c-d)** We show the same comparison of $\Gamma^{\phi\phi}$ and $\tilde{\Gamma}^{\phi\phi}$ but now rotated with the eigenmodes $S^{\phi}_{\mathrm{Quench}}$ of the quench Hamiltonian. Observe, that the eigenmode occupations are rearranged due to a different mode transformation ($n_{\mathrm{GP}} \neq \mathtt{const}$) and minor coherences are introduced by the convolution.

sample size is a smaller limitation than the finite experimental resolution.

SUPPLEMENTARY NOTE 4: EXTENDED DATA

Here we give further results on additional experimental scans that were performed in the study of revivals in Ref. [1]. In total we consider 5 systems (one of them already presented in the main text) with varying system size and particle number — the corresponding values are listed in Supplementary Table I.

Scan	System size $L = 2R_{1\mathrm{D}}$	Average particle number per well $N^{\mathrm{Avg}}_{\mathrm{Well}}$
1	49 µm	3147.5
2	60 µm	3813.6
3	38 µm	2293.5
4	43 µm	2625.7
5	54 µm	3513.3

Supplementary Table I. Table of the experimental scans performed characterized by the system size specified via the external trap and the average particle number per well. The fluctuations of the particle number is about $\delta N^{\mathrm{Avg}}_{\mathrm{Well}} \approx 50$ independent of the system size. These two parameters together with the harmonic longitudinal $\omega_l = 2\pi \times 7\,\mathrm{Hz}$ and radial $\omega_\perp = 2\pi \times 1400\,\mathrm{Hz}$ trapping frequencies allows to calculate the Gross-Pitaevskii profile n_{GP} and hence parametrize the effective model. The first scan is the one presented in the main text.

In Supplementary Figure 7 we show the reconstructed covariance matrices of the initial state as described in the main text for all 5 experimental scans listed in Supplementary Table I. Consistently with the result presented in the main text, we find that the reconstructed covariance matrices are close to being diagonal with significant squeezing suppressing phase fluctuations and enhancing density fluctuations. Furthermore, in Supplementary Figure 8 we show the covariance matrix obtained for the first scan considering wave functions convoluted with a Gaussian distribution (28). Here we find similar $V_{j,k}$ to the covariance matrix shown in the main text for low lying modes but it is noticeable that the higher modes are populated with no clear decay tendency. This can be explained by overfitting noise as the convolution of wave functions for large k vanishes $f^{\phi}_{k}(z) \approx 0$. Indeed, examining (31) we find that the optimizer is not sensitive to changes of $V_{j,k}$ with j, k above the effective cut-off, or in other words the least squares recovery becomes numerically ill-conditioned. We did not observe any significant improvement in quantitatively predicting the revivals using convoluted modes.

Secondly, we investigate in Supplementary Figures 9 and 10 the correlator C defined in the main text based on data obtained in scans 2 to 5. We show the values extracted from the experimental measurement as well as the results obtained from three reconstructions with different input intervals. The results are consistent with the ones presented and discussed in the main text. The experimental data shows a slow dephasing and weakening of the initial phase locking. The reconstructions are able to recover and predict the signal well if the reconstruction interval includes a recurrence. Reconstructions from dephased data (reconstruction regions a) and c)) are able to qualitatively describe the system but fail to predict quantitatively for instance the strength of the recurrence.

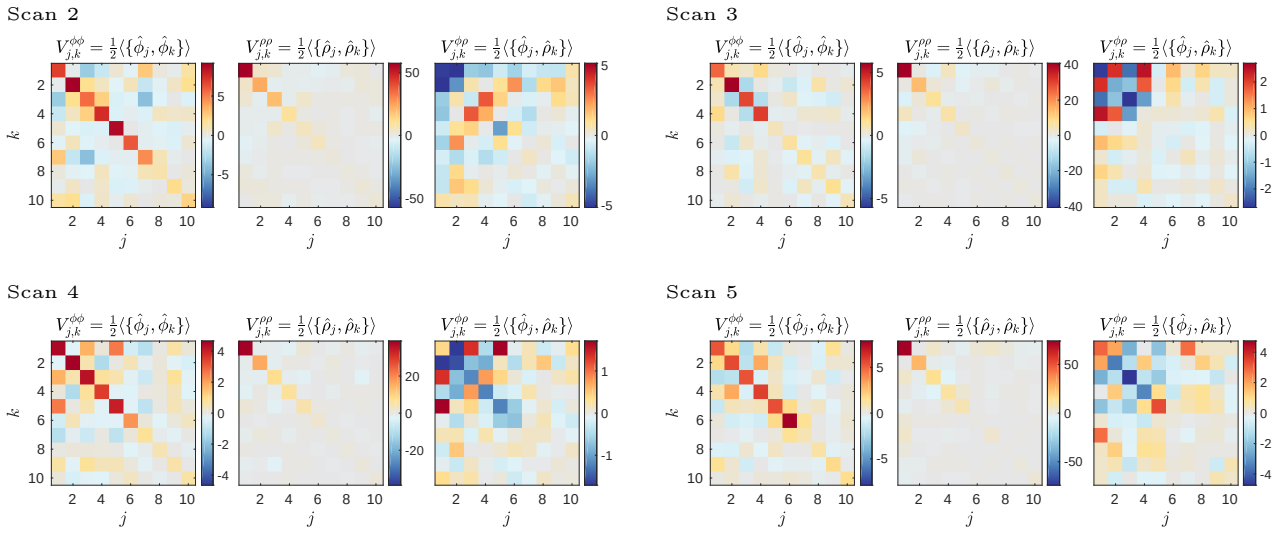

Supplementary Figure 7. We show as in Fig. 2 in the main text the blocks of the covariance matrix of the initial state reconstructed with $\mathcal{N} = 10$ modes for all experimental scans. The system sizes and particle number per well are as given in Table I.

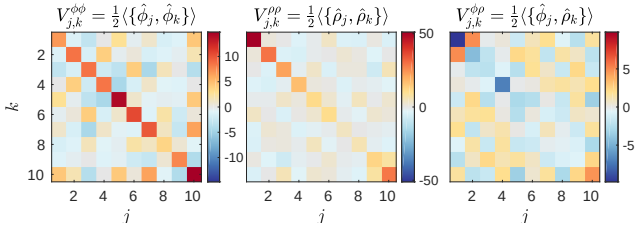

Supplementary Figure 8. We show as above the reconstructed covariance matrix of the initial state of the first scan, but now using convoluted eigenfunctions. As modes with increasing energy display more and more oscillations, the convoluted modes with higher energy become smaller in amplitude once the convolution starts to average over a full oscillation. This renders the least squares less stable and higher modes can have large occupation numbers without changing the real-space correlations because the mode functions are suppressed by the convolution.

Scan 2 Scan 3

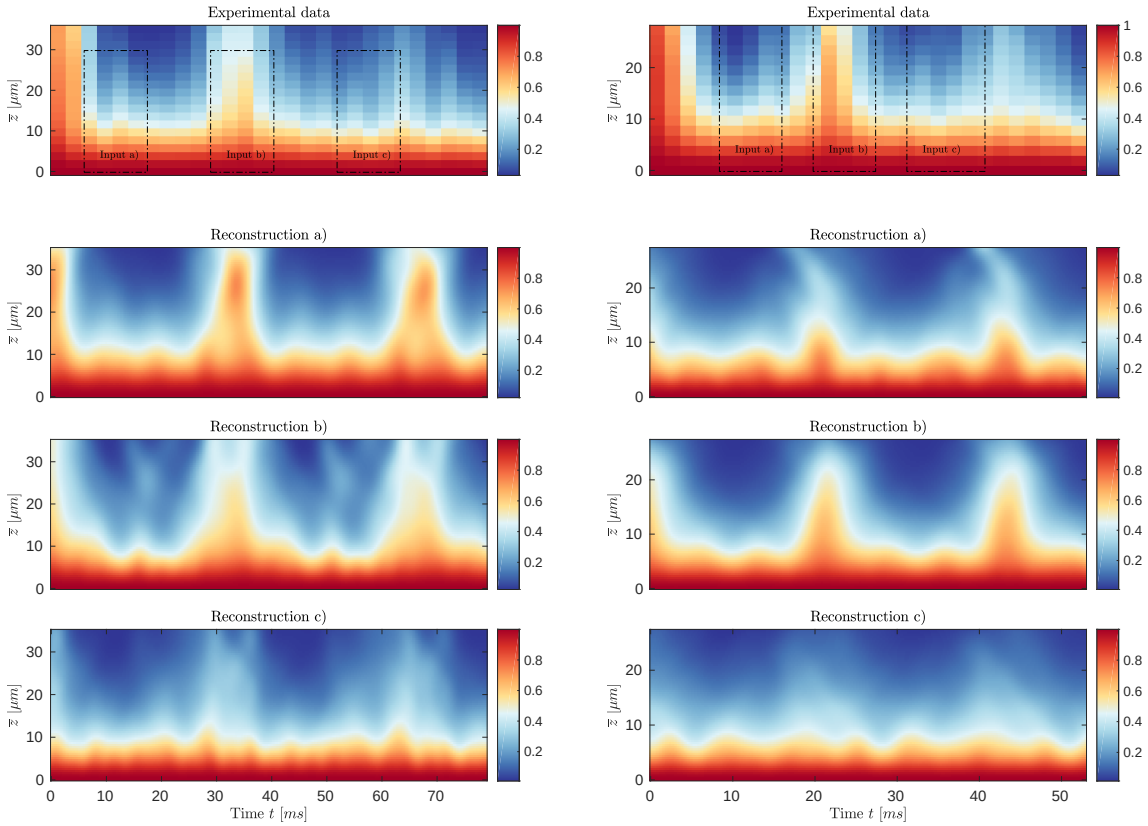

Supplementary Figure 9. Analogous to Fig. 3 from the main text, we show the correlator C calculated from the experimental data and based on three reconstructions with varying input windows (indicated with dashed boxes) for scan number 2 of the largest system size and number 3 of the smallest system size. For the scan number 2 we have moved input window a) to an earlier time which results in very accurate reconstruction of the revival which would not be the case after moving the input window to a later time by one unit Δt. Note, however, that the extrapolation works well which indicates that our method given enough input can yield very good results even with relatively small values of the dynamical phase. For the scan number 3 we can reconstruct reliably in the regions between the revivals. Note that in both cases input window c) does not yield strong reconstructed revivals but they are timed well and also in the experimental data the second revivals are not pronounced.

Scan 4

Scan 5

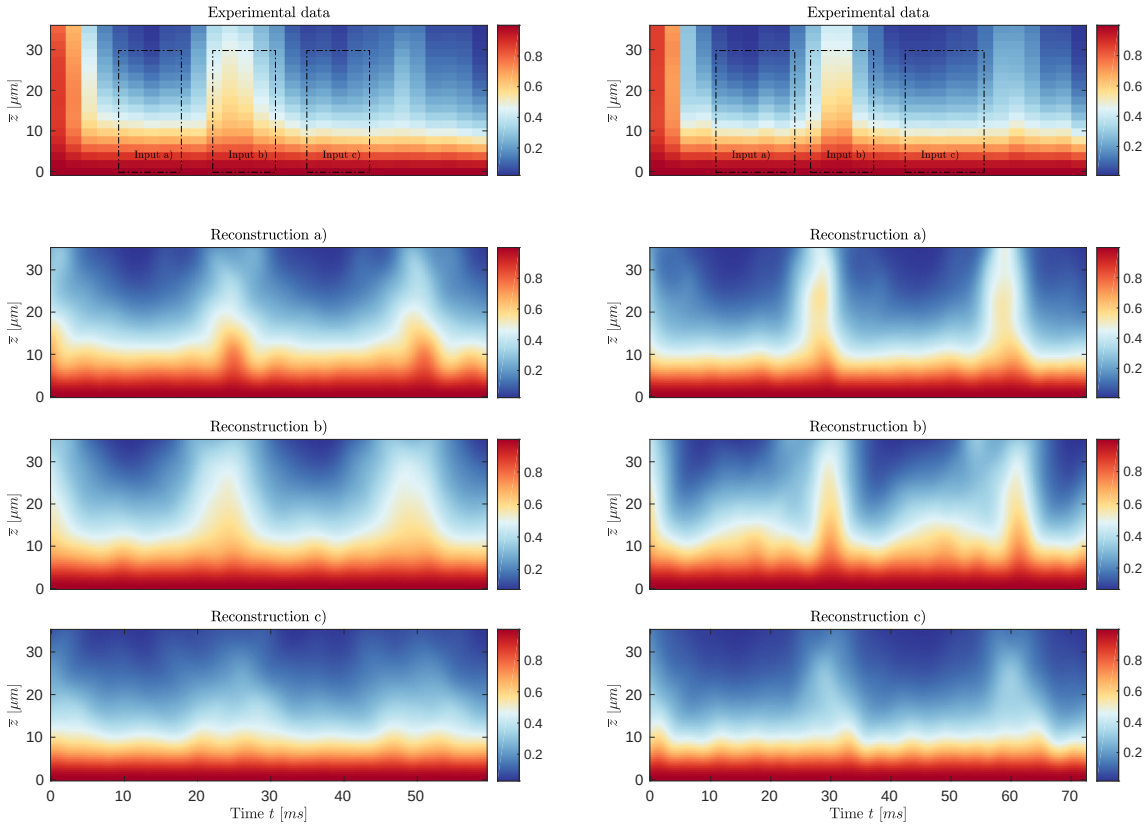

Supplementary Figure 10. As above for scan number 4 with second largest system size and number 5 with second smallest system size.

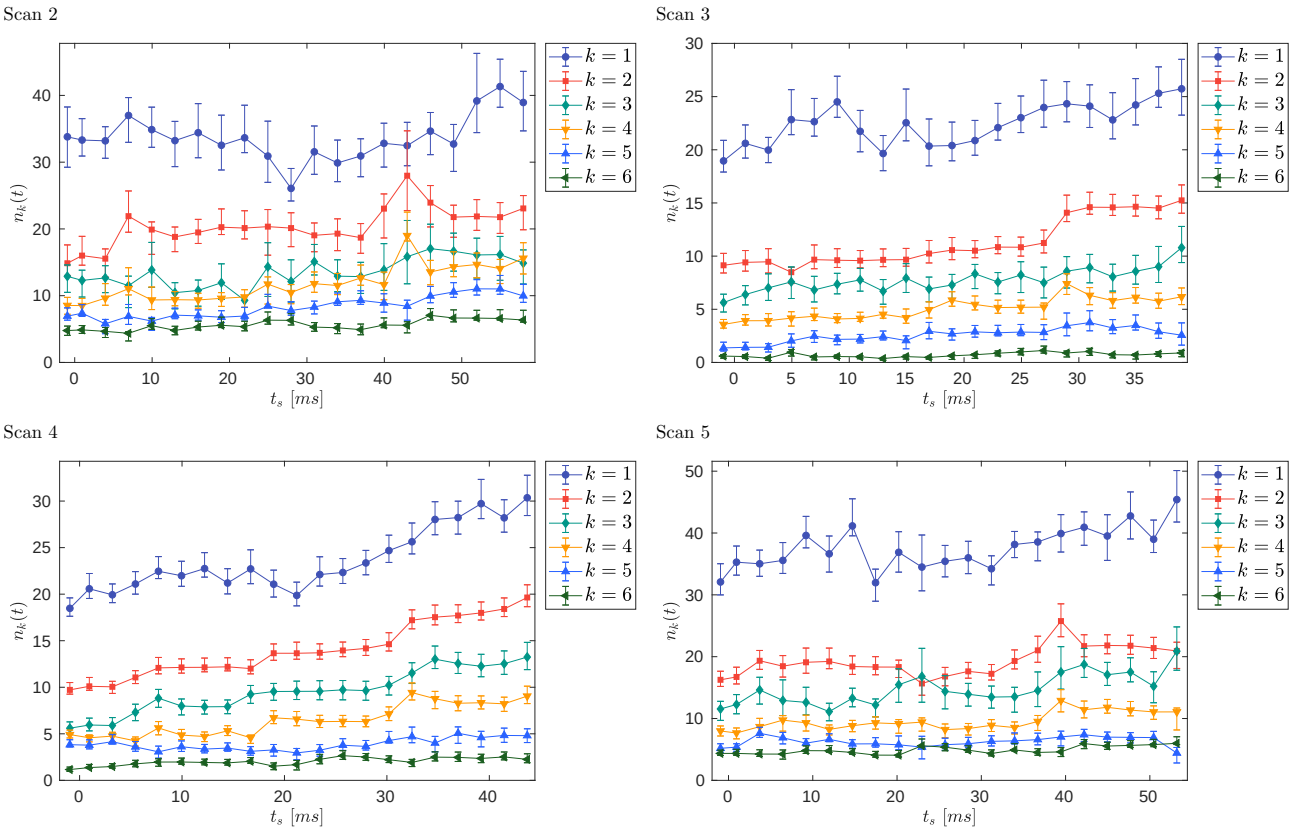

Supplementary Figure 11. Analogous to Fig. 4 in the main text we plot the occupation numbers for scans number 2-5 with parameters given in Table I and bootstrap error-bars by resampling the phase profiles $n_{\text{Bootstrap}} = 500$ times. Note that the fluctuations of the reconstructed occupation of the first modes increase with increasing system sizes which shows that it is important that all the modes acquire enough dynamical phase. Note that often the jumps in the occupation numbers coincide with the input intervals being placed in regions between the revivals where the reconstruction is difficult because of enhanced phase fluctuations due to the in-rotated density fluctuations. We have checked that taking a larger number of input times I does smoothen the occupation numbers but then the size of the input window is large enough so that interaction effects may start playing a role and the value of the occupation numbers need not be accurate.

SUPPLEMENTARY REFERENCES

[1] Rauer, B., Erne, S., Schweigler, T., Cataldini, F., Tajik, M. & Schmiedmayer, J. Recurrences in an isolated quantum many-body system. *Science* **360**, 307 (2018).

[2] Salasnich, L., Parola, A. & Reatto, L. Effective wave equations for the dynamics of cigar-shaped and disk-shaped bose condensates. *Phys. Rev. A* **65**, 043614 (2002).

[3] Weedbrook, C., Pirandola, S., Garcia-Patron, R., Cerf, N. J., Ralph, T. C., Shapiro, J. H. & Lloyd, S. Gaussian quantum information. *Rev. Mod. Phys.* **84**, 621 (2012).

[4] Eisert, J. & Plenio, M. B. Introduction to the basics of entanglement theory in continuous-variable systems. *Int. J. Quant. Inf.* **1**, 479 (2003).

[5] Schweigler, T., Kasper, V., Erne, S., Mazets, I., Rauer, B., Cataldini, F., Langen, T., Gasenzer, T., Berges, J. & Schmiedmayer, J. Experimental characterization of a quantum many-body system via higher-order correlations. *Nature* **545**, 323 (2017).

[6] van Nieuwkerk, Y. D., Schmiedmayer, J. & Essler, F. H. L. Projective phase measurements in one-dimensional bose gases. *arXiv:1806.02626* (2018).

[7] Kalev, A., Kosut, R. L. & Deutsch, I. H. Quantum tomography protocols with positivity are compressed sensing protocols. *njp Quant. Inf.* **1**, 15018 (2015).

[8] Gross, D., Liu, Y.-K., Flammia, S. T., Becker, S. & Eisert, J. Quantum state tomography via compressed sensing. *Phys. Rev. Lett.* **105**, 150401 (2010).

[9] Audenaert, K. M. R., Eisert, J., Plenio, M. B. & Werner, R. F. Entanglement properties of the harmonic chain. *Phys. Rev. A* **66**, 042327 (2002).
[10] Banchi, L., Braunstein, S. L. & Pirandola, S. Quantum fidelity for arbitrary Gaussian states. *Phys. Rev. Lett.* **115**, 260501 (2015).
[11] Zinn-Justin, J. *Quantum field theory and critical phenomena* (Clarendon Press, 1996).

5

FIDELITY WITNESSES FOR FERMIONIC QUANTUM SIMULATIONS

New developments in quantum technologies are being reported at a very fast rate and coherent quantum systems of an increasing number of constituents are becoming available. This experimental advance, however, is bringing about a new theoretical challenge, namely if quantum coherence is extending over many qubits then to describe their state we need an enormous amount of parameters. Nevertheless, while developing large systems with pronounced quantum effects we are in need of methods allowing us to check which state is realized in an experiment and this necessitates new ideas and approaches to circumvent the curse of dimensionality of quantum states.

For a small system the method of choice is full quantum state tomography. This is in practice limited to about a dozen qubits due to the large Hilbert space dimension and number of independent observables that must be measured. Due to this problem post-tomographic tools are being developed. The gold standard of such approaches is randomized benchmarking which allows to do diagnostics of the experimental state on the level of certain non-trivial observables such as entanglement entropies [120]. In certain cases direct fidelity estimation [152] is essentially optimal, allowing to for example assess the preparation of certain entangled states with the number of measurements independent of the number of qubits. One other very promising advance is the development of the so-called matrix-product state tomography [153]. Here the idea is that a certain family of variational wave-functions requiring a polynomial number of parameters is very well-suited to capturing low-energy states of gapped one-dimensional systems. In Ref. [153] based on experimental measurements a matrix-product state was reconstructed allowing to capture larger systems than can be tackled by means of standard tomography. This development suggests that devising *variational* tomographic methods is the way forward to treat coherent many-body systems.

This chapter presents a method answering the question of how to assess the preparation of weakly interacting fermions that may be very entangled obstructing a matrix-product state tomography approach. Such states could appear in future quantum simulation studies of superconductivity involving the formation of Cooper pairs and the presented method would apply for these variational states.

5.1 FORMULATION OF THE PROBLEM

Let $|\psi_t\rangle \in \mathcal{H}$ be a pure target state vector that we would like to prepare and let us denote by $\hat{\rho}_p$ the state that the, possibly imperfect, experimental procedure prepares in the laboratory. We would like to verify that the preparation has high fidelity without resorting to full state tomography which is inefficient in the number of constituents.

Specifically, the task is to *certify* that the fidelity between the uncharacterized preparation state and the target state vector

$$F = \langle\psi_t|\,\hat{\rho}_p\,|\psi_t\rangle$$

is larger than the objective quantified by some threshold value F_{th}. Moreover, we ask for an *efficient* way of verifying that $F > F_{th}$ using polynomially many state preparations even though the Hilbert space dimension grows exponentially fast with the number of qubits. Passing this test implies that the experimental preparation is closer to the target than some ϵ_{th} which depends on F_{th} only.

As a remark, let us point out that in principle a similar certification task could be defined for a mixed target state $\hat{\rho}_t$ in which case the fidelity reads

$$F = \mathrm{tr}\left[(\sqrt{\hat{\rho}_t}\,\hat{\rho}_p^\dagger\,\sqrt{\hat{\rho}_t})^{1/2}\right]^2$$

and again if it exceeds a threshold value, it bounds the single-shot distinguishability between the target and preparation states at a desired accuracy. However, as will be alluded to in the open problems section, devising efficient certification protocols is more challenging - this will become apparent by the discussion of our results in the next section demonstrating in an intuitive way that the purity of the target state is crucially helpful.

5.2 OUR RESULTS

In our studies, we arrived at two ideas offering a way to make progress. Firstly, which will be subject of the next subsection, we conceptualize the possible approaches to the certification task by means of the notion of fidelity witnesses. Secondly, we apply it in the case of non-equilibrium dynamics for the transverse field Ising model which is the standard test-bed model used to benchmark state-of-the-art quantum simulators.

5.2.1 *Fidelity witnesses*

Paralleling the developments that appeared in effort to study entanglement in experiments by means of entanglement witnesses [154] we propose to consider experimentally friendly observables that allow to draw conclusions about the fidelity of a certain state.

Definition 3 (Fidelity witnesses). *An observable $\hat{\mathcal{W}}$ is a* fidelity witness *for $\hat{\rho}_t$ if, for $\mathsf{F}_{\mathcal{W}}(\hat{\rho}_p) \coloneqq \mathrm{tr}[\hat{\mathcal{W}}\,\hat{\rho}_p]$, it holds that*

i) $\mathsf{F}_{\mathcal{W}}(\hat{\rho}_p) = 1$ *if, and only if,* $\hat{\rho}_p = \hat{\rho}_t$, *and*
ii) $\mathsf{F}_{\mathcal{W}}(\hat{\rho}_p) \leqslant \mathsf{F}$ *for all states* $\hat{\rho}_p$.

The term ''witness'' refers to the property that, for any fixed threshold F_T, finding $\mathsf{F}_{\mathcal{W}}(\hat{\rho}_p) \geqslant \mathsf{F}_T$ witnesses that $\mathsf{F} \geqslant \mathsf{F}_T$; but if $\mathsf{F}_{\mathcal{W}}(\hat{\rho}_p) < \mathsf{F}_T$ is found, then nothing can be said about F in relation to the threshold value F_T. As illustrated in Fig. 5.1, fidelity witnesses explicitly realise the extremality-based intuition of ''corralling valid states against the boundary''. The situation is reminiscent of entanglement witnesses, which detect some entangled states and discard all non-entangled ones. Specific fidelity witnesses have been built for ground states of local Hamiltonians [153, 155] and Gaussian as well as non-Gaussian output states of bosonic linear-optical circuits [156]. In the supplementary material of the presented paper we present (possibly non-efficient) fidelity witnesses of arbitrary target states with no assumption other than being pure. A special case of such generic construction is the following (efficient) witnesses for the free-fermionic setting.

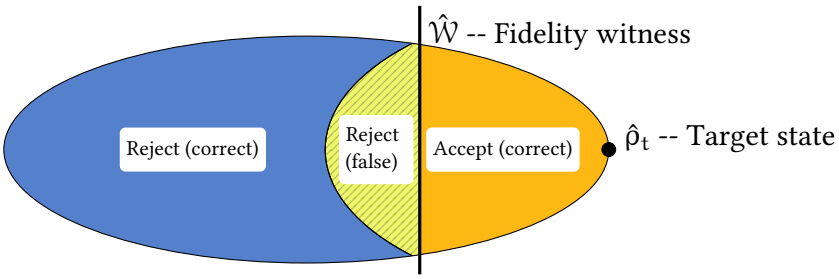

Figure 5.1: **Certifying the membership to the set of high-fidelity preparations.** The set of quantum states is convex and pure states lie on its boundary. Observables act as hyperplanes slicing this set and they separate the states into two classes which are those giving rise to expectation value seither smaller or larger than a prescribed value. A well chosen observable can be used to select a particular target state which is singled out by giving rise to an extremal expectation value of that observable. In the illustration, the citrus-colored areas depict the states that have a sufficiently high fidelity to the target state $\hat{\rho}_t$. Some of these states will be detected by a fidelity witness $\hat{\mathcal{W}}$ but some will be falsely rejected, i.e., the witness may fail to certify that a state preparation has high fidelity. States having very low fidelity depicted by the blue-colored area will be always rejected and hence the fidelity witness test will never lead to a false claim that the fidelity is high when it is not.

5.2.2 *Experimentally relevant fidelity witnesses*

For pure fermionic Gaussian states we have a simple formula to evaluate the fidelity witness but it is necessary to first introduce some essential definitions and notation. It is valid for the most general family of fermionic Gaussian states which includes not only so-called Slater determinants but also entangled BCS states. This family is sometimes referred to as generalized Gaussian or generalized Hartree-Fock states but using the formulation of the problem

using Majorana operators, as is done in the presented paper, it appears to be natural to simply call them Gaussian states.

The crucial insight that we obtained is a generalization of an ubiquitous observation, namely, that the second moments of Majorana operators (defined in detail in the presented paper) specify completely Gaussian states. For example, higher order correlation functions can be obtained from the covariance matrix using the Wick's expansion. In general to determine whether a given state is Gaussian one would have to verify that all of the exponentially many correlation functions satisfy Wick's theorem. Nevertheless, for pure Gaussian states, it turns out to be sufficient to find that their second moments are in fact very special and single out the entire state uniquely. This, in turn, implies the following efficiently measurable value of the fidelity witness

$$F_{\mathcal{W}}(\hat{\rho}_p) = 1 + \frac{1}{4}\,\mathrm{tr}\Big[\big(\mathbf{M}(\hat{\rho}_p) - \mathbf{M}(\hat{\rho}_t)\big)^t \mathbf{M}(\hat{\rho}_t)\Big]\,, \tag{5.2.1}$$

where the covariance matrix $\mathbf{M}(\hat{\rho}_p)$ of the preparation state has to be measured experimentally by estimating polynomially many expectation values of relatively simple physical observables and the covariance matrix $\mathbf{M}(\rho_t)$ of the target state can be assumed to be known as the specification of the target state.

This result is relevant to benchmarking of spin-1/2 chains realized by means of quantum simulation using qubits. Let us denote by X_i, Y_i, and Z_i the Pauli matrices acting at site i of a spin chain. The following Hamiltonian describes the experimentally-relevant spin chain model [157--161]

$$\hat{H}_{\mathrm{TFIM}} = -\sum_{j=1}^{L-1} (J_j^x\, X_j\, X_{j+1} + J_j^y\, Y_j\, Y_{j+1}) - \sum_{j=1}^{L} B_j\, Z_j\,.$$

Here J_j^x, J_j^y and B_j are respectively qubit interactions and transverse-field strengths and L is the length of the spin chain. If we set $J^y \equiv 0$ and other couplings to be independent of position then we obtain the transverse field Ising model. If all couplings are non-zero and position independent then we call the model the XY model. This Hamiltonian can be diagonalized using the Jordan-Wigner transformation which allows to map the one-dimensional interacting spin system to non-interacting fermions. In the case that the couplings depend on position, then we say the model represents a disordered spin chain which then typically gives rise to Anderson localization. Since all these models map to a quadratic Hamiltonian for all parameter regimes, we can efficiently certify quantum simulations of adiabatic ground state preparations or non-equilibrium dynamics following sudden quenches.

5.3 THE IMPLICATIONS OF THE RESULTS

The main merit of the conceptual part of our results is that it unifies other existing ideas for verifying quantum simulations by means of the notion of witnessing the fidelity. This makes touch with the earlier long-standing programme of witnessing entanglement. Viewing both cases in hindsight of the conceptual innovation of introducing the approach of witnesses we find a general feature namely that often in quantum technologies we have some desired quantum objective that has a simple physical meaning and yet it is hard to verify the membership to the class of successful preparations. For entanglement, we would like to establish interesting and resourceful correlations which then can be used to implement powerful protocols. However, in general this is hopeless according to our current knowledge of complexity theory as it has been proven that deciding whether a bipartite quantum state is entangled is an NP-hard task [162]. Nevertheless, with use of entanglement witnesses we can successfully verify the entanglement in simple cases.

Entanglement witnesses have the feature that if the target type of entanglement to be verified is in a specific way simple, e.g., Gaussian, then it can be detected efficiently in the number of modes (the promise of a Gaussian state promotes a general witness to a proper test [163]). Fidelity witnesses exhibit similar features. Indeed, fidelity is inherently difficult to measure, which can be concluded even without natural hardness results but merely by physical intuition that small local imperfections could be amplified by measuring an appropriate global observable The discussion in the supplementary material of the presented paper constructs such an example using a state representing a system with weak symmetry-breaking. This simple observation is further substantiated by the effect known in quantum many-body physics called the 'orthogonality catastrophe' which posits that generic eigenstates of large systems are very sensitive and a slightly perturbed state can easily become orthogonal to an unperturbed state [164--166]. However, fidelity between two pure states measures precisely this overlap and may hence be susceptible to suffering from the orthogonality catastrophe.

Despite these issues, thanks to continued experimental efforts, quantum technologies are becoming increasingly better and it becomes necessary to benchmark systems that are beyond reach of full state tomography. Fidelity witnesses offer an attractive answer for performing pragmatic tests verifying coherence of the emerging and continuously improving quantum simulation platforms. This framework includes the previously known methods and ideas, most prominent of which are based on measuring a small expectation value of an appropriate Hamilton operator which selects the target state uniquely. This special Hamiltonian is typically referred to as parent and gives rise to a fidelity witness.

The specific results concerning Gaussian states give rise to an excellent witness applicable to a range of quantum simulation experiments. This can be directly applied in platforms such as trapped ions, Rydberg arrays, and superconducting qubits. For all these systems interesting non-equilibrium dynamics for dozens of qubits have been reported and our method gives a directly applicable way of measuring the overlap to certain, possible time-dependent, fermionic Gaussian states. The measurements necessary are available in these quantum simulators as they are the same as observables measured in quantum state tomography but their number is significantly smaller. One example, for the possible application is the study performed using the Sycamore quantum processor where fidelity witnesses have been employed to study the preparation of Gaussian studies with the aim of reaching the accuracy necessary for non-trivial computations for quantum chemistry [121].

Notice, that our fermionic Gaussian fidelity witnesses could in principle be also used when the quantum simulator dynamics deviates from Gaussianity. An interesting question to study is how the fidelity towards Gaussian states decays during dynamics influenced by the presence of weak interactions. Even small perturbations to unitary dynamics under quadratic Hamiltonians give generically rise to universal gate sets and we do not know when weak interactions lead to evolutions corresponding to truly BQP-hard instances of unitary dynamics, i.e., circuits that allow to simulate quantum computers. On the other hand, it is still the hope that a quantum analogue of the classical KAM theorem holds [167] hence one would like to expect, on physical grounds, that very weak perturbations lead to dynamics that are close enough to Gaussianity to the extent that the system can still be classically simulable. Currently, the only way to study this question rigorously is essentially via time-dependent perturbation theory which only allows to treat interaction potentials that vanish in the thermodynamic limit. It would be interesting to see if fidelity witnesses could be used in a quantum simulator to show that overlaps to Gaussian states under weakly non-Gaussian dynamics are more persistent than perturbative arguments suggest.

Finally, let us discuss how the formula implies that non-Gaussian states have non-zero Gaussian entropy which is an application independent of the original goal of certifying quantum simulations. The formula (5.2.1) gives the value of a fidelity witness with a pure Gaussian target state and is based exclusively on second moments. Pure Gaussian states have covariance matrices that are orthogonal, i.e., satisfy $\mathbf{M}\mathbf{M}^t = \mathrm{id}$ [168]. Formula (5.2.1) implies the converse, namely, that if a state $\hat{\rho}_p$ has an orthogonal covariance matrix $\mathbf{M}$ then it must be Gaussian. Indeed there exists a pure Gaussian state $|\psi_t\rangle$ with the same second moments as $\hat{\rho}_p$ and by Eq. (5.2.1) we find that the fidelity between $\hat{\rho}_p$ and $|\psi_t\rangle$ has the maximum value and so these two states must be the same. We hence find that non-Gaussian states must have covariance matrices corresponding to mixed Gaussian states.

5.4 OPEN PROBLEMS

Problem 1. Parent Hamiltonians have been used as fidelity witnesses before we defined this notion and the constructions given in the presented paper can in principle also be rephrased in this way. Are parent Hamiltonians the *only* fidelity witnesses?

Problem 2. Do there exist non-trivial fidelity witnesses for *mixed* target states?

Problem 3. What is the precise worst-case computational hardness of estimating the fidelity of a quantum state?

Problem 4. Is it possible to design conditional witnesses, i.e., observables that witness fidelity only given a promise of some physical property, which give tighter bounds than the unconditional witnesses?

Problem 5. Consider a target state which is uniquely selected as the ground state of a gapped local Hamiltonian. Can we construct a practical fidelity witness out of this information without knowing the ground state energy and the spectral gap? Computing the former is QMA-hard while the latter is undecidable but known constructions that work for other computationally hard problems rely on apriori knowledge of these parameters [155].

Fidelity Witnesses for Fermionic Quantum Simulations

M. Gluza,[1] M. Kliesch,[2,3] J. Eisert,[1] and L. Aolita[4,5,6]
[1]*Dahlem Center for Complex Quantum Systems, Freie Universität Berlin, Germany*
[2]*Institute of Theoretical Physics and Astrophysics, University of Gdańsk, Poland*
[3]*Institute for Theoretical Physics, Heinrich Heine University Düsseldorf, 40225 Düsseldorf, Germany*
[4]*Instituto de Física, Universidade Federal do Rio de Janeiro, P.O. Box 68528, Rio de Janeiro, Rio de Janeiro 21941-972, Brazil*
[5]*International Institute of Physics, Federal University of Rio Grande do Norte, 59070-405 Natal, Brazil*
[6]*ICTP South American Institute for Fundamental Research, Instituto de Física Teórica, UNESP-Universidade Estadual Paulista R. Dr. Bento T. Ferraz 271, Bl. II, São Paulo 01140-070, São Paulo, Brazil*

(Received 26 May 2017; published 11 May 2018)

The experimental interest and developments in quantum spin-1/2 chains has increased uninterruptedly over the past decade. In many instances, the target quantum simulation belongs to the broader class of noninteracting fermionic models, constituting an important benchmark. In spite of this class being analytically efficiently tractable, no direct certification tool has yet been reported for it. In fact, in experiments, certification has almost exclusively relied on notions of quantum state tomography scaling very unfavorably with the system size. Here, we develop experimentally friendly fidelity witnesses for all pure fermionic Gaussian target states. Their expectation value yields a tight lower bound to the fidelity and can be measured efficiently. We derive witnesses in full generality in the Majorana-fermion representation and apply them to experimentally relevant spin-1/2 chains. Among others, we show how to efficiently certify strongly out-of-equilibrium dynamics in critical Ising chains. At the heart of the measurement scheme is a variant of importance sampling specially tailored to overlaps between covariance matrices. The method is shown to be robust against finite experimental-state infidelities.

DOI: 10.1103/PhysRevLett.120.190501

Quantum simulators are specific-purpose quantum devices that are able to efficiently simulate phenomena of interest thought to be not directly accessible otherwise [1]. Already at scales of tens of particles they have the potential to outperform today's most powerful supercomputers and help us explain unclear physical effects, as well as give boosts in crucial technological areas [2]. In addition, they constitute an intermediate milestone towards the ultimate goal of realizing large-scale universal quantum computers. This has fueled impressive experimental advances in multiple quantum technologies [3–9]. A type of quantum many-body systems to which experimental simulations have devoted considerable efforts over the past decade is given by one-dimensional lattices of interacting spin-1/2 particles, or spin-1/2 chains, for short. In particular, even though they fall into the regime of efficient classical simulatability, the well-known transverse-field (TF) Ising and XY models have become important basic test beds for the most advanced experimental simulations, e.g., with ion-trap [10–13], superconducting-circuit [14], Rydberg-atom [15], and circuit quantum electrodynamics [16] platforms, including digitalized simulations [12,14,16].

At least two facts justify the significant interest in these specific models. The first one is that they display a vast physical richness: For instance, the TF Ising model—which is, actually, a subclass of the TF XY model—features a quantum phase transition [17–20] as well as topologically and spectrally interesting effects [21–25], and is relevant for quantum speed-ups in certain optimization problems [26]. The second one is that, for nearest-neighbor interactions, they can be analytically solved, e.g., by mapping them into systems of free, i.e., noninteracting, fermions [17]. This allows for in-depth theoretical studies of their dynamics [27–32]. From a broader perspective, these models belong to a more general class of exactly solvable systems known as noninteracting quantum systems, also referred to as fermionic linear optics [33–39]. This class is the fermionic counterpart of the Gaussian formalism for bosons [40,41], which plays a major role in quantum information and quantum optics. It includes, e.g., tight-binding models important in condensed-matter physics, certain interacting bosonic chains that can be fermionized [42–44], and spin-1/2 systems in two-dimensional lattices, such as the celebrated Kitaev's honeycomb model [37], which exhibits non-Abelian excitations.

Unfortunately, the exact analytical solution of a model does not imply that one can efficiently *certify* the correctness of an uncharacterized experimental simulation of it. Furthermore, even if the computational complexity of the target simulation is low, the number of measurements required for its certification can be exponentially high in the lattice size without the adequate certification method. This is the case, e.g., for full state tomography (FST). Characterization tools not relying on FST exist [45–54], each

one efficient on a different subclass of simulations. However, none of these can efficiently handle fermionic linear optics. In fact, almost all [10–12,14,16] the abovementioned experiments relied on FST. The simulation of Ref. [13], in contrast, was certified with matrix-product state tomography [48]. This is a powerful method that covers a broad class of chains but tolerates little long-range entanglement, so that nontrivial evolutions are in practice tractable only over short times [13,48]. Indeed, generic spin chains out of the equilibrium [55], or even very natural, static free-fermionic states [56,57], involve large amounts of entanglement along the lattice. Today, a major roadblock for further experimental progress in spin-chain simulations (and in many-body quantum technologies in general) is their certification.

Here, we develop efficient *fidelity witnesses* for all pure fermionic Gaussian target states. These are experimentally friendly observables whose expectation value (on an arbitrary experimental state) yields a tight lower bound to the fidelity with the target. Hence, they allow for *unconditional* certification, i.e., without any *a priori* knowledge of the experimental setup or imperfections. We derive the witnesses in full generality in the Majorana-fermion representation, and then apply them to experimentally relevant spin-1/2 chains as examples. Among others, we show how to efficiently certify any *sudden quench* (i.e., strongly out-of-equilibrium dynamics) in a critical TF Ising chain with nearest-neighbor interactions. The measurement scheme relies on *importance sampling* tailored to overlaps between covariance matrices, which is potentially interesting on its own. As a result, the number of measurements required for the certification only has a modest scaling with the lattice size, i.e., a small *sample complexity*, for which we present upper bounds. Moreover, the method is robust against finite experimental-state infidelities, in the sense of there always existing a closed ball of valid states that are correctly accepted by the certification test. Finally, we provide also a totally general construction, not restricted to fermions or Gaussian states, of (possibly nonefficient) fidelity witnesses for arbitrary pure target states, which may also be useful in other scenarios.

Preliminaries.—Consider a system of L spinless fermionic atoms, from now on referred to as fermionic modes. By $f_j^\dagger$ and f_j we denote the creation and annihilation operators, respectively, where $j = 1, 2, \ldots, L$. They satisfy the canonical anticommutation relations $\{f_j, f_k^\dagger\} = f_j f_k^\dagger + f_k^\dagger f_j = \delta_{j,k}$ and $\{f_j, f_k\} = \{f_j^\dagger, f_k^\dagger\} = 0$, with $\delta_{j,k}$ the Kronecker symbol. Let us next introduce the self-adjoint Majorana mode operators,

$$m_{2j-1} \coloneqq f_j + f_j^\dagger, \qquad m_{2j} \coloneqq -i(f_j - f_j^\dagger), \tag{1}$$

with anticommutation relations $\{m_j, m_k\} = 2\delta_{j,k}$. We say that the fermionic system is free, Gaussian, or linear optical [33–39] if it is governed by a quadratic Hamiltonian,

$$H = \frac{i}{4}\sum_{j,k=1}^{2L} A_{j,k} m_j m_k, \tag{2}$$

where $\boldsymbol{A} = -\boldsymbol{A}^\top \in \mathbb{R}^{2L\times 2L}$ is called the coupling matrix.

The term "free" or "noninteracting" stems from the fact that H is unitarily equivalent to a Hamiltonian of L fermions not featuring any off-diagonal couplings. In the bosonic realm, this is the defining property of Gaussian systems [40,41], which justifies the term Gaussian. In turn, what is linear about fermionic linear optics is the time evolution of the mode operators in the Heisenberg picture,

$$m_j(t) \coloneqq U^\dagger(t) m_j U(t) = \sum_{k=1}^{2L} Q_{j,k}(t) m_k, \tag{3}$$

where $U(t) \coloneqq e^{-iHt}$, for $t \in \mathbb{R}$, is a fermionic Gaussian unitary and $\boldsymbol{Q}(t) \coloneqq e^{t\boldsymbol{A}} \in \mathbb{SO}(2L)$ its representation in mode space [58]; see Appendix A of Supplemental Material for a simple derivation [59].

Finally, it is useful to introduce, for any state ϱ (Gaussian or not), the real antisymmetric covariance matrix $\boldsymbol{M}(\varrho)$ with elements

$$M_{j,k}(\varrho) \coloneqq \frac{i}{2}\mathrm{tr}([m_j, m_k]\varrho). \tag{4}$$

This matrix contains the expectation values of the single-mode densities $\langle n_j\rangle \coloneqq \langle f_j^\dagger f_j\rangle$ as well as the two-mode currents $\langle f_j^\dagger f_k + \mathrm{H.c.}\rangle$ and pairing terms $\langle f_j^\dagger f_k^\dagger + \mathrm{H.c.}\rangle$.

Fidelity witnesses.—We consider throughout a (known) pure target state ϱ_t and an arbitrary, unknown experimental preparation ϱ_p. Their closeness is measured by their *fidelity*,

$$F \coloneqq F(\varrho_t, \varrho_p) \coloneqq \mathrm{tr}[(\sqrt{\varrho_t}\varrho_p^\dagger\sqrt{\varrho_t})^{1/2}]^2 = \mathrm{tr}[\varrho_t\varrho_p], \tag{5}$$

where the last equality holds because ϱ_t is pure. With this, the pivotal notion of our work can be defined as follows.

Definition 1 [Fidelity witnesses].—An observable $\mathcal{W}$ is a fidelity witness for ϱ_t if, for $F_{\mathcal{W}}(\varrho_p) \coloneqq \mathrm{tr}[\mathcal{W}\varrho_p]$, it holds that (i) $F_{\mathcal{W}}(\varrho_p) = 1$ if, and only if, $\varrho_p = \varrho_t$, and (ii) $F_{\mathcal{W}}(\varrho_p) \leq F$ for all states ϱ_p.

The term "witness" refers to the property that, for any fixed threshold F_T, finding $F_{\mathcal{W}}(\varrho_p) \geq F_T$ witnesses that $F \geq F_T$, but if $F_{\mathcal{W}}(\varrho_p) < F_T$ is found, then nothing can be said about F (see Fig. 1). This is the least information about ϱ_p needed to certify its fidelity with ϱ_t. The situation is reminiscent of entanglement witnesses [62], which detect *some* entangled states and discard all nonentangled ones. The difference is that fidelity witnesses explicitly realize the extremality-based intuition of "corralling valid states against the boundary." Specific witnesses have been built for ground states of local Hamiltonians [48,54,63] and

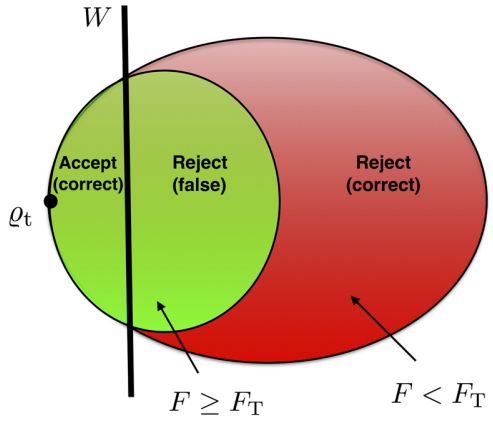

FIG. 1. Geometrical representation of a fidelity witness. A pure target state ϱ_t lies at the boundary of state space. For any fixed fidelity threshold F_T, the valid experimental states are defined by $F \geq F_T$ (green). The states with $F < F_T$ are invalid (red). A fidelity witness $\mathcal{W}$ defines a hyperplane (straight line), to the left of which only valid states are found and to the right of which both valid as well as invalid ones are found. The certification test consists of accepting all states on the left and rejecting all those on the right. Hence, a significant subset of valid states is sacrificed, as in weak-membership problems. However, in return, the experimental estimation is considerably more efficient than in schemes attempting to separate the valid from the invalid states (strong-membership problems).

Gaussian as well as non-Gaussian output states of bosonic linear-optical circuits [52]. In Appendix B of Supplemental Material we present (possibly nonefficient) fidelity witnesses of arbitrary target states with no assumption other than being pure [59]. A special case of such generic construction is the following (efficient) witnesses for the free-fermionic setting.

Any L-mode pure fermionic Gaussian target state ϱ_t can be written as

$$\varrho_t := |\psi_t\rangle\langle\psi_t| \quad \text{with} \quad |\psi_t\rangle := U|\boldsymbol{\omega}\rangle, \tag{6}$$

for a fermionic Gaussian unitary U, as defined below Eq. (3), where $\boldsymbol{\omega} := (\omega_1, \ldots, \omega_L)$ is an L-bit string. The ket $|\boldsymbol{\omega}\rangle$ represents the Fock-basis state vector with $\omega_j \in \{0, 1\}$ excitations in mode j, i.e., $n_j|\boldsymbol{\omega}\rangle = \omega_j|\boldsymbol{\omega}\rangle$, for $j = 1, \ldots, L$, and $n_j := f_j^\dagger f_j$. It is also convenient to introduce $n^{(\boldsymbol{\omega})} := \sum_{j=1}^{L} [(1-\omega_j)n_j + \omega_j(\mathbb{1} - n_j)]$, the total fermion-number operator in the locally flipped basis in which $\boldsymbol{\omega}$ is the null string, i.e., $n^{(\boldsymbol{\omega})}|\boldsymbol{\omega}\rangle = 0$. In other words, $|\psi_t\rangle$ represents the so-called Fermi-sea state and the eigenstates of $n^{(\boldsymbol{\omega})}$ its excitations. In Appendix B [59], we show that the observable

$$\mathcal{W} = U(\mathbb{1} - n^{(\boldsymbol{\omega})})U^\dagger \tag{7}$$

is a fidelity witness for ϱ_t. Expression (7) is the fermionic analogue of the bosonic Gausssian-state witnesses of Ref. [52], with a crucial difference: While for bosons only the Fock-basis state vector $|\mathbf{0}\rangle$ is Gaussian, for fermions all 2^L Fock-basis vectors $|\boldsymbol{\nu}\rangle$ are Gaussian as they satisfy Wick's theorem [36]. In fact, for mixed states, all single-mode states are Gaussian, in sharp contrast to the bosonic case.

Measurement scheme.—Taking the expectation value of Eq. (7) with state ϱ_p yields (see Appendix C [59])

$$F_{\mathcal{W}}(\varrho_p) = 1 + \frac{1}{4}\mathrm{tr}[(\boldsymbol{M}(\varrho_p) - \boldsymbol{M}(\varrho_t))^\top \boldsymbol{M}(\varrho_t)], \tag{8}$$

where $\boldsymbol{M}(\varrho_p)$ and $\boldsymbol{M}(\varrho_t)$ are the covariance matrices of ϱ_t and ϱ_p, respectively. This expression holds also for bosonic Gaussian witnesses [52] and turns out to be very useful for the measurement of $F_{\mathcal{W}}(\varrho_p)$. We call $\Omega := \{(j,k) : M_{j,k}(\varrho_t) \neq 0, \quad \text{for } 1 \leq j < k \leq 2L\}$ the set of nonzero entries of $\boldsymbol{M}(\varrho_t)$. Then Eqs. (4) and (8) imply that if one measures on ϱ_p all $|\Omega| \leq 2L^2 + L$ observables $im_j m_k$ with indices in Ω, then one can estimate $F_{\mathcal{W}}(\varrho_p)$. However, this is not the most efficient procedure (see Appendixes D and E [59]).

A more efficient approach is to exploit importance sampling techniques, where a subset of the $|\Omega|$ observables is randomly selected for measurement according to its importance for $\mathcal{W}$. These techniques have been applied in Hilbert space to the estimation of state overlaps, where they yield efficient schemes only for a specific type of target states [49,50]. Here we apply them in mode space to efficiently estimate overlaps between fully general covariance matrices. The starting point is to identify a random variable X and an importance distribution $P := \{P_\mu\}_\mu$, with X taking the value X_μ with probability P_μ, such that $\mathrm{tr}[\boldsymbol{M}(\varrho_p)^\top \boldsymbol{M}(\varrho_t)]$ is expressed as the mean value of X, i.e.,

$$\mathbb{E}[X] = \sum_\mu P_\mu X_\mu = \mathrm{tr}[\boldsymbol{M}(\varrho_p)^\top \boldsymbol{M}(\varrho_t)]. \tag{9}$$

Then, if one can experimentally sample X from P, $\mathbb{E}[X]$ can be approximated by the finite-sample average $\mathcal{X}^* := \sum_{m=1}^{\mathcal{N}} X_{\mu(m)}/\mathcal{N}$, where $X_{\mu(m)}$ is the value of X at the mth experimental run and $\mathcal{N}$ is the total sample size (number of runs). Next, we present a choice of X and P particularly suited to estimate $F_{\mathcal{W}}(\varrho_p)$.

To this end, let us first define $\hat{m}_{j,k}^{(\beta)}$ as the projector onto the eigenstate of the observable $im_j m_k$ with eigenvalue $\beta = \pm 1$, for $(j,k) \in \Omega$. Then, identifying μ with the triple (β, j, k) and using the short-hand notation

$$|\boldsymbol{M}(\varrho_t)| := \sum_{(j,k)\in\Omega} |M_{j,k}(\varrho_t)| \leq 2L^2, \tag{10}$$

we choose

$$X_{\beta,j,k} := 2|\boldsymbol{M}(\varrho_t)|\beta \mathrm{sgn}[M_{j,k}(\varrho_t)] \tag{11}$$

and

$$P_{\beta,j,k} := \frac{\mathrm{tr}[\hat{m}^{(\beta)}_{j,k}\varrho_p]|M_{j,k}(\varrho_t)|}{|\boldsymbol{M}(\varrho_t)|}. \tag{12}$$

This choice satisfies Eq. (9), as explicitly shown in Appendix D [59]. In the experiment, in turn, for each run one chooses (j,k) according to $P_{j,k} := |M_{j,k}(\varrho_t)|/|\boldsymbol{M}(\varrho_t)|$ and measures im_jm_k on ϱ_p, which outputs β with probability $P_{\beta|j,k} := \mathrm{tr}[\hat{m}^{(\beta)}_{j,k}\varrho_p]$. Substituting the obtained (j,k) and β in Eq. (11), one samples $X_{\beta,j,k}$ with probability $P_{\beta,j,k}$, as desired. As for the experimental accessibility of the observables, for the relevant case of spin-1/2 chains, each im_jm_k corresponds to a product of Pauli matrices, as discussed below.

This single-shot importance sampling approach does not necessarily yield a good estimate of each individual entry of $\boldsymbol{M}(\varrho_p)$, as unlikely observables according to $P_{j,k}$ are measured seldomly. The method is specially tailored to directly obtain $F_{\mathcal{W}}(\varrho_p)$. In fact, the resulting estimate $\mathcal{X}^*$ yields an excellent approximation of $\mathrm{tr}[\boldsymbol{M}(\varrho_p)^\top \boldsymbol{M}(\varrho_t)]$ (in a formal sense given by Theorem 2 below), with which the right-hand side of Eq. (8) can be immediately evaluated. This gives our final finite-sample estimate $F^*_{\mathcal{W}}(\varrho_p)$ of $F_{\mathcal{W}}(\varrho_p)$.

Sample complexity.—Let $\mathcal{N}_{\epsilon,\delta}(\mathcal{W})$ be the minimum number (over all estimation strategies) of single measurements required to estimate $F_{\mathcal{W}}(\varrho_p)$, up to maximal statistical error ϵ and with maximal failure probability δ, i.e., such that

$$\mathbb{P}(|F_{\mathcal{W}}(\varrho_p) - F^*_{\mathcal{W}}(\varrho_p)| \leq \epsilon) \geq 1-\delta, \tag{13}$$

for all ϱ_p. Then the scaling of $\mathcal{N}_{\epsilon,\delta}(\mathcal{W})$ with L is called the sample complexity [51,52,64] of estimating $F_{\mathcal{W}}(\varrho_p)$. In Appendix D we compute the number of single measurements required with the measurement scheme described above [59], which sets the following upper bound on $\mathcal{N}_{\epsilon,\delta}(\mathcal{W})$.

Theorem 2 [Sample complexity of $F_{\mathcal{W}}$].—Let $\epsilon > 0$, $\delta \in (0,1)$, ϱ_t given by Eq. (6), and $\mathcal{W}$ by Eq. (7). Then,

$$\mathcal{N}_{\epsilon,\delta}(\mathcal{W}) \leq \left\lceil \frac{\ln(2/\delta)|\boldsymbol{M}(\varrho_t)|^2}{2\epsilon^2} \right\rceil. \tag{14}$$

Equation (10) implies that the right-hand side of Eq. (14) is never larger than $\lceil 2\ln(2/\delta)L^4/\epsilon^2 \rceil$. The scaling is thus polynomial in L for all ϱ_t, which means that the scheme is efficient in the lattice size. Furthermore, for the physically relevant case of ϱ_t being the unique ground state of a local gapped Hamiltonian, the correlations $\mathrm{tr}([m_j,m_k]\varrho_t)$ decay exponentially with $|j-k|$ [65]. Then, $|\boldsymbol{M}(\varrho_t)| \sim L\log(L)$, which leads to $\mathcal{N}_{\epsilon,\delta}(\mathcal{W}) \leq O(L^2\log^2(L))$.

Finally, in Appendix E, we study also a measurement scheme without importance sampling (where all $|\Omega|$ observables are measured) but exploiting the fact that all commuting observables with indices in Ω can be measured simultaneously in each measurement run [59]. This gives the bound $\mathcal{N}_{\epsilon,\delta}(\mathcal{W}) \leq O(2\ln(2|\Omega|/\delta)L^4/\epsilon^2)$, which, since $|\Omega| \leq 2L^2 + L$, scales logarithmically worse in L than in Eq. (14). We suspect that the bound in Eq. (14) is close to being tight.

Spin-1/2 chains.—We denote a local spin operator acting at site k by $\sigma^\alpha_k = \mathbb{1}_2^{\otimes(k-1)} \otimes \sigma^\alpha \otimes \mathbb{1}_2^{\otimes(L-k)}$, where σ^α for $\alpha = x,y,z$ are the Pauli matrices and $\mathbb{1}_2$ is the single-qubit identity. Via the Jordan-Wigner transformation [66,67]

$$m_{2k-1} = \left(\prod_{j<k}\sigma^z_j\right)\sigma^x_k, \qquad m_{2k} = \left(\prod_{j<k}\sigma^z_j\right)\sigma^y_k, \tag{15}$$

the Hamiltonian in Eq. (2) is equivalent [17] to the experimentally relevant [10–16] spin-1/2 Hamiltonian

$$H_{\mathrm{spin}} = -\sum_{k=1}^{L-1}\left(J^x_k\sigma^x_j\sigma^x_{k+1} + J^y_k\sigma^y_k\sigma^y_{k+1}\right) - \sum_{k=1}^{L}B_k\sigma^z_k, \tag{16}$$

where $J^x_k, J^y_k \in \mathbb{R}$ and $B_k \in \mathbb{R}$ are, respectively, constant coupling and transverse-field strengths. Since these chains are equivalent to free-fermionic systems for all parameter regimes, certifying simulations of, e.g., both adiabatic ground state preparations and sudden quenches amounts to certifying pure fermionic Gaussian states, as described above. Finally, note that Eqs. (15) map each im_jm_k to a product of Pauli matrices, as anticipated in the measurement scheme above.

Sudden quenches in critical Ising chains.—The 1D nearest-neighbor TF Ising Hamiltonian is given by Eq. (16) with $J^x_k = J$, $J^y = 0$, and $B_k = B$, for all $k = 1,\ldots,L$, where $J, B > 0$. In a typical quench, the initial ground state $|\psi(0)\rangle := |\uparrow\rangle^{\otimes L}$ at a noncritical regime $J = 0 < B$, where $|\uparrow\rangle$ is an eigenvector of σ^z, is evolved under the critical regime $J = B$, so as to generate a strong out-of-equilibrium evolution. These quenches are particularly challenging to certify [13,48] because the time-evolved state vector $|\psi(t)\rangle$ rapidly acquires large amounts of entanglement. Let us consider the simulation of such a quench by a digital quantum simulator, which approximates the continuous-time evolution with a Trotter-Suzuki pulse sequence $U(t) = e^{-it(H_B+H_J)} \approx U_T := (e^{-i\Delta t H_B}e^{-i\Delta t H_J})^T$, where $t = T\Delta t$ and H_B and H_J are the Ising Hamiltonians for $J = 0$ and $B = 0$, respectively. The target covariance matrix is then $\boldsymbol{M}(\varrho_t) = \boldsymbol{Q}(t)\boldsymbol{M}(|\uparrow\rangle\langle\uparrow|^{\otimes L})\boldsymbol{Q}(t)^\top$, where $\boldsymbol{Q}(t) = e^{t\boldsymbol{A}(J,B)}$, with $\boldsymbol{A}(J,B)$ the coupling matrix of $H_B + H_J$, is the mode representation of the target time propagator $U(t)$ and

$$\boldsymbol{M}(|\uparrow\rangle\langle\uparrow|^{\otimes L}) := \oplus_{j=1}^{L} \begin{pmatrix} 0 & -1 \\ 1 & 0 \end{pmatrix}. \tag{17}$$

In turn, the preparation's covariance matrix is given by $\boldsymbol{M}(\varrho_p) = \boldsymbol{Q}_T \boldsymbol{M}(|\uparrow\rangle\langle\uparrow|^{\otimes L}) \boldsymbol{Q}_T^{\top}$, where $\boldsymbol{Q}_T = (e^{\Delta t \boldsymbol{A}(J)} e^{\Delta t \boldsymbol{A}(B)})^T$, with $\boldsymbol{A}(J)$ [$\boldsymbol{A}(B)$] the coupling matrix of H_B [H_J], corresponds to the discrete-time experimental evolution U_T. See Fig. 2 for numerical results and Appendix A of Supplemental Material [59] for details.

Discussion.—We have shown how to certify experimental states of dimension 2^{2L} with at most $O(L^4)$ measurements, with no assumption whatsoever on the experimental imperfections, for all pure fermionic Gaussian target states. Moreover, for targets given by ground states of gapped free-fermionic Hamiltonians, the number of experimental repetitions reduces to $O(L^2 \log^2(L))$. In addition, in Appendix F we prove that there always exists a closed ball of valid states that are correctly accepted by the certification test, so that the test is robust against finite experimental deviations [59].

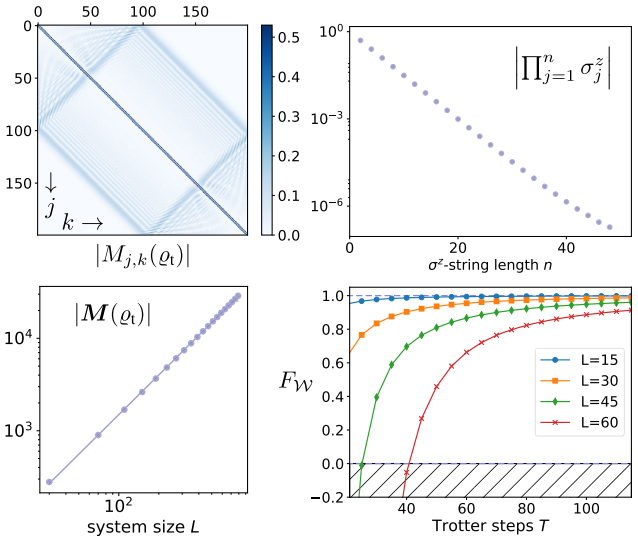

FIG. 2. Certification of a sudden quench in a critical spin-1/2 chain. The target state vector is given by $|\uparrow\rangle^{\otimes L}$ evolved, under the TF Ising Hamiltonian with $J = 1 = B$, up to time $t = L/8$, where L is the number of spins. Top left-hand panel: Absolute values of the $4L^2$ entries of the target covariance matrix for $L = 100$. The plot shows the correlation wave front propagating parallel to the diagonal. At $t = L/8$, the wave front has explored half the lattice size, in the sense that long-range correlations between spins of lattice distance $L/2$ have developed. Top right-hand panel: An extensive amount of Pauli matrix products (only one of which is shown) have exponentially small expectation values on the target state. This renders importance sampling in Hilbert space [49,50] inapplicable. Importance sampling in mode space, in contrast, is efficient for estimating overlaps between arbitrary covariance matrices (see text). Bottom left-hand panel: $|\boldsymbol{M}(\varrho_t)|$ as a function of L, with a power fit yielding the scaling $|\boldsymbol{M}(\varrho_t)| \approx 2.11 \times L^{1.42}$, so that the sample complexity is bounded by $\mathcal{N}_{\epsilon,\delta}(\mathcal{W}) \lesssim O(L^{2.84})$. Bottom right-hand panel: Expectation value of the fidelity witness, as a function of L, on a preparation of the continuous-time evolved state by a digital quantum simulator with T Trotter-Suzuki pulses. As L increases, T needs to increase to keep a value of the fidelity lower bound constant.

Our results are directly relevant to recent experiments with spin chains [7,10–16,68] as well as potential implementations of Kitaev's honeycomb model [69,70]. For instance, concerning the certification of sudden quenches as in Ref. [13], our technique is not limited by the generated long-range entanglement and therefore applies to long-time dynamics, for nearest-neighbor interactions. In turn, as for certifying adiabatic passages of the type of Ref. [15], again for nearest-neighbor interactions, our technique may be useful even for evolutions stopping close to criticality. Additionally, in real-life digital simulations [12,14,16], apart from the Trotterization errors, also heating and noise will of course be present. The fidelity witnesses offer an excellent tool for experimentally quantifying, in an inexpensive way, the detrimental effects of such imperfections on the simulation's performance.

Free-fermionic models are classically tractable, but the importance of their quantum simulations comes from the fact that they constitute a test bed for experimental many-body quantum technologies, with certified simulations of classically intractable models as the ultimate goal. In this respect, the direct certification tools developed here may help bridge the gap between the experimental certification of proof-of-principle simulations and classically intractable ones.

We thank C. Krumnow, D. Hangleiter, D. Gross, and Z. Zimboras for fruitful discussions. The work of J. E. and M. G. was funded by the Templeton Foundation, the EU (AQuS), the ERC (TAQ), and the DFG grants (SPP 1798 CoSIP, EI 519/7-1, EI 519/9-1, EI 519/14-1, and GRO 4334/2-1). The work of M. K. was funded by the National Science Centre, Poland (Polonez 2015/19/P/ST2/03001) within the European Union's Horizon 2020 research and innovation programme under the Marie Sklodowska-Curie Grant Agreement No. 665778. L. A. acknowledges financial support from the Brazilian agencies CNPq, FAPERJ, FAPESP, and CAPES.

[1] R. P. Feynman, Simulating physics with computers, Int. J. Theor. Phys. **21**, 467 (1982).
[2] J. I. Cirac and P. Zoller, Goals and opportunities in quantum simulation, Nat. Phys. **8**, 264 (2012).
[3] A. Aspuru-Guzik and P. Walther, Photonic quantum simulators, Nat. Phys. **8**, 285 (2012).
[4] R. Blatt and C. Roos, Quantum simulations with trapped ions, Nat. Phys. **8**, 277 (2012).
[5] A. A. Houck, H. E. Türeci, and J. Koch, On-chip quantum simulation with superconducting circuits, Nat. Phys. **8**, 292 (2012).

[6] I. Bloch, J. Dalibard, and S. Nascimbene, Quantum simulations with ultracold quantum gases, Nat. Phys. **8**, 267 (2012).
[7] C. Schneider, D. Porras, and T. Schaetz, Experimental quantum simulations of many-body physics with trapped ions, Rep. Prog. Phys. **75**, 024401 (2012).
[8] J. Eisert, M. Friesdorf, and C. Gogolin, Quantum many-body systems out of equilibrium, Nat. Phys. **11**, 124 (2015).
[9] A. Acin, I. Bloch, H. Buhrman, T. Calarco, C. Eichler, J. Eisert, D. Esteve, N. Gisin, S. J. Glaser, F. Jelezko, S. Kuhr, M. Lewenstein, M. F. Riedel, P. O. Schmidt, R. Thew, A. Wallraff, I. Walmsley, and F. K. Wilhelm, The European quantum technologies roadmap, arXiv:1712.03773.
[10] H. Friedenauer, H. Schmitz, J. Glueckert, D. Porras, and T. Schaetz, Simulating a quantum magnet with trapped ions, Nat. Phys. **4**, 757 (2008).
[11] K. Kim, M.-S. Chang, S. Korenblit, R. Islam, E. E. Edwards, J. K. Freericks, G.-D. Lin, L.-M. Duan, and C. Monroe, Quantum simulation of frustrated Ising spins with trapped ions, Nature (London) **465**, 590 (2010).
[12] R. Islam, E. E. Edwards, K. Kim, S. Korenblit, C. Noh, H. Carmichael, G.-D. Lin, L.-M. Duan, C.-C. J. Wang, J. K. Freericks, and C. Monroe, Onset of a quantum phase transition with a trapped ion quantum simulator, Nat. Commun. **2**, 377 (2011).
[13] B. Lanyon, C. Maier, M. Holzäpfel, T. Baumgratz, C. Hempel, P. Jurcevic, I. Dhand, A. Buyskikh, A. Daley, M. Cramer *et al.*, Efficient tomography of a quantum many-body system, Nat. Phys. **13**, 1158 (2017).
[14] R. Barends, A. Shabani, L. Lamata, J. Kelly, A. Mezzacapo, U. Las Heras, R. Babbush, A. Fowler, B. Campbell, Y. Chen *et al.*, Digitized adiabatic quantum computing with a superconducting circuit, Nature (London) **534**, 222 (2016).
[15] H. Bernien, S. Schwartz, A. Keesling, H. Levine, A. Omran, H. Pichler, S. Choi, A. S. Zibrov, M. Endres, M. Greiner, V. Vuletic, and M. D. Lukin, Probing many-body dynamics on a 51-atom quantum simulator, Nature (London) **551**, 579 (2017).
[16] Y. Salathé, M. Mondal, M. Oppliger, J. Heinsoo, P. Kurpiers, A. Potočnik, A. Mezzacapo, U. Las Heras, L. Lamata, E. Solano, S. Filipp, and A. Wallraff, Digital Quantum Simulation of Spin Models with Circuit Quantum Electrodynamics, Phys. Rev. X **5**, 021027 (2015).
[17] P. Pfeuty, The one-dimensional Ising model with a transverse field, Ann. Phys. (N.Y.) **57**, 79 (1970).
[18] S. Sachdev, Quantum phase transitions, Handbook of Magnetism and Advanced Magnetic Materials, DOI: 10.1002/9780470022184.hmm108 (2007).
[19] A. W. Kinross, M. Fu, T. J. Munsie, H. A. Dabkowska, G. M. Luke, S. Sachdev, and T. Imai, Evolution of Quantum Fluctuations Near the Quantum Critical Point of the Transverse Field Ising Chain System $CoNb_2O_6$, Phys. Rev. X **4**, 031008 (2014).
[20] P. di Francesco, P. Mathieu, and D. Sénéchal, *Conformal Field Theory* (Springer-Verlag, New York, 2012), DOI: 10.1007/978-1-4612-2256-9.
[21] A. Y. Kitaev, Unpaired Majorana fermions in quantum wires, Phys. Usp. **44**, 131 (2001).
[22] Y.-Z. You and C. Xu, Symmetry-protected topological states of interacting fermions and bosons, Phys. Rev. B **90**, 245120 (2014).
[23] H. Katsura, D. Schuricht, and M. Takahashi, Exact ground states and topological order in interacting Kitaev/Majorana chains, Phys. Rev. B **92**, 115137 (2015).
[24] F. Pollmann, E. Berg, A. M. Turner, and M. Oshikawa, Symmetry protection of topological phases in one-dimensional quantum spin systems, Phys. Rev. B **85**, 075125 (2012).
[25] U. Grimm, Spectrum of a duality-twisted Ising quantum chain, J. Phys. A **35**, L25 (2002).
[26] H. Nishimori and K. Takada, Exponential enhancement of the efficiency of quantum annealing by non-stochastic Hamiltonians, Front. ICT, DOI: 10.3389/fict.2017.00002 (2017).
[27] P. Calabrese, F. H. Essler, and M. Fagotti, Quantum quench in the transverse field Ising chain: I. Time evolution of order parameter correlators, J. Stat. Mech. (2012) P07016.
[28] P. Calabrese, F. H. Essler, and M. Fagotti, Quantum quenches in the transverse field Ising chain: II. Stationary state properties, J. Stat. Mech. (2012) P07022.
[29] P. Calabrese and J. Cardy, Entanglement entropy and quantum field theory, J. Stat. Mech. (2004) P06002.
[30] J. Dziarmaga, Dynamics of a Quantum Phase Transition: Exact Solution of the Quantum Ising Model, Phys. Rev. Lett. **95**, 245701 (2005).
[31] M. Gluza, C. Krumnow, M. Friesdorf, C. Gogolin, and J. Eisert, Equilibration via Gaussification in Fermionic Lattice Systems, Phys. Rev. Lett. **117**, 190602 (2016).
[32] U. Schneider, L. Hackermüller, J. P. Ronzheimer, S. Will, T. B. S. Braun, I. Bloch, E. Demler, S. Mandt, D. Rasch, and A. Rosch, Fermionic transport and out-of-equilibrium dynamics in a homogeneous Hubbard model with ultracold atoms, Nat. Phys. **8**, 213 (2012).
[33] E. Knill, R. Laflamme, and G. Milburn, A scheme for efficient quantum computation with linear optics, Nature (London) **409**, 46 (2001).
[34] E. Knill, Fermionic linear optics and matchgates, arXiv:quant-ph/0108033.
[35] B. M. Terhal and D. P. DiVincenzo, Classical simulation of non-interacting-fermion quantum circuits, Phys. Rev. A **65**, 032325 (2002).
[36] S. Bravyi, Lagrangian representation for fermionic linear optics, Quantum Inf. Comput. **5**, 216 (2005).
[37] A. Kitaev, Anyons in an exactly solved model and beyond, Ann. Phys. (Amsterdam) **321**, 2 (2006).
[38] F. de Melo, P. Ćwikliński, and B. M. Terhal, The power of noisy fermionic quantum computation, New J. Phys. **15**, 013015 (2013).
[39] S. Bravyi, Classical capacity of fermionic product channels, arXiv:quant-ph/0507282.
[40] A. Ferraro, S. Olivares, and M. G. A. Paris, Gaussian states in continuous variable quantum information, arXiv:quant-ph/0503237.
[41] C. Weedbrook, S. Pirandola, R. García-Patrón, N. J. Cerf, T. C. Ralph, J. H. Shapiro, and S. Lloyd, Gaussian quantum information, Rev. Mod. Phys. **84**, 621 (2012).
[42] F. Haldane, 'Luttinger liquid theory' of one-dimensional quantum fluids. I. Properties of the Luttinger model and their extension to the general 1D interacting spinless Fermi gas, J. Phys. C **14**, 2585 (1981).

[43] J. Von Delft and H. Schoeller, Bosonization for beginners—Refermionization for experts, Ann. Phys. (Berlin) **7**, 225 (1998).

[44] E. Fradkin, *Field Theories of Condensed Matter Physics* (Cambridge University Press, Cambridge, England, 2013).

[45] D. Gross, Y.-K. Liu, S. T. Flammia, S. Becker, and J. Eisert, Quantum State Tomography via Compressed Sensing, Phys. Rev. Lett. **105**, 150401 (2010).

[46] C. A. Riofrio, D. Gross, S. T. Flammia, T. Monz, D. Nigg, R. Blatt, and J. Eisert, Experimental quantum compressed sensing for a seven-qubit system, Nat. Commun. **8**, 15305 (2017).

[47] G. Tóth, W. Wieczorek, D. Gross, R. Krischek, C. Schwemmer, and H. Weinfurter, Permutationally Invariant Quantum Tomography, Phys. Rev. Lett. **105**, 250403 (2010).

[48] M. Cramer, M. B. Plenio, S. T. Flammia, R. Somma, D. Gross, S. D. Bartlett, O. Landon-Cardinal, D. Poulin, and Y.-K. Liu, Efficient quantum state tomography, Nat. Commun. **1**, 149 (2010).

[49] S. T. Flammia and Y.-K. Liu, Direct Fidelity Estimation from Few Pauli Measurements, Phys. Rev. Lett. **106**, 230501 (2011).

[50] M. P. da Silva, O. Landon-Cardinal, and D. Poulin, Practical Characterization of Quantum Devices without Tomography, Phys. Rev. Lett. **107**, 210404 (2011).

[51] S. T. Flammia, D. Gross, Y.-K. Liu, and J. Eisert, Quantum tomography via compressed sensing: Error bounds, sample complexity, and efficient estimators, New J. Phys. **14**, 095022 (2012).

[52] L. Aolita, C. Gogolin, M. Kliesch, and J. Eisert, Reliable quantum certification of photonic state preparations, Nat. Commun. **6**, 8498 (2015).

[53] A. Steffens, M. Friesdorf, T. Langen, B. Rauer, T. Schweigler, R. Hübener, J. Schmiedmayer, C. Riofrío, and J. Eisert, Towards experimental quantum-field tomography with ultracold atoms, Nat. Commun. **6**, 7663 (2015).

[54] D. Hangleiter, M. Kliesch, M. Schwarz, and J. Eisert, Direct certification of a class of quantum simulations, Quantum Sci. Technol. **2**, 015004 (2017).

[55] J. Eisert and T. J. Osborne, General Entanglement Scaling Laws from Time Evolution, Phys. Rev. Lett. **97**, 150404 (2006).

[56] G. Ramírez, J. Rodríguez-Laguna, and G. Sierra, Entanglement over the rainbow, J. Stat. Mech. (2015) P06002.

[57] V. Eisler and Z. Zimborás, Entanglement negativity in two-dimensional free lattice models, Phys. Rev. B **93**, 115148 (2016).

[58] C. V. Kraus and J. I. Cirac, Generalized Hartree-Fock theory for interacting fermions in lattices: Numerical methods, New J. Phys. **12**, 113004 (2010).

[59] See Supplemental Material at http://link.aps.org/supplemental/10.1103/PhysRevLett.120.190501 for details on methods of fermionic linear optics and proofs of properties of fidelity witnesses, which includes Refs. [17,36,52,54,60,61].

[60] M. Gluza, https://github.com/marekgluza/Fidelity_witnesses_example.

[61] M. Wimmer, Algorithm 923: Efficient numerical computation of the Pfaffian for dense and banded skew-symmetric matrices, ACM Trans. Math. Softw. **38**, 1 (2012).

[62] O. Gühne and G. Tóth, Entanglement detection, Phys. Rep. **474**, 1 (2009).

[63] F. Fröwis, M. van den Nest, and W. Dür, Certifiability criterion for large-scale quantum systems, New J. Phys. **15**, 113011 (2013).

[64] C. Gogolin, M. Kliesch, L. Aolita, and J. Eisert, Boson-sampling in the light of sample complexity, arXiv:1306.3995v2.

[65] M. B. Hastings and T. Koma, Spectral gap and exponential decay of correlations, Commun. Math. Phys. **265**, 781 (2006).

[66] P. Jordan and W. Eugene, Über das Paulische Äquivalenzverbot, Z. Phys. **47**, 631 (1928).

[67] E. Lieb, T. Schultz, and D. Mattis, Two soluble models of an antiferromagnetic chain, Ann. Phys. (N.Y.) **16**, 407 (1961).

[68] R. Blatt and C. Roos, Quantum simulations with trapped ions, Nat. Phys. **8**, 277 (2012).

[69] R. Schmied, J. H. Wesenberg, and D. Leibfried, Quantum simulation of the hexagonal Kitaev model with trapped ions, New J. Phys. **13**, 115011 (2011).

[70] M. Mielenz, H. Kalis, M. Wittemer, F. Hakelberg, R. Schmied, M. Blain, P. Maunz, D. Leibfried, U. Warring, and T. Schaetz, Freely configurable quantum simulator based on a two-dimensional array of individually trapped ions, arXiv:1512.03559.

Supplementary material: Fidelity witnesses for fermionic quantum simulations

M. Gluza,[1] M. Kliesch,[2] J. Eisert,[1] and L. Aolita[3,4,5]

[1]*Dahlem Center for Complex Quantum Systems, Freie Universität Berlin, Germany*
[2]*Institute of Theoretical Physics and Astrophysics, University of Gdańsk, Poland*
[3]*Instituto de Física, Universidade Federal do Rio de Janeiro, P. O. Box 68528, Rio de Janeiro, RJ 21941-972, Brazil*
[4]*International Institute of Physics, Federal University of Rio Grande do Norte, 59070-405 Natal, Brazil*
[5] *ICTP South American Institute for Fundamental Research Instituto de Física Teórica, UNESP-Universidade Estadual Paulista R. Dr. Bento T. Ferraz 271, Bl. II, São Paulo 01140-070, SP, Brazil*

(Dated: March 6, 2018)

APPENDIX

In this appendix, we present the technicalities of the calculations mentioned in the main text and additionally provide some further details about our methods. The first section recalls generally known facts concerning fermionic linear optics. The next three sections concern fidelity witnesses. The next two are on sample complexities for evaluating the Gaussian fidelity witness with an estimate. In the last section we provide details on robustness properties of the fidelity witness and the corresponding certification test.

A. Methods of fermionic linear optics

This section gives more details on results of fermionic linear optics used in the main text. The first subsection A 1 discusses unitary evolution in this formalism. The second subsection A 2 contains details on the Jordan-Wigner transformation, covariance matrices of spin product states and which spin operators need to be measured to measure the fermionic covariance matrix. Finally we shortly comment on the numerical simulations in subsection A 3.

1. *Gaussian dynamics*

The Heisenberg evolution of Majorana operators is given as follows.

Lemma 3 (Free fermion propagator)**.** *Let*

$$H(\boldsymbol{A}) = \frac{\mathrm{i}}{4}\sum_{j,k=1}^{2L} A_{j,k} m_j m_k \tag{18}$$

be a free, quadratic fermionic Hamiltonian with $\boldsymbol{A} = -\boldsymbol{A}^\top \in \mathbb{R}^{2L\times 2L}$*. Then*

$$m_j(t) := \mathrm{e}^{\mathrm{i}tH(\boldsymbol{A})} m_j \mathrm{e}^{-\mathrm{i}tH(\boldsymbol{A})} = \sum_{k=1}^{2L} Q_{j,k}(t) m_k \tag{19}$$

where $\boldsymbol{Q}(t) = e^{t\boldsymbol{A}} \in SO(2L)$*.*

Note that the propagator is manifestly real and there is no explicit imaginary unit in the exponent because $\boldsymbol{A}$ is already anti-hermitian.

Proof. We begin by noticing that $t \mapsto m_j(t)$ is differentiable and take a time-derivative obtaining

$$\begin{aligned}\partial_t m_j(t) &= \mathrm{i}H(\boldsymbol{A}) m_j(t) - m_j(t) H(\boldsymbol{A}) \\ &= \mathrm{i}[H(\boldsymbol{A}), m_j(t)]\end{aligned} \tag{20}$$

which is the Heisenberg equation of motion. We further notice that

$$\partial_t m_j(t) = \mathrm{i}\,\mathrm{e}^{\mathrm{i}tH(\boldsymbol{A})}[H(\boldsymbol{A}), m_j]\,\mathrm{e}^{-\mathrm{i}tH(\boldsymbol{A})} \tag{21}$$

which means that we need to evaluate the commutator at $t = 0$. Next we calculate the commutator

$$[m_l m_k, m_j] = 2m_l\delta_{k,j} - 2m_k\delta_{l,j} \tag{22}$$

which leads to

$$\begin{aligned}[H(\boldsymbol{A}), m_j] &= \frac{\mathrm{i}}{4}\sum_{l,k=1}^{2L} A_{l,k}[m_l m_k, m_j] \\ &= \frac{\mathrm{i}}{2}\sum_{l,k=1}^{2L}(A_{l,k} m_l \delta_{k,j} - A_{l,k} m_k \delta_{l,j}) \\ &= \frac{\mathrm{i}}{2}\sum_{k=1}^{2L}(A_{k,j} m_k - A_{j,k} m_k) \\ &= -\mathrm{i}\sum_{k=1}^{2L} A_{j,k} m_k.\end{aligned} \tag{23}$$

This equation allows us to write the above Heisenberg equation of motion explicitly as

$$\partial_t m_j(t) = \sum_{k=1}^{2L} A_{j,k} m_k. \tag{24}$$

This linear system of $2L$ ordinary differential equations is solved by

$$m_j(t) = \sum_{k=1}^{2L} Q_{j,k}(t) m_k, \tag{25}$$

where $\boldsymbol{Q} = e^{t\boldsymbol{A}} \in SO(2L)$. Indeed, this fact becomes apparent as follows. If one considers a vector $m = (m_1, \ldots, m_{2L})^\top$ then we obtain in vector notation

$$\partial_t m(t) = \boldsymbol{A}\, m(t) \quad \Leftrightarrow \quad m(t) = \mathrm{e}^{t\boldsymbol{A}} m. \tag{26}$$

□

Given this lemma we easily obtain the equation of motion of the covariance matrix with entries

$$\begin{aligned} M(\varrho(t))_{j,k} &= \frac{\mathrm{i}}{2}\mathrm{tr}\big([m_j, m_k]\varrho(t)\big) \\ &= \frac{\mathrm{i}}{2}\mathrm{tr}\big([m_j(t), m_k(t)]\varrho\big) \\ &= \sum_{j',k'=1}^{2L} Q_{j,j'}(t)Q_{k,k'}(t)M(\varrho(0))_{j',k'}. \end{aligned} \tag{27}$$

Hence, in matrix notation, we obtain

$$\boldsymbol{M}(\varrho(t)) = (\boldsymbol{Q}(t)\boldsymbol{M}(\varrho(0))\boldsymbol{Q}(t)^\top)_{j,k}. \tag{28}$$

2. *Exploiting the Jordan-Wigner transformation*

This subsection shows how to use the Jordan-Wigner transformation to translate between spins and fermions. We first identify covariance matrices of simple states.

Lemma 4 (Vacuum covariance matrix)**.** *In the notation* $\sigma^z\,|\uparrow\rangle = |\uparrow\rangle$ *we have*

$$\boldsymbol{M}\big(\,|\uparrow\rangle\langle\uparrow|^{\otimes L}\,\big) \coloneqq \oplus_{j=1}^{L}\begin{pmatrix} 0 & -1 \\ 1 & 0 \end{pmatrix}. \tag{29}$$

In general if $|\boldsymbol{\omega}\rangle$ *is a computational basis vector with* $\boldsymbol{\omega} \in \{0,1\}^{\times L}$ *(identifying* $|0\rangle = |\uparrow\rangle$ *and* $|1\rangle = |\downarrow\rangle$*) we have*

$$\boldsymbol{M}\big(\,|\boldsymbol{\omega}\rangle\langle\boldsymbol{\omega}|\,\big) \coloneqq \oplus_{j=1}^{L}\begin{pmatrix} 0 & -(-1)^{\omega_k} \\ (-1)^{\omega_k} & 0 \end{pmatrix}. \tag{30}$$

Proof. The first statement follows directly from the second for $\omega_k = 0$ for all k. To show the latter, we first observe that $\sigma_k^z = -\mathrm{i}\, m_{2k-1}m_{2k}$. Indeed using

$$\sigma^a\sigma^b = \delta_{a,b}\mathbb{1}_2 + \mathrm{i}\sum_{c=x,y,z}\varepsilon_{a,b,c}\sigma^c \tag{31}$$

we obtain

$$\begin{aligned} -\mathrm{i}\, m_{2k-1}m_{2k} &= -\mathrm{i}\big(\prod_{k'<k}\sigma_{k'}^z\big)\sigma_k^x\big(\prod_{k''<k}\sigma_{k''}^z\big)\sigma_k^y \qquad (32)\\ &= -\mathrm{i}\sigma_k^x\sigma_k^y = \sigma_k^z. \qquad (33) \end{aligned}$$

Next, we observe that $\langle\sigma_k^x\rangle_{\boldsymbol{\omega}} = \langle\sigma_k^y\rangle_{\boldsymbol{\omega}} = 0$ and $\langle\sigma_k^z\rangle_{\boldsymbol{\omega}} = (-1)^{\omega_k}$. So, the only non-vanishing elements are

$$\begin{aligned} M_{2k-1,2k} = -M_{2k,2k-1} &= \mathrm{i}\,\langle m_{2k-1}m_{2k}\rangle_{\boldsymbol{\omega}} \\ &= -\langle\sigma_k^z\rangle_{\boldsymbol{\omega}} = -(-1)^{\omega_k}. \end{aligned} \tag{34}$$

□

In an experiment based on qubits the fermionic covariance matrix can be measured by making the Pauli measurements corresponding to the observables in the following lemma.

Lemma 5 (Fermion spin correlation dictionary)**.** *For* $j < k$ *can identify the following terms.*

- *Odd-odd:*

$$m_{2j-1}m_{2k-1} = -\mathrm{i}\sigma_j^y\big(\prod_{j<k'<k}\sigma_{k'}^z\big)\sigma_k^x \tag{35}$$

- *Odd-even:*

$$m_{2j-1}m_{2k} = -\mathrm{i}\sigma_j^y\big(\prod_{j<k'<k}\sigma_{k'}^z\big)\sigma_k^y \tag{36}$$

- *Even-odd:*

$$m_{2j}m_{2k-1} = \mathrm{i}\sigma_j^x\big(\prod_{j<k'<k}\sigma_{k'}^z\big)\sigma_k^x \tag{37}$$

- *Even-even:*

$$m_{2j}m_{2k} = \mathrm{i}\sigma_j^x\big(\prod_{j<k'<k}\sigma_{k'}^z\big)\sigma_k^y. \tag{38}$$

Proof. By straightforward calculation,

$$\begin{aligned} m_{2j-1}m_{2k-1} &= \big(\prod_{j'<j}\sigma_{j'}^z\big)\sigma_j^x\big(\prod_{k'<k}\sigma_{k'}^z\big)\sigma_k^x \qquad (39)\\ &= \sigma_j^x\sigma_j^z\big(\prod_{j<k'<k}\sigma_{k'}^z\big)\sigma_k^x \qquad (40)\\ &= -\mathrm{i}\sigma_j^y\big(\prod_{j<k'<k}\sigma_{k'}^z\big)\sigma_k^x\,. \qquad (41) \end{aligned}$$

The remaining relations follow similarly and by again using the relations (32). □

Considering the reversed direction of this dictionary, we find that the product of two spin operators is a product of again two Majorana operators only when the spins are neighboring in the Jordan-Wigner transformation from which we obtain the following corollary.

Corollary 6 (XY models)**.** *The Hamiltonian* H_{spin} *from main text maps to a quadratic fermionic Hamiltonian* $H(\boldsymbol{A})$ *under the Jordan-Wigner transformation.*

The translation invariant case is physically the most relevant case for which the following result first appeared in Ref. [1] and we state it to make explicit which couplings we have used in our simulations.

Lemma 7 (Transverse field Ising model)**.** *The Hamiltonian of the transverse field Ising model*

$$H_{\mathrm{TFIM}} = -J\sum_{k=1}^{L-1}\sigma_k^x\sigma_{k+1}^x - B\sum_{k=1}^{L}\sigma_k^z \tag{42}$$

maps to free fermions under the Jordan-Wigner transformation and the couplings matrix read

$$\boldsymbol{A}(J,B) = 2\begin{pmatrix} 0 & B & & & & \\ -B & 0 & J & & & \\ & -J & 0 & B & & \\ & & -B & 0 & J & \\ & & & -J & 0 & \\ & & & & & \ddots \end{pmatrix}. \tag{43}$$

Note that for compactness we write in the main text $\boldsymbol{A}(J) := \boldsymbol{A}(J,0)$ and $\boldsymbol{A}(B) := \boldsymbol{A}(0,B)$.

Proof. By the above dictionary lemma we have $\sigma_k^x\sigma_{k+1}^x = -\mathrm{i}\, m_{2k}m_{2k+1}$ and $\sigma_k^z = -\mathrm{i}\, m_{2k-1}m_{2k}$. This gives

$$H_{\mathrm{TFIM}} = \mathrm{i}\sum_{k=1}^{L-1} J m_{2k}m_{2k+1} + \mathrm{i}\sum_{k=1}^{L} B m_{2k-1}m_{2k} \tag{44}$$

which can be put to the standard form

$$H(\boldsymbol{A}) = \frac{\mathrm{i}}{4}\sum_{j,k}^{2L} A_{j,k} m_j m_k \tag{45}$$

by defining the matrix $\boldsymbol{A}$ as in the lemma statement. □

3. *Comments on numerical aspects*

The numerical code used to obtain Fig. 2 in main text is available online [2]. We use Wick's formula [3] to calculate $|\langle\prod_{k=1}^{n}\sigma_k^z\rangle| = \mathrm{Pf}(\boldsymbol{M}_{1\ldots 2n})$, where Pf denotes the Pfaffian which can be calculated using the package PFAPACK [4].

B. Proof that Eq. (7) yields a fidelity witness and general witness construction

Here we first provide an expression for a fidelity witness of any arbitrary, totally generic pure target state, not restricted to the Gaussian fermionic setting.

Proposition 8 (General witness construction)**.** *Let ϱ_t be any pure target state, $0 < \Delta = \lambda_1 \leq \ldots \leq \lambda_N$, and P_1, P_2, …, and P_N positive-semidefinite operators such that $\varrho_t + \sum_{l=1}^{N} P_l = \mathbb{1}$ and $\mathrm{tr}(\varrho_t P_l) = 0$ for all $l = 1,\ldots,N$. Then,*

$$\mathcal{W} := \mathbb{1} - \Delta^{-1}\sum_{l=1}^{N}\lambda_l P_l \tag{46}$$

is a fidelity witness for ϱ_t.

The fact that the observable $\mathcal{W}$ in Eq. (7) defines a fidelity witness for the free-fermionic target state in Eq. (6) follows from Proposition 8 taking $N = 2^L - 1$, identifying l with an L-bit string $\boldsymbol{\nu} \neq \boldsymbol{\omega}$, and taking $\lambda_{\boldsymbol{\nu}} = \sum_{j=1}^{L}[(1-\omega_j)\nu_j + \omega_j(1-\nu_j)]$ and $P_{\boldsymbol{\nu}} = U\,|\boldsymbol{\nu}\rangle\,\langle\boldsymbol{\nu}|\,U^\dagger$.

Proof of Proposition 8. We start with Property i) in Definition 1. Let ϱ_p be such that $\mathrm{tr}[\mathcal{W}\varrho_p] = 1$. Then $\Delta^{-1}\sum_{k=1}^{N}\lambda_l \mathrm{tr}[P_k\varrho_p] = 0$. As all terms are non-negative, we have $\mathrm{tr}[P_k\varrho_p] = 0$. From this, we get

$$1 = \mathrm{tr}[\varrho_p\mathbb{1}] = \mathrm{tr}[\varrho_p\varrho_{\mathrm{t}}] + \sum_{k=1}^{N}\mathrm{tr}[P_k\varrho_p] = \mathrm{tr}[\varrho_p\varrho_{\mathrm{t}}], \tag{47}$$

which means, since ϱ_{t} is pure, that $\varrho_p = \varrho_{\mathrm{t}}$. The converse direction starting from $\varrho_p = \varrho_{\mathrm{t}}$ follows from $\mathrm{tr}[\varrho_{\mathrm{t}}P_k] = 0$. We now prove the validity of Property ii) in Def. 1. For any state vector $|\psi\rangle$ we have

$$\sum_{k=1}^{N}\lambda_l\langle\psi|P_k|\psi\rangle \geq \Delta\sum_{k=1}^{N}\langle\psi|P_k|\psi\rangle \tag{48}$$

$$= \Delta(1 - \langle\psi|\varrho_{\mathrm{t}}|\psi\rangle). \tag{49}$$

This means that

$$\langle\psi|\varrho_{\mathrm{t}}|\psi\rangle \geq \langle\psi|\mathcal{W}|\psi\rangle \tag{50}$$

which one may write $\varrho_{\mathrm{t}} \succeq \mathcal{W} = \mathbb{1} - \Delta^{-1}\sum_{k=1}^{N}\lambda_l P_l$, where $\succeq$ denotes semidefinite ordering. This relation can be used in order to lower bound the fidelity. If we write the preparation state in its eigenbasis $\varrho_p = \sum_k p_k|k\rangle\langle k| \succeq 0$, then we find the following

$$\mathrm{tr}[(\varrho_{\mathrm{t}} - \mathcal{W})\varrho_p] = \sum_k p_k\langle k|\varrho_{\mathrm{t}} - \mathcal{W}|k\rangle \geq 0\,. \tag{51}$$

Thus we arrive at

$$F = \mathrm{tr}[\varrho_{\mathrm{t}}\varrho_p] \geq \mathrm{tr}[\mathcal{W}\varrho_p]\,. \tag{52}$$

□

C. Proof of Eq. (8): Fidelity-witness in terms of covariance matrices

Before the proof, let us first provide useful facts from fermionic linear optics theory. The covariance matrix of any Fock state vector $|\boldsymbol{\omega}\rangle$ is given, introducing the short-hand notation $\boldsymbol{M}_{\boldsymbol{\omega}} := \boldsymbol{M}(|\boldsymbol{\omega}\rangle\langle\boldsymbol{\omega}|)$ by

$$\boldsymbol{M}_{\boldsymbol{\omega}} = \bigoplus_{k=1}^{L}(1-2w_k)\begin{pmatrix} 0 & -1 \\ 1 & 0\end{pmatrix}. \tag{53}$$

This is readily seen from the fact that

$$\mathrm{i}\,[m_{2k-1}, m_{2k}]/2 = (f_k + f_k^\dagger)(f_k - f_k^\dagger) = 2n_k - \mathbb{1} \tag{54}$$

which gives

$$M_{2k-1,2k} = \mathrm{i}\,\langle\boldsymbol{\omega}|\,m_{2k-1}m_{2k}\,|\boldsymbol{\omega}\rangle = 2w_k - 1 = -M_{2k,2k-1} \tag{55}$$

and that all other covariance matrix entries are zero. Put differently, fermionic Fock states are of the most simple product form. In order to introduce coherences in the system one can rotate the state by a Gaussian unitary U with mode action $\boldsymbol{Q}$ which then yields

$$\boldsymbol{M}(U\,|\boldsymbol{\omega}\rangle\langle\boldsymbol{\omega}|\,U^\dagger) = \boldsymbol{Q}\boldsymbol{M}_{\boldsymbol{\omega}}\boldsymbol{Q}^\top. \tag{56}$$

Proof of Eq. (8). In order to evaluate the witness we notice that the numbering operator of mode k is

$$n_k = \frac{\mathbb{1}}{2} + \frac{\mathrm{i}}{4}[m_{2k-1}, m_{2k}] \tag{57}$$

and

$$\mathbb{1} - n_k = \frac{\mathbb{1}}{2} - \frac{\mathrm{i}}{4}[m_{2k-1}, m_{2k}]. \tag{58}$$

This allows us to write the projector $n^{(\boldsymbol{\omega})}$ as

$$n^{(\boldsymbol{\omega})} = \sum_{j=1}^{L} \left[\mathbb{1}/2 + \frac{\mathrm{i}}{4}(1-2\omega_j)[m_{2k-1}, m_{2k}]) \right]. \tag{59}$$

We therefore have

$$\mathrm{tr}(\varrho_p \mathcal{W}) = 1 - \frac{L}{2} - \frac{\mathrm{i}}{4}\sum_{k=1}^{L}(1-2w_k)\mathrm{tr}\big(U^\dagger \varrho_p U \big[m_{2k-1}, m_{2k}\big]\big) \tag{60}$$

$$= 1 - \frac{L}{2} - \frac{1}{2}\sum_{k=1}^{L}(1-2w_k) M(U^\dagger \varrho_p U)_{2k-1,2k}, \tag{61}$$

where the definition of the covariance matrix (4) has been used. As

$$\tilde{\boldsymbol{M}} := \boldsymbol{M}(U^\dagger \varrho_p U) = \boldsymbol{Q}^\top \boldsymbol{M}(\varrho_\mathrm{p}) \boldsymbol{Q} \tag{62}$$

is anti-symmetric, we can write $\tilde{M}_{2k-1,2k}$ as

$$\tilde{M}_{2k-1,2k} = \frac{1}{2}\mathrm{tr}\Big[\begin{pmatrix} 0 & \tilde{M}_{2k-1,2k} \\ \tilde{M}_{2k,2k-1} & 0 \end{pmatrix} \begin{pmatrix} 0 & -1 \\ 1 & 0 \end{pmatrix} \Big]. \tag{63}$$

We further notice that (54) allows us to write

$$\sum_{k=1}^{L}(1-2w_k)\tilde{M}_{2k-1,2k} = \frac{1}{2}\mathrm{tr}[\tilde{\boldsymbol{M}}\boldsymbol{M}_{\boldsymbol{\omega}}]. \tag{64}$$

From the definition of $\boldsymbol{M}(\varrho_\mathrm{t}) = \boldsymbol{Q}\boldsymbol{M}_{\boldsymbol{\omega}}\boldsymbol{Q}^\top$, we finally obtain

$$\mathrm{tr}(\varrho_p \mathcal{W}) = 1 - \frac{L}{2} - \frac{1}{4}\mathrm{tr}[\boldsymbol{M}(\varrho_\mathrm{p})\boldsymbol{M}(\varrho_\mathrm{t})] \tag{65}$$

$$= 1 + \frac{1}{4}\mathrm{tr}\big[(\boldsymbol{M}(\varrho_\mathrm{p}) - \boldsymbol{M}(\varrho_\mathrm{t}))^\top \boldsymbol{M}(\varrho_\mathrm{t})\big]. \tag{66}$$

□

D. Proof of Theorem 3 (sample complexity of $F_{\mathcal{W}}$)

In this section, we compute the number of experimental runs required to get a finite-sample estimate $F^*_{\mathcal{W}}(\varrho_\mathrm{p})$ of $F_{\mathcal{W}}(\varrho_\mathrm{p})$ satisfying Eq. (13) with the measurement scheme with single-shot importance sampling described in the main text. This sets the upper bound on $\mathcal{N}_{\epsilon,\delta}(\mathcal{W})$ in Eq. (14), proving Theorem 2.

Proof of Theorem 2. We begin by noting that one can directly evaluate $F_{\mathcal{W}}(\varrho_\mathrm{p})$ from the value of

$$\mathcal{X} := \mathrm{tr}\big[\boldsymbol{M}(\varrho_\mathrm{p})^\top \boldsymbol{M}(\varrho_\mathrm{t})\big] = 4(F_{\mathcal{W}} + \frac{L}{2} - 1). \tag{67}$$

Indeed, if $|\mathcal{X}^* - \mathcal{X}| \leq 4\epsilon$, then $|F^*_{\mathcal{W}}(\varrho_\mathrm{p}) - F_{\mathcal{W}}(\varrho_\mathrm{p})| \leq \epsilon$. We define conditional probability

$$P_{\beta|j,k} := \mathrm{tr}\Big[\hat{m}^{(\beta)}_{j,k}\varrho_p\Big] \tag{68}$$

and the sampling distribution

$$P_{j,k} = \frac{|M_{j,k}(\varrho_\mathrm{t})|}{|\boldsymbol{M}(\varrho_\mathrm{t})|} \tag{69}$$

for $(j,k) \in \Omega$ with $|\boldsymbol{M}(\varrho_\mathrm{t})| = \sum_{(j,k)\in\Omega}|M_{j,k}(\varrho_\mathrm{t})| \leq 2L^2$. By Bayes' theorem, we have that $P_{\beta,j,k} = P_{\beta|j,k}P_{j,k}$ is a well-defined probability distribution. Additionally, we define the importance sampling variable

$$X_{\beta,j,k} := 2|\boldsymbol{M}(\varrho_\mathrm{t})|\,\beta\,\mathrm{sgn}\big[M_{j,k}(\varrho_\mathrm{t})\big] \tag{70}$$

which is distributed over $P_{\beta,j,k}$. With these definitions we check that the average of X gives $\mathcal{X}$,

$$\mathbb{E}[X] = \sum_{(j,k)\in\Omega,\beta=\pm1} X_{\beta,j,k}P_{\beta,j,k} \tag{71}$$

$$= 2\sum_{(j,k)\in\Omega}\mathrm{sgn}\big[M_{j,k}(\varrho_\mathrm{t})\big]|M_{j,k}(\varrho_\mathrm{t})|\sum_{\beta=\pm1}\beta\mathrm{tr}[\hat{m}^{(\beta)}_{j,k}\varrho^{(p)}] \tag{72}$$

$$= \mathrm{tr}\big[\boldsymbol{M}(\varrho_\mathrm{p})^\top \boldsymbol{M}(\varrho_\mathrm{t})\big]\,. \tag{73}$$

We now use Hoeffding's inequality to see that this results in a (ϵ,δ)-evaluation promise. We have

$$\mathbb{P}\left[|\mathcal{X} - \frac{1}{\mathcal{N}}\sum_{m=1}^{\mathcal{N}} X_{\mu(m)}| > 4\epsilon\right] \leq 2\exp\left(-\frac{2\mathcal{N}\epsilon^2}{|\boldsymbol{M}(\varrho_\mathrm{t})|^2}\right). \tag{74}$$

We impose the RHS to be upper bounded by δ, so we obtain

$$\mathcal{N}_{\epsilon,\delta}(\mathcal{W}) = \left\lceil \frac{\ln(2/\delta)|\boldsymbol{M}(\varrho_\mathrm{t})|^2}{2\epsilon^2} \right\rceil, \tag{75}$$

which is the sample complexity, i.e., yielding the inequality (14).

□

E. Sample complexity for entrywise evaluation

Here, we compute the number of experimental runs required to get a finite-sample estimate $F^*_{\mathcal{W}}(\varrho_\mathrm{p})$ of $F_{\mathcal{W}}(\varrho_\mathrm{p})$ satisfying Eq. (13) with a measurement scheme that does not exploit importance sampling, i.e., where all $|\Omega|$ observables are deterministically measured, but that exploits the fact that

commuting observables with indices in Ω can be measured simultaneously in each run. As we show, the resulting bound is less tight than the one in Eq. (14). More precisely, we consider a procedure where all $|\Omega|$ observables are measured the same number of times

$$\eta = \epsilon^{-2} L^3 \ln(2|\Omega|/\delta) \tag{76}$$

and we obtain the sample complexity $\mathcal{N}_{\epsilon,\delta}(\mathcal{W}) = 4L\eta$.

We denote the estimator of $\boldsymbol{M}$ by $\boldsymbol{M}^*$. The fact that the covariance matrix entries are bounded and lie in the interval $-1 < M_\mu < 1$ allows us to use Hoeffding's inequality. Taking $b = \ln(2|\Omega|/\delta)$ and making a union bound we find

$$\mathbb{P}\Big[\forall \mu \in \Omega : \big|M_\mu - M^*_\mu\big| \leq \sqrt{2b/\eta}\Big] = \tag{77}$$

$$1 - \mathbb{P}\Big[\exists \mu \in \Omega : \big|M_\mu - M^*_\mu\big| \geq \sqrt{2b/\eta}\Big] \geq \tag{78}$$

$$1 - |\Omega| \max_{\mu\in\Omega} \mathbb{P}\Big[\big|M_\mu - M^*_\mu\big| \geq \sqrt{2b/\eta}\Big] \geq 1 - 2|\Omega|\mathrm{e}^{-b}, \tag{79}$$

where we have used that $\mathbb{P}[A \cup B] \leq \mathbb{P}[A] + \mathbb{P}[B]$ for any probability measure $\mathbb{P}$. We check that $2|\Omega|\mathrm{e}^{-b} = \delta$ and additionally

$$\sqrt{2b/\eta} = \sqrt{2\epsilon^2 L^{-3}} = \sqrt{2} L^{-3/2} \epsilon \tag{80}$$

and therefore we have

$$\mathbb{P}\left[2^{-1/2} L^{3/2} \left\|\boldsymbol{M} - \boldsymbol{M}^*\right\|_{\max} \leq \epsilon\right] \geq 1 - \delta. \tag{81}$$

Eq. (13) follows thanks to the following Lemma which tells us that one can efficiently estimate the fidelity lower bound from estimates of the covariance matrix of ϱ_p with small errors.

Lemma 9 (Stability)**.** *The fidelity lower bound $F_{\mathcal{W}}(\varrho_p)$ is Lipschitz continuous with Lipschitz constant $L^{3/2}/\sqrt{2}$ with respect to the max-norm, i.e., for any two covariance matrices $\boldsymbol{M}$ and $\boldsymbol{M}^*$ we have for the respective values of the fidelity witnesses*

$$|F_{\mathcal{W}}(\varrho_p) - F^*_{\mathcal{W}}(\varrho_p)| \leq 2^{-1/2} L^{3/2} \left\|\boldsymbol{M} - \boldsymbol{M}^*\right\|_{\max}. \tag{82}$$

In the following proof, we denote the trace-norm by $\|\cdot\|_1$, the Schatten 2-norm (or Frobenius norm) by $\|\cdot\|_2$, and the spectral norm by $\|\cdot\|_\infty$.

Proof of Lemma 9. Let

$$\boldsymbol{\mathcal{J}}_L = \oplus_{k=1}^{L} \begin{pmatrix} 0 & 1 \\ -1 & 0 \end{pmatrix}. \tag{83}$$

It is enough to show that the linear map $\boldsymbol{M} \mapsto \mathrm{tr}[\boldsymbol{Q}\boldsymbol{M}\boldsymbol{Q}^\top \boldsymbol{\mathcal{J}}_L]$ is Lipschitz continuous at the origin with Lipschitz constant $(2L)^{3/2}$.

By Hölders inequality we have

$$\left|\mathrm{tr}[\boldsymbol{Q}\boldsymbol{M}\boldsymbol{Q}^\top \boldsymbol{\mathcal{J}}_L]\right| = \left|\mathrm{tr}[\boldsymbol{M}\boldsymbol{Q}^\top \boldsymbol{\mathcal{J}}_L \boldsymbol{Q}]\right| \tag{84}$$

$$\leq \|\boldsymbol{M}\|_1 \left\|\boldsymbol{Q}^\top \boldsymbol{\mathcal{J}}_L \boldsymbol{Q}\right\|_\infty = \|\boldsymbol{M}\|_1, \tag{85}$$

where we have used that $\|\cdot\|_\infty$ unitarily invariant and that $\|\boldsymbol{\mathcal{J}}_L\|_\infty = 1$ in the last step. It remains to show that $\|\boldsymbol{M}\|_1 \leq 2L$. But for any $2L \times 2L$ matrix $\boldsymbol{M}$ it holds that

$$\|\boldsymbol{M}\|_1 \leq \sqrt{2L}\, \|\boldsymbol{M}\|_2 \leq \sqrt{2L} 2L\, \|\boldsymbol{M}\|_{\max}, \tag{86}$$

where we have used (i) a general norm inequality for the Schatten 1- and 2-norm, (ii) that the Schatten 2-norm is the same as the vector 2-norm of the vectorized matrix, (iii) a general norm inequality for the vector 2-norm and the vector ∞-norm, and (iv) that the vector ∞-norm of a vectorized matrix is the max-norm of the matrix. Note that the bound (87) is tight for general matrices, as can be seen by choosing $\boldsymbol{M}$ as the discrete Fourier transform matrix on $\mathbb{C}^{2L}$. Inserting Eq. (87) into (86) completes the proof. □

Finally, in order to derive the sample complexity, we need to partition the set $[2L] \times [2L]$ such that the corresponding elements of the covariance matrix commute. We do it by considering bands parallel to the diagonal of the covariance matrix. Let us consider the non-trivial elements closest to the diagonal $\mu = (i, i+1)$. We bi-partition this band into indices starting with an even or an odd number. By construction, all associated covariance matrix observables will commute. As there are in total $2L - 1$ such off-diagonals, the total number of i.i.d. state preparations is bounded by

$$\mathcal{N}_{\epsilon,\delta}(\mathcal{W}) = 4L\eta = \frac{4L^4 \ln(2|\Omega|/\delta)}{\epsilon^2}. \tag{87}$$

Since $|\Omega| \leq 2L^2 + L$, this scaling is logarithmically worse in L than in Eq. (14).

F. Robustness of the certification test

Ref. [5] established a framework of certification where the notion of *robust quantum state certification* has been defined. In particular, in such a certification test, one desires to accept states above a threshold fidelity F_{T} and requires to reject states below F_{T}. But a realistic certification test cannot resolve fidelities F very close to F_{T} and thus one needs to allow for a fidelity region that remains undetermined. This idea leads to a robust certification test [5, 6], where one allows for a fidelity gap $\Delta < 1 - F_{\mathrm{T}}$. A *robust* test is guaranteed to accept a preparation ϱ_p if $F \geq F_{\mathrm{T}} + \Delta$, to reject it if $F < F_{\mathrm{T}}$, and possibly accept it in the intermediate region. These conditions for the test concern the exact fidelity and need to be translated to a statement concerning the estimate of the witness $F^*_{\mathcal{W}}(\varrho_{\mathrm{p}})$. We will show that for all preparations ϱ_p in a certain class of states $\mathcal{S}_\perp(\Delta, \epsilon)$ it suffices to compare the estimator $F^*_{\mathcal{W}}(\varrho_{\mathrm{p}})$ to the number $F_{\mathrm{T}} + \epsilon$. In other words, such test is robust

i) if ϱ_p is such that $F < F_{\mathrm{T}}$ then in the same time the witness will testify this i.e. $F^*_{\mathcal{W}}(\varrho_{\mathrm{p}}) < F_{\mathrm{T}} + \epsilon$. This means that whenever the test *has to* reject a preparation, then it will.

ii) if $F \geq F_{\mathrm{T}} + \Delta$ then we have $F^*_{\mathcal{W}}(\varrho_{\mathrm{p}}) \geq F_{\mathrm{T}} + \epsilon$. That is, whenever the fidelity is larger then the threshold fidelity enlarged by the fidelity gap, then the preparation is accepted by the test.

Note, that if $F \in [F_{\mathrm{T}}, F_{\mathrm{T}}+\Delta]$, then the certification test might accept or reject the preparation. Specifically, the class $\mathcal{S}_\perp(\Delta,\epsilon)$ characterizes the set of preparations ϱ_p where the witness behaves as a weak oracle separating $F \leq F_{\mathrm{T}}$ from $F \geq F_{\mathrm{T}}+\Delta$. We now construct this class. With a given target state $U|\boldsymbol{\omega}\rangle$ and its corresponding fidelity witness in mind, we define a mismatch parameter of some preparation state ϱ_p to be

$$n_\perp(\varrho_p) \coloneqq \mathrm{tr}[\hat{n}^{(\boldsymbol{\omega})} U^\dagger \varrho_p U] \geq 0\,. \tag{88}$$

Let us note that the preparation ϱ_p can be decomposed with the Hilbert-Schmidt inner product into the target state ϱ_{t} and a orthogonal contribution $\varrho_\perp \coloneqq \varrho_\perp(\varrho_{\mathrm{t}},\varrho_p)$, that is $\varrho_p = F\varrho_{\mathrm{t}} + (1-F)\varrho_\perp$ for $0 \leq F = \mathrm{tr}[\varrho_p\varrho_{\mathrm{t}}] \leq 1$ and $\mathrm{tr}[\varrho_{\mathrm{t}}\varrho_\perp]=0$. Using linearity of our witness for this decomposition yields

$$\begin{aligned} F_{\mathcal{W}}(\varrho_{\mathrm{p}}) &= F + (1-F)(1-\mathrm{tr}[U\hat{n}^{(\boldsymbol{\omega})}U^\dagger\varrho_\perp]) \\ &= 1-(1-F)n_\perp(\varrho_\perp)\,. \end{aligned} \tag{89}$$

Therefore the mismatch content has the properties $n_\perp(\varrho_{\mathrm{t}}) = 0$ and $n_\perp(\varrho_p) = (1-F)n_\perp(\varrho_\perp)$. For a given maximum estimation error $0<\epsilon<(1-F_{\mathrm{T}})/2$, fidelity gap $\Delta > 2\epsilon$ and fidelity threshold $F_{\mathrm{T}} < 1$ we define the *mismatch content threshold*

$$n_{\perp,\mathrm{T}}(\Delta,\epsilon) \coloneqq \frac{1-F_{\mathrm{T}}-2\epsilon}{1-F_{\mathrm{T}}-\Delta}\,. \tag{90}$$

This allows us to consider the following subset of all states $\mathcal{S}$

$$\mathcal{S}_\perp(\Delta,\epsilon)(\Delta,\epsilon) = \{\varrho\in\mathcal{S} | n_\perp(\varrho) \leq n_{\perp,\mathrm{T}}(\Delta,\epsilon)\}\,. \tag{91}$$

It is a convex set containing mixtures of states with possibly very large mismatch content $n_{\perp,\mathrm{T}}$ and which includes the target state ϱ_{t} in its interior. The following theorem states that our fidelity witness leads to a robust certification test.

Theorem 10 (Robust certification of pure Gaussian states)**.** *Let $F_T < 1$ be a threshold fidelity, $\delta > 0$ a maximal failure probability , $0<\epsilon<(1-F_T)/2$ a maximal estimation error and $2\epsilon < \Delta < 1-F_T$ a fidelity gap. Let ϱ_t be a pure Gaussian state and ϱ_p a preparation state. Let $F^*_{\mathcal{W}}(\varrho_p)$ be the estimator of the fidelity witness from Theorem 2. The test accepting the preparation if $F^*_{\mathcal{W}}(\varrho_p) \geq F_T+\epsilon$ and rejecting if $F^*_{\mathcal{W}}(\varrho_p) < F_T+\epsilon$ yields a robust certification of ϱ_t if $\varrho_p \in \mathcal{S}_\perp(\Delta,\epsilon)$. For states with high enough fidelity $F > 1-L^{-2}$ the witness yields a non-trivial lower bound $F_{\mathcal{W}}(\varrho_p) \geq 0$.*

Proof. The rejection Property i) follows by observing that according to Theorem 2 we have with probability at least $1-\delta$ that

$$|F^*_{\mathcal{W}}(\varrho_{\mathrm{p}}) - F_{\mathcal{W}}(\varrho_{\mathrm{p}})| \leq \epsilon \tag{92}$$

from which it follows that

$$F^*_{\mathcal{W}}(\varrho_{\mathrm{p}}) - \epsilon \leq F_{\mathcal{W}}(\varrho_{\mathrm{p}})\,. \tag{93}$$

Next we use that the fidelity witness is a lower bound to the fidelity F and that in case i) we have $F < F_{\mathrm{T}}$ to get the chain

$$F^*_{\mathcal{W}}(\varrho_{\mathrm{p}}) - \epsilon \leq F_{\mathcal{W}}(\varrho_{\mathrm{p}}) \leq F < F_{\mathrm{T}}\,. \tag{94}$$

Therefore, if $F < F_{\mathrm{T}}$ then $F^*_{\mathcal{W}}(\varrho_{\mathrm{p}}) < F_{\mathrm{T}}+\epsilon$. In this step we did not need to assume anything on the preparation ϱ_p.

Secondly, we show that the test has the acceptance Property ii) as well. We now use $F \geq F_{\mathrm{T}}+\Delta$ and assume that $n_\perp(\varrho_p) \leq n_{\perp,\mathrm{T}}$ to obtain from Eq. (90)

$$\begin{aligned} F_{\mathcal{W}}(\varrho_{\mathrm{p}}) &= 1-(1-F)n_\perp \\ &\geq 1-n_{\perp,\mathrm{T}}+Fn_{\perp,\mathrm{T}} \\ &\geq 1-n_{\perp,\mathrm{T}}+(F_{\mathrm{T}}+\Delta)n_{\perp,\mathrm{T}}, \end{aligned} \tag{95}$$

which with the definition of the mismatch content (91) becomes

$$\begin{aligned} F_{\mathcal{W}}(\varrho_{\mathrm{p}}) &\geq 1-(1-F_{\mathrm{T}}-\Delta)n_{\perp,\mathrm{T}} \\ &\geq 1-(1-F_{\mathrm{T}}-2\epsilon) \\ &\geq F_{\mathrm{T}}+2\epsilon. \end{aligned} \tag{96}$$

Therefore, we find with probability at least $1-\delta$ the inequality for the estimator of the fidelity witness

$$F^*_{\mathcal{W}}(\varrho_{\mathrm{p}}) \geq F_{\mathcal{W}}(\varrho_{\mathrm{p}}) - \epsilon \geq F_{\mathrm{T}}+\epsilon\,. \tag{97}$$

These two steps show that the test is robust for $\varrho\in\mathcal{S}_\perp(\Delta,\epsilon)$.

Finally let us assume $F_{\mathrm{T}} \geq 1-L^{-2}$. We need to show that if $F \geq F_{\mathrm{T}}+\Delta$ then $F^*_{\mathcal{W}}(\varrho_{\mathrm{p}}) \geq F_{\mathrm{T}}+\epsilon$. By Fuchs-van der Graaf inequality we have $D(\varrho_p,\varrho_{\mathrm{t}}) \leq \sqrt{1-F} \leq \sqrt{1-F_{\mathrm{T}}} = L^{-1}$. From this bound it follows that

$$\eta = \sum_{k=1}^{L}\left[(1-w_k)\mathrm{tr}[n_k U^\dagger\varrho_p U] + w_k\mathrm{tr}[(\mathbb{1}-n_k)U^\dagger\varrho_p U]\right] \tag{98}$$

$$\leq \sum_{k=1}^{L} L^{-1} = 1. \tag{99}$$

From this bound, we find

$$F_{\mathcal{W}}(\varrho_{\mathrm{p}}) = 1-\eta \geq 0\,. \tag{100}$$

□

Note that the witness is exact $F_{\mathcal{W}}(\varrho_{\mathrm{p}}) = F$ for preparation state vectors supported on the Hilbert space subspace $\mathrm{Span}(\{U|\emptyset\rangle, Uf_1^\dagger|\emptyset\rangle,\ldots,Uf_L^\dagger|\emptyset\rangle\})$. Finally, Eq. (90) allows to intuitively understand when exactly the witness fails to be an oracle, which we illustrate with one last example.

Example: symmetry breaking

Consider a scenario, where the system has initially a $\mathbb{Z}_2$ symmetry between the vacuum $|\emptyset\rangle$ and the fully occupied state vector $|\overline{1}\rangle$, and then at some point *spontaneous symmetry breaking* occurs such that the system must choose one of the two states. If the preparation is given by $\varrho_p = U\left[(1-\lambda)|\emptyset\rangle\langle\emptyset| + \lambda|\overline{1}\rangle\langle\overline{1}|\right]U^\dagger$ then the mismatch is a very good way of quantifying the fidelity of symmetry breaking, namely $n_\perp(\varrho_p) = \lambda\langle\overline{1}|\hat{N}|\overline{1}\rangle = \lambda L$ is a good order parameter. The mismatch is low for $\lambda \ll 1/L$ which occurs for high

values of our witness and it therefore allows to show that the system chose the vacuum in the $\mathbb{Z}_2$ symmetry breaking. Note, that the mismatch parameter will be high for many-particle GHZ states, but those are expected to be unstable and will not occur for no reason e.g. due to incoherent noise. In particular, low mismatch is also a natural assumption when certifying a digital simulation of the transverse field Ising Hamiltonian. As a final corollary to this example, note that for an L-mode system we have $\|n^{(\boldsymbol{\omega})}\| = L$ and therefore for all states ϱ in a ball defined by $\|\varrho - \varrho_{\mathrm{t}}\|_1 \leq 1/L$ we will find $F_{\mathcal{W}}(\varrho_{\mathrm{p}}) \geq 0$.

[1] P. Pfeuty, *The one-dimensional Ising model with a transverse field*, Ann. Phys. **57**, 79 (1970).

[2] M. Gluza, https://github.com/marekgluza/Fidelity_witnesses_example (2018).

[3] S. Bravyi, *Lagrangian representation for fermionic linear optics*, arXiv preprint quant-ph/0404180 (2004).

[4] M. Wimmer, *Algorithm 923: Efficient Numerical Computation of the Pfaffian for Dense and Banded Skew-Symmetric Matrices*, ACM Trans. Math. Softw. **38**, 30:1 (2012).

[5] L. Aolita, C. Gogolin, M. Kliesch, and J. Eisert, *Reliable quantum certification of photonic state preparations*, Nature Comm. **6**, 8498 (2015).

[6] D. Hangleiter, M. Kliesch, M. Schwarz, and J. Eisert, *Direct certification of a class of quantum simulations*, Quantum Sci. Technol. **2**, 015004 (2017).

SUMMARY

This thesis is very thematic to the vibrant age of emerging quantum technologies. Indeed, it demonstrates on first hand examples how novel experimental advances motivate various avenues of theoretical research. For physicists, the possibility of working with systems with pronounced quantum effects is particularly exciting. Accordingly, at all times of the theoretical research presented here there were specific quantum systems that we had in mind and we could always rely on the availability of complex and insightful experiments to guide, i.e., both stimulate and discipline, the ideas explored. We encountered cold atoms which can be trapped in various geometries, e.g., in an optical lattice, where the gas is restricted to a discrete set of available positions, or on an Atom Chip where the particles are free to roam in a continuous one-dimensional container. For these two cold atoms platforms we have seen diverse examples where paradigmatic scenarios pertaining to quantum many-body systems have been explored. Besides numerous beautiful realizations of key physical effects, that were discussed to set our work in context of a larger research program, we have seen that highly controlled experiments with cold atoms can tackle questions regarding the emergence of statistical mechanics [1, 2, 12, 13], or a quantitative experimental investigation [3] of aspects of one-dimensional systems that have been studied with methods of quantum field theory almost half a century ago and only now have entered the experimental domain.

In fact, even more is true concerning the experiments with cold atoms that we have discussed. At the moment we are still used to the important paradigm in physics 'predict and test' which in practice involves various theoretical arguments, approximations or measurements yielding oftentimes only indirect evidence for the questions at hand. This approach has been unquestionably successful in the past and can be largely expected to capture our scientific undergoings also in the future. However, already now, at the current development stage of quantum technologies, it appears to be fruitful to think of a newly emerging paradigm, namely 'simulate and read out'. This stresses the fact that a given highly controlled quantum system can reveal to us some properties of a system at first glance appearing to be completely different. We do have a growing body of evidence that this is technologically feasible and to sketch the long-term goals of the community it may suffice to give as fruit for thought a single example, which of course is not the only possibility: At the time of writing it is not unrealistic to believe that quantum simulation experiments with cold atoms will one day allow us to obtain conclusive results concerning specific aspects of high-temperature superconducting materials.

How can a gas of atoms reveal information about a specific solid-state material? The precise implementation details will have to be worked out in upcoming studies but on a higher level we have the answer and it lies in the idea of quantum simulation. Indeed we have seen in this thesis that cold atoms experiments are highly flexible, to the extent that we can even envision building quantum field thermal machines in these platforms [14]. Thus, if we establish precise ways to control the interaction parameters of an ultra-cold atomic gas such that the physics of the system will match the effective description of some desirable material, we will be able to simulate that physical system by a quantum simulation experiment. Once this is done, we have to ascertain the correctness of the result. This, surprisingly, turns out to be a particularly uncharted endeavor, possibly due to the fact that only recently did we become able to build up and control quantum aspects of synthetic systems. Thus if in the past there was a lack of easily available quantum systems, then there was no demand for developing quantum read-out techniques, i.e., methods of measuring non-commuting observables. The recent technological developments have rendered this issue a crucial bottle-neck and the results presented in this thesis provide possible ways of making progress on this matter [3, 4, 11, 13].

Quantum simulation experiments with ultra-cold atoms have served as the main motivation for the investigations presented in the first two chapters where foundational questions about quantum mechanics and statistical mechanics were considered [1, 2]. We have discussed that quantum simulators can realize exotic states where, e.g., steady states of thermodynamically large systems are non-thermal and have seen how to describe and rigorously derive this effect by proving time-scales for convergence to generalized Gibbs ensembles. Hence, these chapters give a first-hand account of what may become in the future the standard means of inquiry into the ongoings in complex quantum many-body systems, prominently featuring the guidance coming from quantum simulation experiments [12].

In the third chapter we have shown how to efficiently look into quantum simulators in a way that allows us to draw physical conclusions. That is to say, we were able to show how to improve the considered quantum

simulation platform thanks to an overall understanding of the physics of the system. Specifically, we developed a novel toolbox of tomographic analysis which allows to perform quantum state tomography of weakly interacting continuous fields [3]. This is particularly appealing, as thanks to the collaboration with a leading experimental group we were able to study quantitative physics of a one-dimensional quantum many-body system and in essence have verified experimentally the effective model of the ultra-cold gas which has been proposed about half a century ago by pioneering quantum field theorists.

Besides being able to study paradigmatic quantum systems in a very clear fashion it is also important to search for possibilities of improving future quantum simulators in ways that anticipate future challenges and yet are not too far fetched from being realised. In the last chapter we have shown that the fidelity of preparing weakly interacting systems of fermions in quantum simulators can be estimated efficiently, even in cases where the system features the formation of Cooper pairs. Fidelity witnessing [4] seems to be an excellent way forward to benchmark the coherence of large quantum systems where the target Hamiltonian is far from the basic interactions of the constituents. Arguably our method is one of the most practical ways of demonstrating the correct functioning of a dynamical quantum simulation, and so indirectly also the presence of quantum coherence and entanglement, on platforms devised in a bottom-up approach where the constituents on their own would not have pronounced quantum effects. One example is the Sycamore quantum processor where superconducting qubits have to be coupled by appropriately controlled operations which then allows to obtain interesting quantum states and fidelity witnesses allowed to successfully reveal the correct functioning of such quantum algorithms in an independent experiment [121].

All three themes of research laid out in this thesis are already accompanied by an experimental realization which illustrates how accessible exciting experiments on quantum systems have become. This would not have been possible without the prior work of the experimentalists building up towards devising quantum simulators and we were already now in a position to profit from the various possibilities of performing controllable experiments. This hints at a prognosis for future developments in physics: We should anticipate that quantum simulators will realize experimentally novel theoretical ideas by simulating an effect rather than hard-coding it into a given physical setup. Such programmable functionalities will allow to use a single well-controlled system for studying a wealth of physical questions and the time between a theoretical insight and the experimental observation will be dramatically shortened by quantum simulators in the future.

BIBLIOGRAPHY

[1] Gluza, M., Krumnow, C., Friesdorf, M., Gogolin, C. & Eisert, J. Equilibration via gaussification in fermionic lattice systems. *Phys. Rev. Lett.* **117**, 190602 (2016). URL https://link.aps.org/doi/10.1103/PhysRevLett.117.190602.

[2] Gluza, M., Eisert, J. & Farrelly, T. Equilibration towards generalized Gibbs ensembles in non-interacting theories. *SciPost Phys.* **7**, 38 (2019). URL https://scipost.org/10.21468/SciPostPhys.7.3.038.

[3] Gluza, M. *et al.* Quantum read-out for cold atomic quantum simulators. *Communications Physics* **3**, 1--8 (2020).

[4] Gluza, M., Kliesch, M., Eisert, J. & Aolita, L. Fidelity witnesses for fermionic quantum simulations. *Phys. Rev. Lett.* **120**, 190501 (2018). URL https://link.aps.org/doi/10.1103/PhysRevLett.120.190501.

[5] Goihl, M., Gluza, M., Krumnow, C. & Eisert, J. Construction of exact constants of motion and effective models for many-body localized systems. *Phys. Rev. B* **97**, 134202 (2018). URL https://link.aps.org/doi/10.1103/PhysRevB.97.134202.

[6] Jahn, A., Gluza, M., Pastawski, F. & Eisert, J. Holography and criticality in matchgate tensor networks. *Science advances* **5**, eaaw0092 (2019).

[7] Bielas, K., Flieger, W., Gluza, J. & Gluza, M. Neutrino mixing, interval matrices and singular values. *Phys. Rev. D* **98**, 053001 (2018). URL https://link.aps.org/doi/10.1103/PhysRevD.98.053001.

[8] Jahn, A., Gluza, M., Pastawski, F. & Eisert, J. Majorana dimers and holographic quantum error-correcting codes. *Phys. Rev. Research* **1**, 033079 (2019). URL https://link.aps.org/doi/10.1103/PhysRevResearch.1.033079.

[9] Goihl, M., Krumnow, C., Gluza, M., Eisert, J. & Tarantino, N. Edge mode locality in perturbed symmetry protected topological order. *SciPost Phys.* **6**, 72 (2019). URL https://scipost.org/10.21468/SciPostPhys.6.6.072.

[10] Haferkamp, J., Hangleiter, D., Eisert, J. & Gluza, M. Contracting projected entangled pair states is average-case hard. *Phys. Rev. Research* **2**, 013010 (2020). URL https://link.aps.org/doi/10.1103/PhysRevResearch.2.013010.

[11] Baez, M. L. *et al.* Dynamical structure factors of dynamical quantum simulators. *arXiv preprint arXiv:1912.06076* (2019).

[12] Schweigler, T. *et al.* Decay and recurrence of non-gaussian correlations in a quantum many-body system. *arXiv preprint arXiv:2003.01808* (2020).

[13] Gluza, M. & Eisert, J. Recovering quantum correlations in optical lattices from interaction quenches. *arXiv preprint arXiv:2005.09000* (2020).

[14] Gluza, M. *et al.* Quantum field thermal machines. *arXiv preprint arXiv:2006.01177* (2020).

[15] Deutsch, D. Quantum theory, the church--turing principle and the universal quantum computer. *Proceedings of the Royal Society of London. A. Mathematical and Physical Sciences* **400**, 97--117 (1985).

[16] Bernstein, E. & Vazirani, U. Quantum complexity theory. *SIAM Journal on computing* **26**, 1411--1473 (1997).

[17] Shor, P. W. Polynomial-time algorithms for prime factorization and discrete logarithms on a quantum computer. *SIAM review* **41**, 303--332 (1999).

[18] Blatt, R. & Roos, C. F. Quantum simulations with trapped ions. *Nature Physics* **8**, 277 (2012).

[19] Krantz, P. *et al.* A quantum engineer's guide to superconducting qubits. *Applied Physics Reviews* **6**, 021318 (2019).

[20] Bloch, I., Dalibard, J. & Zwerger, W. Many-body physics with ultracold gases. *Reviews of modern physics* **80**, 885 (2008).

[21] Browaeys, A., Barredo, D. & Lahaye, T. Experimental investigations of dipole--dipole interactions between a few Rydberg atoms. *Journal of Physics B: Atomic, Molecular and Optical Physics* **49**, 152001 (2016).

[22] Barends, R. *et al.* Superconducting quantum circuits at the surface code threshold for fault tolerance. *Nature* **508**, 500--503 (2014).

[23] Nigg, D. *et al.* Quantum computations on a topologically encoded qubit. *Science* **345**, 302--305 (2014).

[24] 2018, I. Global warming of 1.5°c. an ipcc special report on the impacts of global warming of 1.5°c above pre-industrial levels and related global greenhouse gas emission pathways, in the context of strengthening the global response to the threat of climate change, sustainable development, and efforts to eradicate poverty. *IPCC* (2018). URL https://www.ipcc.ch/sr15/.

[25] Ballance, C., Harty, T., Linke, N., Sepiol, M. & Lucas, D. High-fidelity quantum logic gates using trapped-ion hyperfine qubits. *Physical review letters* **117**, 060504 (2016).

[26] Monz, T. Aqtion - advanced quantum computing with trapped ions (2020). URL https://qt.eu/understand/projects/aqtion-advanced-quantum-computing-with-trapped-ions/.

[27] Kokail, C. *et al.* Self-verifying variational quantum simulation of lattice models. *Nature* **569**, 355 (2019).

[28] Metz, C. Google claims a quantum breakthrough that could change computing. *New York times* (2019). URL https://www.nytimes.com/2019/10/23/technology/quantum-computing-google.html.

[29] Arute, F. *et al.* Quantum supremacy using a programmable superconducting processor. *Nature* **574**, 505--510 (2019).

[30] Aaronson, S. *Quantum computing since Democritus* (Cambridge University Press, 2013).

[31] Terhal, B. M. & DiVincenzo, D. P. Adaptive quantum computation, constant depth quantum circuits and arthur-merlin games. *arXiv preprint quant-ph/0205133* (2002).

[32] Aharonov, D. & Vazirani, U. *Is quantum mechanics falsifiable? A computational perspective on the foundations of quantum mechanics* (Computability: Turing, Gödel, Church, and Beyond. MIT Press, 2013).

[33] Poulin, D. & Wocjan, P. Preparing ground states of quantum many-body systems on a quantum computer. *Physical review letters* **102**, 130503 (2009).

[34] Poulin, D., Kitaev, A., Steiger, D. S., Hastings, M. B. & Troyer, M. Quantum algorithm for spectral measurement with a lower gate count. *Physical review letters* **121**, 010501 (2018).

[35] Fradkin, E. *Field theories of condensed matter physics* (Cambridge University Press, 2013).

[36] Anderson, P. W. More is different. *Science* **177**, 393--396 (1972).

[37] Barahona, F. On the computational complexity of ising spin glass models. *Journal of Physics A: Mathematical and General* **15**, 3241 (1982).

[38] Cubitt, T. S., Montanaro, A. & Piddock, S. Universal quantum hamiltonians. *Proceedings of the National Academy of Sciences* **115**, 9497--9502 (2018).

[39] Cubitt, T. S., Perez-Garcia, D. & Wolf, M. M. Undecidability of the spectral gap. *Nature* **528**, 207 (2015).

[40] Arora, S. & Barak, B. *Complexity theory: A modern approach* (Cambridge University Press, 2009).

[41] Nielsen, M. A. & Chuang, I. L. *Quantum computation and quantum information* (Cambridge University Press, 2010).

[42] Gharibian, S., Huang, Y., Landau, Z., Shin, S. W. *et al.* Quantum hamiltonian complexity. *Foundations and Trends® in Theoretical Computer Science* **10**, 159--282 (2015).

[43] Osborne, T. J. Hamiltonian complexity. *Reports on Progress in Physics* **75**, 022001 (2012).

[44] Rauer, B. *et al.* Recurrences in an isolated quantum many-body system. *Science* **360**, 307--310 (2018).

[45] Trotzky, S. *et al.* Probing the relaxation towards equilibrium in an isolated strongly correlated one-dimensional Bose gas. *Nature Phys.* **8**, 325 (2012).

[46] Lohse, M., Schweizer, C., Zilberberg, O., Aidelsburger, M. & Bloch, I. A Thouless quantum pump with ultracold bosonic atoms in an optical superlattice. *Nature Physics* **12**, 350 (2016).

[47] Cheneau, M. *et al.* Light-cone-like spreading of correlations in a quantum many-body system. *Nature* **481**, 484 (2012).

[48] Aidelsburger, M. *et al.* Realization of the Hofstadter Hamiltonian with ultracold atoms in optical lattices. *Physical review letters* **111**, 185301 (2013).

[49] Greiner, M., Mandel, O., Esslinger, T., Hänsch, T. & Bloch, I. Quantum phase transition from a superfluid to a Mott insulator in an ultracold gas of atoms. *Nature* **415**, 39--44 (2002).

[50] Schreiber, M. *et al.* Observation of many-body localization of interacting fermions in a quasirandom optical lattice. *Science* **349**, 842--845 (2015).

[51] Murthy, P. A. *et al.* Quantum scale anomaly and spatial coherence in a 2d Fermi superfluid. *Science* **365**, 268--272 (2019).

[52] Mazurenko, A. *et al.* A cold-atom Fermi--Hubbard antiferromagnet. *Nature* **545**, 462 (2017).

[53] Bohrdt, A. *et al.* Classifying snapshots of the doped Hubbard model with machine learning. *Nature Physics* **15**, 921--924 (2019).

[54] Chiu, C. S. *et al.* String patterns in the doped Hubbard model. *Science* **365**, 251--256 (2019).

[55] Gring, M. *et al.* Relaxation and prethermalization in an isolated quantum system. *Science* **337**, 1318--1322 (2012).

[56] Langen, T. *et al.* Experimental observation of a generalized gibbs ensemble. *Science* **348**, 207--211 (2015).

[57] Schweigler, T. *et al.* Experimental characterization of a quantum many-body system via higher-order correlations. *Nature* **545**, 323 (2017).

[58] Kinoshita, T., Wenger, T. & Weiss, D. S. A quantum Newton's cradle. *Nature* **440**, 900 (2006).

[59] Schemmer, M., Bouchoule, I., Doyon, B. & Dubail, J. Generalized hydrodynamics on an atom chip. *Phys. Rev. Lett.* **122**, 090601 (2019). URL https://link.aps.org/doi/10.1103/PhysRevLett.122.090601.

[60] Bernien, H. *et al.* Probing many-body dynamics on a 51-atom quantum simulator. *Nature* **551**, 579 (2017).

[61] de Léséleuc, S. *et al.* Observation of a symmetry-protected topological phase of interacting bosons with rydberg atoms. *Science* **365**, 775--780 (2019).

[62] Bohnet, J. G. *et al.* Quantum spin dynamics and entanglement generation with hundreds of trapped ions. *Science* **352**, 1297--1301 (2016).

[63] Jurcevic, P. *et al.* Quasiparticle engineering and entanglement propagation in a quantum many-body system. *Nature* **511**, 202 (2014).

[64] Zhang, J. *et al.* Observation of a many-body dynamical phase transition with a 53-qubit quantum simulator. *Nature* **551**, 601 (2017).

[65] Mazurenko, A. *et al.* A cold-atom Fermi-Hubbard antiferromagnet. *Nature* **545**, 462 (2017).

[66] Childs, A. M. & Su, Y. Nearly optimal lattice simulation by product formulas. *Phys. Rev. Lett.* **123**, 050503 (2019). URL https://link.aps.org/doi/10.1103/PhysRevLett.123.050503.

[67] Landau, L., Lifshitz, E. & Pitaevskii, L. Statistical physics, part 2. *Course of theoretical physics* **9**, 67 (1981).

[68] Ruelle, D. *Thermodynamic formalism: the mathematical structure of equilibrium statistical mechanics* (Cambridge University Press, 2004).

[69] Huang, K. *Introduction to statistical physics* (Chapman and Hall/CRC, 2009).

[70] Polkovnikov, A., Sengupta, K., Silva, A. & Vengalattore, M. Colloquium: nonequilibrium dynamics of closed interacting quantum systems. *Rev. Mod. Phys.* **83**, 863--883 (2011). URL https://link.aps.org/doi/10.1103/RevModPhys.83.863.

[71] Eisert, J., Friesdorf, M. & Gogolin, C. Quantum many-body systems out of equilibrium. *Nature Physics* **11**, 124 (2015).

[72] Goold, J., Huber, M., Riera, A., del Rio, L. & Skrzypczyk, P. The role of quantum information in thermodynamics—a topical review. *J. Phys. A* **49**, 143001 (2016). URL http://stacks.iop.org/1751-8121/49/i=14/a=143001.

[73] Gogolin, C. & Eisert, J. Equilibration, thermalisation, and the emergence of statistical mechanics in closed quantum systems. *Rep. Prog. Phys.* **79**, 056001 (2016). URL http://stacks.iop.org/0034-4885/79/i=5/a=056001.

[74] D'Alessio, L., Kafri, Y., Polkovnikov, A. & Rigol, M. From quantum chaos and eigenstate thermalization to statistical mechanics and thermodynamics. *Advances in Physics* **65**, 239--362 (2016).

[75] Mori, T., Ikeda, T. N., Kaminishi, E. & Ueda, M. Thermalization and prethermalization in isolated quantum systems: a theoretical overview. *Journal of Physics B: Atomic, Molecular and Optical Physics* **51**, 112001 (2018). URL https://doi.org/10.1088%2F1361-6455%2Faabcdf.

[76] Cramer, M., Dawson, C. M., Eisert, J. & Osborne, T. J. Exact relaxation in a class of nonequilibrium quantum lattice systems. *Phys. Rev. Lett.* **100**, 030602 (2008). URL http://link.aps.org/doi/10.1103/PhysRevLett.100.030602.

[77] Rigol, M., Dunjko, V. & Olshanii, M. Thermalization and its mechanism for generic isolated quantum systems. *Nature* **452**, 854--858 (2008).

[78] Rigol, M., Dunjko, V., Yurovsky, V. & Olshanii, M. Relaxation in a completely integrable many-body quantum system: An ab initio study of the dynamics of the highly excited states of 1D lattice hard-core bosons. *Phys. Rev. Lett.* **98**, 050405 (2007).

[79] Caux, J.-S. & Essler, F. H. L. Time evolution of local observables after quenching to an integrable model. *Phys. Rev. Lett.* **110**, 257203 (2013).

[80] Vidmar, L. & Rigol, M. Generalized Gibbs ensemble in integrable lattice models. *J. Stat. Mech.* **2016**, 064007 (2016).

[81] Calabrese, P., Essler, F. H. & Fagotti, M. Quantum quench in the transverse field Ising chain: I. time evolution of order parameter correlators. *J. Stat. Mech.* **2012**, P07016 (2012).

[82] Wouters, B. *et al.* Quenching the Anisotropic Heisenberg Chain: Exact Solution and Generalized Gibbs Ensemble. *Phys. Rev. Lett.* **113**, 117202 (2014).

[83] Schreiber, M. *et al.* Observation of many-body localization of interacting fermions in a quasi-random optical lattice. *Science* **349**, 842--845 (2015).

[84] Huse, D. A., Nandkishore, R. & Oganesyan, V. Phenomenology of fully many-body-localized systems. *Phys. Rev. B* **90**, 174202 (2014).

[85] Langen, T. *et al.* Experimental observation of a generalized Gibbs ensemble. *Science* **348**, 207--211 (2015).

[86] Abanin, D. A., Altman, E., Bloch, I. & Serbyn, M. Many-body localization, thermalization, and entanglement. *Rev. Mod. Phys.* **91**, 021001 (2019).

[87] Kinoshita, T., Wenger, T. & Weiss, D. S. A quantum newton's cradle. *Nature* **440**, 900 (2006).

[88] Bernien, H. *et al.* Probing many-body dynamics on a 51-atom quantum simulator. *Nature* **551**, 579 (2017).

[89] Turner, C. J., Michailidis, A. A., Abanin, D. A., Serbyn, M. & Papic, Z. Weak ergodicity breaking from quantum many-body scars. *Nature Phys.* **14**, 745--749 (2018).

[90] Li, C. *et al.* Dephasing and relaxation of bosons in 1D: Newton's Cradle revisited (2018). 1804.01969v1.

[91] Wilming, H., Goihl, M., Krumnow, C. & Eisert, J. Towards local equilibration in closed interacting quantum many-body systems (2017). 1704.06291.

[92] de Oliveira, T. R., Charalambous, C., Jonathan, D., Lewenstein, M. & Riera, A. Equilibration time scales in closed many-body quantum systems. *New Journal of Physics* **20**, 033032 (2018). URL https://doi.org/10.1088%2F1367-2630%2Faab03b.

[93] Rigol, M. Quantum quenches and thermalization in one-dimensional fermionic systems. *Phys. Rev. A* **80**, 053607 (2009).

[94] Cramer, M., Flesch, A., McCulloch, I., Schollwöck, U. & Eisert, J. Exploring local quantum many-body relaxation by atoms in optical superlattices. *Phys. Rev. Lett.* **101**, 063001 (2008).

[95] Zangara, P. R. *et al.* Time fluctuations in isolated quantum systems of interacting particles. *Phys. Rev. E* **88**, 032913 (2013).

[96] Eckstein, M., Kollar, M. & Werner, P. Interaction quench in the hubbard model: Relaxation of the spectral function and the optical conductivity. *Phys. Rev. B* **81**, 115131 (2010).

[97] Bernier, J.-S., Citro, R., Kollath, C. & Orignac, E. Correlation dynamics during a slow interaction quench in a one-dimensional bose gas. *Phys. Rev. Lett.* **112**, 065301 (2014).

[98] Torres-Herrera, E. J., Kollmar, D. & Santos, L. F. Relaxation and thermalization of isolated many-body quantum systems. *Physica Scripta* **2015**, 014018 (2015).

[99] Santos, L. F. & Torres-Herrera, E. J. Nonequilibrium quantum dynamics of many-body systems (2017). 1706.02031.

[100] Khodja, A. & Gemmer, J. Effect of short-range order on transport in one-particle tight-binding models. *Phys. Rev. E* **88**, 042103 (2013).

[101] Tasaki, H. From quantum dynamics to the canonical distribution: general picture and a rigorous example. *Phys. Rev. Lett.* **80**, 1373 (1998).

[102] Reimann, P. Foundation of statistical mechanics under experimentally realistic conditions. *Phys. Rev. Lett.* **101**, 190403 (2008).

[103] Linden, N., Popescu, S., Short, A. J. & Winter, A. Quantum mechanical evolution towards thermal equilibrium. *Phys. Rev. E* **79**, 061103 (2009).

[104] Short, A. J. & Farrelly, T. C. Quantum equilibration in finite time. *New J. Phys.* **14**, 013063 (2012).

[105] Reimann, P. & Kastner, M. Equilibration of isolated macroscopic quantum systems. *New J. Phys.* **14**, 043020 (2012).

[106] Goldstein, S., Hara, T. & Tasaki, H. Time scales in the approach to equilibrium of macroscopic quantum systems. *Phys. Rev. Lett.* **111**, 140401 (2013).

[107] Malabarba, A. S., García-Pintos, L. P., Linden, N., Farrelly, T. C. & Short, A. J. Quantum systems equilibrate rapidly for most observables. *Phys. Rev. E* **90**, 012121 (2014).

[108] Garcia-Pintos, L. P., Linden, N., Malabarba, A. S. L., Short, A. J. & Winter, A. Equilibration time scales of physically relevant observables (2015). 1509.05732.

[109] Farrelly, T. Equilibration of quantum gases. *New J. Phys.* **18**, 073014 (2016).

[110] Essler, F. H. L. & Fagotti, M. Quench dynamics and relaxation in isolated integrable quantum spin chains. *J. Stat. Mech.* **2016**, 064002 (2016).

[111] Masanes, L., Roncaglia, A. & Acín, A. Complexity of energy eigenstates as a mechanism for equilibration. *Phys. Rev. E* **87**, 032137 (2013).

[112] Brandão, F. G. S. L. *et al.* Convergence to equilibrium under a random Hamiltonian. *Phys. Rev. E* **86**, 031101 (2012).

[113] Cramer, M. Thermalization under randomized local Hamiltonians. *New J. Phys.* **14**, 053051 (2012).

[114] Vinayak & Žnidarič, M. Subsystem dynamics under random Hamiltonian evolution. *J. Phys. A* **45**, 125204 (2012).

[115] Ududec, C., Wiebe, N. & Emerson, J. Information-theoretic equilibration: the appearance of irreversibility under complex quantum dynamics. *Phys. Rev. Lett.* **111**, 080403 (2013).

[116] Reimann, P. Typical fast thermalization processes in closed many-body systems. *Nat. Commun.* **7**, 10821 (2016).

[117] Braun, S. *et al.* Emergence of coherence and the dynamics of quantum phase transitions. *Proceedings of the National Academy of Sciences* **112**, 3641--3646 (2015).

[118] Schneider, U. *et al.* Fermionic transport and out-of-equilibrium dynamics in a homogeneous hubbard model with ultracold atoms. *Nature Physics* **8**, 213 (2012).

[119] Kaufman, A. M. *et al.* Quantum thermalization through entanglement in an isolated many-body system. *Science* **353**, 794--800 (2016).

[120] Eisert, J. *et al.* Quantum certification and benchmarking. *Nature Reviews Physics* 1--9 (2020).

[121] Arute, F. *et al.* Hartree-fock on a superconducting qubit quantum computer. *arXiv preprint arXiv:2004.04174* (2020).

[122] Lieb, E. & Robinson, D. The finite group velocity of quantum spin systems. *Communications in Mathematical Physics* **28**, 251--257 (1972). URL http://dx.doi.org/10.1007/BF01645779.

[123] Neumann, J. Beweis des ergodensatzes und desh-theorems in der neuen mechanik. *Zeitschrift für Physik* **57**, 30--70 (1929). URL http://dx.doi.org/10.1007/BF01339852.

[124] Cramer, M. & Eisert, J. A quantum central limit theorem for non-equilibrium systems: exact local relaxation of correlated states. *New J. Phys.* **12**, 055020 (2010). URL http://stacks.iop.org/1367-2630/12/i=5/a=055020.

[125] Cushen, C. D. & Hudson, R. L. A quantum-mechanical central limit theorem. *Journal of Applied Probability* **8**, 454--469 (1971).

[126] Hudson, R. L. A quantum-mechanical central limit theorem for anti-commuting observables. *Journal of Applied Probability* **10**, pp. 502--509 (1973). URL http://www.jstor.org/stable/3212771.

[127] von Waldenfels, W. An algebraic central limit theorem in the anti-commuting case. *Zeitschrift für Wahrscheinlichkeitstheorie und Verwandte Gebiete* **42**, 135--140 (1978). URL http://dx.doi.org/10.1007/BF00536049.

[128] Haag, R., Kadison, R. & Kastler, D. Asymptotic orbits in a free fermi gas. *Communications in Mathematical Physics* **33**, 1--22 (1973).

[129] Hastings, M. B. & Koma, T. Spectral gap and exponential decay of correlations. *Communications in mathematical physics* **265**, 781--804 (2006).

[130] Nachtergaele, B. & Sims, R. Lieb-robinson bounds and the exponential clustering theorem. *Communications in mathematical physics* **265**, 119--130 (2006).

[131] Kliesch, M., Gogolin, C., Kastoryano, M. J., Riera, A. & Eisert, J. Locality of temperature. *Physical Review X* **4**, 031019 (2014).

[132] Molnar, A., Schuch, N., Verstraete, F. & Cirac, J. I. Approximating Gibbs states of local hamiltonians efficiently with projected entangled pair states. *Phys. Rev. B* **91**, 045138 (2015). URL https://link.aps.org/doi/10.1103/PhysRevB.91.045138.

[133] Murthy, C. & Srednicki, M. Relaxation to gaussian and generalized gibbs states in systems of particles with quadratic hamiltonians. *Physical Review E* **100**, 012146 (2019).

[134] Caux, J.-S. & Mossel, J. Remarks on the notion of quantum integrability. *Journal of Statistical Mechanics: Theory and Experiment* **2011**, P02023 (2011).

[135] Flesch, A., Cramer, M., McCulloch, I., Schollwöck, U. & Eisert, J. Probing local relaxation of cold atoms in optical superlattices. *Phys. Rev. A* **78**, 033608 (2008).

[136] Calabrese, P., Essler, F. H. & Fagotti, M. Quantum quench in the transverse-field ising chain. *Phys. Rev. Lett.* **106**, 227203 (2011).

[137] Fagotti, M. & Essler, F. H. Reduced density matrix after a quantum quench. *Phys. Rev. B* **87**, 245107 (2013).

[138] Sotiriadis, S. Memory-preserving equilibration after a quantum quench in a one-dimensional critical model. *Phys. Rev. A* **94**, 031605 (2016).

[139] Sotiriadis, S. & Calabrese, P. Validity of the gge for quantum quenches from interacting to noninteracting models. *J. Stat. Mech.* **2014**, P07024 (2014).

[140] Short, A. J. Equilibration of quantum systems and subsystems. *New J. Phys.* **13**, 053009 (2011).

[141] Farrelly, T., Brandão, F. G. & Cramer, M. Thermalization and return to equilibrium on finite quantum lattice systems. *Phys. Rev. Lett.* **118**, 140601 (2017).

[142] Ilievski, E. *et al.* Complete generalized Gibbs ensembles in an interacting theory. *Phys. Rev. Lett.* **115**, 157201 (2015).

[143] Rauer, B. *Non-Equilibrium Dynamics Beyond Dephasing Recurrences and Loss Induced Cooling in One-dimensional Bose Gases.* Ph.D. thesis (2019).

[144] Schweigler, T. *Correlations and dynamics of tunnel-coupled one-dimensional Bose gases.* Ph.D. thesis, TU Wien (2019).

[145] Schumm, T. *et al.* Matter-wave interferometry in a double well on an atom chip. *Nat. Phys.* **1**, 57--62 (2005).

[146] van Nieuwkerk, Y. D., Schmiedmayer, J. & Essler, F. H. L. Projective phase measurements in one-dimensional bose gases. *arXiv:1806.02626* (2018).

[147] Langen, T., Geiger, R., Kuhnert, M., Rauer, B. & Schmiedmayer, J. Local emergence of thermal correlations in an isolated quantum many-body system. *Nature Physics* **9**, 640--643 (2013).

[148] Erne, S., Bücker, R., Gasenzer, T., Berges, J. & Schmiedmayer, J. Universal dynamics in an isolated one-dimensional bose gas far from equilibrium. *Nature* **563**, 225--229 (2018).

[149] Popov, V. N. *Functional integrals in quantum field theory and statistical physics*, vol. 8 (Springer Science & Business Media, 2001).

[150] Giamarchi, T. *Quantum physics in one dimension*, vol. 121 (Clarendon press, 2003).

[151] Langmann, E. & Moosavi, P. Construction by bosonization of a fermion-phonon model. *Journal of Mathematical Physics* **56**, 091902 (2015).

[152] Flammia, S. T. & Liu, Y.-K. Direct fidelity estimation from few pauli measurements. *Phys. Rev. Lett.* **106**, 230501 (2011). URL https://link.aps.org/doi/10.1103/PhysRevLett.106.230501.

[153] Cramer, M. *et al.* Efficient quantum state tomography. *Nature Comm.* **1**, 149 (2010).

[154] Terhal, B. M. Bell inequalities and the separability criterion. *Physics Letters A* **271**, 319 -- 326 (2000). URL http://www.sciencedirect.com/science/article/pii/S0375960100004011.

[155] Hangleiter, D., Kliesch, M., Schwarz, M. & Eisert, J. Direct certification of a class of quantum simulations. *Quantum Sci. Technol.* **2**, 015004 (2017).

[156] Aolita, L., Gogolin, C., Kliesch, M. & Eisert, J. Reliable quantum certification of photonic state preparations. *Nature communications* **6** (2015).

[157] Friedenauer, H., Schmitz, H., Glueckert, J., Porras, D. & Schaetz, T. Simulating a quantum magnet with trapped ions. *Nature Phys.* **4**, 757--761 (2008).

[158] Kim, K. *et al.* Quantum simulation of frustrated ising spins with trapped ions. *Nature* **465**, 590--593 (2010).

[159] Islam, R. *et al.* Onset of a quantum phase transition with a trapped ion quantum simulator. *Nature Comm.* **2**, 377 (2011).

[160] Salathé, Y. *et al.* Digital quantum simulation of spin models with circuit quantum electrodynamics. *Phys. Rev. X* **5**, 021027 (2015).

[161] Barends, R. *et al.* Digitized adiabatic quantum computing with a superconducting circuit. *Nature* **534**, 222--226 (2016).

[162] Doherty, A. C., Parrilo, P. A. & Spedalieri, F. M. Complete family of separability criteria. *Phys. Rev. A* **69**, 022308 (2004). URL https://link.aps.org/doi/10.1103/PhysRevA.69.022308.

[163] Hyllus, P. & Eisert, J. Optimal entanglement witnesses for continuous-variable systems. *New Journal of Physics* **8**, 51 (2006).

[164] Anderson, P. W. Infrared catastrophe in fermi gases with local scattering potentials. *Phys. Rev. Lett.* **18**, 1049--1051 (1967). URL https://link.aps.org/doi/10.1103/PhysRevLett.18.1049.

[165] Peierls, R. E. & Peierls, R. *Surprises in theoretical physics* (Princeton University Press, 1979).

[166] Fogarty, T., Deffner, S., Busch, T. & Campbell, S. Orthogonality catastrophe as a consequence of the quantum speed limit. *Phys. Rev. Lett.* **124**, 110601 (2020). URL https://link.aps.org/doi/10.1103/PhysRevLett.124.110601.

[167] Brandino, G. P., Caux, J.-S. & Konik, R. M. Glimmers of a quantum kam theorem: Insights from quantum quenches in one-dimensional bose gases. *Phys. Rev. X* **5**, 041043 (2015). URL https://link.aps.org/doi/10.1103/PhysRevX.5.041043.

[168] Bravyi, S. Classical capacity of fermionic product channels. *eprint arXiv:quant-ph/0507282* (2005). quant-ph/0507282.

[169] CO2nduct-community. Scientific co2nduct: Raising awareness for the climate impact of science, https://scientific-conduct.github.io.

CLIMATE FOOTPRINT ESTIMATES

Given the current climate change crisis that has arisen from human activities it is urgently needed to assess transparently various branches in the overall economy, this also includes scientific research. While an urgent call of action has been voiced by the Intergovernmental Panel on Climate Change (IPCC) [24] improvements regarding our overall impact on the climate seems to be rather slow. This is to the extent that even in science the methodology for assessing the climate footprint is unclear and we only now begin to start developing possible ways of doing that [169].

My footprint had three dominating factors. The most important are *i)* travels and flying in particular and *ii)* numerical computations on a cluster. Additionally *iii)* there are the daily activities such as commuting to work, running computers and laptops, video calls. The daily routines can be estimated similarly as for other inhabitants of a given city. Three projects out of 14 publications over the course of 5 years demanded heavy cluster usage and the largest use was Ref. [5] with whooping 576000 of kernel hours. As mentioned, there is no standard methodology of keeping track of the footprint and so the kernel hours of Ref. [11] have to be estimated to be somewhere between the use documented in Refs. [9] and [5] as these publications involved similar types of calculation. Thus the amount of emitted CO_2 can be estimated to about 1484+5000?+9274 kg CO_2 which is comparable to one year footprint of one person living in Germany. A similar figure can be obtained for my travels which over the course of 5 years amount again to the yearly footprint of a person living in Germany. It seems to be standard to frequently travel for research visits or workshops and the course of PhD studies seems to be an example of that. Below I list the different destinations and means of transport giving the CO_2 estimates obtained from the *atmosfair* calculator. The flights connected to the research presented in this thesis were: *Berlin (B)* $\leftrightarrow$ *Gothenburg (288 kg), 1.5* $\times$ *Vienna (387 kg), 2*$\times$ *Barcelona (1700 kg), Granada (1281 kg), Toronto (3853 kg).*Additionally, these were the train travels inland $B \leftrightarrow$ *2*$\times$ *Dresden, 2*$\times$ *Hannover, 2*$\times$ *Heidelberg, Mainz, Erlangen, Regensburg, Bielefeld, Bonn* and international $B \leftrightarrow 3 \times$ *Vienna (3* $\times$ ~~*258 kg*~~*), Copenhagen (*~~*212 kg*~~*), Aarhus (*~~*287 kg*~~*), Obergurgl (*~~*307 kg*~~*)* and additionally it proved useful to connect travels $B \rightarrow$ *Katowice* $\rightarrow$ *Vienna* $\rightarrow B$ *(*~~*258 kg*~~*),* $B \rightarrow$ *Vienna* $\rightarrow$ *Ljubljana* $\rightarrow B$ *(*~~*453 kg*~~*),* $B \rightarrow$ *Split* $\rightarrow$ *Vienna* $\rightarrow B$ *(*~~*700 kg*~~*),* $B \rightarrow$ *Vienna* $\rightarrow$ *Florence* $\rightarrow B$ *(*~~*611 kg*~~*)* where the stroked out numbers are the estimates for flights.

Most of the international train travels could have been flights and I attribute this substitution solely to raised awareness concerning flights thus showing that information campaigns can be effective.

It should be noted that only recently it became possible to offset research travels via university funding and there is no standard way for doing this which constitutes a systemic obstacle for implementing some measures of accounting for carbon impact of science related travels. Additionally, a wider implementation of SAP-type systems to do accounting at universities, where the administration organization tends to be rather outdated and not digitalized, would allow to much more systematically gather travel data to assess the climate impact of science related travels.

In theoretical physics peers tend to be working at distanced institutes because we often tackle rather unusual subjects and for developing scientific insights staying connected is a key essential aspect of the work we do. As evidenced by the recent events, there seems to be a major shift toward video conferencing due to the pandemic. It can be expected that a number of future conference and workshop-type events will be held online and institutions such as universities, ministries of science and funding agencies should provide incentives for creating more online events. For 2 out 14 of my publications it was possible to predominantly work via video conferencing which could include all project participants and allowed for programming together via screen sharing over the Internet without the need for joint visits in person. Again institutions should encourage such innovative ways of working on projects with the ultimate goal that research visits become largely reserved for meetings with peers dedicated to exchanging ideas via personal communication and scientific discussions which is the only indispensable aspect of research that cannot be done online as effectively.

ACKNOWLEDGMENTS

I would like to thank my supervisor Jens Eisert that I had a chance during my studies to be part of the impressive research environment which he has created. It has been extremely inspiring to learn first hand to stay always positive and committed to tackling relevant research subjects. This experience has been for me absolutely unique and I'm grateful for how it enriched me in so many ways, something that will remain invaluable for me for the rest of my life. Many, many thanks Jens!

I also extended my warmest thanks to the many colleagues and collaborators for their continuous generosity in sharing their insights and knowledge. It seems to me that first hand seeing the power of collaborative research is the most important thing I have learnt so far, even more than solving the harmonic oscillator! My gratitude goes towards: Abdul Afzal, Leandro Aolita, Paul Appel, Ben Balz, Laura Baez, Andi Bauer, Jörg Behrmann, Juani Bermejo-Vega, Krzysiek Bielas, Paul Boes, Winton Brown, Federica Cataldini, Roberto di Candia, Terry Farrelly, Wojtek Flieger, Mathis Friesdorf, Janusz Gluza, Christian Gogolin, Marcel Goihl, David Gosset, Lucas Hackl, Jonas Haferkamp, Frederik Hahn, Dominik Hangleiter, Marcus Huber, Alex Jahn, Si-Cong Ji, Markus Kesselring, Michael Keyl, Martin Kliesch, Christian Krumnow, Ivan Kukuljan, Richard Küng, Sophia Lachs, Jaqueline Lekscha, Igor Mazets, Nelly Ng, Papalex Nietner, Yasser Omar, Fernando Pastawski, Sebastian Päckel, Marco Pezzutto, Jeremi Piotrowski, Philipp Preiss, Mariusz Przybycień, Bernhard Rauer, Tord Riemann, Carlos Riofrío, Ingo Roth, João Sabino, Sidhant Saraogi, Jörg Schmiedmayer, Martin Schwarz, Thomas Schweigler, Kanu Sinha, Spyros Sotiriadis, Adrian Steffens, Ryan Sweke, Amin Tajik, Nick Tarantino, Giuseppe Vitagliano, Yuri van Nieuwkerk, Albert Werner, Carolin Wille, Henrik Wilming, Jacek Wosiek, Zoltán Zimborás.